CRANFIELD UNIVERSITY

SCHOOL OF AEROSPACE, TRANSPORT AND MANUFACTURING

Doctor of Philosophy

Academic Year 2012 - 2015

JINCHUN ZHU

DEVELOPMENT OF NOVEL FLAX BIO-MATRIX COMPOSITES FOR NON-STRUCTURAL AND STRUCTURAL VEHICLE APPLICATIONS

Supervisor: Dr Hrushikesh Abhyankar
Dr Huijun Zhu

This thesis is submitted in fulfilment of the requirements for the degree of PhD

ABSTRACT

The use of natural fibres (e.g. flax, hemp etc.) instead of synthetic fibres (carbon and glass etc.) as composite reinforcements not only benefits the environment, but also provides economical lightweight products for transports. Although there are a few studies reported in literature on use of flax fibres, there is no comprehensive guide on use of flax fibres with bio-resins to re-engineer bio-composite systems that can be used in vehicle structures. The state-of-art of the current research towards using natural fibre reinforced composites is reviewed by the thesis. The review covers the performances of flax composites, concentrating on the effect of matrix types and existing development methods. The review also identifies the rational of selecting tannin resins and bio-epoxy resins to combine with flax fibre reinforcements.

In the experimental work, mimosa tannin resin (natural phenolic resin) and pine-oil derived supersap epoxy resin are selected to manufacture the fully renewable flax composites. By tailoring the fibre configurations and chemical surface treatments, the resultant composites were investigated to provide information for engineers to understand the composite behaviours and properties. Mechanical properties (tension, flexural, shear, impact etc.) and physical properties (moisture, ageing etc.) were assessed through adequate tests and analysing methods. In addition, bio-sandwich structures based on the novel studied composites and commercial bio-foams were evaluated to study the energy absorption which could be very important in vehicle design. Based on the results, flax/supersap epoxy and flax/tannin composites are suitable for possible exterior structural and interior non-structural applications, respectively. The developed flax fibre composites with innovative bio-matrices have a potential to prevail in modern vehicle applications, due to the competitive performances, economic viability and environmental acceptability.

Keywords:

Flax fibres, Tannin, bio-epoxy, fibre configuration and surface treatment, bio-sandwiches, mechanical performance

ACKNOWLEDGEMENT

I am grateful to the FP 7 and ECHOSELL (project no. 265838) for the financial support for this research.

I am deeply indebted to my main supervisor, Dr Hrushikesh Abhyankar, at the Centre of Automotive Technology (CAT), Canfield University. His suggestions and comments are very helpful for me to carry this study. Without his patient guidance, I would not have gone in the correct direction.

I would like to express my gratitude to all others who gave me the possibility to complete the study. I want to thank to Dr Huijun Zhu, Dr David Ayre, Mr Ben Hopper and my college - Elias, Laura and Ian for their help in my material preparation, characterisation, and analysis. I also would like to thank my friends (Zihang Zhu etc.) who helped me through my study in Cranfield. With special to Dr Hrushikesh Abhyankar again for his kind support to take me through after the movement of my previous supervisor Dr James Njuguna who also gave my lots of help to build up this research base.

Above all I would like to express my sincere thanks to my parents, for their on-going support all these years since I studied in UK. They can only see me once a year, but always encourage me with their best wishes, which have led me there.

Thanks and love you

CONTRIBUTIONS TO THE THESIS

Journal publications:

- Zhu, J., Abhyankar, H., Nassiopoulos and Njuguna, J. (2012), "Tannin-based flax fibre reinforced composites for structural applications in vehicles", *IOP Conference Series: Materials Science and Engineering*, vol. 40, no. 1, pp. 012030.
- Zhu, J., Njuguna, J., Abhyankar, H., Zhu, H., Perreux, D., Thiebaud, F., Pizzi, A., Sauget, A., de Larminat, A. and Nicollin, A. (2013), "Effect of fibre configurations on mechanical properties of flax/tannin composites", *Industrial Crops and Products*, vol. 50, pp. 68-76.
- Zhu, J., Zhu, H., Njuguna, J. and Abhyankar, H. (2013), "Recent development of flax fibres and their reinforced composites based on different polymeric matrices", *Materials,* vol. 6, no. 11, pp. 5171-5198.
- Zhu, J., Brighton, J., Zhu, H. and Abhyanhkar, H. (2014), "Effect of Alkali, Esterification and Silane Surface Treatments on Properties of Flax Fibres", Journal of Scientific Research and Reports, Vol. 4, pp. 1-11.
- Zhu, J., Zhu, H., Brighton, J and Abhyanhkar, H. (2014), "Improving mechanical properties of novel flax/tannin composites by different treatments", *Industrial Crops and Products*, (submitted).
- Zhu, J., Immonen, K., Avril, C., Zhu, H., Brighton, J and Abhyanhkar, H. (2014), "Novel hybrid flax reinforced supersap composites for automotive applications", *Fibres*, (submitted)
- Zhu, J., Zhu, H., Brighton, J and Abhyanhkar, H. (2014), "Low-velocity impact response of fully bio-sandwich composites", *International Journal of Polymer Science*, (submission invitation).

Conference papers and presentations:

- Zhu, J., Abhyankar, H., Avril, C., Pizzi, A. and Sauget, A. Structural performances of flax reinforced composites from bio-epoxy and tannin resins. TRA2014, Paris, April 2014 (conference proceeding paper)

- Zhu, J., Abhyankar, H., and Njuguna, J.: Effects of fibre pre-treatments on water adsorption of non-woven flax mat-reinforced tannin composites. ICMR2013, Cranfield, UK (conference proceeding paper)
- Zhu, J., Abhyankar, H., and Njuguna, J. et.al: Effects of chemical treatments on physical properties of flax fibres, MPM2013, Cracow, May 2013 (conference proceeding paper).
- ECOSHELL workshop-Superlight City car, 27 June, 2013, Belgium, Brussels. (Presentation)
- Zhu, L., Abhyankar, H., and Njuguna, J. et.al: Effects of chemical treatments on performances of flax/tannin composites, Euromat 2013, Seville, Spain, September 2013. (Presentation)

MAIN ABBREVIATIONS

PP	Polypropylene
PS	Polystyrene
PLA	Poly (lactic acid)
UPE	Unsaturated polyester
FT	Flax/tannin composites
FE	Flax/supersap bio-epoxy composites
BTCA	Butanetertracarboxylic acid
APS	Amionproply triethoxy siloxane
LD	Laccase-dodecyl gallate
ASTM	American Society for Testing and Materials
ISO	International Organization for Standardization
$_{wt}$%	Weight content ratio
$_{vol}$%	Volume content ratio
DIC	Digital image correlation
DMA	Dynamic mechanical analysis
DSC	Differential Scanning Calorimetry
TGA	Thermogravimetry analysis
FTIR	Fourier transformation infrared spectroscopy
SEM	Scanning electronic micropscope

TABLE OF CONTENTS

ABSTRACT i
ACKNOWLEDGEMENT iii
CONTRIBUTIONS TO THE THESIS v
MAIN ABBREVIATIONS 7
TABLE OF CONTENTS 9
LIST OF FIGURES 13
LIST OF TABLES 19
LIST OF FIGURES IN APPENDICES 21
LIST OF TABLES IN APPENDICES 21
Chapter 1. Introduction 1
1.1 Background 1
1.2 Literature gaps 3
1.3 Aims and objectives 5
1.4 Outline of the thesis 5
Chapter 2. Literature review 9
2.1 Polymer composite 9
2.2 Bio-composites 9
2.2.1 Bio-matrix based polymer composites 10
2.2.2 Natural fibre reinforced composites 12
2.2.3 Environmental impacts of bio-composites 15
2.3 Flax fibres and their composites 17
2.3.1 Origin of flax fibres 18
2.3.2 Properties of flax fibres 19
2.3.3 Development of surface treatment on flax fibres 22
2.3.4 Properties and characterization of flax polymeric composites 28
2.4 The fibre reinforcement mechanism in polymer composites 41
2.4.1 Prediction of stiffness: Elastic solution 42
2.4.2 Effects on the prediction of stiffness 43
2.5 Key findings of the literature review 46
Chapter 3. Influence of fibre configurations and surface treatments on properties of flax fibres 49
3.1 Introduction 49
3.2 Methodology 51
3.2.1 Materials 51
3.2.2 Characterisation and tests 52
3.3 Results and discussion 55
Part 1-effect of fibre configuration 55
3.3.1 Microscope on single fibre and fibre bundles 55
3.3.2 Tensile characterisation of fibre bundles and fibre fabric 57
Part 2-effect of fibre treatments 62

3.3.3 Effects of fibre pre-treatments on fibre compositions 62
3.3.4 Effects of surface treatments on fibre thermal properties 67
3.3.5 Effects of surface treatments on tension properties of fibres 71
3.4 Conclusions 73
Chapter 4. Influence of fibre configurations on properties of untreated flax/tannin composites 75
4.1 Introduction 75
4.2 Methodology 80
4.2.1 Materials 80
4.2.2 Cured resin preparation 80
4.2.3 Composite manufacturing (provided by ENSTIB) 80
4.2.4 Characterisation and tests 81
4.3 Results and discussion 84
4.3.1 Resin formation 84
4.3.2 DSC analysis of cured composites 85
4.3.3 Effects of configurations on dynamic mechanical properties 86
4.3.4 Effects of fibre configurations on tensile properties 89
4.3.5 Effects of fibre configurations on flexural properties 95
4.3.6 Effects of fibre configurations on impact properties 98
4.4 Conclusions 102
Chapter 5. Influence of surface treatments on properties of nonwoven flax mat/tannin composites 103
5.1 Introduction 103
5.2 Methodology 105
5.2.1 Materials 105
5.2.2 Aqueous resin preparation 106
5.2.3 Composite manufacturing 106
5.2.4 Characterisation and tests 107
5.3 Results and discussion 109
5.3.1 SEM investigations 109
5.3.2 Effect of fibre treatment on dynamic mechanical properties 111
5.3.3 Effect of treatments on tensile properties of flax/tannin 114
5.3.4 Effect of treatments on shear properties of flax/tannin 120
5.3.5 Effect of treatments on flexural properties of flax/tannin 123
5.3.6 Effect of treatments on impact properties of flax/tannin 125
5.3.7 Effects of treatments on water absorption of flax/tannin 130
5.4 Conclusions 134
Chapter 6. Influence of treatments on properties of hybrid flax/supersap bio-epoxy composites 135
6.1 Introduction 135
6.2 Methodology 137
6.2.1 Materials 137

6.2.2 Pure bio-resin formation 138
6.2.3 Preparation of composites (provided by MahyTec) 138
6.2.4 Characterisation and tests 139
6.3 Results and discussion 140
Part 1-mechanical properties 140
6.3.1 Effect of treatments on tensile properties of hybrid FE 140
6.3.2 Effect of treatments on shear properties of hybrid FE 144
6.3.3 Effect of treatments on flexural properties of hybrid FE 146
6.3.4 Effect of treatments on impact properties of hybrid FE 148
Part 2-environmental resistance 151
6.3.5 Differential Scanning Calorimetry (DSC) 151
6.3.6 Effect of treatments on thermal-mechanical properties 153
6.3.7 Effect of treatment on water absorption properties 157
6.3.8 Effect of treatment on UV and Xenon ageing properties 161
6.4 Conclusions 163
Chapter 7. Impact response of fully renewable bio-sandwiches based on flax bio-composites 165
7.1 Introduction 165
7.2 Methodology 168
7.2.1 Materials and fabrication of sandwich panels 168
7.2.2 Microscopy analysis 170
7.2.3 Compression analysis on foams 170
7.2.4 Falling weight impact testing 170
7.3 Results and discussion 171
7.3.1 Foam structure analysis 171
7.3.2 Compressive properties of bio-foams 173
7.3.3 Influence of foams and face sheets on impact response (3 m/s) 175
7.3.4 Influence of foams and face sheets on impact response (5 m/s) 180
7.3.5 Influence of foams and face sheets on impact response (7 m/s) 184
7.4 Conclusions 186
Chapter 8. Conclusions and future work 189
8.1 Conclusions of the thesis 189
8.2 Suggestions to the future work 191
REFERENCES 193
APPENDICES 227
Apendix 1. Statistical analysis 227
Apendix 2. Mechanical testing campaign 231
Apendix 3. Digital image correlation (DIC) 237
Apendix 4. Composite machining 241
Apendix 5. Procedure of bonding tensile specimens with tabs 251

LIST OF FIGURES

Figure 1. Current plant fibre composites for car applications [1; 7; 8]..... 2

Figure 2. Proposed superlight electric vehicle. 3

Figure 3. Current gaps found in literature for flax composites for vehicle applications..... 4

Figure 4. Classification of natural fibres according to origin [34]. 13

Figure 5. Environmental impact study of (a) under-door panels made of PP and glass fibres and flax fibres; (b) interior side panel made of ABS and hemp/epoxy [52]. 16

Figure 6. Composition and cross section of flax stems [63]. 18

Figure 7. Structure of a flax fibre [67]. 19

Figure 8. Schematic representation of failure mechanism of flax fibres. At 25 mm clamping length, elementary fibres slip over each other. At 3 mm, cracks have to run through the cross section of elementary fibres [67]. 20

Figure 9. Loop test for compression. The ratio c/a changes at failure point. 21

Figure 10. Grafting of silanols on flax fibre surface (redraw from Singha er al.[86])..... 24

Figure 11. Chemical structure of (a) APS and (b) BTCA. 24

Figure 12. The reaction between –OH groups of flax fibres and (a) methacrylic (b) propionic anhydrides [40]. 25

Figure 13. Moisture content of flax/PP composites as a function of time [108]. 30

Figure 14. Moisture versus mechanical properties: (a) stiffness; (b) strength [108]..... 31

Figure 15. Normalised young's modulus (modulus/modulus at time=0) versus normalised immersion time (test time/saturation time) [121]..... 32

Figure 16. SEM images of flax/epoxy composites: (a) origin specimen; (b) after 8 wet-dry cycles [130]. 33

Figure 17. Tensile properties of flax/PLA compared to flax/PP composites [131]. 34

Figure 18. Weave types: (A) plain; (B, C) two different twill; (D) Dobby [105]. . 36

Figure 19. The chemical structure of tannin: (a) hydrolysable; (b) condensed [140]..... 37

Figure 20. Decomposition of hexamine [144]. 38

Figure 21. Further reaction between tannin and hexamine [144]. 38

Figure 22. Interaction forces between two constituent atomic planes. 41

Figure 23. Elastic solution: (a) isostrain response; (b) isostress response. 42

Figure 24. Interface situations between matrix and fibres (same loading direction). 44

Figure 25. Representation of upper and lower limit modulus enhancement. 45

Figure 26. Dependence of Young's modulus, E(θ). 46

Figure 27. Flax fabrics (a) non-woven; (b) balanced fabric; (c) UD fabric. 51

Figure 28. Fibre fixed on a paper frame. 53

Figure 29. Experimental set-up of tensile tests on flax yarns (a) clamped paper frame; (b) side section of clamping jaws. 54

Figure 30. TGA equipment for thermal analysis. 55

Figure 31.SEM images of flax fibres (a) elementary flax; (b) flax bundles. 56

Figure 32. Typical optical images: (a) origin flax (UD); (b) post-analysed flax (UD); (c) optical origin flax (balance); (d) post-analysed flax (balance). 57

Figure 33. Typical stress-strain curves of tested flax bundles. 58

Figure 34. Dependence of gauge length on tensile properties (ref [155]). 59

Figure 35. Failed fibre bundle (balance): (a) front view; (b) side view. 60

Figure 36. Weibull plots of survival probability versus applied stress for UD and balance fibre bundles with the 40 mm and 75 mm clamping length. 61

Figure 37. Tensile deformation of the non-woven mat (from a to d). 62

Figure 38. FTIR spectra of unmodified and NaOH treated flax fibres. 64

Figure 39. FTIR spectra of unmodified and BTCA treated flax fibres. 65

Figure 40. FTIR spectra of unmodified and APS treated flax fibres. 66

Figure 41. FTIR spectra of unmodified and Laccase-Doga treated flax fibres. . 67

Figure 42. TGA curves of investigated flax fibres. 68

Figure 43. DTG curves of investigated flax fibres. 71

Figure 44. Load-displacement of representative non-woven flax mats with treatments. 72

Figure 45. Modulus of elasticity of flax/tannin composites during curing [10]. .. 76

Figure 46. Lay-up angles of individual fibre ply [102]. 77

Figure 47. (a) Illustrations of stacking sequence and (b)symmetric laminates. 77

Figure 48. DIC technique for tension (a) preparation of speckled samples; (b) DIC set-up; (c) evaluated gauge area. 82

Figure 49. Drop tower machine for impact tests (a) view of tower; (b) sample position. 84

Figure 50. Resin formation (a) glass mould type; (b) cured resin after removing mould; (c) cracked resin after a few hours. 84

Figure 51. DSC thermograms of flax/tannin composites (single run and dual run programme). 85

Figure 52. Variation of storage modulus of the flax/tannin composites. 87

Figure 53. Variation of loss modulus (E'') of flax/tannin composites. 88

Figure 54. Variation of tanδ of flax/tannin composites. 88

Figure 55. Typical micro-scale stress-strain curves obtained through DIC method. 90

Figure 56. Tension load-elongation curves (macro-scale) for flax/tannin composites. 92

Figure 57. Tested samples during tension (a) delamination; (b) fracture. 93

Figure 58. SEM micrographs of a cut non-fractured sample: (a) cross-section of the delaminated sample, (b) magnified graph. 93

Figure 59. SEM micrographs of tensile fractured composites: (a) fracture area; (b) fibre pull-out, (c) fibre breakage, (d) brittle failure of resin matrix. 94

Figure 60. Flexural strength and modulus of the nonwoven and woven flax composites. 96

Figure 61. Flexural load-displacement curves of the selected flax/tannin composites. 97

Figure 62. Flexural failure of composite samples during three point bending: (a) i- UD flax composite with no crack on the tension surface; ii-crack failure of nonwoven flax mat composite; (b) side section of non-woven composite without breaking into two piece; (c) the delamination of $[0, 90]_4$ composite after bending; (d) buckling of the layers away from each other (magnification of the delaminated $[0, 90]_4$ composite. 98

Figure 63. Impact force-displacement curves for different composites. 99

Figure 64. Examined samples after impact test: (a) Flax mat; (b) 100 %UD flax; (c) $[0, 90°]_4$; (d) $[0, +45°, 90°, -45°]_2$ 100

Figure 65. Speed-displacement curves for composite A and B. 100

Figure 66. 3D-time-force-energy for flax/tannin composites. 101

Figure 67. Impact energy for different composite types. 101

Figure 68. Overview of composites manufacturing (a) water content adjustment; (b) aluminium plate mould; (c) compression machine; (d) examples of composites. 107

Figure 69. Shear tests method and sample location with DIC method. 108

Figure 70. The SEM morphology of untreated single flax fibre. 109

Figure 71. SEM morphologies of treated flax fibres: (a) 5% NaOH treated; (b) BTCA treated; (c) APS treated; (d) LD treated. 110

Figure 72. Variation of storage modulus of flax/tannin composites with different treatments as a function of temperature. 112

Figure 73. Variation of loss modulus (a) and tanδ (b) as a function of temperature for flax/tannin composites with different treatments. 113

Figure 74. Tension properties of untreated and treated composites. 114

Figure 75. Example of computation of tensile failure initiation for flax/tannin. 117

Figure 76. Strain distribution and localisation of flax/tannin composite at 13 and 40 s. 119

Figure 77. Representative failure progress monitored by strain change for nonwoven flax mat/tannin composites. 120

Figure 78. Typical failure stages of tensile fracture for flax/tannin composites: (1) no-crack; (2) fibre orientation and crack initiation; (3) crack propagation; (4) failure. 120

Figure 79. Image analysis of shear strain at +45° and -45°. 121

Figure 80. Comparison of shear properties of flax/tannin composites with treatments. 121

Figure 81. Example of computation of shear failure initiation for flax/tannin composites. 122

Figure 82. Example of shear strain field up to failure for flax/tannin composites. 123

Figure 83. Waterfall description of impact force-displacement for flax/tannin composites with different treatments. 126

Figure 84. Speed change as a function of time during impact tests. 127

Figure 85. 3D description of time-force-energy for flax/tannin composites. 128

Figure 86. Average moisture uptake of flax composites at 100% of relative humidity. 131

Figure 87. Thickness swelling of flax composites at 100% of relative humidity. 133

Figure 88. (a) Composites plates; (b) Machined specimens for testing..... 138

Figure 89. Tensile strength and modulus of hybrid FE composites. 140

Figure 90. Stress-strain curves of hybrid FE composites. 141

Figure 91. SEM micrographs of cross-sectional area of neat composites. 142

Figure 92. SEM images of fracture surface of composites with treatments. ... 143

Figure 93. Failure progress of LD specimens: (a) crack occurring; (b) crack occurring; (c) Shear strain distribution at failure. 145

Figure 94. Failure progress of BTCA specimens:(a) upper notch failure; (b) crack propagation and lower notch failure; (c) shear strain distribution at failure. 145

Figure 95. Flexural properties of hybrid FE composites. 146

Figure 96. Stress-strain curves for representative FE composites during bending. 147

Figure 97. Force versus displacement of FE composites under impact. 148

Figure 98. Damage of hybrid FE composites (a) typical damage (b) the worst case. 149

Figure 99. 3D curves of force-time-energy of FE composites..... 150

Figure 100. DSC curves of pure epoxy and flax/supersap composites. 151

Figure 101. DSC curves after baseline subtraction for further comparison. ... 152

Figure 102. Variation of storage modulus of resin and FE composites. 153

Figure 103. Effect of treatments on loss modulus of resin and FE composites. 154

Figure 104. Effect of treatments on tan δ of resin and FE composites. 156

Figure 105. Water content versus time root of FE composites. 159

Figure 106. Thickness swelling behaviour of FE composites. 160

Figure 107. Surface change by water immersion (a) before; (b) after. 161

Figure 108. Flax/supersap bio-epoxy composites samples with and without treatments after ageing condition: (a) UV radiation for 552 h; (b) Xenon light for 500h. 162

Figure 109. (a) Schematic drawing of a sandwich plate and (b) Aptera electric car. 165

Figure 110. Sandwich preparation (a) bonding; (b) clamping (c) final sandwich. 169

Figure 111. Drop tower impact test co-operated with high speed camera. 171

Figure 112. Test surface of the bio-foams based on the 3D directions. 172

Figure 113. Cell structure of PLA (left column) and bio-PS foam (right column) through SEM investigation at three planes. 173

Figure 114. Compression load-deflection curves for bio-foams..... 174

Figure 115. Comparison of load and speed vs displacement plotted for three different bio- sandwiches (3 m/s). 175

Figure 116. Comparison of damage area on the top skin surface of sandwiches. 177

Figure 117. Load and energy versus time plots for bio-sandwiches impacted at 3 m/s. 178

Figure 118. Impact response moment of FT/PLA sandwiches at 3 m/s. 179

Figure 119. Impact response moment of FT/bio-PS sandwiches at 3 m/s. 179

Figure 120. Impact response moment of FE/bio-PS sandwiches at 3 m/s. 180

Figure 121. Load and speed versus displacement response at 5 m/s. 181

Figure 122. Load and energy versus time plots for bio-sandwiches impacted at 5 m/s. 182

Figure 123. Back sheet of FT/bio-PS sandwiches after impacting at different velocity. 182

Figure 124. Impact response moment of FT/PLA sandwiches at 5 m/s. 183

Figure 125. Impact response moment of FT/bio-PS sandwiches at 5 m/s. 183

Figure 126. Impact response moment of FE/bio-PS sandwiches at 5 m/s. 183

Figure 127. Load and speed versus displacement of sandwiches impacted at 7 m/s. 184

Figure 128. Impact response moment of FT/PLA sandwiches at 7 m/s. 185

Figure 129. Impact response moment of FT/bio-PS sandwiches at 7 m/s. 185

Figure 130. Impact response moment of FE/bio-PS sandwiches at 7 m/s. 186

Figure 131. Load and energy versus time of sandwiches impacted at 7 m/s. 186

Figure 132. Literature comparison of tensile properties for natural composites (fibre content in weight fraction). 189

LIST OF TABLES

Table 1. Information of selected bio-polymers as composite matrix [3; 24; 25]. 11

Table 2. Repeat units of common bio-degradable aliphatic polyesters [3]. 12

Table 3. Chemical composition of the cell wall in different plant fibres [33]. 13

Table 4. Typical properties of some bast fibres compared to E-glass [38]. 14

Table 5. Tensile properties of glass and flax fibres [67]. 21

Table 6. Different treatments of flax-reinforced composites. 23

Table 7. Testing data of mechanical properties of flax reinforced composites. 29

Table 8. Physical properties of studied flax fibres. 51

Table 9. Diameter of studied flax fibres. 56

Table 10. Tensile properties for flax fabrics. 62

Table 11. Infrared band characteristics for neat flax fibres. 63

Table 12. Summary of TGA results for treated and untreated flax fibres. 69

Table 13. Effect of treatments on tension properties of non-woven flax mats .. 72

Table 14. Flax/tannin composites with different fibre configurations. 80

Table 15. Summary of DMA results of flax/tannin composites. 86

Table 16. Tensile properties of flax/tannin composites. 90

Table 17. Untreated and treated non-woven flax mat tannin composites. 105

Table 18. Dynamic mechanical properties of flax/tannin composites. 112

Table 19. Flexural properties of untreated and treated flax/tannin composites. 124

Table 20. Computed ‘flexural failure initiation strength’ of flax/tannin. 125

Table 21. Impact characteristics of flax/tannin composites. 126

Table 22. Water absorption properties of flax/tannin composites with surface treatments. 132

Table 23. Examples of mechanical properties of flax-thermoset composites. 135

Table 24. Qualitative evaluation of constituents for composites manufacturing. 137

Table 25. The hybrid flax reinforced bio-epoxy composites with treatments. . 138

Table 26. Shear properties of hybrid FE composites with treatments. 144

Table 27. Energy-absorbing characteristics of FE composites for impact tests. 149

Table 28. Flexural and storage modulus of FE composites. 154

Table 29. Thermal-mechanical properties of untreated and treated composites. 155

Table 30. Summarised water absorption properties of FE composites with and without treatments. 158

Table 31. Tension properties of hybrid flax/supersap bio-epoxy composites with different treatments in weathering conditions. 162

Table 32. Property comparison between PLA bio-foam and EPS [240-242]. . 168

Table 33. Prepared bio-sandwich structures for characterisation 169

Table 34. Morphology properties of PLA and bio-PS polymer foams. 172

Table 35. Compressive properties of bio-foams. 175

Table 36. Average impact parameters for sandwich samples impacted at 3, 5 and 7 m/s. 176

Table 37. Other properties of the novel flax composites compared to literature. 190

LIST OF FIGURES IN APPENDICES

Figure 2-1. (a) Sample geometry, (b) Drawing and dimensions, (c) Assembly of the samples with the pads for the tensile tests. 232

Figure 2-2. (a) Sample geometry, (b) Drawing and dimensions, (c) Assembly of the samples in the testing fixture for the shear tests. 233

Figure 2-3. (a) Sample geometry, (b) Drawing and dimensions for the 3-point bending tests. 234

Figure 2-4. (a) Sample geometry, (b) Drawing and dimensions. 235

Figure 3-1. Image correlation of facets. 237

Figure 3-2. 2D in-plane deformation. 238

Figure 4-1. The CNC machine for composite machining. 241

Figure 4-2. The drawing pattern designed by Draftsight. 241

Figure 4-3. Optimised tooling path and machining parameters. 242

Figure 4-4. Simulation of g-code by cut viewer 249

Figure 5-1. Preparation of (a) tab abrasion and (b) specimen abrasion. 251

Figure 5-2. Adhesive tab bonding procedure on tensile specimens. 252

LIST OF TABLES IN APPENDICES

Table 1-1. Weibull calculations for flax bundle (UD) at 40 mm gauge. 229

Table 1-2. Weibull calculations for flax bundle (Balance) at 40 mm gauge. ... 229

Table 1-3. Weibull calculations for flax bundle (UD) at 75 mm gauge. 230

Table 1-4. Weibull calculations for flax bundle (Balance) at 75 mm gauge. ... 230

Table 2-1. Quasi-static mechanical tests. 231

Table 2-2. Dynamic mechanical tests. 231

Chapter 1. Introduction

1.1 Background

To date, crude oil-derived composites (glass/PP, glass/epoxy etc.) have been commercially used to produce lightweight parts, such as doors, panels, chassis pillars etc., for vehicles and other transports [1; 2]. However the concerns on the disposal issues after the service-life have always existed with the development of composites technology. The interest towards new renewable raw material based composites has been increasing very fast, which is mainly due to the increasing environmental awareness (e.g. increased pollution, increasing demand for biodegradable materials, material need for CO_2 neutrality and low greenhouse gas emissions, new environmental laws and regulations) and innovations offering new opportunities (new enhanced materials, employment etc.) [3]. One of the important achievements as a viable alternative to common composites is the investigation and usage of 'green composites', providing the unusual biodegradability characteristics. The production cost, processing flexibility, mechanical properties and environmental resistance, together with the material recyclability are the crucial factors for car manufacturers to consider the use of bio-composites [4]. Due to the limited crude oil in the earth (only for 45 to 60 years maximum) and the rapid price increase (over $100 per barrel at 2015), bio-fibre based composites have been paid more and more attention [4].

A bio-composite normally is referred to a composite material which has at least one of the components (matrix and fibres) derived from renewable resources. The bio-fibres could be either natural fibres from a natural origin like plants or the fibres during industry recycling production. Composites from natural fibres and oil-derived polymer matrices, such as flax/PP (interior door panels, instrument panels, insulation hood), kenaf/PP (seat back boards) and flax/synthetic PLA (seat for F1), are well known [5; 6]. Figure 1 shows the existing use of natural fibre composites in vehicle exterior and interior applications. However, for similar applications, composites using natural matrices have not been developed nor commercialised to the same extent. This

is due to the difficulty in finding matrices of natural origin capable of imparting the required performance to the composites.

Figure 1. Current plant fibre composites for car applications [1; 7; 8].

The new environment regulations of the governments and authorities have spurred effort for the manufactures and scientists to develop novel bio-materials. For example, European end of life vehicle directive states that by 2015 vehicles must be constructed of 95% recyclable materials with 85% recoverable through reuse or mechanical recycling and 10% through energy recovery or thermal recycling. Hence the EU FP 7 project lauched ECOSHELL named ‘Development of new light high-performance environmentally benign composites made of bio-materials and bio-resins for electric car application’. ECOSHELL aims to develop the structural and non-structural components, for electric superlight cars (see Figure 2). The superlight electric vehicles made by composites have a possibility to be acceptable due to the competitive price and energy consumption. The sponsored PhD research was part of ECOSHEEL project and mainly focused on the novel bio-composites innovation and development.

Figure 2. Proposed superlight electric vehicle.

1.2 Literature gaps

Of all the natural fibre reinforcements, flax fibre is commonly selected for bio-composite investigation, due to their extraordinary mechanical properties (e.g. 1.5 times of tensile strength to hemp fibres) and good anti fungus property [9]. In addition, its specific E-modulus is comparable to E-glass fibre, let alone other advantages, such as environmental benefits and low cost. Therefore, flax fibres in particular can be combined with suitable matrix materials to impart desirable characteristics such as reduced final cost and good load bearing properties.

Tannin resins used as wood panel adhesives (less than 10 $_{wt}$%) can be expected to impart as high content bio-matrix in bio-composites reinforced by natural fibres. Tannins are non-toxic natural products and therefore more environmentally friendly than the synthetic (polluting) materials. The technologies for tannin auto-condensation and hexamine hardening are ready for industrial use. The use of hexamine as a hardener for a tannin is a very environmentally-friendly proposition without formaldehyde emmission. A pioneering research work by Pizzi et al. [10] very recently studied the mimosa tannin/non-woven flax fibre mat composites. Very serious industrial interest exists in the products, always with an eye on the environmental acceptability and also on the economic and technical viability.

Epoxies usually provide excellent chemical, high temperature resistance and good electric insulating properties, as well as their good mechanical performances when a thermosetting epoxide polymer cures with a catalyzing

agent or "hardener". A range of bio-epoxy resins are extracted from epoxidised vegetables oils (EVOs) like pine oil waste and soya oil. Excellent inexpensive bio-epoxy based composites could be made using natural fibres such as hemp, straw, flax and wood etc. However, most of the work has done only for low-fibre-content (below 50 $_{wt}$%) composites based on soy bean oil-derived epoxy [11-15].

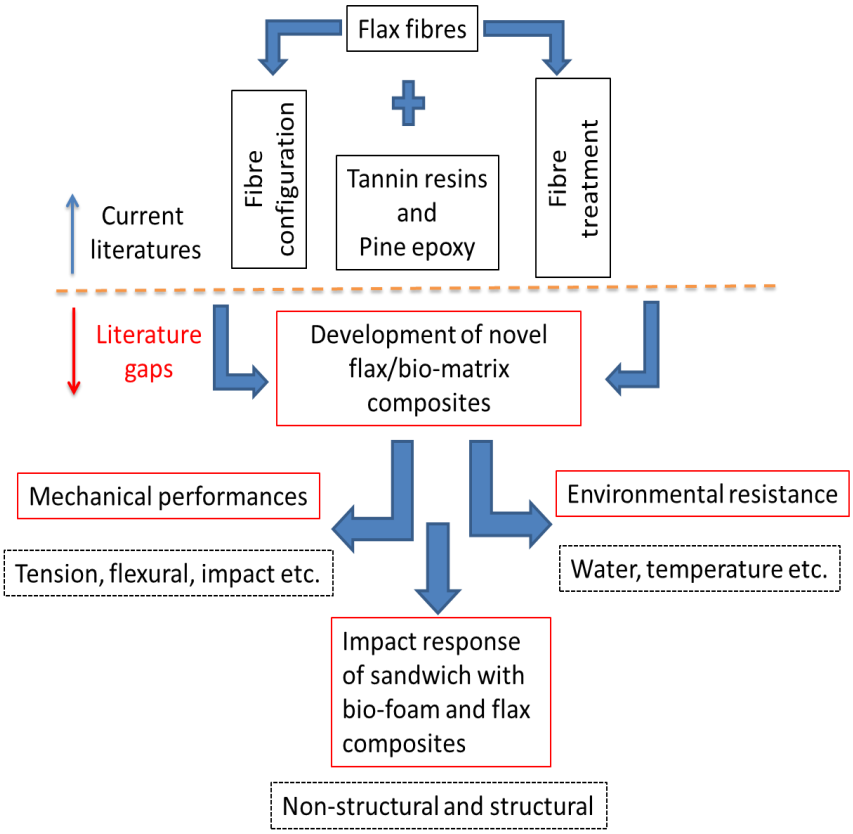

Figure 3. Current gaps found in literature for flax composites for vehicle applications.

At present, no technical data on pine-oil derived epoxy and tannin based flax reinforced composites with high fibre content has been reported yet, which has resulted in their limited uptake by the engineering society in vehicle applications. There is also lack of studies on the influence of flax textile change, including fibre configuration and treatments, on properties of these novel composites. The specific knowledge gaps on flax composites are summarised in Figure 3. The use of renewable matrix material (natural phenolic (tannin) and pine oil-derived epoxy resin) in flax composite could develop ecologically sustainable technologies by using less crude-oil in order to gain fully bio-

resourced composites. Bio-sandwiches based on the flax composites ideally will offer good energy absorption, more weight savings, as well as environmental advantages. This study will try to fill this gap by establishing a knowledgebase for flax reinforced tannin and innovative bio-epoxy composites for various loading and environmental conditions, enabling engineers to use these composites in vehicle interior (seats, pedals, dashboards, expansion tanks etc.) or exterior applications (fenders, wipers, grills, chassis pillars etc.).

1.3 Aims and objectives

This project is carried out to study and assess the feasibility of the fully renewable flax composites using mimosa tannin and supersap pine-oil derived epoxy for potential vehicle applications. The main objectives are:

- To investigate the effects of fibre configuration and treatments on properties (tensile, chemical and thermal) of flax fibres.
- To investigate the effects of fibre configuration on mechanical (e.g. tensile, flexural, shear, impact etc.) properties of flax/tannin
- To investigate the effects of fibre treatments on properties of non-woven flax/tannin composites.
- To investigate the effects of fibre treatments on properties and environmental resistance of flax/supersap bio-epoxy composites with optimised fibre configuration
- To systematically study the low energy impact response of fully bio-sandwiches (flax composites as skins and bio-foams as core).

1.4 Outline of the thesis

Chapter 1 gives the relevant background of this study, the defined literature gaps, thesis aims, objectives and plans. The interesting point is on the structure-property relationship of the novel flax/bio-matrix composites to be potentially used in automotive industries.

Chapter 2 provides a literature review by detailing the current state-of-the art of green composites based on natural fibres like flax fibres. The existing work and knowledge are presented to obtain the key information regarding on properties

of flax fibre composites based on different matrices. The gap and advantages for using bio-polymers (tannin and bio-epoxy) as matrix is well defined. An insight to the current work in development of flax reinforced polymer composites is also given. Finally, key findings of the literature are drawn.

Chapter 3 assesses the mechanical and physical properties of flax fibres by adjusting fibre configurations (non-woven and woven) and surface chemical treatments. This builds the base information to predict and understand the performances of resulted flax/bio-matrix (tannin and supersap bio-epoxy) composites through the different development approaches.

Chapter 4 investigates the influence of fibre configurations on properties of flax/tannin composites. Mainly dynamic (DMA-dynamic mechanical analysis and impact) and static mechanical properties (tensile and flexural etc.) were obtained. This study inspects the consequences of using four fibre configurations that can be tailored to improve mechanical properties.

Chapter 5 exams the influence of chemical treatments on properties of nonwoven flax/tannin composites. Except mechanical tests, the water absorption measurement of the composites upon the fibre treatments was also carried out. This study emphasises the selection of suitable surface treatments for performance improvement of flax/tannin composite.

Chapter 6 investigates the properties of flax/supersap bio-epoxy composites using a hybrid fibre configuration along with the different four surface treatments. Studies were performed to point out the effect of fibre treatments on mechanical properties and environmental resistance (moisture and light ageing) of flax/supersap bio-epoxy composites.

Chapter 7 analyses the impact response of bio-sandwich structures made of these novel flax composites and commercial bio-foams (biodegradable polystyrene and poly-lactic acid foam). Falling weight impact testing was performed at the velocity from low to relative high. This chapter looks at the energy absorption and damage resistance of renewable sandwich composites for potential applications under impact loading.

Chapter 8 makes conclusions of the research work, summarising the obtained engineering database of flax/tannin and flax/supersap composites in terms of their structure-property relationships. Future material and product development are also suggested.

Chapter 2. Literature review

2.1 Polymer composite

Composites consist of two materials or phases, together offering a combination of properties and applications [16; 17]. The increasing interest of polymer matrix composites (PMC) is due to the combination of low cost and improved properties. Fibres are generally utilised to incorporate in the polymer matrix so as to provide increased strength and stiffness. Fibres used for reinforcement are commonly used in two forms: short fibres and long (continuous) fibres. Short fibres (1cm or less), called staples, are often incorporated randomly in the composites. The long and continuous fibres are placed into prepregs, which comprise of layers of fibre mats or fabrics in the un-polymerized resins.

Thermosets are highly cross-linked polymers which do not soften at elevated temperature. Epoxy resins, vinyl Ester, polyesters, novolac and polyamide are widely produced as polymer matrices. With the concern of better processing feasibility (e.g. low cure temperature), unsaturated polyesters reinforced by a wide range of cellulosic fibres have been investigated in the industry [18].

The significant advantage of thermoplastics compared to thermosets is their softening behaviour without chemical transformation when heated. However, the high viscosity in molten thermoplastics makes the process difficult and reduces the contact between the fibres and matrix [18; 19]. It is therefore very important to lower the processing viscosity to avoid damage to fibres, on account of the strong shear stresses. Commercial thermoplastic matrix materials are mainly produced by the injection moulding of pre-compounded molten materials containing matrix and short fibres (e.g. glass-filled nylon) [19].

2.2 Bio-composites

Considering the increasing price of oil and oiled-derived products together with the after-service environmental pollutions, bio-composites have attracted growing interest and been developing for quite some time now [20; 21]. Natural fibres are employed in plastics due to their good mechanical properties, which

can compete with glass fibre but are lighter than glass fibre. They also give nice 'natural' look, warmth and grip to composites and not to speak of reduced environmental impact. The above characteristics of bio-composites make them very attractive for bio-degradable packaging uses and automotive components from compress moulding.

Both bio-polymers and synthetic polymers are acceptable as matrix for natural fibre-reinforced composites, offering environmental benefits. However, the idea matrix for natural composites is 100% bio-resourced material (e.g. bio-epoxy resins, polylactic-acid-based resins, bio-polyester resins) derived from soybean oil, epoxidised pine oil waste, castor oil, cellulose and proteins etc. [3]. Unlike the commercial synthetic matrix materials, bio-matrices from the renewable resources develop sustainable technologies by using less crude-oil. The current manufactures also employ the mixed matrix containing various bio-based content and have produced some commercial goods, such as ENVIREZ-1807 (Bio 18 $_{wt}$%) from Ashland, EpoBioX^{TM} (Bio 50-90 $_{wt}$%) from Anroy Europe Oy, ENVIROLITETM (Bio25 $_{wt}$%) from Reinchhold, Palapre ECO P 55-01(Bio 55 $_{wt}$%) from DSM and other bio-resins.

Bio-polymers also provide good bio-degradability for the sake of ease recycling. Except change in chemical structures, chemical reactions during polymer degradation also change the physical properties caused by the external stresses, which are related to the breakdown of polymer molecular bonds [22]. The typical polymer degradation could be caused by chemical deteriogens (e.g. oxygen, humidity, nitrogen oxides, ozone) and physical stresses (e.g. heat, mechanical forces, radiation and ablation). Biodegradation is an irreversible process and similar to normal polymer degradation. Bond scissions on the molecule backbone for bio-degradation could be induced by the influence of some living organisms [23].

2.2.1 Bio-matrix based polymer composites

The term 'bio-matrix' means that the composite matrix is partly or wholly biodegradable. According to their biodegradation, a solution of waste-disposal problems of petroleum-derived plastics is offered by enlarging the market for

bio-polymers. These polymers are classified by scientists into three types: biosynthetic, semi-biosynthetic, and chemosynthetic biopolymers [3]. They can be both thermoplastics and thermosets. Biosynthetic polymers are almost fully biodegradable within a time scale because of their origin of renewable sources. The presence of natural occurring chemical bonds in semi-biosynthetic and chemosynthetic biopolymers also provides good bio-degradability. The plant oils (e.g. pinel oil, castor oil), proteins, polysaccharides (starch and cellulose), even petroleum-based raw materials, can be used to extract or synthesis bio-polymer. In Table 1, some commercial bio-based thermosets are presented with their applications.

Table 1. Information of selected bio-polymers as composite matrix [3; 24; 25].

Bio-matrix	bio (%)	Origin	Applications
Unsaturated polyester	18	Soybean oil	e.g. tractor panels
Natural phenols	50-90	Pine oil waste	Kayaks, boats
Unsaturated polyester	55	-	SMC applications
Furfuryl alcohol resin	100	Biomass	Varied applications
Unsaturated polyestes	25	-	SMC/pultrusion

* SMC-sheet moulding compound

Bio-epoxy resins are extracted from natural sources which could mainly be the epoxidised vegetables oils (EVOs) like pine oil waste and soya oil. Waste streams of industry processes could also produce bio-epoxy resins [26]. Sorbitol and glycerol, respectively derived from corn starch and triglyceride vegetable oil, are the most known bio-epoxy types. They are basically bio-based aliphatic polyols with inexpensive cost for usage in textile and paper processing agents, and reactive diluents etc. For example, glycerol polyglycidyl ether (GPE) and polyglycerol polyglycidyl ether (PGPE) epoxies have been already industrial commercially [24]. Takada et al. [27] investigated the use of glycerol-epoxy bio-resins for the production of composites. They reported that due to their good mechanical properties, outstanding heat resistance and environmental advantages, glycerol-epoxy resins are expected to replace petroleum-based polymers for composite manufacturing in vehicle industries.

Aliphatic polyesters are also widely used for bio-composites. Based on the mode of bonding of constituent monomers, chemically there are two groups: polyhydroxyalkanoates (only one repeating unit of O-R-COO) and poly (alkylene dicarboxylate) from the condensation polymerisation of diols and dicarboxylic acids. The chemical structures of some typical biodegradable aliphatic polyester are shown in Table 2. Poly(lactic acid), PLA, is a crystalline polymer with high melting point, has been increasingly studied for a variety of applications, such as containers, automotive, trays, film and other packaging and assembly. PLA can not only be degraded by microorganisms or enzymes but can also undergo hydrolytic degradation. It is often blended with fibres, and natural additives to inhibit degradability, reduce brittleness.

Table 2. Repeat units of common bio-degradable aliphatic polyesters [3].

Chemical structure	**Examples**
$(O\text{-}CHR\text{-}CO)_n$	R=H, Poly (glycolic acid), PGA
Poly(α-hydroxy acid)	$R=CH_3$, Poly(l-lactic acid), PLLA
$(O\text{-}CHR\text{-}CH_2\text{-}CO)_n$	$R=CH_3$, Poly(β-hydroxybutyrate), PHB
Poly(β-hydroxyalkanoate)	$R=CH_3$, C_2H_5, Poly(β-hydroxybutyrate-co-valerate), PHVB
$[O\text{-}(CH_2)_x\text{-}CO]_n$	x=5, Poly(ε-carolactone), PCL
Poly(w- hydroxyalkanoate)	
	x=2, y=2, Poly(ethylene succinate), PES
$[O\text{--}(CH_2)_x\text{-}O\text{-}CO\text{--}(CH_2)_y\text{-}CO]_n$	x=4, y=2, Poly(butylene succinate), PBS
Poly(alkylene dicarboxylate)	x=4, y=4, Poly(butylene succinate-co-butylene adipate), PBSA

2.2.2 Natural fibre reinforced composites

Natural fibres are divided into the groups of animal (wool and silk), mineral (asbestos) and plant/vegetable (bast, leaf, seed, wood, and grasses) [28-30] as shown in Figure 4. Yu and his coworkers [31], Saheb and Jog [32], and Holbery

and Houston [33] have reviewed natural fibre composites with their advantages, classifications, properties and potential applications. The common natural fibres used for composites include cotton (seed hairs), wheat, wood, flax (bast), hemp (bast) and sisal (leaf), chemical compositions of which are shown in Table 3.

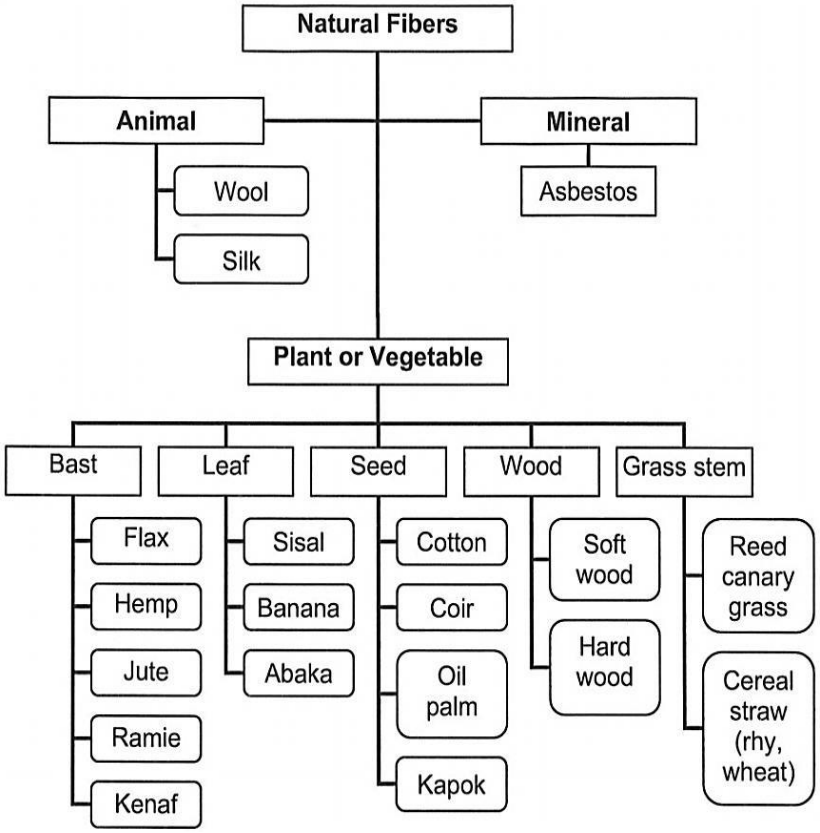

Figure 4. Classification of natural fibres according to origin [34].

Table 3. Chemical composition of the cell wall in different plant fibres [33].

Plant	Fibre type	Cell wall chemical composition ($_{wt}$%)		
		Cellulose	Hemisellulose	Lignin
Hemp	bast	70.2-74.4	17.9-22.4	3.7-5.7
Flax	bast	71	18.6-20.6	2.2
Sisal	leaf	43-62	21-24	7-9
Cotton	seed	85-96	1-3	0.7-1.6

The development of bast fibres and their composites has been reviewed by Summerscales et al. [35], Anandjiwala and Blouw [36], and Cao et al. [37]. Bast fibres obtained from the outer cell layers of the plant stems have a high young's

modulus up to 70 GPa. Table 4 shows the property comparison within some typical bast fibres and E-glass fibres. The mechanical merits (e.g. modulus/density) together with their biodegradability make bast fibres a viable option as reinforcements for composites.

Table 4. Typical properties of some bast fibres compared to E-glass [38].

Fibres	Density (kg/m^3)	E-modulus (GPa)	Tensile strength (MPa)	Elongation at break (%)
E-glass	2550	71	3400	3.4
Flax	1530	58±15	1339±486	3.27±0.4
Hemp	1520	70	920	1.7
Jute	1520	60	860	2
Kenaf	1193	14-38	240-600	-

Flax fibre, a kind of bast fibres, is extracted from the skin of the stem of the flax plants abundantly from west Europe. The high cellulose content in flax fibres together with the low microfibril angle result in a high tensile strength of fibres up to 1000 MPa [39; 40]. The outstanding specific mechanical properties (tensile strength and modulus/weight), cost and the planting origin area make them one of the mostly investigated green fibres in Europe for bio-composite applications. Wambua et al. [41] reported that flax/HDPE (ultrahigh molecular weight polyethylene) showed better ability to absorb ballistic impact energy than hemp and jute composites. The mechanical properties of flax reinforced composites are highly influenced by three factors: properties of fibres and matrix, and the interfacial adhesion properties [42]. The main problem associated with the use of biofibres as reinforcements in thermoplastics are the incompatibility between hydrophilic natural fibres and hydrophobic synthetic polymers, resulting in weak bonding on the fibre/matrix surface. It was observed that the melting point of HDPE and LLDPE (linear low density polyethylene) increased after adding flax fibres with surface treatments [43]. The fibre/matrix interfacial shear stress was found to improve in flax/PP composites by treating flax fibres with MAA-PP (maleic acid anhydride modified polypropylene) [44]. Tensile and flexural strengths of flax/PP composites were found to increase with

increasing degree of acetylation up to 18% and then decreased [45]. It was found that mercerization of flax fibres improved the mechanical properties of polystyrene composites reinforced with chemically treated flax fibres [46].

The development and use of natural fibre composites is to some extent limited by issues like [32; 47-50].: (1) the thermal degradation of natural fibres can decrease the mechanical properties (toughness and bending strength), resulting in poor organoleptic properties (odour and colour) and possible production of volatiles at processing time over 200°C; (2) high moisture content of natural fibres, especially for cellulosic fibres, can lead to poor dimensional stability and process-ability, and porous issues; (3) composites exposed to the environment may bio-degrade; (4) dispersion of natural fibres affected by the strong inter-fibre bonding; (5) incompatibility between hydrophobic polymer matrix and hydrophilic natural fibres.

2.2.3 Environmental impacts of bio-composites

The driving force for using bio-composites like natural fibre composites as substitution of synthetic polymers is their superiority in environmental impacts. Life cycle assessment (LCA) has been widely adopted nowadays to compare and quantify the environmental impact of bio-based products and their oil-derived counterparts. The LCA studies show great environmental benefits contributed by using bio-composites, which will be discussed in following paragraphs.

Comparing to synthetic polymers, bio-polymers show lower production energy related to material use [51]. As an example, starch polymer pellets require lower production energy up to 75 % than polyethylene. 20% to 80% greenhouse gas emissions (GHG) also are reduced. The large value range is due to the different starch/copolymer blends, different polyethylene references and different waste treatment methods [52-57]. In the case of PLA (polylactic acid) energy requirements for cradle-to-factory gate are in the range of 20 % to 30% below those for polyolefin materials, and greenhouse emissions are up to 25 % lower. The cradle-to-factory gate energy requirements for PHA (polyhydroxyalkanoates) are about 66 GJ/t, which is about 10-20% lower,

compared to polyethylene [58]. Epoxidised linseed oil has been found to be very attractive due to the super-high production energy savings and GHG emissions reduction (90 %).

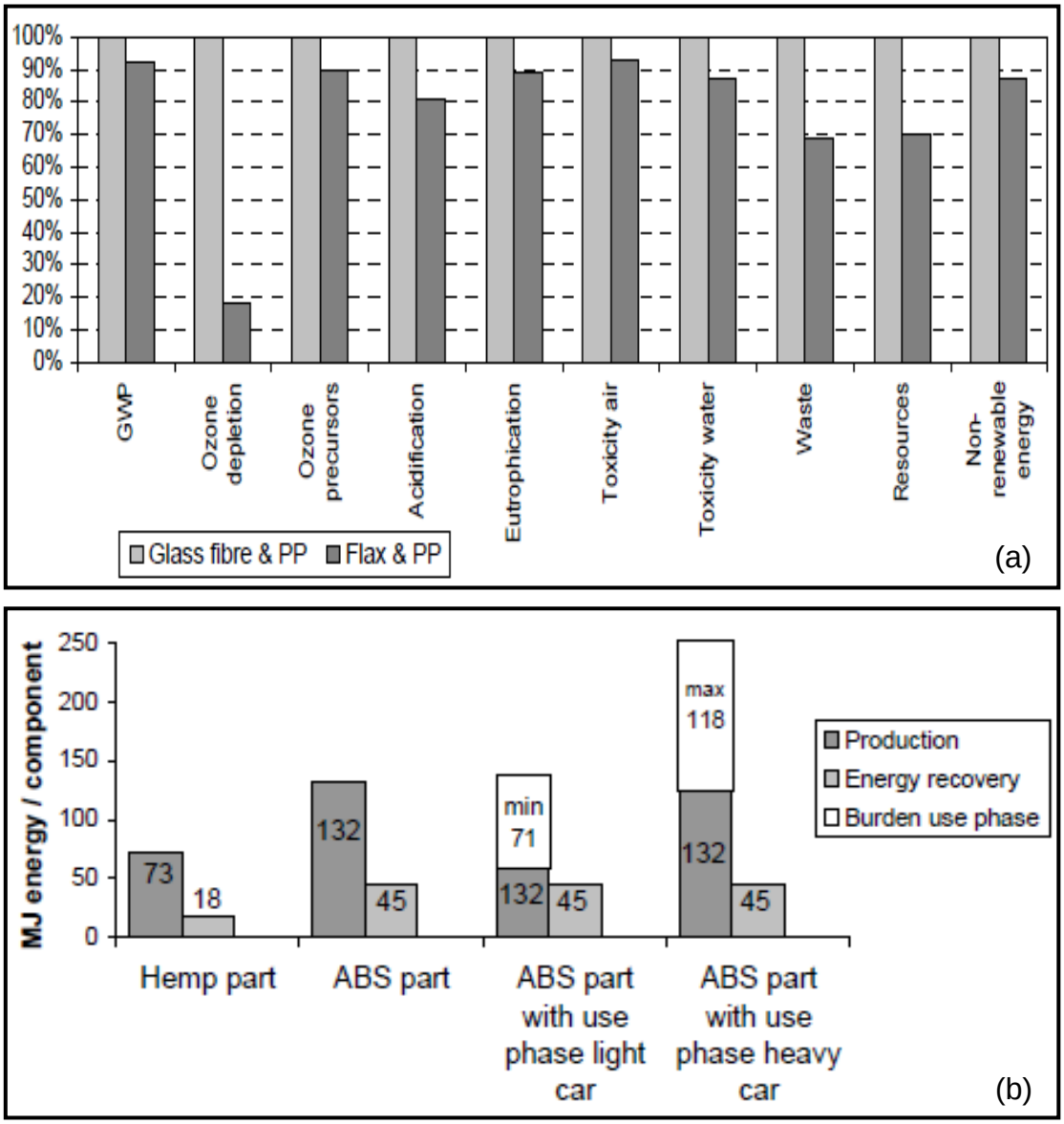

Figure 5. Environmental impact study of (a) under-door panels made of PP and glass fibres and flax fibres; (b) interior side panel made of ABS and hemp/epoxy [52].

Using natural fibres as composite reinforcement could also give considerable energy and GHG savings [52; 59; 60]. About 80% energy is saved by replacing glass fibre mats with flax fibre mats [52; 61]. Diener and Siehler [62] carried out life cycle assessment (LCA) for the under-floor panels for a Mercedes A class

car (Figure 5). The panel was initially manufactured by glass fibre reinforced PP (polypropylene) composites to protect car chassis and improve aerodynamics. Flax fibre/PP composite-made panel was also studied concerning on the technical demands for this panel application. The results of the flax/PP panel not only passed the mechanical and thermal testing, but also indicated better environmental impacts than the glass fibre/PP panel (as shown Figure 5 (a)). About 14 % energy for the under-door panel was saved. Focusing on the interior side panel, Wötzel et al. [59] studied the possibility of using bio-composites through LCA testing (as seen in Figure 5 (b)). The side panel was made in one case from acrylonitrile-butadiene-styrene (ABS) by injection moulding and in the other from epoxy (34 $_{vol}$%) composites reinforced with hemp fibres (66 $_{vol}$%) through compression moulding. The weight of the interior panel was 1125 g for ABS and 820 g for hemp/epoxy. The substitution of hemp/epoxy composites saves non-renewable energy about 30-45%, and GHG emissions of 13 %.

Corbière-Nicollier et al. [60] investigated the environmental impacts of two polymer pallets. One is glass fibre (42 $_{wt}$%)/PP pallet (GF) with weight of 15 kg, the other is china reed (53 $_{wt}$%)/PP pallet (CR) which is 3.2 kg lighter. Although they have the same expected life time of 5 years, the poor bio-fibre/matrix interface property still needs further R&D development. Better scores of the environmental impacts (eight sub-sectors) and fuel savings were found for the CR pallet than the GF pallet through LCA (life cycle assessment). For a distance of 5000 km, the saving amount is about 660 MJ, which achieves about 90% of the production energy for manufacturing a new CR pallet. Assuming a transport distance of 200000 km, over three times of the non-renewable energy (2300 MJ) is saved to produce a CR pallet.

2.3 Flax fibres and their composites

This section focusses mainly on composites reinforced by flax fibres from plants. As stated, many reasons, such as oil-use capacity, government environment legislation as well as sustainability, have resulted in the increased emphasis on natural fibre composites [63-65]. Flax fibres are perceived to meet

most of these requirements and have extra advantages (e.g. specific modulus-modulus to weight ratio, safer working conditions, low machine wear, heath advantages, recyclability etc.) over established synthetic fibres [66-68]. It is inevitable that the inherent detriments of flax, including moisture adsorption and incompatibility with some polymeric system due to its high hydrophilicity, bring lots of challenges in their composite design and applications.

2.3.1 Origin of flax fibres

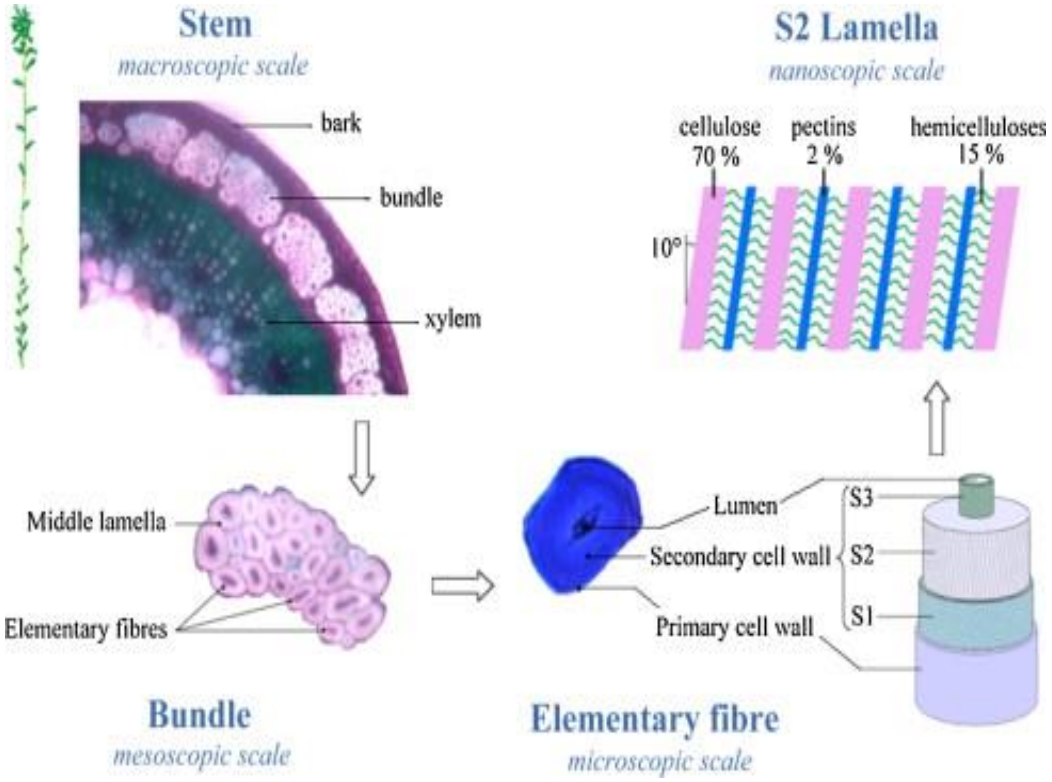

Figure 6. Composition and cross section of flax stems [63].

Naturally flax is from flax plant, one species of Linum usitatissimum bred, and is widely cultivated in West Europe where the daily temperature is generally below 30°C [63]. The flax plant has a life cycle of 90 to 125 days including vegetative, flowering and maturation period. The diameter of flax stem is in the range of 1 to 2 mm, with the height about 80 cm. It can be seen from Figure 6 that there are three layers—bark, bundle and xylem in the flax stem. The outer layer of bark functions as a protect cover from the external attacks except the penetration of water and other nutrients [63].

During the fibre processing, the bark, together with xylem is removed, to leave fibre bundles consisting of elementary fibres as shown in Figure 6. Technical fibres are extracted by partially separating the fibre bundles in the flax plant and can be as long as the stem length (approximately 1 m). Unlike the technical fibres, the length of elementary fibres varies between 2 and 5 cm, and the diameter is about 19 to 25 µm. The polyhedron shapes (5 to 7 sides) help pack the elementary fibres together [69]. The elementary fibres have the primary and secondary cell walls, both of which are cellulose material. Cellulose fibrils (diameter between 0.1-0.3 µm) are embedded in concentric lamella composed of about 2% pectins and 15% hemicellulose which contribute to thermal degradation and water uptake of fibres [70]. They can be highly oriented with the fibre axis and thus crystallised in the cell walls to provide high tensile strength [69]. There is also a hollow part called lumen and filled by cytoplasm in the elementary fibres [63].

2.3.2 Properties of flax fibres

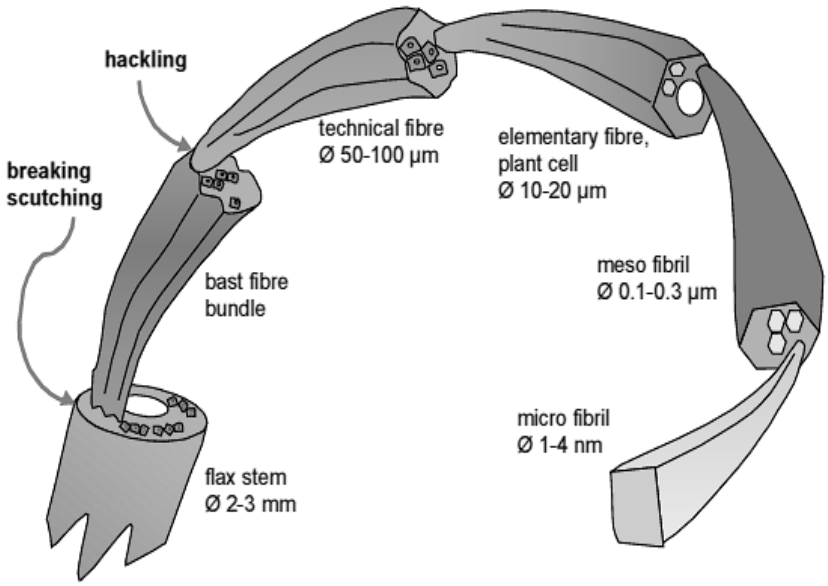

Figure 7. Structure of a flax fibre [67].

Figure 7 gives a description of the flax structure from stem to micro fibril. The commonly used flax fibres are after scutching and hackling. Technical fibres consist of 10 to 40 elementary fibres with 2-5 cm length. The primary wall of

elementary fibres is only 0.2 µm thickness, while the second cell wall is the major component composed of cellulose and hemicellulose [67; 71]. In addition to the orientation and crystallisation of cellulose, the hydrogen bonds within cellulose also contribute to the mechanical properties (e. g. stiffness) [67]. It is found that the strength of the fibre is reduced dramatically without the presence of hemicellulose [67]. The micro-fibrils have a diameter between 1 to 4 nm and are packed at the angle of 10° with the fibre axis [67].

Tensile properties. It is reported that there is no large scale plastic deformation of flax fibres in stress-strain behaviour as the amorphous region between fibril are oriented [67]. Baley et al. [72] found that the longitudinal Young's modulus of 59 GPa and transverse modulus of approximately 8 GPa. The clamping length of fibres, however, has a great effect on the tensile strength. Bos found that the tensile strength of the technical fibres has a plateau value of 500 MPa, which increases significantly below the clamping length of 25 cm [67]. Two main reasons are mentioned in his report: (1) less critical flaws, (2) changes in failure mechanism. Flaws, such as kink bands resulted from isolate process etc., are reduced by decreasing fibre length to increase the fibre strength. In the other side, for large clamping length, failure takes place through the weak interphase, while the cracks can only propagate through cell walls at the clamping length below elementary fibre length lying between 20 to 50 mm as seen in Figure 8. The mean value of tensile strength of technical fibres is only 57% of the elementary fibre strength, 1522 ± 440 MPa, due to the bulk effect.

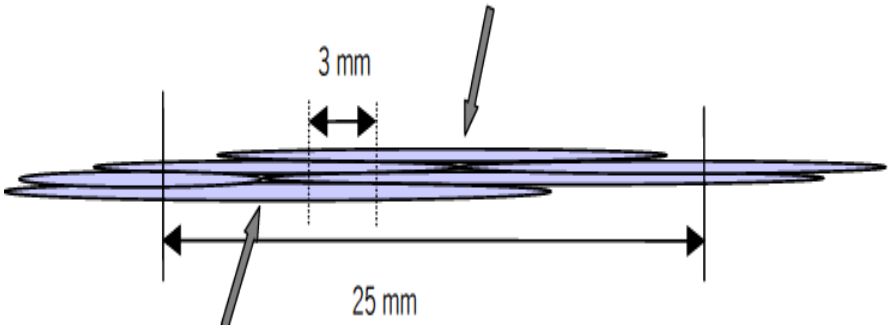

Figure 8. Schematic representation of failure mechanism of flax fibres. At 25 mm clamping length, elementary fibres slip over each other. At 3 mm, cracks have to run through the cross section of elementary fibres [67].

In some applications, flax fibres are as good as the glass fibres, and hence are accepted as a replacement. Except the specific properties of flax fibres as shown in Table 5, three other reasons have been stated to make the application of flax fibre more attractive: (1) cheaper than glass fibres, (2) less toxic, (3) high strength to weight ratio. Normally, the flax fibres have a relatively low price compared to glass fibres. In addition, glass fibres are suspected to cause lung cancer, but there is no such problem for natural fibres [67]. The thermal recycling of the flax fibres (burning of flax fibres with few slags left) is a great advantage over glass fibres.

Table 5. Tensile properties of glass and flax fibres [67].

Property	**E-glass**	**Flax fibres**
Diameter (μm)	8-14	10-80
Density (g/cm^3)	2.56	1.4
E-modulus (GPa)	76	50-70
Tensile strength (GPa)	1.4-2.5	0.5-1.5
Specific E-modulus (GPa per g/cm^3)	30	36-50
Specific tensile strength (GPa per g/cm^3)	0.5-1	0.4-1.1

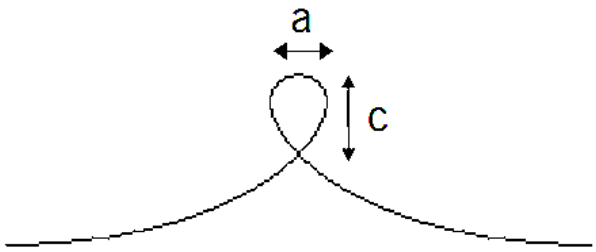

Figure 9. Loop test for compression. The ratio c/a changes at failure point.

Compressive properties. Similar to glass fibres, the compressive strength of flax fibres could be measured by the elastic loop test (Figure 9). Flax fibres usually fail in the top of the loop because of the highly oriented structure. The compressive strength, σ_c, is calculated from [67]:

$$\sigma_c = \frac{1.34 E_C d}{C_c} \qquad (2.1)$$

Here the E_c is the elastic modulus for both tensile and compressive, d the fibre diameter, Cc the point of failure. Fibre samples were tested and a compressive strength range of 830 to 1570 MPa was obtained [67].

Physical properties. The degradation of flax fibres is a crucial aspect in the development of natural fibre composites and thus has a bearing on the curing temperature in the case of thermosets and extrusion temperature in thermoplastic composites. Cellulose is the main component of natural fibres, and thus controls the major degradation behaviour of flax fibres. The degradation routes for cellulose upon heating were discussed by the literature [73]. The glycosyl units generally are decomposed at low temperature, followed by their depolymerisation at high temperatures. Then the formed substances like levoglucosan decompose into gas at higher temperatures.

The effect of thermal degradation on mechanical properties of flax fibres were investigated by Gassan and Bledzki [74]. They placed the untreated flax fibres in a laboratory oven between 170°C to 210°C for a maximum 120 minutes. Then the tenacity of flax fibres was measured by a tensile test. The tenacity decreased slightly below 170°C, whereas there is a rapid decrease of tenacity and polymerisation degree at temperature above 170°C. The behaviour strongly depends on the exposure time and temperature. Additionally, a slight increase of crystallinity was observed after heat treatment, as a result of chain scissions.

Stamboulis, Baillie and Peijs [75] demonstrated that moisture absorption varied between Duralin flax fibres and Green flax fibres. Duralin fibres absorbed less water and retained a more smooth fibre surface after fibre separation than Green flax fibres. The tensile strength of Duralin flax fibres increased to a maximum tensile strength at a humidity of 66% and decreased afterwards. The reason is that water plasticised the fibres at low absorbed water content but this effect was less important at large moisture content.

2.3.3 Development of surface treatment on flax fibres

To improve the adhesion between hydrophilic flax and hydrophobic polymer matrix, many studies on using chemical or physical treatments have been

published [76-79]. Some typical treatment routes from published articles are collected in Table 6. Common treatments include mercerization, dewaxing, silane treatment, acrylation, peroxide treatment, coatings, and impregnation with a dilute epoxy [25; 80; 81].

Table 6. Different treatments of flax-reinforced composites.

Fibre/matrix	Treatment	Conditions	Effect on properties	Ref
Flax/PP	Esterification	10 $_{wt}$% MA, 25h, 50°C	Highest flexural and tensile strength	[78]
Flax/phenolic	Esterification	25 $_{wt}$% MMA, 30min, 210 W	More moisture retardant	[79]
Flax/epoxy	Alkali treatment	5 $_{wt}$% NaOH,30 min	Tensile strength 21.9%; Flex. Strength 16.1%	[82]
Flax/epoxy	Alkali treatment	4 $_{wt}$% NaOH,45s	Transvers strength, 30% increment	[83]
Flax/polyester	Silane treatment	0.05 $_{wt}$%, 24hRT	Hydric fibre/matrix interface	[84]
Flax/PP	Esterification	MA-PP coupling agent	Interphase compatibility	[85]

*MMA-methylmethacrylate, MA-maleic-anhydride

2.3.3.1 Silane treatment

Coupling agents usually improve the degree of crosslinking in the interface region and offer a perfect bonding. Among the various coupling agents, silane coupling agents are found to be effective in modifying the natural fibre-matrix interface. The incorporation of proper silane treated fibres in composites could lead to improvement of the fibre/matrix compatibility. Hence the mechanical properties and outdoor performances of the resulting composites are improved. Silane is hydrolyzed forming reactive silanols and is then adsorbed and condensed on the fibre surface (sol-gel process). The hydrogen bonds are formed between the adsorbed silanols and hydroxyl groups of natural fibres

may be further converted into covalent bonds by heating the treated fibres at a high temperature (see Figure 10).

Xie and his coworkers [39] has reviewed silane coupling agent modification to natural fibre composites and found out improvements in strength, moisture absorption and fungal resistance for UP and epoxy composites. The suggested suitable silane modification for fibres in epoxy composites was aminopropyl triethoxy siloxane (APS-Figure 11(a)) and methacryloxypropyl trimethoxysilane (MPS). 3% APS solution combined with alkali treatment was found to provide better moisture resistance [86].

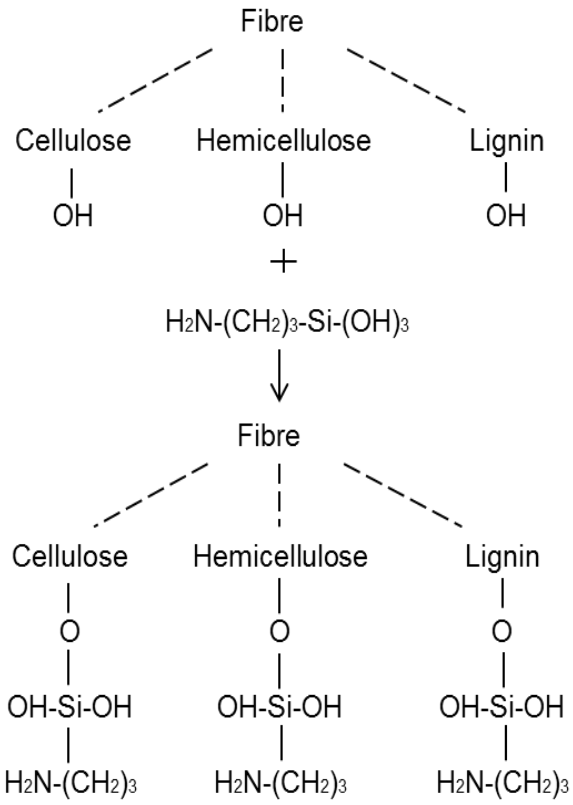

Figure 10. Grafting of silanols on flax fibre surface (redraw from Singha er al.[86]).

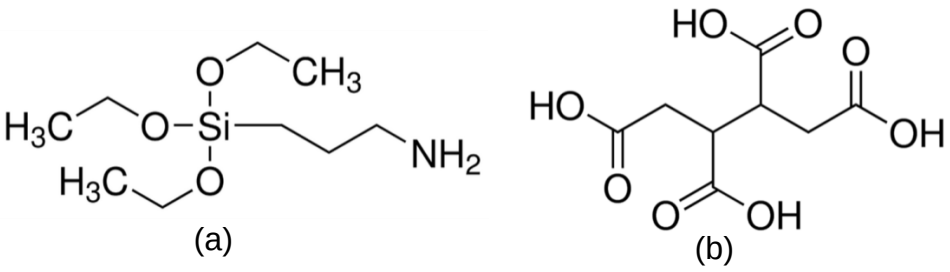

Figure 11. Chemical structure of (a) APS and (b) BTCA.

2.3.3.2 Acetylation

Acetylation is a well-known esterification method originally applied to wood cellulose to stabilize the cell walls against moisture, improving dimensional stability and environmental degradation. In lignocellulosic material the acetic anhydride (like BTCA-Butanetetracarboxylic acid- as seen in Figure 11(b)) reacts with more reactive hydroxyl groups (OH), in lignin and hemicellulose (amorphous material). The hydroxyl groups of cellulose, the crystalline structure can prevent the diffusion of reagent [87]. About 25% tensile and flexural strength improvement in 18% acetylated flax fibre with PP-flax fibre composites (30% fibre) was recently reported [88]. Acetylation is beneficial in reducing the moisture absorption of natural fibres.

2.3.3.3 Anhydride treatment

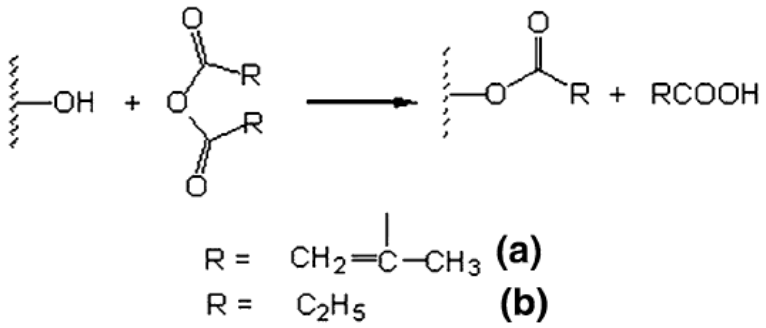

Figure 12. The reaction between –OH groups of flax fibres and (a) methacrylic (b) propionic anhydrides [40].

Anhydride treatment is usually carried out by utilizing maleic anhydride or maleated polypropylene (or polyethylene) in a toluene or xylene solution, where the fibres are immersed for impregnation and reaction with the hydroxyl groups on the fibre surface. Hugues, Carpenter and Hill [76] reported that methacrylic and propionic anhydrides modification showed a marked effect on yield properties (yield point, on set of yield etc.) of flax composites. There are two modification mechanisms used: (a) reactive vinylic group introduced by methacrylic anhydride (MA); (b) hydrocarbon coating on the surface to improve the hydrophobic by propinic anhydrides (PA) (see in Figure 12). The trend of bond strength was observed: MA>PA>unmodified, and was related to the work

of fracture trend: unmodified>PA>MA. This is due to the fact that the debonding behaviour was inhibited by good bonding strength. The treatment of grafting MAPP copolymer decreased the fibre surface energy to a similar value of PP and hence improved the wettability [78].

2.3.3.4 Mercerization / Alkali treatment

Alkali treatment of natural fibres, also called mercerization, is the common method to produce high-quality fibres. Mercerization has an effect on the chemical composition of the flax fibres, degree of polymerization and molecular orientation of the cellulose crystallites. The cementing substances like lignin and hemicellulose which are removed during the mercerization process [85]. Alkali treatment also transferred crystalline form cellulose I into cellulose II [83]. The extent of this transformation could be to some extent reflected by the intensity ratio of the stretching modes of symmetric (C-O-C) and asymmetric (C-O-C) through FT Raman spectroscopy [77].

The changes in surface morphology and chemical compositions, along with mercerization greatly influence the thermal degradation of flax fibres and hence the processing temperatures. Bledzki et al. [88] reported that the degradation temperature of flax fibres increased from 319°C to 360°C after mercerization (34% acetylation). It was stated that the thermal stability of flax fibres increased after alkali treatment, due to the removal of lignin and hemicellulose [89].

2.3.3.5 Enzymatic treatments

Enzymes are an increasingly interesting option as such or when combined with chemical and mechanical methods for modification and processing of biomaterials. This is due to the fact that enzymes are highly specific and efficient catalysts and they work in mild, energy-saving conditions. Oxidative enzymes, such as laccase or peroxidases, can be used to activate and further functionalise lignocellulosics [90]. The primary reaction of laccase is the oxidation of phenolic hydroxyls to phenoxy radicals in the presence of oxygen. Laccase can thus be used to activate lignin, lignans, and different types of lipophilic extractives present in the complex lignocellulosic materials [91]. It was

found that the lignin content of single cellulose fibres decreased from 35% to 24% with laccase treatment. Further co-polymerisation or grafting with selected hydrophobic components (e.g. dodecyl gallate-Doga) could be applied on laccase-catalysed lignocellulosic materials. Lauryl gallate (LG), a hydrophobic compound with strong internal sizing effect, was grafted on cellulosic fibres, and the results showed significant reduction of water penetration [92; 93].

2.3.3.6 Graft copolymerisation

Required properties could be added through graft copolymerisation, which is the polymerisation of functional molecule groups with the active sites on the polymeric back-bone to form a graft copolymer. A specialised chemical group is normally considered as an active site to react with an appropriate monomer through ionic or condensation polymerisations. Vinyle monomers were successfully grafted on flax fibres through the investigation of Kaith and Kalia [79]. Three different reaction process factors, such as air, microwave radiation and pressure, were investigated. The highest grafting percentage of 41.7 % was observed when graft copolymerisation occurred in air. The grafting percentage of 36.4 % and 24.6 % was found for the process done under pressure (0.8 MPa) and microwave radiation (210 W), respectively.

2.3.3.7 Other treatments

A number of available pre-treatments, such as benzoylation [94], etherification [95], isocyanate treatment [96], peroxide treatment [46], sodium chlorite [97] and stearic acid treatment [98] have been reported in the literature. In benzoylation treatment, benzoyl chloride is most often used in fibre pre-treatment. The inclusion of benzoyl group in the fibre is responsible for the decreased hydrophilic nature of the treated fibre, decreasing its water absorption, but also increasing its strength properties. For the modification of cellulosic fibres by etherification Sodium hydroxide plays an important role in forming a charged intermediate species with the fibre, which allows the faster nucleophilic. Addition of epoxides, alkyl halides, benzyl chloride, acrylonitrile, and formaldehyde. Isocyanate group can react with the hydroxyl groups on fibre

surface forming covalent bonds, thus improving the interface adhesion. Organic peroxides tend to decompose easily to free radicals (RO.), which further react with the hydrogen group of the matrix and cellulose fibres. Sodium chlorite ($NaClO_2$) usually is used in bleaching fibres; however, it could dignify lignocellulosics. Fibre treatment of stearic acid ($CH_3(CH_2)_{16}COOH$) in ethyl alcohol solution can remove non-crystalline constituents of the fibres, thus altering the fibre surface topography. It could be interesting to add that these treatments are not very eco-friendly and the better way to use natural fibre is to use them as received without chemical treatments.

2.3.4 Properties and characterization of flax polymeric composites

Like common polymer composites, either thermoplastics or thermosets could be used with flax fibres and offer varying mechanical properties. From the matrix point of view, thermoplastic matrices like polypropylene (PP) and polyethylene (PE) are ductile, easy to process and simple to recycle. On the other hand, processing temperature and time must be properly controlled so as to decrease the viscosity for suitable wetting and not to degrade the fibres. Concerning on the increasing needs of recyclable materials, bio-degradable polymeric matrices (polylactic acid-PLA, soy protein epoxy and tannin phenolic resin) have attracted more and more attention from academics and industries. Table 7 shows the mechanical properties of flax-reinforced composites based on some different matrices. Physical information of flax fibres and the associated composites, could be obtained through various approaches, such as DSC (differential scanning calorimetry) [99], DMA (dynamic mechanical analysis), TGA (thermogravimetry analysis) [99], X-ray diffraction [85], SEM (scanning electron microscope) [99; 100] and FTIR [98; 101].

2.3.4.1 Thermoplastic polypropylene (PP) based flax composites

Many studies [45; 109-112] have concentrated on flax/thermoplastic composites and provided valuable information. From Van de Velde and Kiekens [45] investigations, polypropylene (PP) is the most suitable thermoplastic matrix for flax-reinforced composites due to its various advantages, such as low density,

Table 7. Testing data of mechanical properties of flax reinforced composites.

Fibre/ matrix	**Processing method**	**Tensile Strength (MPa)**	**Tensile Modulus (GPa)**	**Flexural Strength (MPa)**	**Impact strength (kJ/m^2)**	**Ref**
Flax/bio-thermoset(MSO)	Compression moulding	≈50-120	≈6-15	180 (max)		[102]
Flax/bio-thermoset (MMSO)	Compression moulding	≈50-120	≈7-15	201 (max)		[102]
Arctic Flax/ Epoxy(50:50)	Resin transfer moulding	280	40			[103]
Plain woven flax/epoxy	Hand lay-up			≈78-100 ($MPa/g{\cdot}cm^{-3}$)	≈17-35 ($kJ/m^2/G{\cdot}cm^{-3}$)	[104]
Plain-woven flax/thermoset	Compression Moulding	280	32	250	15 (Charpy)	[105]
Flax/Lactic acid resins(70:30)	Compression moulding	62	9	96		[106]
Flax/PLA	Injection moulding	≈40-55	≈3-6		≈9-11(Charpy)	[107]

low thermal expansion, good resistance to water and recyclability. The adhesion between hydrophilic flax fibres and hydrophobic PP being the biggest problem; modification technologies were therefore applied to improve it. Boiling of flax and use of chemicals (e.g. maletic acid) was proved to be good for adhesion modification in order to increase mechanical properties [113-115]. Garkhail, Heijenrath and Peijs [116] prepared flax/ maletic-anhydride grafted PP (MA-PP) composites by two production methods, called film-stacking and paper-making process. The effect of fibre length on composite stiffness and tensile strength was very little, showing agreement with the model predictions shared with other scientists [117; 118]. The critical length was thought to be reduced by the addition of MA-PP, compared to PP/flax. Fibre volume however had a significant effect on the final mechanical properties of composites. The influence of the physical structure of the flax fibres on mechanical properties were investigated by Van Den Oever, Bos and Van Kemenade [119]. 40 vol% hackled and 40 vol% scutched fibre/PP were used to compare with the theoretical predictions. The results indicates that combing the flax fibres (hackled fibres) will remove some weak lateral bonds, which are detriment to tensile and flexure strength. The compressive behaviour of composites is also relative to the presence of kink bands which can be removed by combing [120].

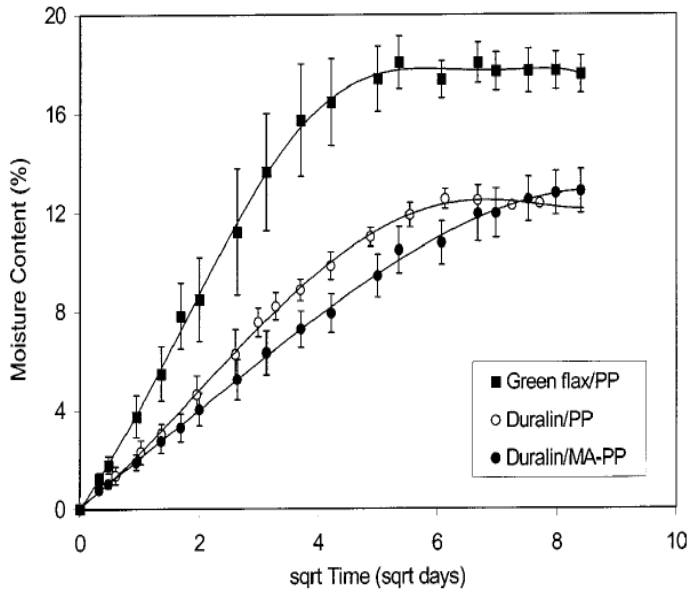

Figure 13. Moisture content of flax/PP composites as a function of time [108].

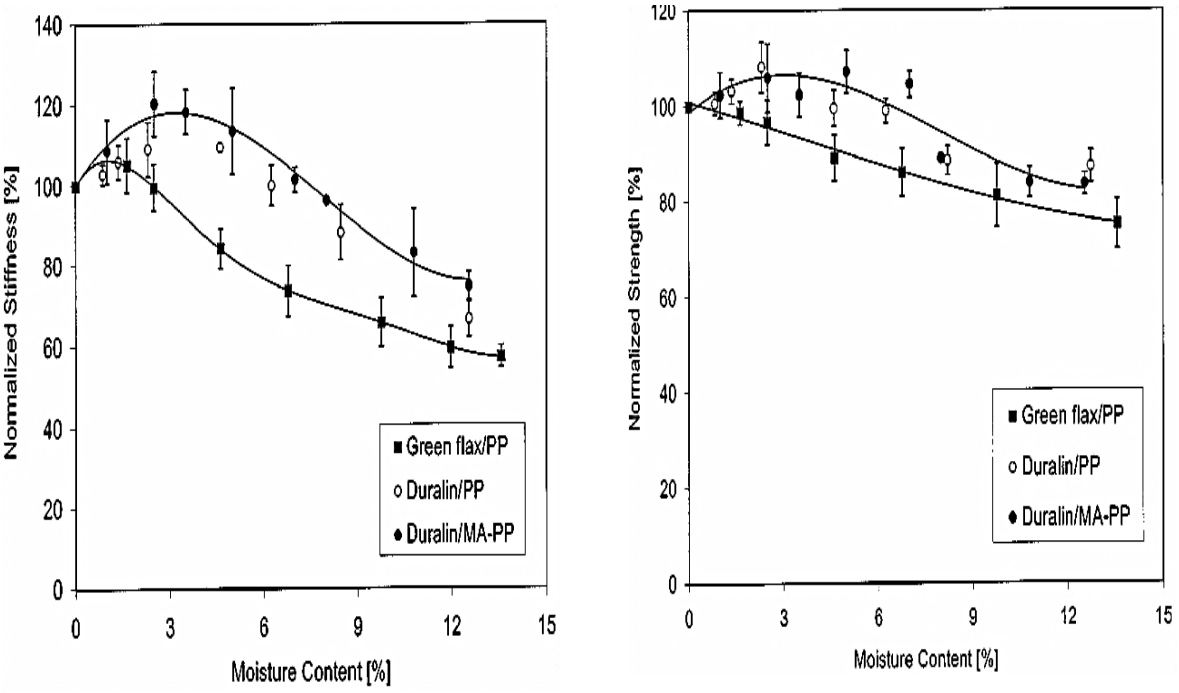

Figure 14. Moisture versus mechanical properties: (a) stiffness; (b) strength [108].

The hydrophilic character of bio-composites cannot be neglected. The water absorption/ageing plays an important role in degradation and decrease of mechanical properties. Recent studies [75; 108; 121; 122] have reported the effect of water uptake in bio-composites limits their outdoor applications. In general, there are three ways to understand the term 'water absorption': (1) water diffuses directly into the matrix; (2) through the interphase matrix/reinforcements; (2) by imperfections. A study of moisture absorption and environmental durability of flax (Green and Duralin)/PP composites was conducted by Stamboulis and his co-workers [69]. The moisture content versus root time curve (Figure 13) could be explained by Fick's law. Green flax/PP composites were clearly more sensitive to water than Durbin flax ones, meanwhile the addition of MA (maleic-anhydride)-PP lowered the initial water uptake rate with little effect on the maximum moisture content. In terms of mechanical properties, the moisture content affected stiffness of flax/PP composites more than tensile strength (Figure 14). The stiffness increased somehow at low moisture content due to the filled interfacial gap by swelling flax fibres, while it decreased significantly at 7% moisture content.

2.3.4.2 Thermoset-epoxy resin based flax composites

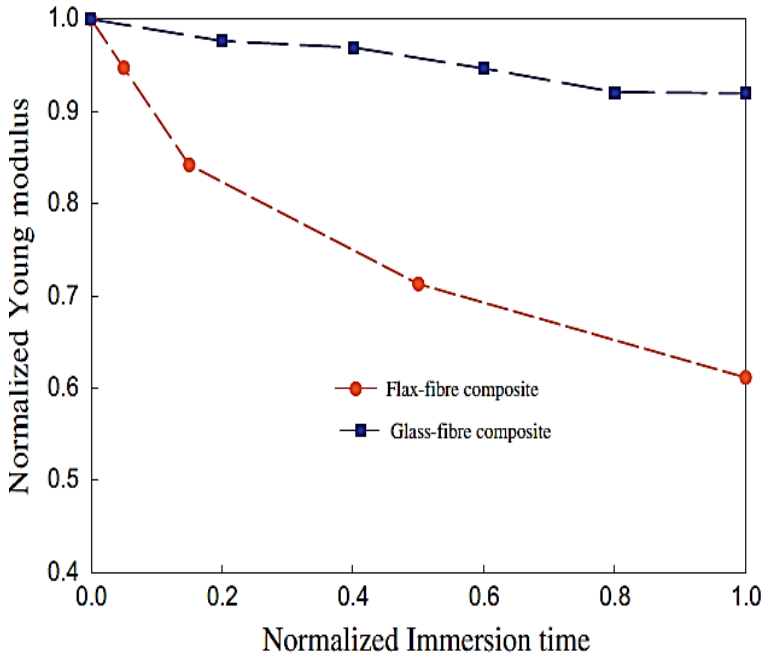

Figure 15. Normalised young's modulus (modulus/modulus at time=0) versus normalised immersion time (test time/saturation time) [121].

The mechanical performance of epoxy based flax composites have been widely investigated [103; 123-125]. Hughes et al. [126] produced unidirectional flax/epoxy composites and directed their investigation towards the tensile deformation behaviour. The work revealed the non-linear stress-strain relationship under tensile loading with respect to the flax/matrix adhesion and the presence of kink bands. Muralidar [127; 128] studied the epoxy composite reinforced by flax in the form of hybrid preform (plain weave fabric and rib knitted structure) through lay-up method. He pointed out that the compressive properties were mainly contributed by the matrix whereas the tensile properties of woven composites were highly influenced by the flax volume fraction in the tension direction. The effect of woven flax fabric on fracture toughness of flax/epoxy composites were reported by Liu and Hughes [129]. The well-packed fibres in the textile lead to a high fibre volume fraction and hence the improvement of fracture toughness up to 9 $MPa \cdot m^{1/2}$ compared to pure resin (about 1.8 $MPa \cdot m^{1/2}$). Additionally, the results strongly depended on the testing directions (weft and warp) with different fibre densities. Oksman [103] found that

Arctic Flax /epoxy composites had outstanding mechanical properties (e.g. maximum tensile strength of 280 MPa) and presented better specific modulus of 29 GPa/g·cm^{-3} than that of glass/epoxy composites. Liang and his co-workers [123] compared fatigue behaviours between glass fibre/epoxy and flax fibre/epoxy composites. They reported that flax composites had the advantages of relatively stable modulus under cycling load over glass fibre-reinforced composites.

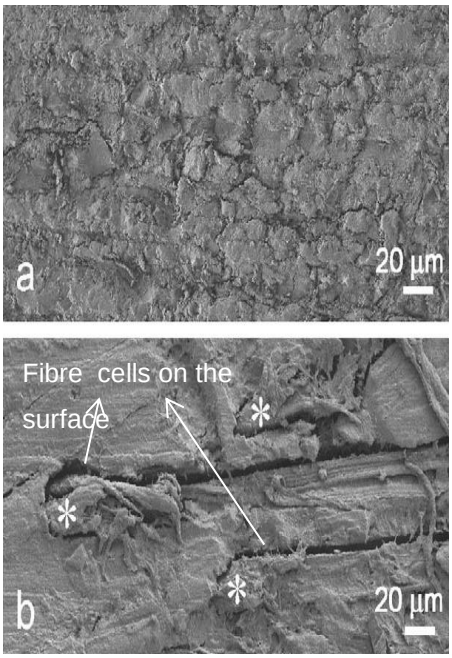

Figure 16. SEM images of flax/epoxy composites: (a) origin specimen; (b) after 8 wet-dry cycles [130].

Like all the natural fibre composites, the environmental durability is a major concern in flax/epoxy composites. Assarar and his co-workers [121] reported the influence of water ageing on properties of epoxy composites with 11 flax unidirectional plies. The failure stress decreased around 13% after first 1-day water immersion. Then the reduction of failure stress was only an extra 2% between 1 and 20 days of immersion. From Figure 15, a 30% decrease of normalised young's modulus of flax/epoxy in the first 10 days showed a much worse result from water ageing than glass fibre composites. Hewman [130] tested the water damage of plain-weave flax/epoxy composites (8 plies) through the wet-dry cycle procedure. The tensile strength after the first wet-dry cycle was found to be 89% of the unconditioned value, and dramatically dropped to

16% after 4th cycles. Penetrated water expanded the flax fibres and created in matrix/technical fibres gaps (SEM images in Figure 16) after drying. This is attributed to the different shrinkage degrees of fibres and matrix. The increased number of wet-dry cycles enlarged these gaps (auto-accelerative process) and consequently weakened the composite.

2.3.4.3 Bio-degradable poly(lactic acid) (PLA) based flax composites

The use of natural fibre (e.g. hemp, flax, jute and sisal) reinforced composites has been well-established for several years because of the increasing environmental awareness. Nevertheless, due to the petroleum-based polymer matrices (e.g. PP and epoxy), the composites are not fully degradable, leading to the difficulty in recycling process. Hence, new generation of fully bio-materials need to be developed.

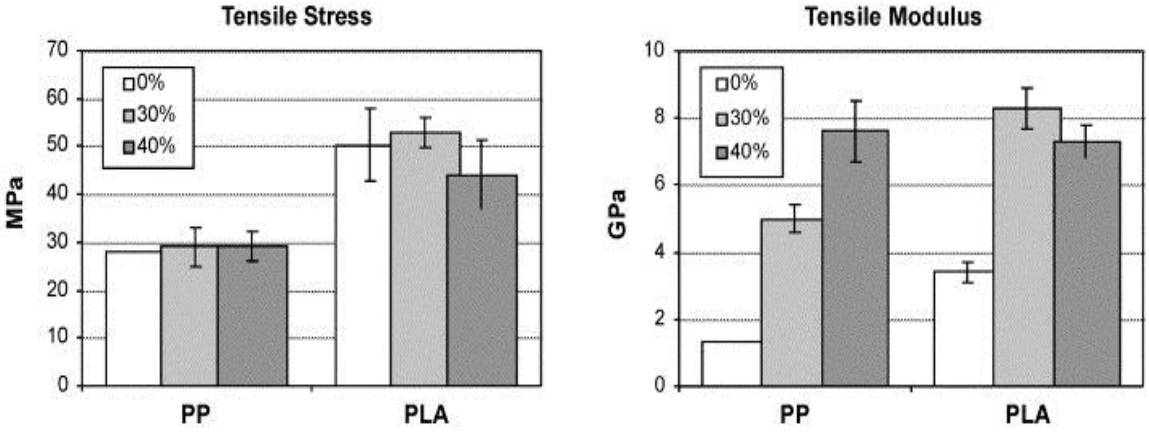

Figure 17. Tensile properties of flax/PLA compared to flax/PP composites [131].

To improve the sustainability and eco-efficiency, bio-degradable poly(lactic acid) has been increasingly used together with flax fibres [3; 131-133]. PLA can be derived from corn starch, sugarcane etc., while it is also able to be synthesised, especially for industrial production. Akesson et al. [106] produced and studied fully biodegradable composites from PLA and flax fibres. The mechanical properties of final composites were increased by varying the fibre content from 40 $_{wt}$% to 70 $_{wt}$%, but drastically reduced with a fibre ratio of 75 $_{wt}$%. The humidity ageing tests showed that the tensile modulus was reduced from 9 GPa to 2.5 GPa after 1000-h exposure time at 95 % humidity and 38°C, meanwhile

the tensile strength was reduced about 70 %. It was demonstrated by Bax and Müssig [134] that the flax / PLAcomposites had a higher Young's modulus of 6.31 GPa than Cordenka/PLA composites. The impact strength increased to 11 KJ/m^2 with fibre mass fraction of 30 $_{wt}$%. Oksman et al. [131] manufactured flax (long heckled fibres)/PLA composite by compression moulding and then compared them to the commercial flax/PP composites used for automotive panels. The composites with 40 $_{wt}$% flax content showed good fibre dispersion and over 50% higher tensile modulus up to 7.3 GPa than flax/PP composites (as seen in Figure 17). The DMA results indicated that the reinforcement of flax fibres increased T_g from 50°C for pure PLA to 60°C for the composite, and presented a cold crystallization at 80°C. For the adhesion bonding measurement of flax/PLA composites, Le Duigou and his coworkers [135] designed a microbond test to estimate the interfacial shear strength. With decreasing the thermal treatment rate, the shear strength increased from 33 MPa for 93 °C/min to 38 MPa for 1.5 °C/min, as a result of the thermal residual stress from the crystallization.

2.3.4.4 Bio-epoxy resin based flax composites

The vegetable oil-derived renewable epoxy resin is a potential substitute of petroleum-based resin for flax composites to be used in automotive and construction applications [105; 136-139]. Flax yarn and flax woven fabric reinforced soy protein concentrated resins (SPC) were prepared by Huang and Netravali [70] for the comparison of tensile and flexural properties. Two layers of unidirectional flax yarns were impregnated with resin solution by winding fabrication, and then air cured at 35°C for 24 hours, followed by a 25-minute hot pressing at 120°C of 8 MPa. Flax fabric composites were made of four resin-coated flax fabrics cured at the same hot pressing condition. Flax yarn composites showed the highest tensile strength of 298 MPa and flexural strength of 117 MPa, while for flax fabric composites, failure stress of 62 MPa and 83 MPa were observed in the warp and weft direction, respectively. The reinforcement of both flax yarns and flax fabrics results in high failure strain and high toughness.

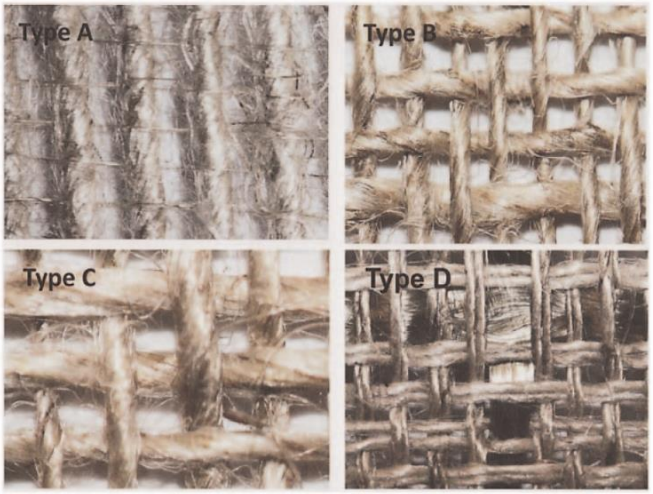

Figure 18. Weave types: (A) plain; (B, C) two different twill; (D) Dobby [105].

Adekunle et al. [102] prepared bio-epoxy composites reinforced by hybrid nonwoven and woven flax fabrics. MMSO (methyacrylic anhydride modified soybean oil) concentrate bio-epoxy resins and MSO (methacrylated soybean oil) resin were applied. The composite laminates consisted of three non-woven flax mats sandwiched between four woven fabrics (0°, 45°, 90° orientation) with different stacking sequences. The composite tensile strength up to 119 MPa and modulus up to 14 GPa was found for fibre configuration of $[0_4/N_3]$. A flexural strength of 201 MPa and modulus of 24 GPa was also achieved. MMSO offered the additional methacrylate function groups, and hence the final composites exhibited better mechanical properties with higher level of cross-linking. The extra addition of styrene in the bio-thermosets improved the mechanical (e.g. brittle) properties. The low viscosity of molten styrene results in better fibre/matrix adhesion.

A study of the influence of weave architecture on the mechanical properties of flax fibre/ bio-epoxy composites was conducted by Adekunle et al [105]. The woven fabrics were in the forms of plain, twill and dobby as shown in Figure 18. The tensile, flexural and impact properties were found to follow the trend: Plain weave type <twill type <dobb type. The inherent thin weft yarns in plain weave fabric were neglected, and hence the almost unidirectional properties along the warp yarn. The T_g of flax/bio-epoxy composites was around 85°C from the tanα plot, which was little higher than T_g of 70°C from loss modulus data.

2.3.4.5 Bio-phenolic (tannin) flax composites

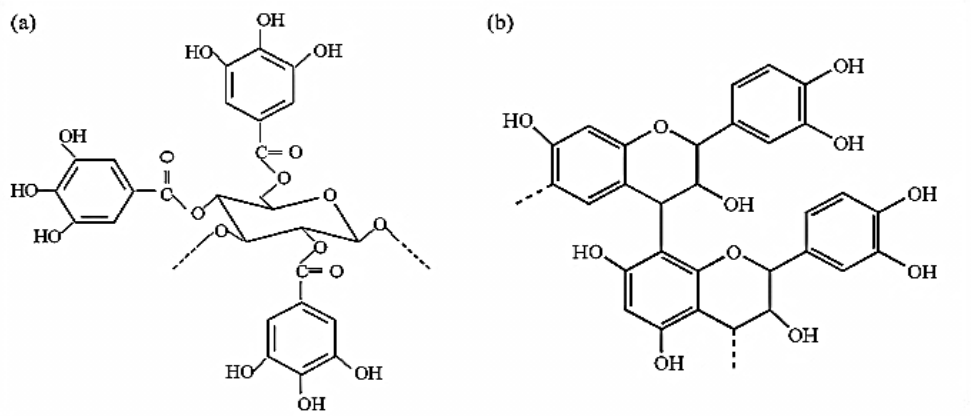

Figure 19. The chemical structure of tannin: (a) hydrolysable; (b) condensed [140].

One possible matrix for fully bio-degradable flax composites is tannin resins (naturally occurring polyphenolic compounds) from plant resources (e.g. wattle, myrtle, pine etc.) [20-23]. The environmental and economic advantages of tannin composites have attracted lots of attention from auto industry. The composite made from tannin and flax fibres could potential offer desirable characteristics aiming at reduction the environmental footprint of vehicles through the use of bio-materials for possible load-bearing parts such as vehicle body panels, crash elements, side panels and body trims.

Tannins contain many phenolic rings and have a high molecular range of 500 to 2000 and chemically are grouped into hydrolysable and condensed tannin (Figure 19). The hydrolysable tannin is capable of hydrolysing in certain conditions (e.g. alkalis, acids and enzymes), whereas the condensed tannin is more stable and suitable to produce resins [141]. Hydrolysable tannins comprises of simple phenols such as pyrogallol and ellagic acid and of esters of a sugar, mainly glucose, with gallic and digallic acids. Condensed (or flavonoid) tannin on the other hand (which constitute 90% of the commercially available tannins) have being used as adhesives and resins since 1971. Their reactivity is comparable to that of synthetic polymers, and they can be reacted either by autocondensation (for interior applications only) or by reaction with an aldehyde. Formaldehyde has been for long among the best choices for hardener. Tannin crosslinking by formaldehyde via methylene or methylene ether bridges in a

polycondensation reaction is the traditional chemistry for tannins to function as exterior-grade weather resistant word adhesives [141-143].

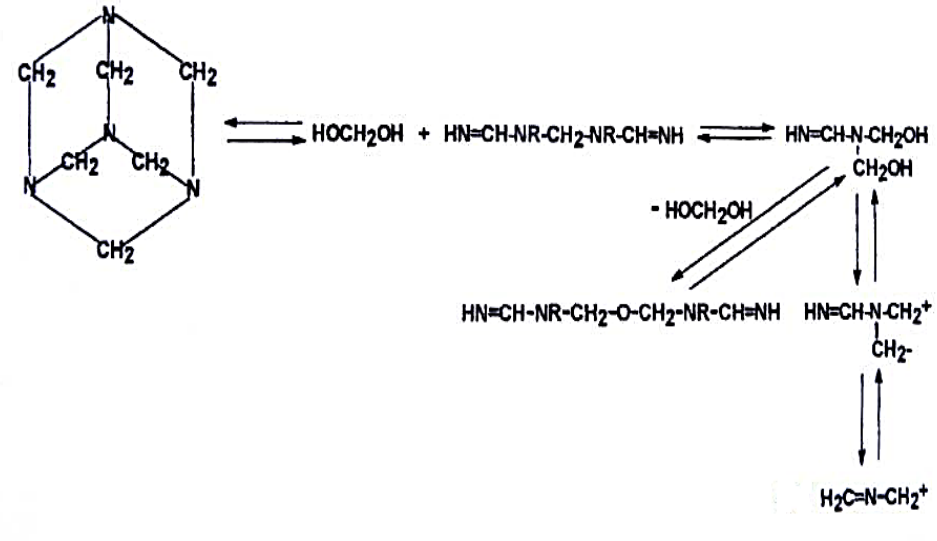

Figure 20. Decomposition of hexamine [144].

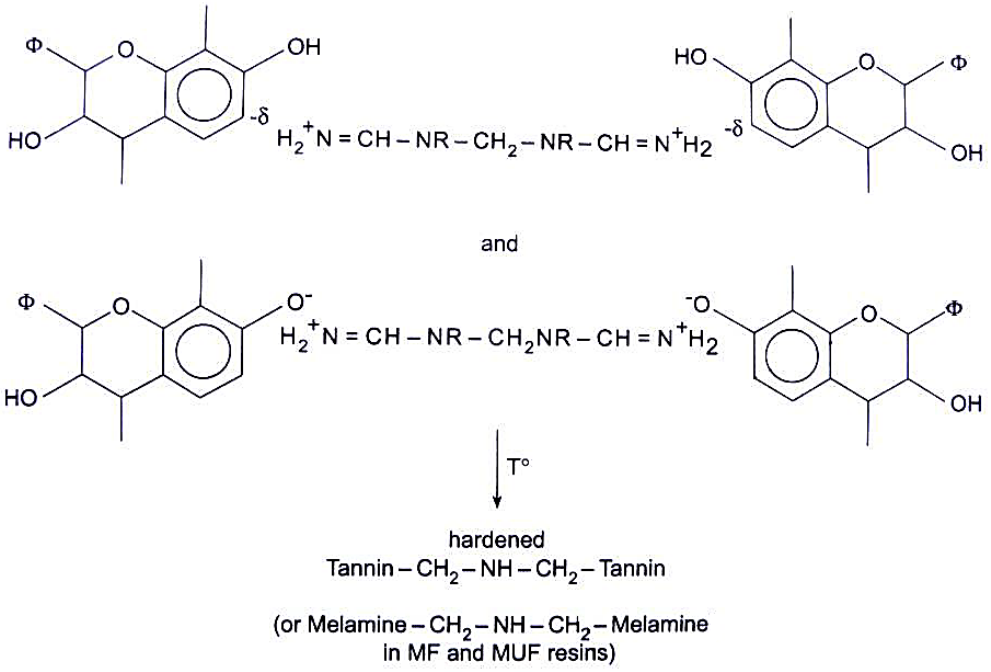

Figure 21. Further reaction between tannin and hexamine [144].

To decrease or completely eliminate formaldehyde emission during processing, the use of hexamethylenetetramine (hexamine) has been developed as an effective alternative to traditional hardeners like paraformaldehyde. When

making tannin/hexamine resin, condensed tannins are solubilized into water firstly. The alkaline solution makes this solubilisation easier because of the formation of OH- ions. Hexamine should turn into formaldehyde and trimethylamine in this alkaline environment after going through unstable molecule like $+CH_2$-NH-CH_2+ (Figure 20), but as tannins are negatively charged, they immediately react with these unstable molecules to form $–CH_2$-NH-CH_2- bonds molecules (Figure 21).

To date, tannins have been widely reported to produce wood adhesives, anti-corrosive, rust inhibitor etc.[145], however there are only a small number of papers about tannin matrix composites for other applications. Recently, there has been growing interest on tannin-based resins [2]. Coir fibre reinforced tannin composites were recently studied by Vilmar et al. [140] to show a potential for automotive applications as internal parts. Ndazi and his co-workers [146] manufactured composite panel boards from rice husks and mimosa tannin resins with adequate stiffness. Barbos et al. [140] prepared tannin-phenolic based composites reinforced with coir fibres. The impact strength was highly improved by coir fibres to show the potential for vehicle applications.

2.3.4.6 Flax composites based on other matrices

In addition to PP, epoxy, PLA, bio-epoxy and tannin resin, a few other polymeric matrices for flax composites are also available. Saiah and his co-workers [147] fabricated and characterised flax-reinforced composites based on thermoplastics from wheat flour. The stress at failure increased from 4.4 MPa at fibre content with 5 $_{wt}$% to 8.9 MPa at 20 $_{wt}$%, while there was an increment of 270% in tensile modulus. They used X-ray diffraction to analyse the crystallinity of the flax fibre. The increase in fibre content leads to the increase in intensity of peaks at 2θ by 15.1°, 16.8°, 22.7° and 34.4°, corresponding to crystalline structure of flax fibres. In terms of the thermal degradation, an observed mass loss peak in 300-360°C range of the composites was found to increase with increasing the fibre content. Andersons and Joffe [148] pointed out only at low fibre volume fraction (up to 20%) that experimentally tensile strength of vinyl ester resin/flax composite can reach the theoretically predicted values.

2.3.4.7 Nanotechnology applied in flax composites

Nano-level technology also has been developing at a high speed in flax fibre polymer composites. The recent research activities and developments of nano-level cellulose fibre reinforced composites were reviewed by Eichhorn et al. [149]. With respect to the production of cellulose nanofibres and their composites, the review pointed out some issues that are worth noting: (1) structure damage may occur during extraction of nanofibres; (2) lots of energy is required by mechanical ways to separate fibres; (3) the dispersion of nanofibres is crucial to control the composite quality and can be greatly enhanced by layer-by-layer deposition. Due to the high surface/volume ratio of cellulose nanowhiskers, the efficiency of stress transfer is highly improved and the modification like grafting of DNA and coupling of chromophores can be applied for different purposes.

Flax bast fibres are one of the major sources to produce the cellulose nanofibres, showing great potential for composite applications. Bhantnagar and Sain [150] investigated the flax fibre-derived cellulose nanofibres with the diameter range between 10-60 nm and prepared 10 $_{wt}$% nanofibre containing polyvinyl alcohol (PVA) composite films. The strong orientation of flax nanofibres gives rise to the high crystallinity of 59 $_{wt}$% obtained from the X-ray diffractograms. The tensile modulus increased from 2.29 GPa of pure PVA to 6.1 GPa of PVA composites using 10 $_{wt}$% flax nanofibres. The glass transition temperature of flax nanofibre/PVA composites was found to shift up to 58°C with increasing fibre content from 5 $_{wt}$% to 40 $_{wt}$% [151]. Qua and his coworkers[152] found the three degradation steps of the nanofibre/PVA composite films by considering the weight change in TGA curves. The second degradation peak corresponding to the dehydration of PVA, significantly increased by the addition of nanofibres due to the difficulty to break down the strong hydrogen bonding between PVA matrix and fibres.

Except the nanofibre reinforcement, Huang and Netravali [70] added nano-clay particles to SPC (soy protein concentrated) composites reinforced by flax fibres (yarns and fabrics). The presence of nano-clay particles enhanced composite

stiffness (e.g. tensile modulus and flexural modulus), however reduced the failure strain. The reduction of maximum strain may be due to the increased rigidity of the polymer chains and defects introduced by clay particles. The highest tensile strength and flexural strength of flax/SPC composites is 298 and 117 MPa, respectively.

2.4 The fibre reinforcement mechanism in polymer composites

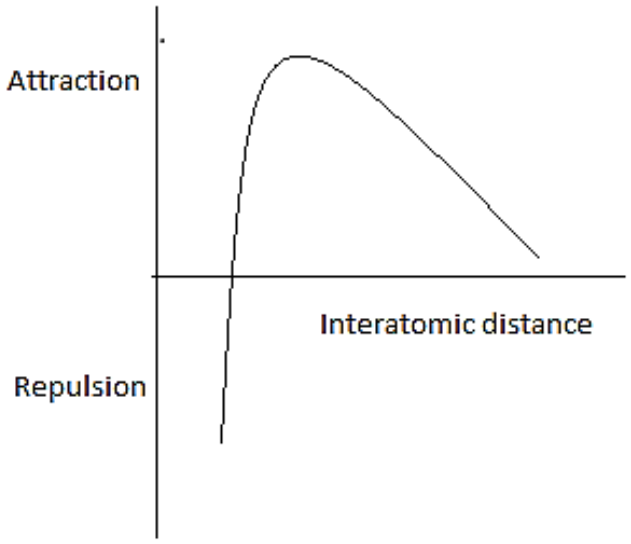

Figure 22. Interaction forces between two constituent atomic planes.

In composites, reinforcements are done to improve properties in the origin matrix. Ideally, the modulus and strength of fibres should be much greater than the polymer matrix so as to obtain a significant improvement in these mechanical properties. There are many prediction approaches and modes, depending on the chosen equivalent hypotheses (e.g. 'effective moduli', 'self-consistent', 'bounding', and 'average method'), for characteristics of composites [2; 12; 16]. All these modes are from calculation of theoretical cleavage stress and shear strength. By considering interaction forces varying with the distance between two atomic planes (Figure 14), the theoretical cleavage stress can be obtained from:

$$\sigma_{max} = \sqrt{\frac{E\gamma}{a_0}} \qquad (2.2)$$

Where E is the fundamental value of Young's modulus, γ is the surface energy represented by the area under the curve, and a_0 the distance between planes. The estimation of the mechanical properties, such as stiffness and strength, is based on the different composite conditions, including fibre length, nature of bonding, fibre orientation, continuity of fibres, and composite homogeneity etc. [153]. The following chapter discusses the conditions for prediction.

2.4.1 Prediction of stiffness: Elastic solution

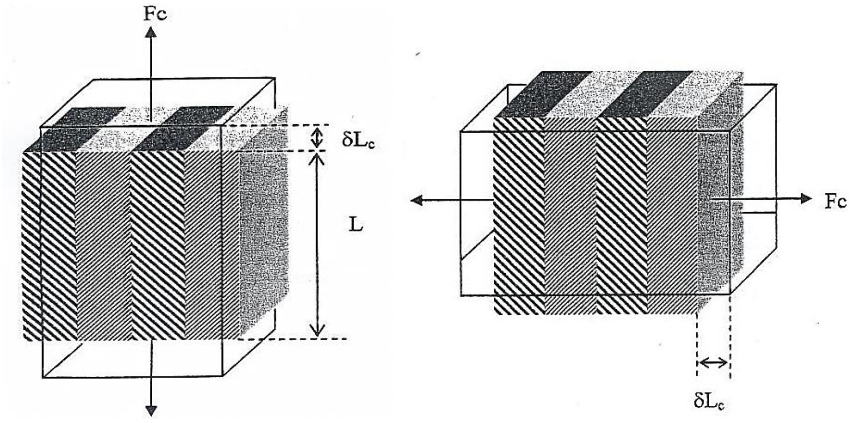

Figure 23. Elastic solution: (a) isostrain response; (b) isostress response.

The initial assumptions of elastic solution to estimate stiffness are: (a) Perfect bonding—no movement at the interface; (b) elastic behaviour in both phases—ignore the time-dependant deformation; (c) same poisson's ratio through all sections---no triaxial stress occurring from applied axial stress. Even in the above hypotheses, it is not possible to predict the modulus of a composite accurately. It ranges from the highest modulus, known as upper limits of reinforcement, to lowest modulus from lower limit of reinforcement. When the two constituent phases exhibit isometric deformation as shown Figure 23(a), modulus at the direction of force is the highest. Figure 23(b) shows that the lowest modulus takes place at isostress condition.

Upper limit of reinforcement : isotrain condition ($\varepsilon_c=\varepsilon_1=\varepsilon_2$)

The load on the composite F_c equals to the sum of loads applied on each phase. It is also known that load=stress×area, we have the following equation:

$$A_c \times \sigma_c = \sum a_1 \times \sigma_1 + \sum a_2 \times \sigma_2 \ (\mathrm{A}_c, \mathrm{a}_1 \text{and } \mathrm{a}_3 \text{ are the surface areas}) \quad (2.3)$$

It could be divided by strain ($\varepsilon_c=\varepsilon_1=\varepsilon_2$), we can write:

$$E_c = f_1 E_1 + f_2 E_2 \quad (2.4)$$

Where E_c is the total modulus. E_1, E_2 and f_1, f_2 are the modulus and volume fractions of each phase, respectively.

Lower limit of reinforcement: isostress condition ($\sigma_c= \sigma_1=\sigma_2$)

The total deformation equals to the sum of deformation of each phase, so that $A_c\varepsilon_C L_c=A_1\varepsilon_1 L_1+A_2\varepsilon_2 L_2$, dividing by A_cL_c ($A_c=A_1=A_2$) to give:

$$\varepsilon_c = \varepsilon_1 \times \frac{L_1}{L_c} + \varepsilon_2 \times \frac{L_2}{L_c} \quad (2.5)$$

$$\frac{L_1}{L_c} = f_1; \frac{L_2}{L_c} = f_2; 1 = f_1 + f_2 \ (volume\ fraction) \quad (2.6)$$

So we can obtain:

$$\frac{1}{E_c} = \frac{f_1}{E_1} + \frac{(1-f_1)}{E_2} \quad (2.7)$$

2.4.2 Effects on the prediction of stiffness

There are many factors influencing the resulting stiffness of composites. These parameters mainly include the length-diameter ratio, orientation of fibres and strength of the bond between the matrix and the fibres [154]. The combination of them leads to the uncertainty in prediction of mechanical properties.

2.4.2.1 Effects of discontinuity of fibres

Unidirectional continuous fibre-reinforced

The isostrain condition can be applied in unidirectional-continuous fibres composite to calculate the longitudinal modulus (position (a) in Figure 24) by :

$$\frac{E_c}{E_m} - 1 = f_f \left(\frac{E_f}{E_m} - 1 \right) \quad (2.8)$$

Where E_m, E_f, and E_c represent the modulus of the matrix, the modulus of the fibre and the modulus of the composite, respectively. The f_f refers to the volume fraction of reinforcement phase.

This is widely used to estimate the transvers modulus (position (b) in Figure 24) in the unidirectional continuous fibres composites. In the transverse direction, the stresses acting on the two components can obey the inverse rule of mixture. The transverse modulus could be therefore written as:

$$\frac{E_c}{E_m} = \frac{E_f}{f_f E_m + (1 - f_f) E_f} \tag{2.9}$$

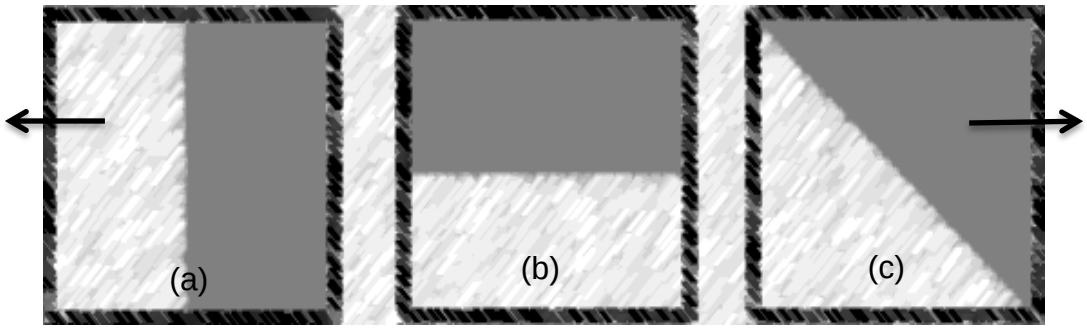

Figure 24. Interface situations between matrix and fibres (same loading direction).

This calculation is just idea and not applicable in some practical cases. The first problem is the Poisson effect in matrix caused by strain concentrations, so matrix modulus is divided by (1-Φ_m^2 (matrix Poisson ratio)) to introduce a 'constrained' modulus for modification [19]:

$$\frac{1}{E_c} = \frac{f_f}{E_f} + \frac{f_m(1 - \emptyset_m^2)}{E_2} \tag{2.10}$$

In addition, the fibres in the transverse plane are not in an idealised geometry. The position (c) in Figure 24 clearly shows a condition, where shear stresses occur at the interface, hence neither isostress nor isostrain are applicable. The adhesion properties play a very important role in this situation, while the volume fractions are unimportant. The reinforcing efficiency of the upper and lower limits is shown in Figure 25. It is noted that no matter what the value of Ef/Em is, the transverse modulus increases more largely when more than 50% by volume of fibres are included in composites.

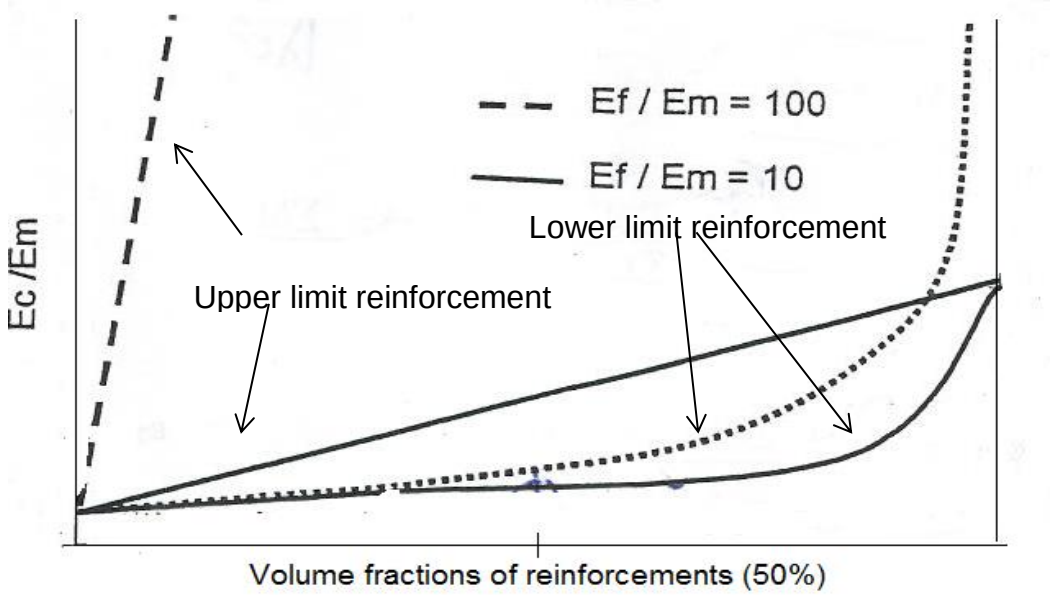

Figure 25. Representation of upper and lower limit modulus enhancement.

Unidirectional discontinuous fibre-reinforced

For a discontinuous or short fibre-reinforced composite under longitudinal force, it is observed that shear deformation develops at the two tips of each fibre meanwhile other parts undergo tensile deformation. Therefore, the upper and lower limits of reinforcement are partly applied in this situation.

New models have been tried to minimise or eliminate the prediction errors. Most of them are computational procedures to get exact data. Haplipin-Tsai interpretation can reduce many rigorous mathematical models to show the approximately relationships [19].

$$\frac{M_c}{M_m} = \frac{1 + \xi\eta\phi_f}{1 - \eta\phi_f} \tag{2.11}$$

$$\eta = \frac{\left(\frac{M_f}{M_m}\right) - 1}{\left(\frac{M_f}{M_m}\right) + \xi} \tag{2.12}$$

Where M_c , M_f, M_m are the modulus of composites, fibres and matrix, respectively. ξ refers to the geometric factor depending on the fibre length and loading conditions.

$$\xi = 1, \qquad for\ prediction\ of\ shear\ modulus$$

$$= 2\left(\frac{l}{d}\right), \qquad for\ prediction\ of\ young'modulus \qquad (2.13)$$

The Halpin-Tsai interpretation makes a great contribution to predict stiffness of unidirectional short fibre-reinforced composites.

2.4.2.2 Effects of the angle to the stress direction

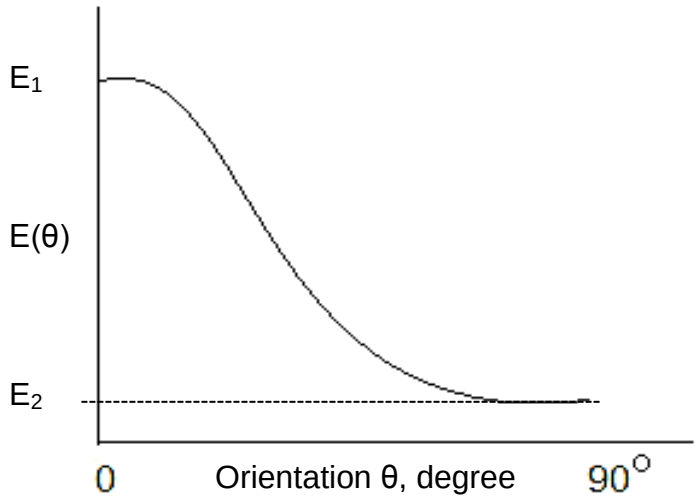

Figure 26. Dependence of Young's modulus, E(θ).

To suit design requirements in different directions, composites often contain some unidirectional plies at some specific angle to the applied stress. The orthotropic plate theory could give a basic understanding of the combination elastic properties of the multi-ply composites [19; 153]:

$$\frac{1}{E(\theta)} = \frac{cos^4\theta}{E_1} + \frac{sin^4\theta}{E_2} + \left(\frac{1}{G_{12}} - \frac{2\vartheta_{12}}{E_1}\right) cos^2\theta sin^2\theta \qquad (2.14)$$

2.5 Key findings of the literature review

Flax fibres with good mechanical properties (e.g. high tensile strength up to 1000 MPa) and physical properties have been reported as a potential reinforcement replacement for composites used for non-structural and structural applications. It is inevitable that the inherent detriments of flax, including moisture adsorption and incompatibility with some polymeric system due to high hydrophilicity, present lots of challenges with respect to the composite design

and applications. Various chemical treatments, such as mercerization, silane treatment and benzoylation etc., of flax fibres can improve the interface between fibres and matrix.

The flax fibre composites have a wide range of properties, depending on the matrix type, such as thermoplastic, thermosets and biomaterials. Flax/PP composite is the most commonly studied composite and has been commercially used in automotive applications (e.g. vehicle panels). Anhydride treatment is a very efficient way to improve the flax/PP adhesion and hence the mechanical properties. The humidity sensitivity is still a problem as it decreases the long-term material properties. The properties of flax/epoxy composites are strongly influenced by the processing methods and fibre lay-up configurations. Resin transfer moulding and compression moulding are preferred for high performance flax/epoxy composites. The mechanical performance at similar conditions could follow the fibre form trend: plain weave type < twill type < dobb type. The investigation of flax/bio-epoxy composites is mainly on epoxies derived from soybean oil and the final composites have similar independent factors to flax/epoxy composites. Flax/tannin composites have been studied just in the last 2-3 years, mostly for potential automotive applications. Also, the use of nanotechnology (flax nanofibres and the addition of nanoclays in flax composites) highly improves the mechanical performances, giving a good outlook for future development. However there is missing engineering database (e.g. processing method, treatment approaches, mechanical performances, environmental resistance etc.) on flax/tannin and flax/innovative bio-epoxy composites with high fibre content (over 50 $_{wt}$%) to enable future engineers with dataset that they can use to design products. Based on the missing information, the literature gaps are discussed and detailed in previous chapter 1.

Chapter 3. Influence of fibre configurations and surface treatments on properties of flax fibres

3.1 Introduction

Over the recent years, flax fibres derived from flaxseed straw are being looked at in a whole new light. For a long history, Flax fibre is being utilised in the textile industry for making durable materials, and also in the paper industry where it is used in many products like cigarette paper. Nowadays, flax fibres have been used as laminate reinforcements with polymer matrix materials to form natural composites, providing outstanding environmental benefits and other characteristics such as reduced cost and light weight. It is very important to know the properties of the fibres that form the composite in order to correctly guage the performance of the composites.

Load-bearing properties of resulting composites depend on fibre configurations (laminate type, fabric arrangement angles etc.) with different fibre property performances [67; 155-157]. The properties of technical fibres and elementary flax fibres have been mostly investigated in the research [158; 159]. Technical fibres extracted from plants are composed of 10-14 elementary fibres (2-5 cm long, diameter of 5-35 μm). Elementary fibres are held together by pectin and hemicellulose, which exists mainly in the primary and second cell wall as inter-fibrillar matrix. It was reported [72] that the tensile strength of elementary fibres could go up to 1000-2000 MPa, while that of technical fibres could increase with decreasing gauge length. The technical fibres tested at gauge length of 80 mm had the strength of 250 MPa with a big variation around 150MPa. This observation indicates the inconsistent properties using technical fibre. Hence, short fibre non-woven mats and woven fibre fabrics are introduced to make composites so as to offer stable enhancement.

Fibre pre-treatments, used to reduce the incompatibility between hydrophilic natural fibre and hydrophobic polymer matrix, also greatly influence the fibre properties, such as thermal stability and mechanical properties, influencing the final performances and applications [87; 160; 161]. The hydroxyl groups in flax

fibres can be modified for hydrogen bonding or to introduce new moieties that form effective interlocks with matrix [162]. Due to the dissolution of pectin and hemicellulose (mainly in primary cell wall), rougher fibre surface is created to enhance the fibre/matrix wettability. Mercerisation, acetylation, silane treatment, enzyme and some other treatments are commonly used for flax reinforced composites [81; 163; 164]. The previous literature review has detailed these treatment methods and their reaction mechanisms. Determining the thermal degradation of flax fibres is crucial to the development of natural fibre composites for ensuring good composites with wide operating and service temperature range. The thermal degradation of fibres is affected by the chemical content and the energy to breakdown the chemical bonds or to degrade the chemicals [74; 165]. Ahmed and his co-workers [166] pointed out the addition of $M_g(OH)_2$ can produce low combustible flax/PP composites with improved thermal stability. Saiah et al. [147] referred that the wheat flour thermoplastic based flax composites showed a great observed mass loss in 300-360°C, contributed by the fibre content. Bledzki et al. [88] reported that the degradation temperature of flax fibres increased from 319°C to 360°C after acetylation (34% acetylation). The thermal stability of flax fibres increased after alkali treatment due to the composition change of the removal of lignin and hemicellulose [89]. In addition to the thermal stability, the surface treatment may have a great effect on mechanical properties of fibres, mainly the tensile strength, directly influencing the reinforcement efficiency. Li and his colleagues [167] observed a decrease in flexural modulus (-6.1%) for MPS-g-PLA (Polylactide grafted r methaacryloxypropyltrimethoxysilane) treated sisal/PLA composites in comparison to the untreated composites.

It is necessary to study fibre reinforcement efficiency with various configurations and treatments before developing new flax bio-composite systems. This chapter is divided into two parts: the effects of (1) fibre configurations and (2) treatments on flax properties to build structure-property relationship database. SEM and optical microscopy were used to ascertain the fibre morphology and to obtain the diameter of elementary fibres and fibre bundles. Tension tests of flax fibres (various configuration and pre-treatments) were conducted based on the ASTM

standards (seen in the methodology). The chemical changes of flax fibres after pre-treatments were evidenced by the Fourier transformation infrared spectroscopy (FTIR) spectrums. The effects of fibre pre-treatments on thermal properties and kinetics were investigated through thermal gravimetric analysis (TGA). The tension properties of non-woven flax mats after treatments were obtained as well.

3.2 Methodology

3.2.1 Materials

Part 1-Configuration.

Considering the cost and production feasibility, flax fibres in the form of non-woven mats (carding/cross-lapping/needle punching) and woven fabrics were purchased (Table 8 and Figure 27). The non-woven flax mats are very thick and show an inhomogeneous appearance owing to the presence of coarse and short fibres among thinner filaments. The UD fabrics have more fibre bundles in the warp direction than in the weft direction to form the woven shape with good longitudinal strength, while the balanced fabrics show even fibre bundle distribution in both principle directions.

Table 8. Physical properties of studied flax fibres.

Type	Dry fabric areal (g/cm^2)	Thickness (mm)	Supplier
Non-woven mat	600	3	Ecotechlin
UD fabric	180	0.35	LINEO
Balanced fabric	300	0.6	LINEO

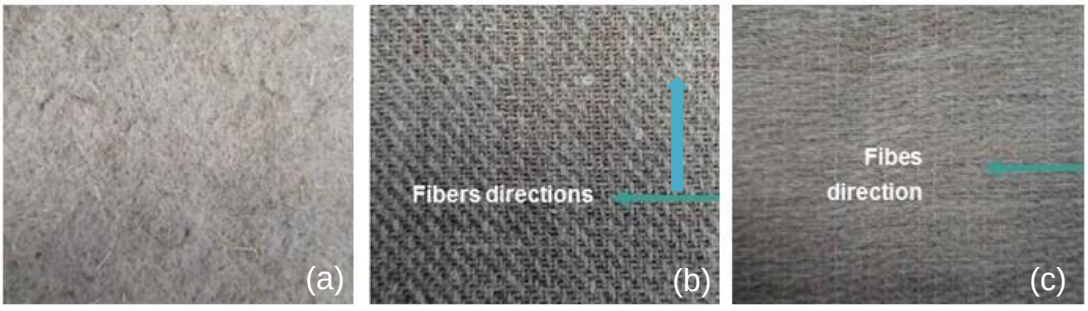

Figure 27. Flax fabrics (a) non-woven; (b) balanced fabric; (c) UD fabric.

Part 2-Treatment.

Non-woven flax fibre mats were sent to Valtion Teknillinen Tutkimuskeskus (VTT Ltd) for surface treatments as below:

The mercerization (NaOH) was made by immersing the flax mats into 5 $_{wt}$% NaOH solution for one hour, washing them two times thoroughly with water and drying in 50 °C for 12 h. It was made as pre-treatment for butanetetracarboxylic acid (BTCA) and amiopropyltriethoxysilane (APS) treated mats.

The BTCA treatment was done by spraying 2.5 $_{wt}$% BTCA-water solution on both mat surfaces to contain 5 $_{wt}$% of BTCA (Butanetertracarboxylic acid), followed by heating at 80 °C for 20 min and drying at 50 °C for overnight.

APS- treatment was done with ethanol (98%): water-solution (80:20) containing 1 $_{wt}$% APS (Amionproply triethoxy siloxane). The mats were sprayed 'full' with solution on both sides and let stand in room temperature for 2 h. APS was attached on fibres in heat oven at 80 °C for 4h followed by washing with ethanol-water solution and water and drying in heat oven in 50 °C for overnight.

The laccase Doga (LD) treatments were carried out as described in the following steps: a) wetting of the samples with distilled water, b) activation with laccase, c) treatment with DOGA, d) rinsing with water and d) drying. Activation of the wetted samples was carried out by spraying commercial laccase solution (Ecopulp) on both sides of the samples and placing the samples into plastic bags and submerging them into water bath of 45 °C for 30 min. Thereafter DOGA solution at a molar dosage of 0.12 mol/g was poured onto both sides of the samples and the plastic bags were placed back into the water bath of 45 °C for additional 90 min.

3.2.2 Characterisation and tests

Part 1-effect of fibre configuration

3.2.2.1 Scanning electron microscope (SEM)

Single/elementary fibres from non-woven fibre mats were examined using a XL30 SFEG analytical high resolution scanning electron microscopy (SEM),

supplied by FEI. The fibre cross section was considered as round shape for area prediction. The images were analysed using Image J software.

3.2.2.2 Optical microscopy

Optical microscopy was used to analyse the diameter of flax bundles separated from UD and balanced fabrics. Due to the residual waviness, measurements were taken from images of 5 bundles each sample at different locations with the help of Image J, identifying the fibre edges and determining the diameter. The bundles were also considered as round for the sake of simplicity.

3.2.2.3 Tensile testing

Tensile properties of untreated flax fibres were grouped into two parts: (1) on fibre bundles; (2) on untreated fibre fabrics/mats. ASTM D 3379-75 standard was adopted for the tests on flax fibre bundles. The tests for fibre fabrics and mats were based on ASTM D 5035-11 standard. Normal statistical and Weibull analysis was adopted (seen in Appendix 1).

Tensile testing on fibre yarns

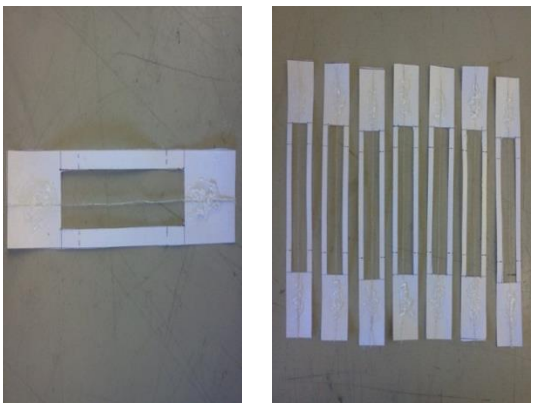

Figure 28. Fibre fixed on a paper frame.

Flax bundles were manually drawn from the woven fabrics. According to the preparation procedure of ASTM D 3379-75, flax fibres were cut at the required distance and glued by an epoxy adhesive into a paper frame as shown in Figure 28. During mounting, the specimens were handled only by the paper frame. The tests were carried out on an electromechanical Instron 5/100KN 5500R machine. Load displacement curves were recorded during the test. Two

aluminium plates were placed at both sides of each paper frame end to give a flat clamping face. Before their tensile fracture, the paper frame was cut allowing the undisturbed loading of the fibre as seen in Figure 29.

Tensile testing was performed at an ambient temperature at a deformation rate of 1 mm/min with a load cell of 5 KN. At least 20 fibre bundles were tested separately at two clamping lengths: 40 and 75 mm. A Weibull statistics model was applied due to the independent nature of fibre bundles.

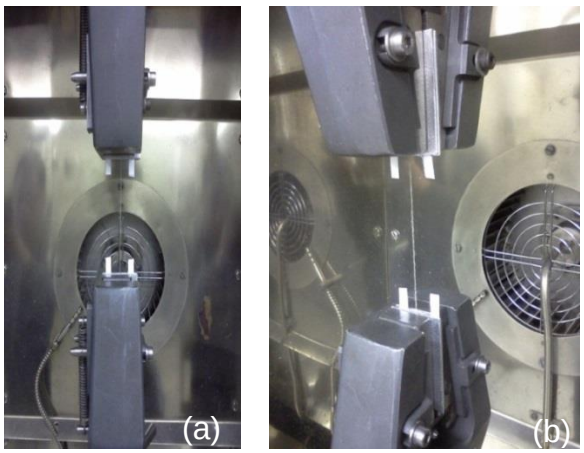

Figure 29. Experimental set-up of tensile tests on flax yarns (a) clamped paper frame; (b) side section of clamping jaws.

Tensile testing on flax fabrics with different configuration and treatments

According to ASTM D 5035-11 standard, ravelled and cut strips were prepared for woven fabrics (UD and balance) and non-woven flax mats, respectively. The specimen size was 150X25 mm. The tensile tests were conducted with a gauge length of 75 mm and a loading rate of 300 mm/min. A 5KN load cell was applied. The use of aluminium plates was necessary to give a tight clamping. At least 4 specimens were tested for each sample type.

Part 2-effect of fibre treatment

3.2.2.4 Fourier transformation infrared spectroscopy (FTIR)

FTIR spectroscopy was carried out with a shimadzu FTIR 8400S to characterize all the samples to identify the chemical change of flax fibres. The scan number was 64 per minute with the band range from 600 to 4000 cm^{-1}.

3.2.2.5 Thermal gravimetric analysis (TGA)

The thermal analysis of untreated and treated flax fibres was carried out by a TGA STA 449 instrument supplied by NEZSCH (as shown in Figure 30) at Cracow University of Poland. Around 20 mg of each specimen was heated from room temperature to 600°C at the heating rate of 10 °C/min.

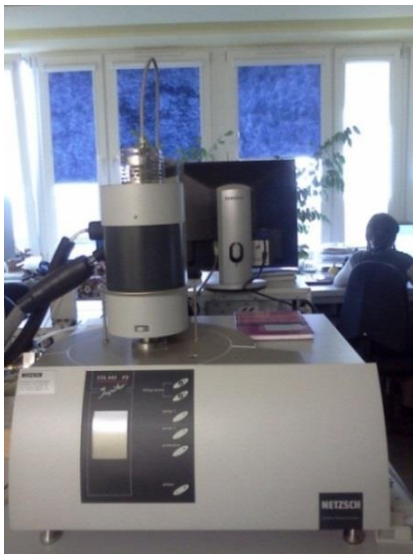

Figure 30. TGA equipment for thermal analysis.

3.2.2.6 Tension tests on fibres with different treatments

To investigate the influence of chemical surface treatments on mechanical properties of flax fibres, the tension properties of treated flax fibre nonwoven mats were also tested (ASTM D 3055-11) for the purpose of comparison with the properties of virgin fibre mats.

3.3 Results and discussion

Part 1-effect of fibre configuration

3.3.1 Microscope on single fibre and fibre bundles

SEM micrograph

Figure 31(a) shows the SEM image of elementary flax fibres selected from non-woven mats and fibre yarns separated from flax fabrics. The length of

elementary fibres was unknown as the fibres were partially folded. It was noted that the elementary fibres were not separated completely as evident from some tight-contacted single fibres (Point A). The obstacles on the fibre surface was believed to be the remaining pectin after the separation of elementary fibres through the pectin interphase. Point B indicated the kink bands, which were introduced by the isolation process, but not from growing. Kink bands tend to be weak points as local stress concentrations by which cracks occur easily over other positions under overloading [67]. The presence of kink bands can be minimised through deterioration process to reduce their negative effect on fibre properties. Diameter of single flax fibres varies in different fibre and different locations. The average diameter from Image analysis is shown in Table 9.

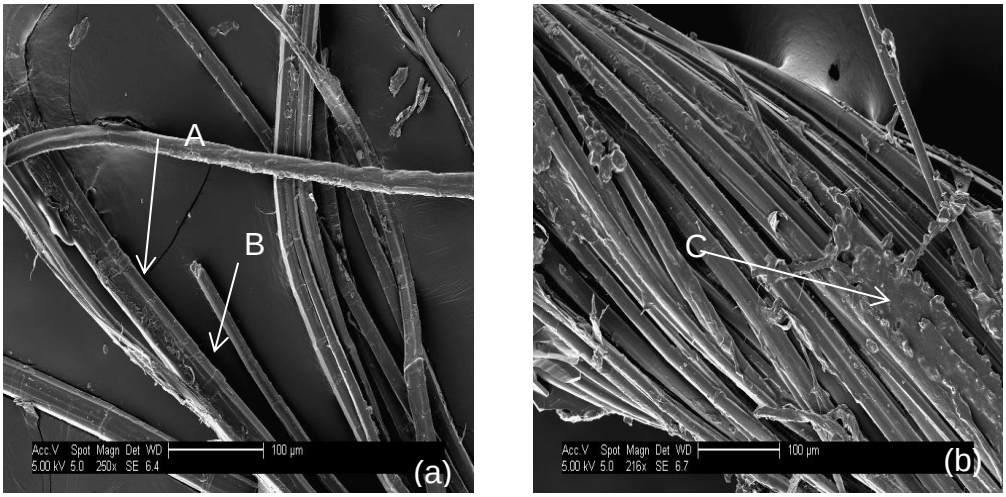

Figure 31.SEM images of flax fibres (a) elementary flax; (b) flax bundles.

Table 9. Diameter of studied flax fibres.

Fibre Diameter (mm)	Mean	SD	Min	Max
Elementary fibre	0.032	0.005	0.028	0.035
Fibre yarn (UD)	0.278	0.02	0.221	0.316
Fibre yarn (balance)	0.494	0.069	0.379	0.646

Figure 31(b) showed the topography of flax yarns. Obviously, the flax yarn was a cluster of single/elementary fibres. There was a lack of interphase bonding observed although a few fibres still bonded together as pointed by area ‘C’. It could lead to the weak intra-fibre shear strength and possible fibre slippage

during tension. Since it was difficult to determine the boundary line of fibre bundles in SEM images, optical microscopy images, discussed later, gave more accurate diameter measurement.

Optical microscopy

The optical images and post-analysed images of flax bundles from UD and balanced woven fabrics are respectively shown in Figure 32. According to the figures, there were some elementary fibres detached/pulled out from the fibre bundle. Both bundle types exhibited some degree of waviness as they were woven to form fabric. At least five bundles for each type were taken for optical scanning at different locations for image analysis (examples seen in Figure 32). Table 9 displays diameters of flax fibre bundles.

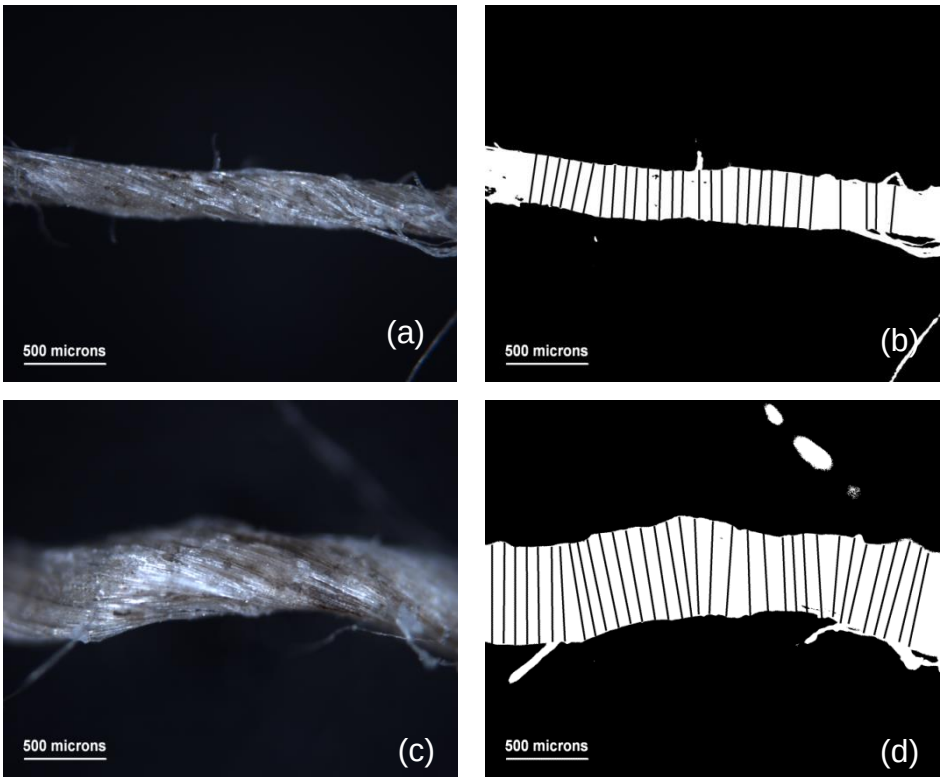

Figure 32. Typical optical images**:** (a) origin flax (UD); (b) post-analysed flax (UD); (c) optical origin flax (balance); (d) post-analysed flax (balance).

3.3.2 Tensile characterisation of fibre bundles and fibre fabric

Cellulose and hemicellulos are the main chemical components of flax fibres, and thus strongly control the mechanical properties. The strong hydrogen bonds

formed between cellulose molecules offer the stiffness to flax fibres. The chief portion of the cellulose is arranged in crystallites with interspersed amorphous regions. The highly crystalline structure of the secondary cell wall makes the fibre strong in the length direction. However, due to the orientation of the crystallites and the presence of amorphous regions between crystallites, both stiffness and strength of flax fibres are expected to differ greatly.

Tensile behaviour of fibre yarns

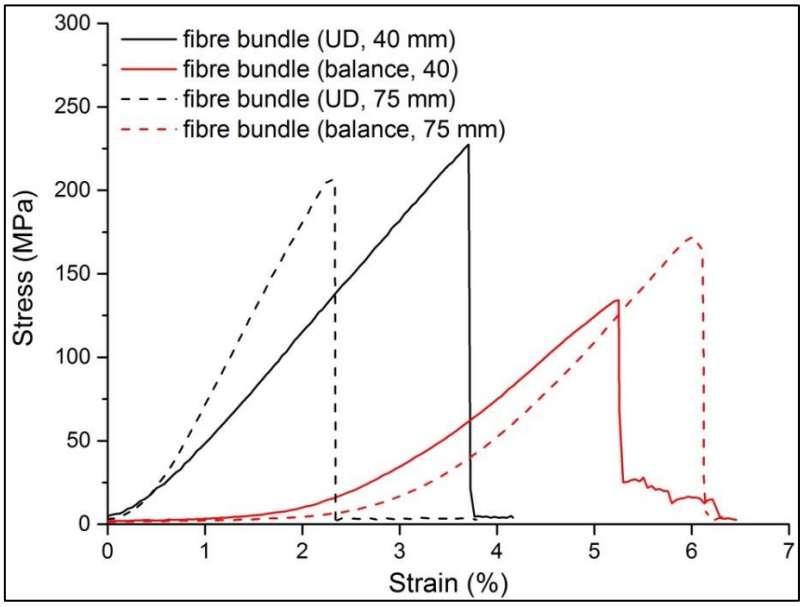

Figure 33. Typical stress-strain curves of tested flax bundles.

The indicative stress-strain responses of the two types of flax fibre bundles (UD and balance) are shown in Figure 33. Stress was determined by dividing applied force with the apparent circular cross-section area. The macro-strain was obtained using the machine recorded displacement. The initial strain with little stress increase for all fibre bundles is attributed to the stretching phenomenon of twisted fire bundles. The subsequent loading was linear elastic up to the maximum stress. There was little plastic deformation in the fibre upon straining due to the fact that the amorphous regions between cellulose micro fibrils were already oriented, and therefore not capable of deforming plastically. Charlet and Beaku [155] reported two breaking points in a Z-like peak. The first damage point indicated the beginning of the sliding. The following rupture point corresponds to the failure of interphase. Only the damage point was noticed in

author's stress-strain curves, indicating the lack of interphase between elementary fibres.

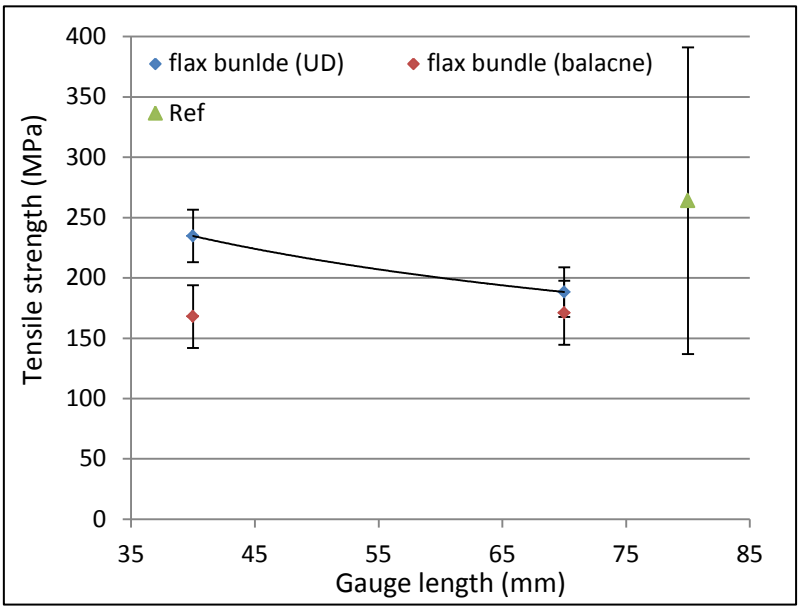

Figure 34. Dependence of gauge length on tensile properties (ref [155]).

The tensile strength of flax bundles at 40 and 75 mm clamping length are shown in Figure 34. The macro-strain was improper to present the real fibre strain due to the uncertain fibre slippage; hence the modulus calculation was not done. However, the tensile strength of flax fibres was more reliable. The flax fibres (UD) with smaller diameter showed tensile strength around 39% higher than that of flax fibres (balance) at the gauge length of 40mm. As empty space or voids exits between elementary fibres, the fibre number per unit area may increase with decreasing the yarn diameter. The strength of flax fibre bundles (UD) at a clamping length of 75 mm was around 196 MPa, which increased to 240 MPa by reducing the gauge length to 40 mm. The same effect of clamping length on tensile strength was also found by Romhany et al. [156]. At the clamping length below the elementary fibre length (20-50mm), the crack propagation is less able to follow the pectin interphase, but has to take place through the elementary fibres with strong cell walls. The reduction of presence of critical flaws also contributes to the strength increase with decreasing gauge length. It was likely that with long clamping length, fibre failure occurred at the relatively weak points, such as kink bands and pectin interphase, resulting in

slippage and breakage. The gauge length had much less effect on strength of fibre bundles (balance), indicating that the fibre slippage may dominated the failure mechanism for this bundle type. Figure 35 displays the fibre (balance) after the damage point during tension. The fibres slipped apart in the middle of the gauge section as a result of shear failure of the interphase.

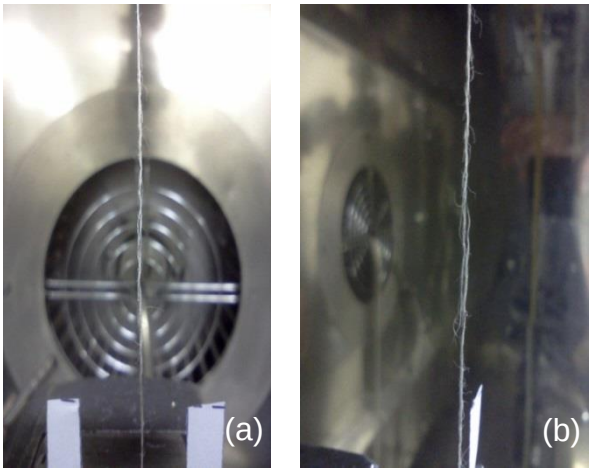

Figure 35. Failed fibre bundle (balance): (a) front view; (b) side view.

The flaws and weak interphase areas are randomly distributed along the fibre bundle length; as a result, no two supposedly identical bundles will have the same strength, just like ceramics. A simplified Weibull equation usually used to describe ceramic failure strength is adopted:

$$P_s\,(V) = 1 - \exp\left[V\left(\frac{\sigma - \sigma_u}{\sigma_0}\right)^m\right] \tag{3.1}$$

Where $P_s(V)$ is the probability of survival for a sample of volume V, σ is the applied stress, σ_u is the zero point stress at which $P_s(V)=1$ (usually made equal to zero), σ_0 is a normalizing constant (usually made equal to σ_m, the mean strength of the samples), m is the scale parameter in Weibull distribution. The equation can be further transferred into:

$$\ln\left[\ln\left(\frac{1}{P_s\,(V)}\right)\right] = lnV + m\ln\left(\frac{\sigma - \sigma_u}{\sigma_0}\right) \tag{3.2}$$

At $\sigma_u=0$, the value of $\ln(\sigma/\sigma_0)$ is linear to $\ln(\ln(1/P_s))$ with the slope of m. The relationships obtained from the fibre failure strength were plotted in Figure 36.

Details of the calculations are shown in Appendix 1. The fitted m value presented the reproducibility or reliability of strength values in a range of fibre bundles. The higher the m value, the better the reliability of the samples. The m value for all tests is over 10, which is not extremely good but very typical in failure strength measurements.

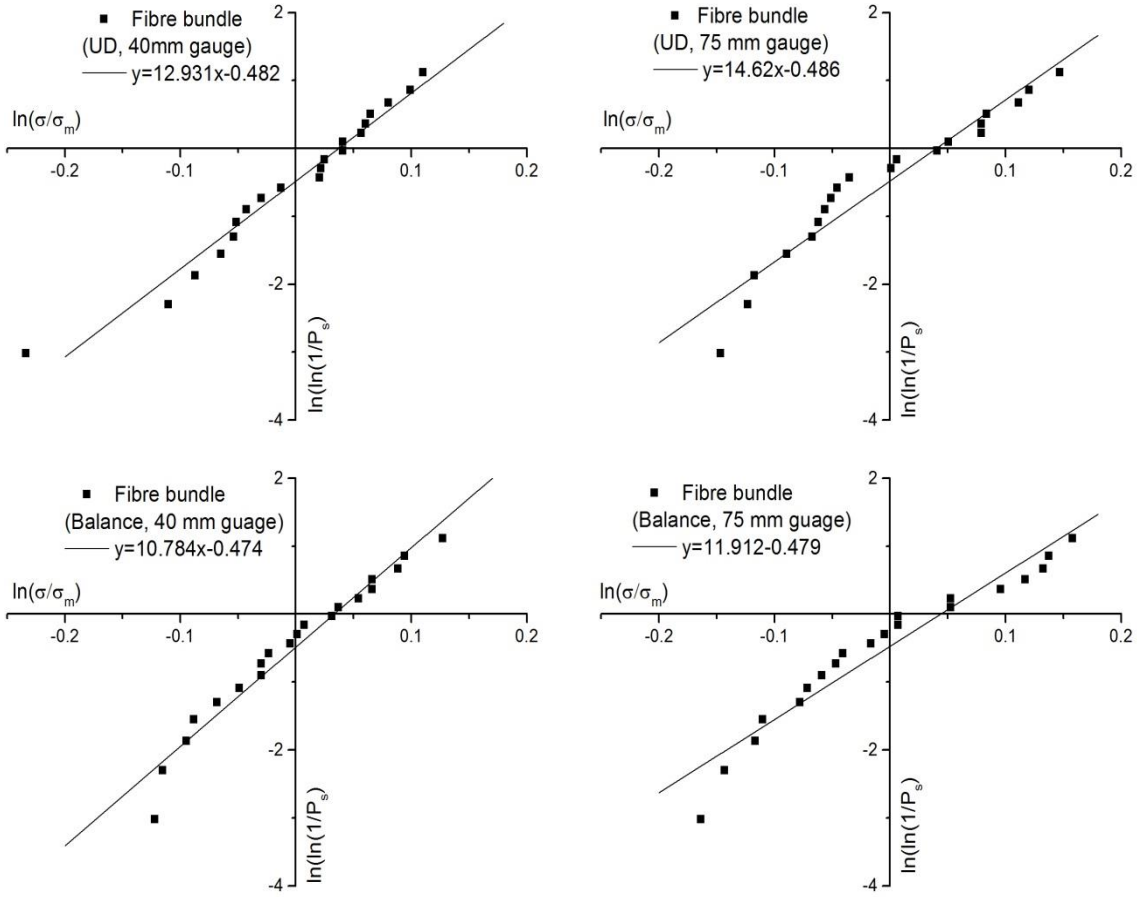

Figure 36. Weibull plots of survival probability versus applied stress for UD and balance fibre bundles with the 40 mm and 75 mm clamping length.

Tensile properties of fabrics

The tensile properties, such as breaking force and apparent elongation, of flax fabrics are summarised in Table 10. UD woven fabric showed 21% increase in the breaking force than balance woven fabric. Non-woven flax mat showed a much lower breaking force due to the lack of fibre orientation in the tension direction. In terms of the apparent elongation, non-woven flax mat represented the highest value of around 50%. The high apparent elongation of non-woven

mat is the consequence of the re-alignment of flax fibres in the load direction. Figure 37 shows a plastic-deformation-like behaviour of non-woven flax mat, which may have a bearing on the plasticity of the composites.

Table 10. Tensile properties for flax fabrics.

Type	Number of bundles	Breaking force (N)	Apparent elongation at max load (%)
Non-woven mat	-	131.2±5.3	48±4.2
UD woven	50±7	892.5±14.5	4.3±1.2
Balanced woven	25±5	732.1±83.9	5.1±2.9

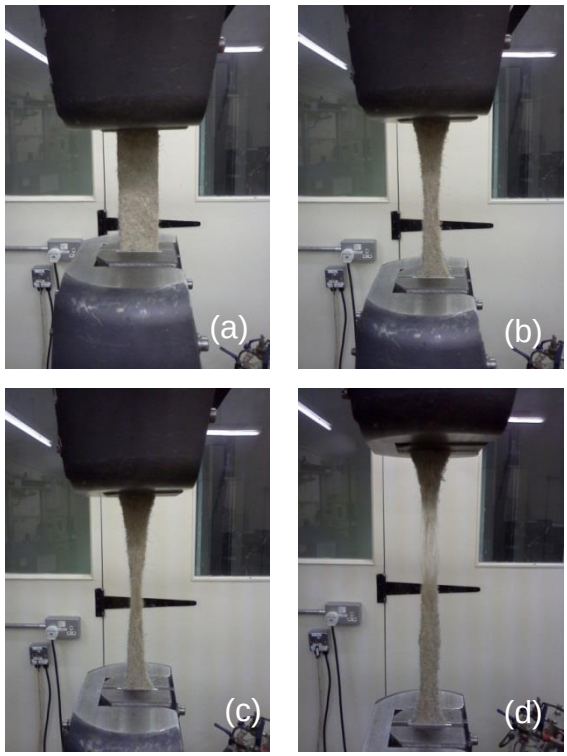

Figure 37. Tensile deformation of the non-woven mat (from a to d).

Part 2-effect of fibre treatments

3.3.3 Effects of fibre pre-treatments on fibre compositions

The flax fibre mainly comprises of polysaccharides including cellulose (64.1%), hemicellulose (16.7%), pectin (1.8%) and lignin (2.0%), with minor components such as bound water, waxes, and other inorganic materials. The fibrills of

cellulose in the crystalline form are deposited within the hemicellulose and lignin acting as an amorphous phenolic polymer matrix. Pectin found in the primary cell wall of the fibres contains strong polar carboxyl groups (COOH), resulting in poor interfacial compatibility to non-polar compounds like polypropylene. Garside and Wyeth [1] introduced the use of Fourier transform infrared (FTIR) with attenuated total reflectance (ATR) spectroscopy technique. FTIR-ATR could identify and distinguish cellulosic fibres (e.g. flax, hemp, jute etc.) as an alternative simple and highly reproducible way to micro-spectroscopy. Through the ATR FTIR spectroscopy, the predominant components of flax fibres (cellulose, hemicellulose, prectin and lignin) were identified and analysed at certain associated peaks.

Table 11. Infrared band characteristics for neat flax fibres.

Position/cm^{-1}	**Assignment**	**Belonged chemicals**
~3335	v (OH) free	-
~2850	v (CH2) symmetrical	Organic compounds
~1735	v (C=O) ester	Pectin
~1635	Adsorbed water	All the chemicals
~1595	v (C=C) aromatic	Lignin
~1505	v (C=C) aromatic	Lignin
~1155	v (C-C) ring breathing	Largely from cellulose
~1105	v (C-O-C) glycosidic	Cellulose

*v-vibration mode

Based on the reference data [98], the important characteristic band assignments for neat flax fibres are summarised in Table 11. The peak at around 1735 cm^{-1} is associated with C=O stretching for ester groups, indicating the presence of galacturonic acid from prectin in the fibres. Two peaks appearing at around 1600 cm^{-1} and 1505 cm^{-1} are attributed to the aromatic C=C in-plane stretching from lignin, However, as indicated in the literature [2], if there is absorbed water in crystalline form, due to the hydrophilicity of cellulose elements, the broad peak at 1600 cm^{-1} should be the result after overlap between water and aromatic C=C bands (lignin). The cellulose structure peaks

were at 1158 cm^{-1} and 1105 cm^{-1}, accounting for the asymmetric v(C-C) ring breathing and the v(C-O-C) glycoside ether bands, respectively. Two peaks for other non-aromatic organic materials in flax fibres were also observed as sp3 C-H stretching at around 2900 cm^{-1} and symmetrical CH_2 stretching at 2850 cm^{-1}.

5wt% NaOH.

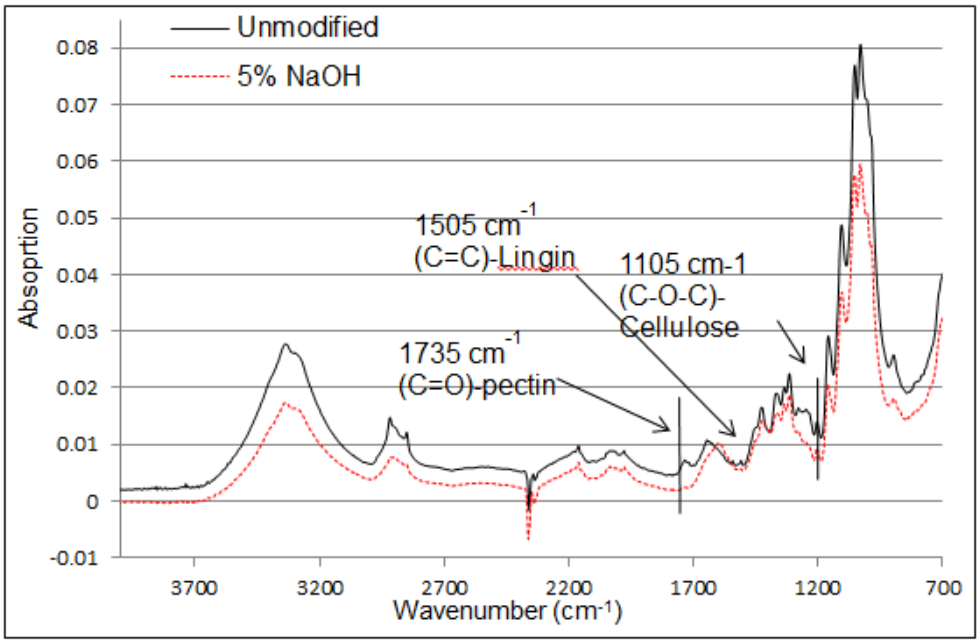

Figure 38. FTIR spectra of unmodified and NaOH treated flax fibres.

There was no big difference for the major chemical constituents between unmodified and 5 $_{wt}$% NaOH mercerised flax fibres due to the similarity of the two spectrums as shown in Figure 38. However, the peak around 1735 cm^{-1} standing for the existence of pectin has disappeared in the FTIR spectra of flax fibres modified with 5 $_{wt}$% NaOH. The absence of this peak is attributed to the removal of the pectin component within the primary cell wall. The peak at 1505 cm^{-1} disappeared, showing the removal of the lignin after alkali treatment. As a result, the presence of absorbed water mainly contributes to the peak shifting to 1582 cm^{-1}, a lower frequency compared to 1632 cm^{-1} for the IR spectra of unmodified flax fibres. A possible explanation in this case is that the crystalline form containing absorbed water has been transferred from the crystalline lattice of cellulose-I to cellulose-II with better thermodynamic stability. The distance between lattice planes was expanded by replacing OH groups with bigger ONa

groups. Scientific work [77; 168] has demonstrated three main effects of the sodium hydroxide modification on cellulose fibres: (i) transform of crystalline structure from cellulose-I to polymorphous cellulose-II; (ii) removal of non-cellulosic cementing constituents (pectin, lignin and hemicellulos), creating the rougher topography, smaller fibre diameter (increased aspect ratio) and weak interface between fibrils; (iii) neutralisation with substances like acidic hydroxyl groups and carboxyl groups to reduce the hydrophilicity.

NaOH+BTCA treatment

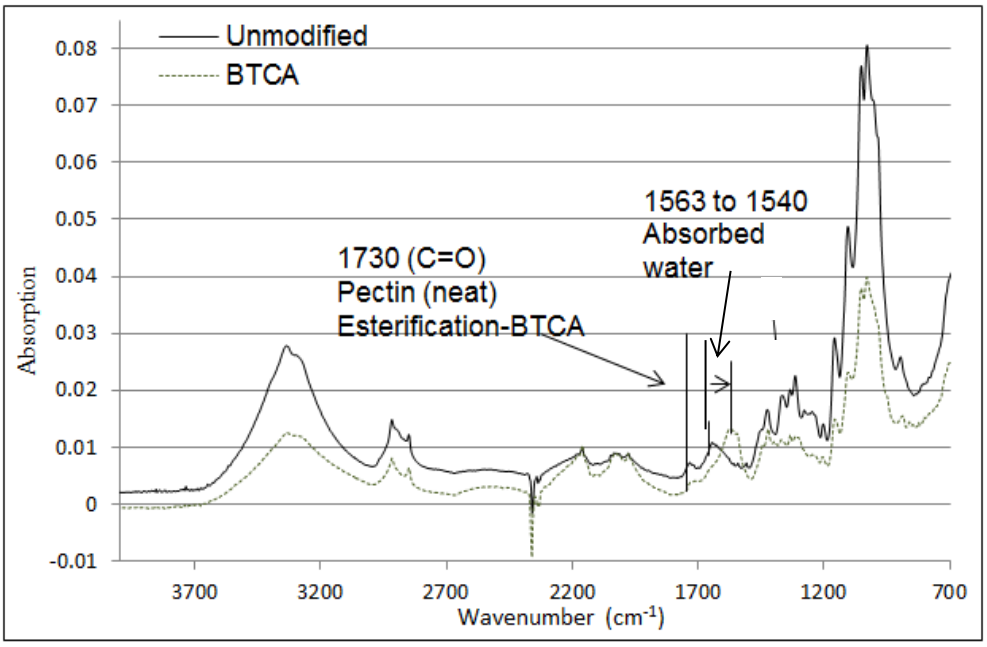

Figure 39. FTIR spectra of unmodified and BTCA treated flax fibres.

The most significant change in the FTIR spectra before and after BTCA treatment was observed in the range of 1500-1700cm^{-1} as in Figure 39. According to the reaction mechanism, the appearance of peak around 1730 cm^{-1} is related to the ester bonds introduced by BTCA reacting with OH groups, but not to the C=O bonds of pectin that were eliminated during the NaOH treatment. The peak (1635 cm^{-1}) representing the absorbed water in cellulosic crystalline shifted towards the low-frequency side (1563 cm^{-1}) along with a new partially-overlapped peak at 1540 cm^{-1}. The shift of the peak position is probably correlated with removal of the primary wall protecting from the water

penetration, while the absorption band at 1540 cm^{-1} is assigned to the carboxylate carbonyl via NaOH treatment.

NaOH+APS treatment

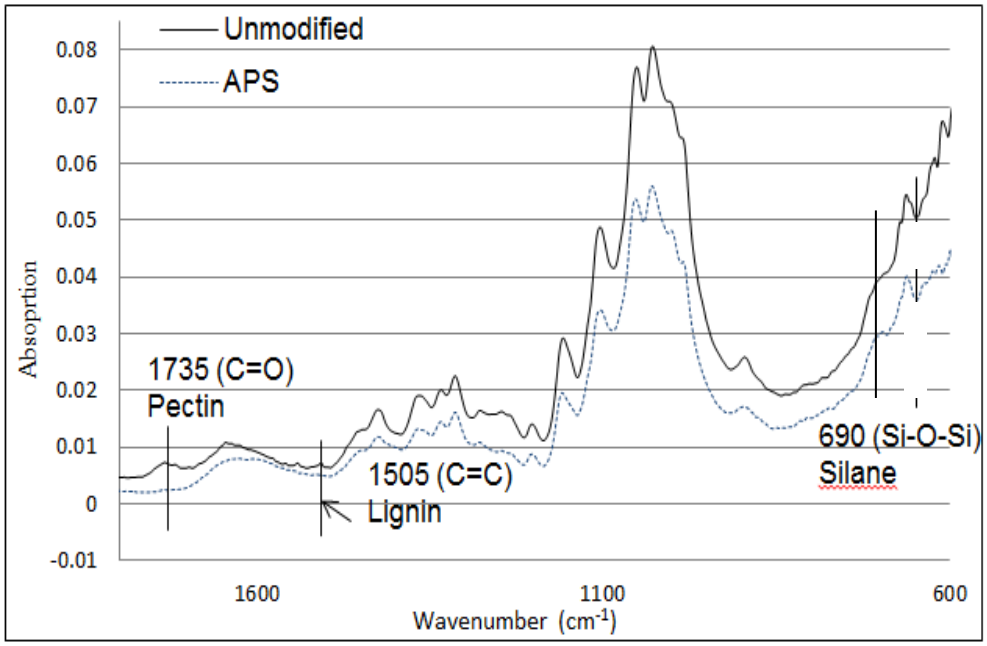

Figure 40. FTIR spectra of unmodified and APS treated flax fibres.

Efficiency of silane treatment, such as aminopropyl triethoxy siloxane (APS), was reported higher than for the mercerisation treatment because more reactive sites can be generated for silane reactions [86]. The function mechanism of silane treated fibres and polymer matrix was briefly described in the literature review. According to Figure 40, NaOH treatment before APS addition, which removed (fully or partially) the waxy epidermal tissues, lignins, adhesive pectins and hemicellulose, can account for the disappearance of peaks at 1735 cm^{-1} and 1505 cm^{-1}. In the APS treated flax fibres, the well-defined absorption band at around 690 cm^{-1} was obtained due to the symmetric stretching of –Si-O-Si- structure on the APS treated fibres derived. The increment of the peak intensity at 1000 cm^{-1} and 982 cm^{-1} was attributed to the presence of Si-O-C bonds derived from the silane chemical treatment. In addition, the Si-O-Si asymmetric stretching peak around 1060 cm^{-1} was completely overlapped with C-C ring breathing (cellulose) absorption band at 1055 cm^{-1}.

Laccase-Doga

Oxidative enzyme, laccase, was used to activate and further functionalise lignocellulosics. The primary reaction of laccase is the oxidation of phenolic hydroxyls to phenoxy radicals in the presence of oxygen. After laccase treatment, phenolic dodecyl gallates (Doga) were grafted to the fibre material to increase properties such as charge, hydrophobicity or bonding capability.

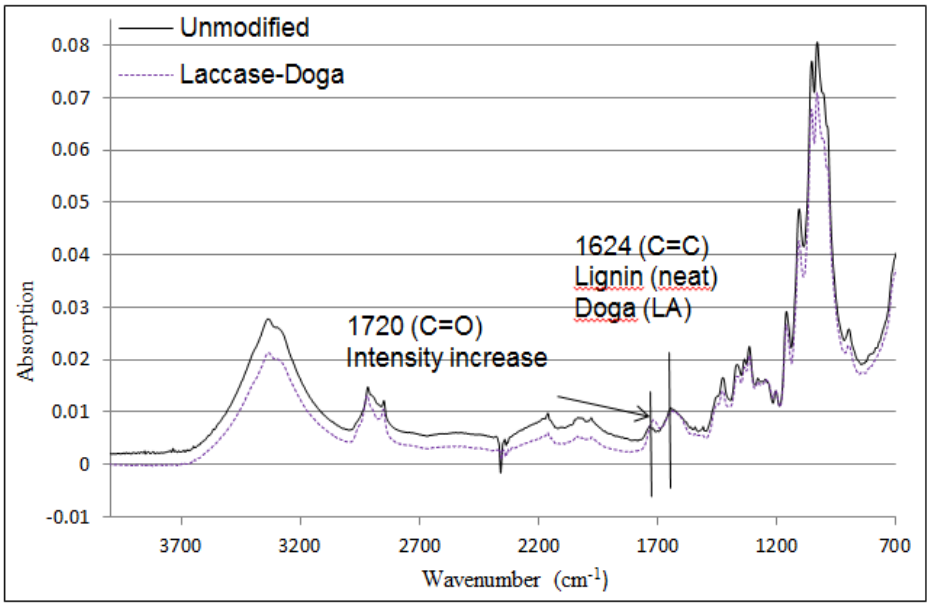

Figure 41. FTIR spectra of unmodified and Laccase-Doga treated flax fibres.

The IR spectrum of LD treated flax fibres are shown in Figure 41. The broad peak around 1624 cm^{-1} was contributed not only from the absorbed water and aromatic C=C from lignin, but also from aromatic C=C-C stretching vibration in Doga moiety. The intensity of the peak (around 1720 cm^{-1}) attributed to ester band C=O stretching was found to increase due to the new C=O bonds from Doga introduced via the laccase-activated graft polymerisation. Additionally, the shift of the peak from 1735 to1717 cm^{-1} indicates the presence of saturated ketone and suggests that the laccase oxidised the phenolic rings to quinone or cleaved the phenolic rings.

3.3.4 Effects of surface treatments on fibre thermal properties

Thermogravimetric analysis (TGA) uses heat to drive reactions and physical changes, providing a quantitative measurement of mass change in materials

associated with a transition of thermal degradation due to chemical dehydration, decomposition, or oxidation [169]. TGA analysis was undertaken for neat, NaOH, NaOH-BTCA and NaOH-APS treated flax fibres so as to investigate the effects of different treatments on their thermal degradation properties. The chemical changes in fibres during modifications certainly have an effect on their thermal degradations. From the TGA curves, data on moisture content, onset of degradation, main decomposition temperatures, degradation stages, residue contents and other thermal degradation characteristics was obtained.

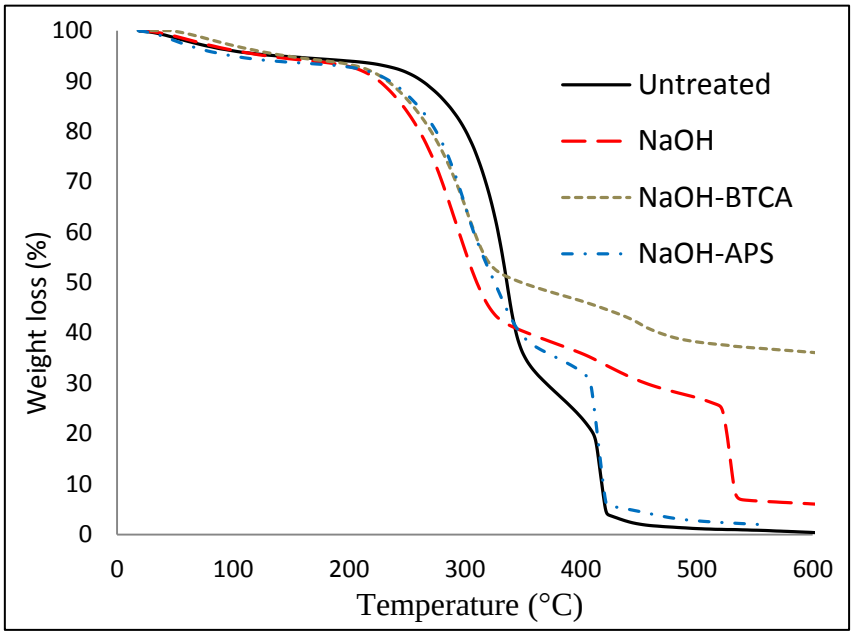

Figure 42. TGA curves of investigated flax fibres.

Figure 42 shows the mass-loss of flax fibres as a function of temperature. The decomposition profile of untreated flax fibres shows strong agreement to the typical TGA-air of flax fibres [74]. Cellulose is the main component of natural fibres, and thus controls the major degradation behaviour of flax fibres. The degradation routes for cellulose upon heating have been discussed in the literature [73]. The glycosyl units decompose at low temperature, followed by their depolymerisation at high temperatures. Then the substances like levoglucosan decompose into gas at higher temperatures. From Figure 42, it was obvious that some weight loss of around 5.47 % occurred up to 150°C due to the evaporation of (absorbed) water from the flax fibres. Then the biggest weight loss of 65.94% mainly due to the cellulose degradation occurring in the

temperature range of 250 to 380 °C, followed by the second weight loss of 24.99 %, referring to non-cellulose components (from 380 to 420 °C). After that, a weight loss of 3.28 % took place until 600 °C with a residual content of 0.32 %. The main decomposition temperature was obtained at 305 °C, which is similar to the temperatures observed in the literature [70; 85; 170]. Also, the onset of degradation was seen at much lower temperature of approximate 200 °C, in line with literature findings [35; 74; 171]. The onset of degradation of treated fibres was also observed around 200°C, whereas their decomposition temperature decreased from 305 °C to about 250-260 °C after the treatments. For the pure NaOH treated flax fibres, the non-cellulose decomposition was at a higher temperature of 500 °C than those of neat and NaOH-APS flax fibres, which were found around 410 °C (Table 12). NaOH-BTCA exhibited the lowest weight loss between 300-500 °C with 35 % residue, indicating the improved thermal stability for non-cellulose content.

Table 12. Summary of TGA results for treated and untreated flax fibres.

Flax type	Moisture ($_{wt}$%)	Main decomposition temperature (°C)	DTG peaks (°C)		
			1st	2nd	3rd
Untreated	5.47	305.5	50.2	336.5	417.4
NaOH	5.88	250.3	59.6	293.0	528.1
NaOH-BTCA	5.83	258.5	78.2	301.5	451.3
NaOH-APS	6.49	261.8	48.3	299.9	421.4

With regards to the moisture content, no hydrophobic enhancement of flax fibres after modifications was detected. Neat flax fibres had the water content around 5.5 %, while NaOH, NaOH-BTCA and APS showed slightly higher values. The highest water content of 6.9 % was displayed by the NaOH-APS sample. As noted earlier, one of the functions of alkali treatment is to remove the primary cell wall containing pectin with high moisture sensitivity. However, the new exposed fibre surface after primary wall removal was still hydrophilic due to the polar OH groups of cellulose and other polar ingredients.

To further understand the degradation of flax fibres, the resultant DTG (derivative thermogravimetric) curves (Figure 43) were used to present the

kinetics upon heating. For untreated fibres, the first DTG peak was broad and below 100 °C as a result of water removal. The second DTG peak is caused by cellulose degradation while the third DTG peak of around the 417 °C is largely attributed to the degradation of non-cellulose components. It is worth noting that the cellulose degradation continued after the first peak until 500 °C since cellulose suffered different degradation reactions depending on temperatures. Generally, in the temperature range from 300 to 500 °C, cellulose is first converted into active form to yield phenol, followed by the ring scission at approximately 340 °C to form anhydrosugars such as levoglucosan and formation of polycyclic aromatic compounds (350 °C) that mainly constitute the ash content in the 400-500 °C temperature range [73]. After the third DTG peak, most of the decomposition products integrated into tar, volatile hydrocarbons and condensable gases (e.g. H_2O, CO). It left around 0.3 % inorganic residue after 600 °C. Hornsby et al. [170] found that TGA of flax fibres showed nearly 10 % carbonaceous residue formed between 300 to 500 °C because of a nitrogen atmosphere. The degradation progressed much faster in air condition than in a nitrogen or inert atmosphere because free radicals are easier to generate in air. Amongst all the fibres, the highest 1st peak temperature of 80 °C of NaOH-BTCA sample suggests that BTCA treatment leads to strong hydrogen bonding with water. The second peak temperature related to cellulose degradation decreased from 336 °C of untreated fibres to the temperature range of 290-300 °C for all the modified samples. This may correlate to the increase of amorphous cellulose which the degradation began with. In addition, the 2nd peak magnitude, which is the maximum decomposition rate, of all modified samples decreased compared to that of untreated flax fibres. This reduced decomposition rate is attributed to the removal of part of lignin and hemicellulose, which exhibits lower degradation stability. The degradation of hemicellulos happened in the 200-280 °C, and the degradation at high temperature of 280-300 °C was from lignin (activation energies: hemicellulose-28 kcal/mol; lignin-25 kcal/mol) [32]. Many researchers [73; 172; 173] reported the positive influence of alkali treatment on thermal stability of natural fibres. The 3rd peak temperature of pure NaOH treated flax fibres was around 100 °C

higher than that of the untreated type. Apparently the thermal stability of non-cellulose part is highly improved by alkali treatment on flax fibres. NaOH-BTCA flax sample showed the lowest 3rd peak value, indicating that esterification may result in the slowest decomposition stage of non-cellulose components.

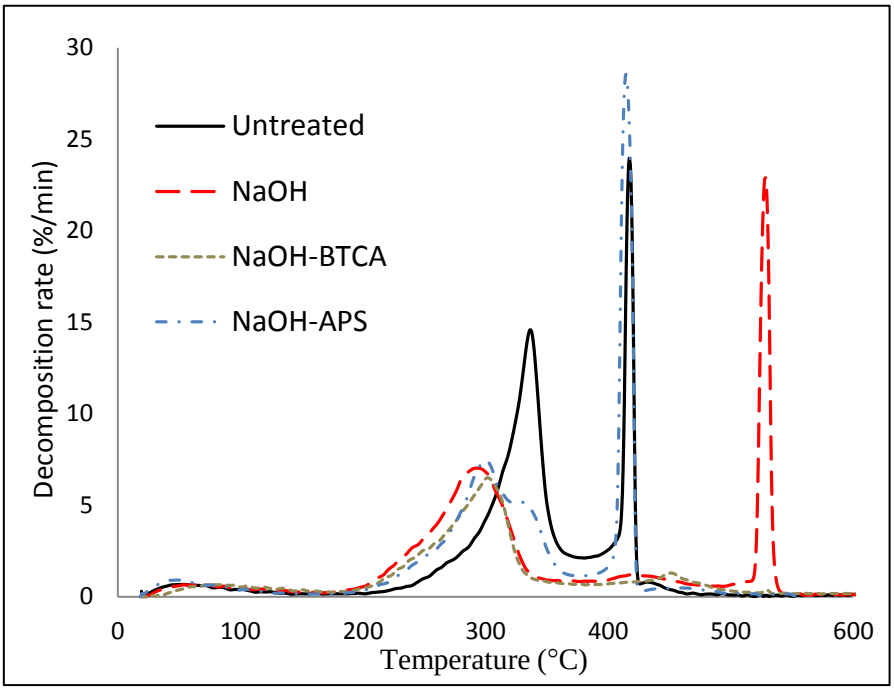

Figure 43. DTG curves of investigated flax fibres.

3.3.5 Effects of surface treatments on tension properties of fibres

Tension properties like breakage force and apparent elongation were obtained for the non-woven flax mats with and without treatments as shown in Table 13. Neat flax mats respectively exhibited the breakage force and apparent elongation of 131 N and 48%. From the results, to various extents, the surface treatments deteriorated the tensile properties of non-woven flax mats. NaOH+ APS treated fibres showed average values of breakage force around 110 N, about 20 N less than that of untreated flax fibres. The highest reduction of 33 % in peak load was observed for BTCA treated non-woven flax mats. As discussed before, the hemicellulose, pectin and lignin were partially removed from fibres after the treatments. However the excess removal of these constituents leads to the severe loss of inter-fibrillra matrix, causing less load transfer between elementary fibres in comparison with the virgin fibres. Singha

et al. [86] reported that the APS treatment destroyed packing of the cellulose chains to a certain extent, causing disorder in the crystalline pattern of the main polymeric backbone. The reduced properties of flax mats after acrylic acid and other acid treatment were also found by Erasmus and Anandjiwala [174], and were contributed to the possible fibre degradation resulting from the harsh treatment environment. However, hydroxyethyl-cellulose (HEC) treatment can improve the mechanical properties of stiffness of twist flax fibres by 75 % [175]. It can be concluded that the mechanical properties of flax fibres can be affected either positively or negatively by using different surface treatments.

Table 13. Effect of treatments on tension properties of non-woven flax mats

Type	Max. force (N)	Apparent elongation at Load peak (%)	Max elongation (load<10%)
Untreated	131.2±5.3	48±4.2	67.5±2.4
NaOH	107.1±2.1	45.6±3.5	60.9±2.6
BTCA	87.7±5.8	30.9±4.3	47.7±2.5
APS	109.6±10.2	45.0±4.7	58.5±3.8
LD	108.9±2.1	34.6±3.2	51.1±1.9

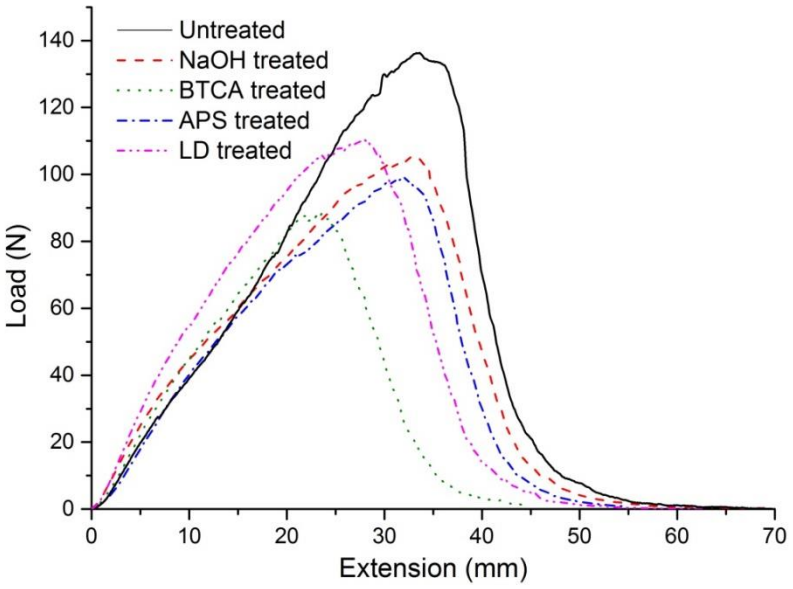

Figure 44. Load-displacement of representative non-woven flax mats with treatments.

In terms of the apparent elongation, non-woven flax mat represents the highest value of around 50 %. Again BTCA treated fibres showed the lowest elongation

value at 30 %. The high apparent elongation of non-woven mat is the consequence of the re-alignment of flax fibres in the load direction. Plastic deformation behaviour of non-woven flax mat during tension was shown in Figure 44. Due to the rule of mixtures for fibre/matrix composites, the decreased tensile properties of flax fibres may compensate the effect of improved fibre/matrix wettability. The resulting composite tensile performance may not be able to achieve the best improvement degree from the treatments.

3.4 Conclusions

The effect of fibre configurations and treatments on properties of flax fibres was studied. The tensile strength of flax bundles from UD and balance woven fabrics depended on the testing gauge length, and showed big variations. The non-woven mat displayed a low tension breaking force but a long extension. The physical changes like the removal of pectin and lignin (form the primary cell wall) during the NaOH treatment were verified by the disappearance of their characteristic IR band at 1735 cm^{-1} and 1505 cm^{-1} respectively. FTIR results also indicated the presence of cross-linked BTCA (ester bond) and the new APS (Si-O-Si) bond. As a result of the changes in fibre physical structure, the treated fibre can potentially provide good fibre/matrix contact. The onset degradation temperature for flax fibres occurred at around 200°C, indicating the processing and service temperature below 200°C. NaOH-BTCA was found to provide the best improvement on thermal stability of the non-cellulose content in the flax fibres. Additionally, the fibre tensile properties decreased to some extent after the treatments, possibly due to the loss of inter-fibrillar matrix or the degradation from harsh reaction environment. New bio-sourced matrix such as bio-epoxy and bio-phenolic resins could be used in the future with flax fibres by optimising treatments and configurations to develop the composite properties.

Chapter 4. Influence of fibre configurations on properties of untreated flax/tannin composites

4.1 Introduction

Natural fibres (e.g. bast, leaf and seed) are employed as reinforcement because of their competitive specific properties to synthetic fibres like glass fibres. They also give nice 'natural' look, warmth to composites and not to speak of reduced environmental impact.

In addition to the synthetic polymer matrices, the use of bio-matrices from renewal resources (e.g. soybean oil, pine oil waste, castor oil, cellulose and proteins etc.) to replace synthetic plastics could further develop the sustainability technologies [3]. Saiah and his co-workers [147] reinforced the thermoplastic from wheat flour by flax fibres and used X-ray diffraction to analyse the crystallinity of the composites, suggesting that the intensity of crystalline peaks increased with increasing fibre content. Adhekunle et al. [102] manufactured flax/bio-thermoset (methacrylated soybean oil and methyacrylic anhydride modified soybean oil) composites with different fibre stacking sequences and lay-up angles, leading to maximum tensile strength of 119 MPa and Young's modulus of 14 GPa. Akesson et al. [106] fabricated the flax-reinforced composites based on polylactic acid-based (PLA) resins, which was cured at elevated temperature via compression moulding. From the DMA analysis, the storage modulus of PLA composites reinforced with 70 $_{wt}$% flax fibres is 9.32 GPa and 3.29 GPa at 20°C and 140 °C, respectively.

The use of tannin as matrix has received more and more attention for the following reasons: (i) non-toxic nature of tannin and related hardeners; (ii) wide availability of tannin and low cost; (iii) fast curing rate of tannin resins. The advantage of bio-degradability is also applied to the tannins from large varieties of plants (e.g. wattle, myrtle, pine etc.) through the extraction with water [145]. As stated in literature review (Chapter 2), the rigid carbon-carbon bonds between the phenol rings make condensed tannins more stable and suitable to produce resins [141]. Tannin crosslinking by formaldehyde via methylene or methylene ether bridges in a polycondensation reaction is the traditional way for

tannins to function as exterior-grade weather-resistant wood adhesives [141-143]. Theoretically, tannin can partially or fully substitute phenol to form resins and the associated composites. Ramires et al. [176] optimised the sisal fibre content at about 50 $_{wt}$% in tannin-phenolic composites to present the highest stiffness and impact strength. The 100% use of tannin instead of phenol as matrix was initially investigated by Ndazi and his co-workers [146] who successfully manufactured composite panel boards from rice husks and mimosa tannins.

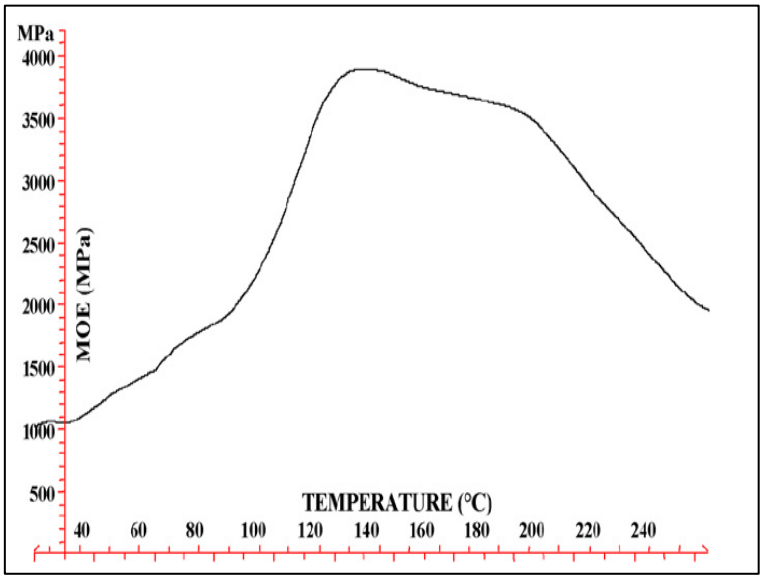

Figure 45. Modulus of elasticity of flax/tannin composites during curing [10].

Pizzi et al. [10] used flax fibres to produce mimosa tannin based composites. 5 $_{wt}$% hexamine was applied as hardener for tannin resins to eliminate formaldehyde emission. There were two natural matrices used: (1) mimosa tannin with 5% hexamine as hardner; (2) mixed tannin/ lignin resins in 50/50 solid content. The low density (8 mm thickness) and high density (1.2 mm thickness) composites were prepared, and followed by tensile tests, three point bending tests and Brinell hardness tests. The tensile strength was found to vary with changes in density. The low density composites had 50 % increase of tensile strength from 536 to 727 kg/m^3. The modulus of elasticity was characterised as a function of temperature during the curing of tannin-based resins (Figure 45). Additionally, by stacking several layers together to obtain

required thickness, it was unavoidable to have weak interfacial planes causing delamination rather easily.

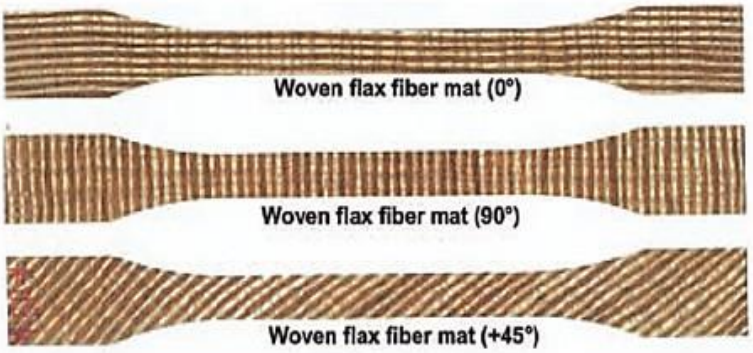

Figure 46. Lay-up angles of individual fibre ply [102].

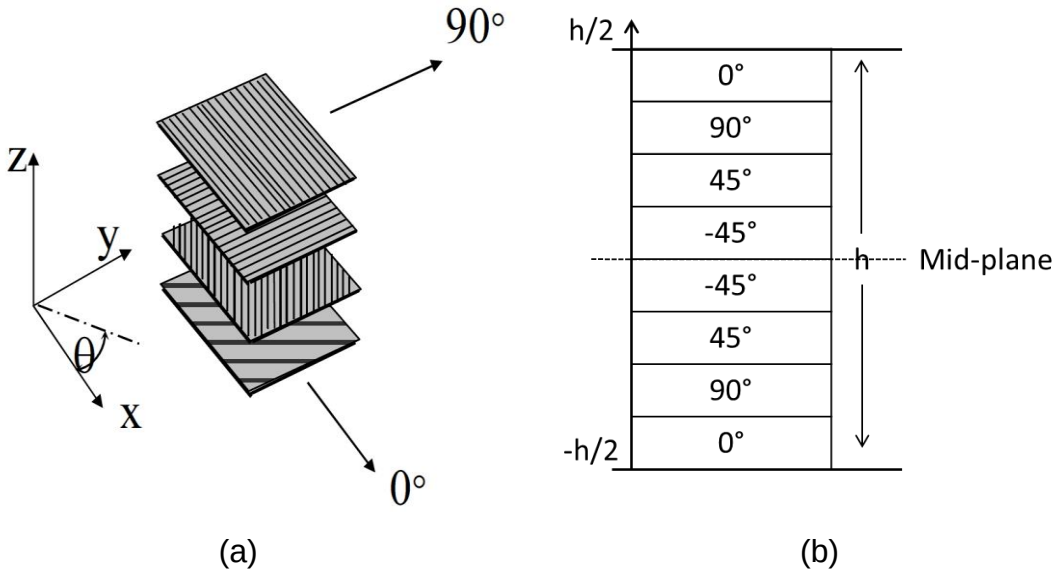

Figure 47. (a) Illustrations of stacking sequence and (b)symmetric laminates.

The selection of fibre laminate stacking orientations has a significant effect on the mechanical performances of resulted composites. Three fibre orientations in individual sample ply, as shown in Figure 46, are normally used. Flax/bio-thermoset composites with unidirectional (0°) plies showed improved flexural properties and as much as 30 % of increased tensile strength [102]. Muralidhar et al. [104] investigated the effects of lay-up angle and ply numbers on the flexural and impact properties of flax composites. The plies at [$0°_4$/$+45°_4$/$-45°_4$/$0°_4$] of woven fibres were the optimum layers and resulted in improvement

in flexural strength by up to 120% and high-impact strength (13.8 kJ/m^2) due to the better shear between laminates. The reduction of flexural and impact properties were caused by over stacking fabric layers, resulting in poor wettability between resins and fibres. The knitted preform laminate composites were also investigated and showed that the change in lay-up angle had little influence. Similar to Muralidahar's finding, Liang et al. [123] reported that fibre/epoxy composite at stacking sequence of [+45°, -45°]$_3$ showed better fatigue properties than [0°, 90°]$_3$ flax composites. The stacking order was reported to have little effect (±5 %) on fracture toughness of flax/epoxy composites with the weft oriented notch [129].

The in-plane stress-strain relationship of fibre laminate reinforced composites, highly depending on the fibre orientations, has been described by suitable models [177]. Individual plies in practise are stacked with different lay-up angles at certain oriented axis (x, y) to offer desired mechanical properties for design purpose (Figure 47(a)). A symmetric laminate as seen in Figure 47(b) is normally produced and studied for simplification of stress analysis. It shows same properties, such as ply type and orientation at the equal distance from the mid-plane. Consequently, the average stress ($\bar{\sigma}$) is presented as below when the strains of each ply are constant:

$$\bar{\sigma} = \frac{1}{h}\int_{-\frac{h}{2}}^{\frac{h}{2}} \sigma \, dz \tag{4.1}$$

Where h is the total thickness of a symmetric laminate. Hence we find:

$$\begin{bmatrix} \bar{\sigma}_1 \\ \bar{\sigma}_2 \\ \bar{\tau}_{12} \end{bmatrix} = {}^{1}/_{h} \begin{bmatrix} Q_{11} & Q_{12} & Q_{16} \\ Q_{12} & Q_{22} & Q_{26} \\ Q_{16} & Q_{26} & Q_{66} \end{bmatrix} \begin{bmatrix} \varepsilon_1 \\ \varepsilon_1 \\ \gamma_{12} \end{bmatrix} \tag{4.2}$$

$$Q_{ij} = h\int_{-\frac{h}{2}}^{\frac{h}{2}} D_{ij}(\theta, E_{ij})dz \tag{4.3}$$

Where D_{ij} is a function of lay-up angle (θ) and stiffness matrix (E_{ij}) of each ply. The stress-strain relationship of the composite can also be inverted to:

$$\begin{bmatrix} \varepsilon_1 \\ \varepsilon_1 \\ \gamma_{12} \end{bmatrix} = h \begin{bmatrix} A_{11} & A_{12} & A_{16} \\ A_{12} & A_{22} & A_{26} \\ A_{16} & A_{26} & A_{66} \end{bmatrix} \begin{bmatrix} \bar{\sigma}_1 \\ \bar{\sigma}_2 \\ \bar{\tau}_{12} \end{bmatrix} \quad (4.4)$$

The longitudinal (E_L), transverse (E_T) and shear modulus (G) are given by

$$E_L = \frac{1}{A_{11}h};\ E_T = \frac{1}{A_{22}h};\ G = \frac{1}{A_{66}h}; \quad (4.5)$$

The laminate mixture rule [178] is the simplest method to estimate the laminate stiffness and strength without inter-laminate coupling effects. It is assumed that the composite properties are dominated by fibres with ply fibre failure only at fracture. The stiffness are the summation of contribution from each fibre ply:

$$E_x = \sum K_\theta E \frac{t_\theta}{t} \quad (4.6)$$

Where E_x is the longitudinal modulus of the final laminate, t the total thickness, t_θ the thickness of layers with the angel of θ, K_θ the contribution factor, influenced by θ relative to the stress directions, E is a constant elastic modulus of fibre laminate at θ=0. The strength contribution is very similar to the above equation. The Hart-smith rule [179] suggests that there is only 10 % stiffness and strength contribution (K_θ=0.1) for layers at 45° and 90° with respect to the 0° layer (K_θ=1).

The lack of understanding and studies in flax/tannin composites has limited their applications, especially for vehicle applications. The fibre configuration for this novel composite is not investigated in the literature and as such is yet to be reported in the open literature. In this chapter, the effects of fibre configurations on mechanical properties of flax/tannin composites were investigated. The temperature dependency was indicated by physical changes through DMA characterisation, offering both quantitative and qualitative information. Tensile properties including the values and the failure mechanisms were obtained using the DIC (digital image correlation), followed by the SEM scanning on the failed samples. In addition to tensile performances, the falling weight low energy tests and three point bending tests were performed to show the impact and flexural properties.

4.2 Methodology

4.2.1 Materials

As discussed in previous chapter, non-woven flax mats (areal weight 1200 g/mm^2) were provided by CETELOR, Epinal, France. A thinner nonwoven mat type (600 g/mm^2) was provided as well. The unidirectional fabrics (areal weight 180 g/mm^2) provided by LINEO were pre-coated for epoxy impregnation. Mimosa tannin resin was supplied by Silva Chimica, S. Michele Mondovi, Italy. As shown in Table 14, the two non-woven flax mats/tannin composites were thereby denoted as type A, while woven fabric-reinforced laminate composites were manufactured as type B, C and D with different lay-up angles.

Table 14. Flax/tannin composites with different fibre configurations.

Types	Fabric characteristic	Number of layers	Layer thick
A	Non-woven	2	3 and 5 mm
B	UD lay-up	8	0.35 mm each
C	$[0, 90]_4$	8	0.35 mm each
D	$[0, +45, 90, -45]_2$	8	0.35 mm each

4.2.2 Cured resin preparation

The tannin resin formation followed the formulation: 21 / 25 / 5 / 4.75 of water / tannin / hexamine 33 $_{wt}$% solution / NaOH 33 $_{wt}$% solution. The required tannins were completely dissolved in water to form tannin solutions as first step, followed by the addition of hexamine and NaOH parts. The mixture was stirred using a magnetic stirrer at 40 °C for 20 minutes. The final aqueous resin was poured in the a glass mould and cured at different temperatures (room temperature for 1 week, 80°C for 2 hours, 130 °C for 40 minutes.)

4.2.3 Composite manufacturing (provided by ENSTIB)

Laminated composite preparation was conducted by ENSTIB using compression moulding process and the same resin formulation. Proper drying of flax fibres was conducted prior to the fabrication to avoid poor adhesion between fibres and matrix. The woven flax-reinforced composite plates were

fabricated using a 100 ton hydraulic press with servo-component allowing an accurate control of the consolidation pressure. The pressing blocks of the press were surrounded by an electric furnace with multi-segments controller for programming polymerization cycle. Additionally, a small-diameter thermocouple was placed in the mould in order to measure the temperature as close as possible to the composite material. The laminates were hot pressed at 80 °C for two hours with an initial pressure of 15 bar. All the laminates had the fibre content of around 50-55 % in weight and a target thickness of 2.5-3 mm.

4.2.4 Characterisation and tests

4.2.4.1 Differential scanning calorimetry

Thermal analysis L60 was used for DSC (differential scanning calorimetry) for flax/tannin composites. A composite of around 21 mg was sealed in an encapsulated pan. A standard heating rate 10°C/min was used under a nitrogen purge to heat the temperature from room temperature to 250°C. Dual-run progress was carried out the next day.

Note: the mechanical testing approaches (e.g. tensile, three-point bending etc.) was detailed in the below. They are also detailed in Appendix 2 to be cited in other experimental chapters.

4.2.4.2 Dynamic mechanical thermal analysis

Dynamic mechanical analysis was conducted in a Thermal Analysis Instruments Q800 DMA using single cantilever bending mode. It was heated from room temperature to 250 °C at a heating rate of 3 °C/min and a frequency of 1 Hz. Two specimens were tested for every type to ensure the consistency. The testing surface area was about 35×12 mm. The effect of temperature on storage modulus, loss modulus and tanδ was analysed.

4.2.4.3 Quasi-static tensile tests

The flat coupon tensile test was carried out on the Instron 5/100 kN 5500 R machine according to ASTM D3039 at the cross head speed of 2 mm/min. The test specimens were cut to the standard size of 250×25 mm and aluminium tabs

were glued to prevent stress concentration and sample damage by the fixing jaws (Figure 48). Five specimens, conditioned at same environment for 24 hours prior to the experiments, were tested at room temperature for each type.

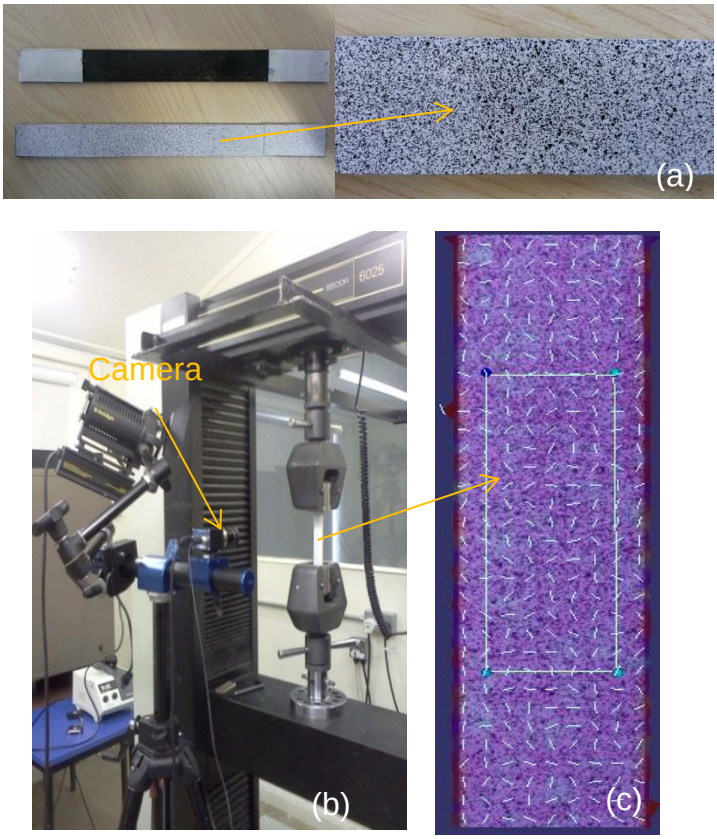

Figure 48. DIC technique for tension (a) preparation of speckled samples; (b) DIC set-up; (c) evaluated gauge area.

For accurate micro-scale strain measurement, a Q-400 system from Dyantec Dynamics (digital image correlation –DIC [180]) was used (Figure 48). The sample surface was sprayed with plain white paint, followed with a random speckled pattern of black dots (Figure 48(a)). With the testing going, the images were sequentially recorded at sub-pixel (micro-strain) resolution and then the patterns were used to identify the two-dimensional displacement through Istra 4 software. The principle strain for the selected area with gauge length of 50 mm was recorded (Figure 48(c)). Its non-contact nature of measurements (DIC method) can avoid the influence of attachment skills. Also, the advantages include the high data precision, wide measurement area, and good stability etc. More details and advantages of DIC are described in Appendix 3.

The cross-section topographies of the composite fracture surfaces after tensile testing were examined using a XL30 SFEG analytical high resolution scanning electron microscope (SEM), supplied by FEI. Voltage of 5 V was applied, and images were taken at selected magnifications.

4.2.4.4 Quasi-static three-point bending tests

The rectangular coupon flexural tests were performed according to ASTM D7264, on the Instron 5/100kN machine at 1 mm/min rate of loading. The specimen with the size of 154×13 mm was placed in three-point bending using a standard span to thickness ratio of 32:1. A 30 kN load cell was used. At least four specimens were tested for every lay-up fabric angles to average the flexural results.

Flexural stress is calculated from the applied load (F), span length (L), specimen wide (w) and thickness (d):

$$\sigma_{max} = \frac{3FL}{2wd^2} \tag{4.7}$$

The flexural strain is obtained from:

$$\varepsilon = \frac{6\delta d^3}{L^2} \tag{4.8}$$

Where δ is the mid-span deflection.

4.2.4.5 Low-energy impact tests

Impact strength of composites is the resistance of materials to the applied stress at certain speed and is greatly influenced by factors like the fibre architecture and matrix/fibre adhesions. The impact tests were performed using an Instrumented Falling Weight Impact Tester, Type 5, according to ASTM D7136, to provide damage resistance properties of composites subjected to a drop-weight impact event (Figure 49). The total impact mass and the nominal impact velocity were 2.280 kg and 3 m/s, respectively. The impactor has a hemispherical striker tip with diameter of 20 mm. Three 100×150mm specimens (regular plaques) were tested for each sample type.

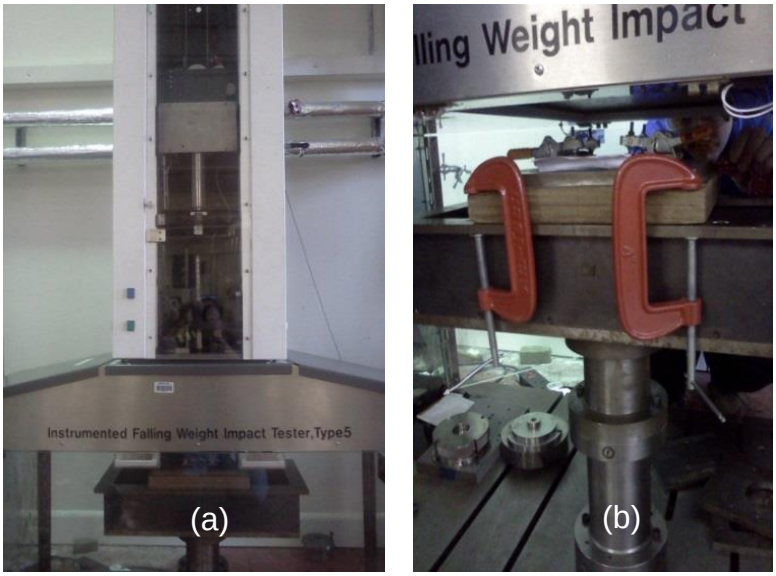

Figure 49. Drop tower machine for impact tests (a) view of tower; (b) sample position.

4.3 Results and discussion

4.3.1 Resin formation

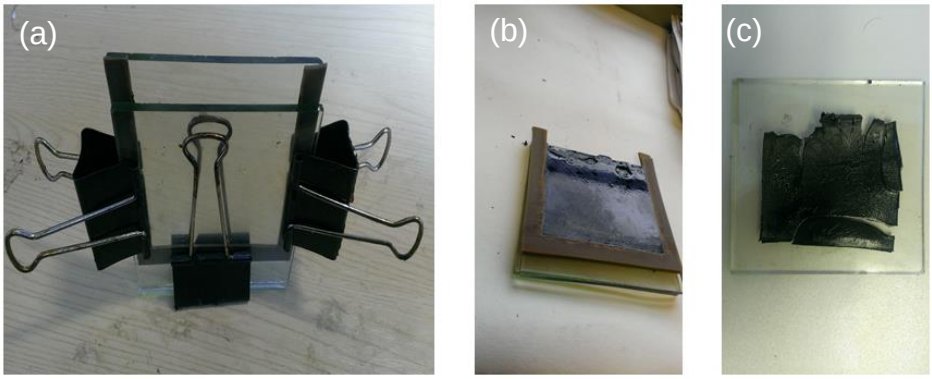

Figure 50. Resin formation (a) glass mould type; (b) cured resin after removing mould; (c) cracked resin after a few hours.

It was found that the aqueous resin was transferred into solid plate with shining black surface after curing and water removal at elevated temperature (Figure 50). However after opening the glass mould, the resin could not withstand the internal stress, resulting in severe warpage and crack formation after a few hours (as seen in Figure 50(c)). The fast curing at high temperature (130 °C) to slow reaction (cure at room temperature) had little effect to minimise or reduce this phenomenon. It could possibly be due to the acceleration of further reaction

within the hexamine-cured tannin resins, releasing NH_3 and increasing cross-link degrees, at the open air environment. Flax fibres not only exhibit good mechanical properties in the length directions for reinforcement but also are expected to act as 'tougher agent' (from their flexible nature) to avoid resin damage in tannin/flax composites.

4.3.2 DSC analysis of cured composites

The DSC results of flax/tannin composites are shown in Figure 51**.** In the curve of the single run carried out, there was an initial broad endotherm, which was attributed to the loss of water absorbed flax. On further heating, a second minor endotherm took place, followed by a heat flow increase due to the composite degradation. The onset of degradation temperature could be roughly indicated as the minor endothermic peak at 215 °C, at which the cellulose degradation was reported [181].

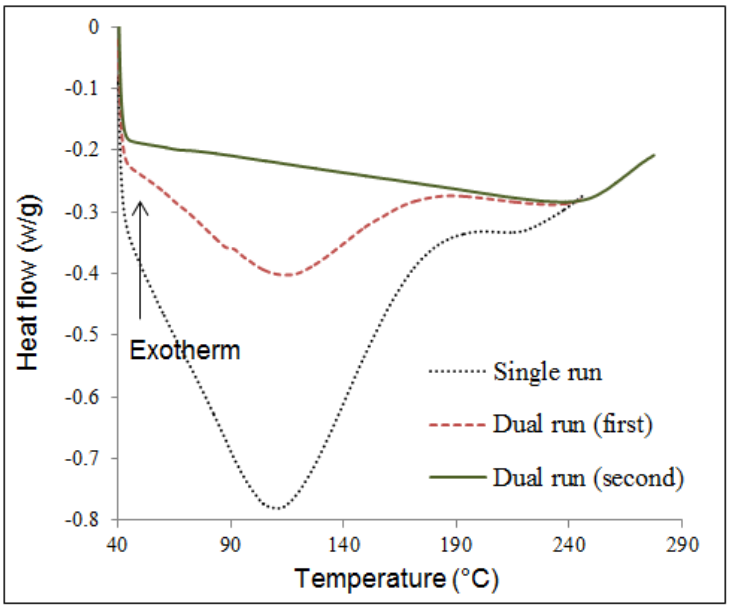

Figure 51. DSC thermograms of flax/tannin composites (single run and dual run programme).

Dual-run DSC programme was employed (same conditions and set up) on the same sample the next day for the purpose of comparison. It was clear that water-related endothermic peak was presented again in the first run, just like in the single run programme. The high water sensitivity of flax fibres allowed the

composite to absorb water overnight before the dual-run programme the next day. The peak area was significantly reduced, indicating less moisture content due to less absorbed energy to evaporate water. In the DSC curve of the second run, heat flow decreased gradually from the beginning as a result of enthalpy relaxation (the water was almost removed by the first heating). The degradation indicated by an exothermic increase took place again on further heating. Compared to the first run, the onset temperature of degradation (2nd run, no water) increased slightly to 237 °C. The exiting water accelerated the degradation progress of tannin/flax composite, resulting in the lower degradation temperature (215 °C).

4.3.3 Effects of configurations on dynamic mechanical properties

The viscoelastic data from DMA are plotted as Figure 52, Figure 53 and Figure 54 on the basis of each parameter, and Table 15 summarizes the characteristic properties. The DMA analysis could be further clarified with tannin resins, however to date, the author has not managed to cure tannin resins without fibres as a flat testing piece. This can also be explained by the complete lack of literature on DMA properties of cured tannin resins, except for cured neat tannin adhesives [182], the results of which are not comparable to the resins used for the study.

Table 15. Summary of DMA results of flax/tannin composites.

Composite type	E' at 27°C (GPa)	E'' at 27°C (MPa)	T_g (°C)	γ transition (°C)
A	5.3	194	61	150
B	7.5	516	-	160
C	6.2	345	60	-
D	5.1	379	60	158

The storage modulus of nonwoven flax mat reinforced composite (type A) at 27°C was 5.4 GPa, corresponding to tensile results (Young's modulus of 6.4 GPa) (see in 4.3.4). In terms of the woven flax/tannin composites (type B, C and D), the initial storage modulus follows the trend B>C>D. The UD (0°) composite (type B) showed the highest the modulus (7.5 GPa) that can be attributed to

reinforcement at 0°. The storage modulus decreases with increasing the fibre orientation from 0° to 90° according to the equation [183].

$$1/E'_c = \cos^2\theta/E'_L + \sin^2\theta/E'_T \qquad (4.9)$$

Where θ is the fibre orientation, E' is the storage modulus of composites, E_L' is the modulus along the direction of the fibre alignment, E_T' is the transverse modulus. The fibre fabrics in flax/tannin composites could be assumed as one-directional reinforcement. The composite $[0, 90°]_4$ (type C) had a higher storage modulus at 27°C than the composite $[0, +45°, 90°, -45°]_2$ (type D) due to the fact that type C contains more UD-aligned fibre fabrics. The initial storage modulus of the composite $[0, +45°, 90°, -45°]_2$ (type D) (27°C) was almost the same as the one of the nonwoven flax/tannin composite (type A). This indicates that the fabric lay-up structure of $[0, +45°, 90°.-45°]_2$ nonwoven flax mat (2 plies) at room temperature show similar mechanical properties.

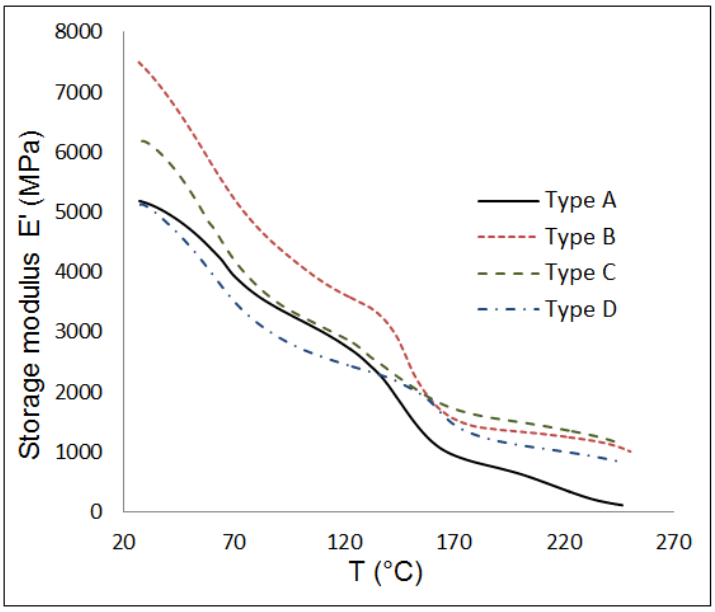

Figure 52. Variation of storage modulus of the flax/tannin composites.

Figure 52 shows the temperature dependency of the storage modulus (E') on various composite samples. The storage modulus of non-woven flax mat/tannin composite (type A) dropped from 5.3 GPa at 27°C to 636 MPa at 200°C with a transition around 150°C, on account of degradation. A similar transition

temperature of 160 °C was observed for composites B, C and D. The slight transition change at around 50 °C reflects the progressive glass transition of the composites. Only the onset of the glass transition was observed.

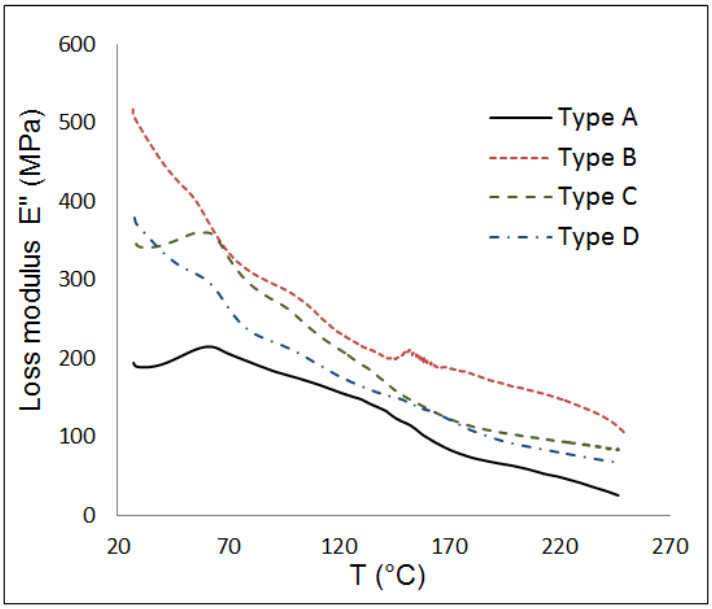

Figure 53. Variation of loss modulus (E'') of flax/tannin composites.

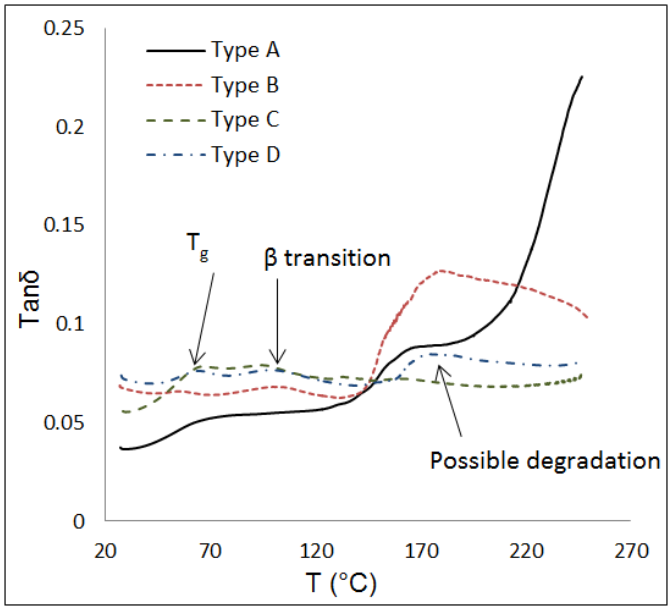

Figure 54. Variation of tanδ of flax/tannin composites.

The variation in loss modulus of the flax/tannin composites is shown in Figure 53. It has been reported that it is more reliable to obtain glass transition temperature (T_g) from the peak of loss modulus than from the tanδ peak which

tends to overestimate T_g [102]. The T_g of composites type A, C and D on average was about 60.5 °C, whereas a broad and fuzzy T_g peak at around 50 °C was observed for type B (UD type). Increase in constraints on the motion of molecules with increase in the fibre angle (θ) results in the increase of T_g [184]. In addition, the composite type B have more UD fibre fabrics as reinforcement at 0°, thus the resin matrix at the fibre surface is stiffer and deformed less than the absorbed resin layer in other composite systems. Consequently, the larger gradients in modulus of tannin resins caused a broader glass transition range.

Figure 54 shows variation of tanδ as a function of temperature. The tanδ trend is indicative of the energy dissipation with changes in physical properties. There were three tanδ peaks observed in the curve of the composite (type D). The first peak with increasing temperature expressed as T_g at around 65 °C, slightly higher than that obtained from loss modulus-temperature curve. The second peak, called β transition, may be attributed to the water evaporation phenomenon or due to the motion of side groups grafted on molecular chains on the account of the absorbed kinetic energy. The third peak close to 200 °C probably arises from the onset degradation of flax fibres, affecting the fibre load-carrying ability and hence the properties of the attached reins. This shows agreement with the published fibre degradation temperature [35].

4.3.4 Effects of fibre configurations on tensile properties

Using DIC to reduce the factor of dimension change under stress, Figure 55 shows the relationship between stress and strain of tested composites at micro-scale level. The obtained principle strain even after interpolation for sub-pixel resolution is not continuously ascending due to the stepped and discrete data input, hence the quantitative values were plotted as scatter diagrams. It can be seen that non-woven flax/tannin composites exhibited typical non-linear stress-strain response, whereas UD composite (type B) showed a more linear-like relationship. By using stacking sequences like $[0, 90]_4$ and $[0, +45°, 90°, -45°]_2$, the flax/tannin composites was approaching isotropic material-like response, more like homogenized non-woven mat composites, presenting non-linear curves.

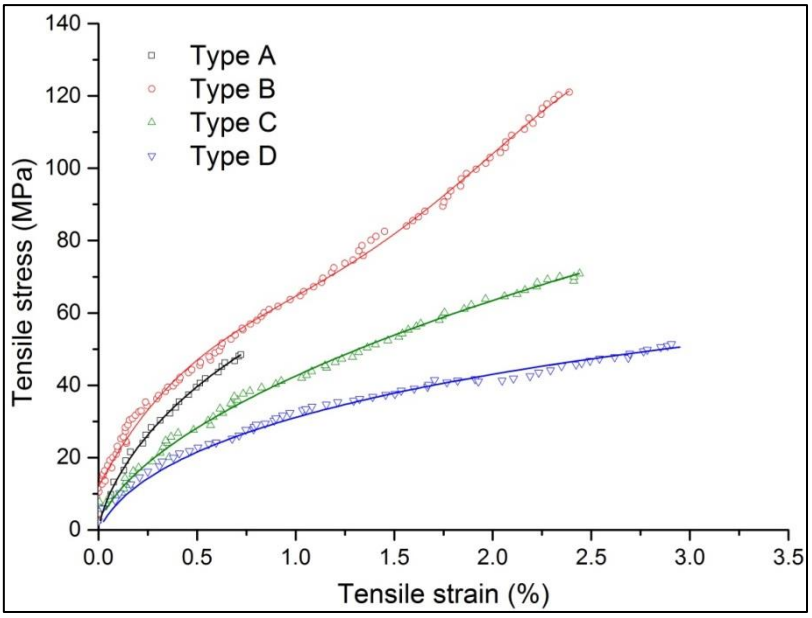

Figure 55. Typical micro-scale stress-strain curves obtained through DIC method.

Table 16. Tensile properties of flax/tannin composites.

Composite Type	Strength (MPa)	Predicted strength (MPa)	Modulus (Gpa)	Predicted modulus (GPa)
A	48±3.68	-	6.4±0.3	-
B	130±2.9	-	9.6±0.25	-
C	70±3.6	71.5	4.8±0.25	5.28
D	51±1.3	43.25	3.1±0.14	3.12

Tensile strength and elastic chord modulus (between the strain range of 0.001 to 0.003) of flax/tannin composites are shown in Table 16. UD (0°) samples (type B) had average tensile strength of 140 MPa, which is in line with the reported value (150MPa) of the dobby weave flax/bio-thermoset composite [102; 106]. The $[0, +45°, 90°,-45°]_2$ (type D) composite with lower tensile strength but higher maximum strain was found to be tougher than the $[0, 90°]_4$ type-C. The tensile strength and maximum strain of nonwoven flax mat/mimosa tannin composites (type A) reached relatively low values of 55 MPa and 0.7 %, respectively, due to the random distribution of short flax fibres in non-woven fibre mats. The Young's modulus of woven fabric reinforced specimens follows

the trend B>C>D. The unidirectional fibres in type B give rise to the maximum Young's modulus of approximately 9.6 GPa. In accordance with the tensile strength, the $[0, 90°]_4$ layer arrangement (type C) produced higher Young's modulus of 4.8 GPa than the $[0, 45°, 90°, -45°]_2$ composite (type D). One thing noticed is that the non-woven flax mat reinforced tannin composites (type A) also showed a relatively high Young's modulus (6.4 GPa). Due to the different manufacturing details, tensile modulus of type A is not comparable with the values of other types (B, C and D).

Prediction of stiffness and strength for off-axis orientations

According to the rule of mixture [177; 185], the longitudinal stiffness and strength of type C-$[0, 90]_4$ and type D-$[0, +45, 90, -45]_2$ could be estimated based on the tensile results of type B (UD composites). For type C and type D, the tensile stiffness (E_c and E_B) could be expressed by:

$$E_c = K_0 E_0 \frac{t_0}{t} + K_{90} E_0 \frac{t_{90}}{t} \tag{4.10}$$

$$E_B = K_0 E_0 \frac{t_0}{t} + K_{45} E_0 \frac{t_{45}}{t} + K_{-45} E_0 \frac{t_{-45}}{t} + K_{90} E_0 \frac{t_{90}}{t} \tag{4.11}$$

Where E_0 is the modulus of UD laminates, equal to 9.6 GPa, K_0 (contribution factor) is 1 for UD layers, $K_{90,}$ K_{45} and K_{-45} is 0.1 as a result of off-axis loading, t the thickness of related layer. The equation can hence be inverted to:

$$E_c = E_0 \frac{1}{2} + 0.1 \times E_0 \frac{1}{2} = 5.28 \tag{4.12}$$

$$E_c = E_0 \frac{1}{2} + 0.1 \times E_0 \frac{1}{4} + 0.1 \times E_0 \frac{1}{4} + 0.1 \times E_0 \frac{1}{4} = 3.12 \tag{4.13}$$

The estimated modulus of type C and type D shows strong agreement with the testing results with 8% and 0.6% difference, respectively (as seen in Table 16). Similarly, the tensile strength of type C and D composites were also estimated. It was noted that the practical tensile strength of type D $[0, +45, 90, -45]_2$ is 7 MPa higher than the estimation. This is attributed to the fact that this configuration can lead to less voids through thickness, keeping more resin as matrix within the laminates than type B and type C composites.

Failure analysis

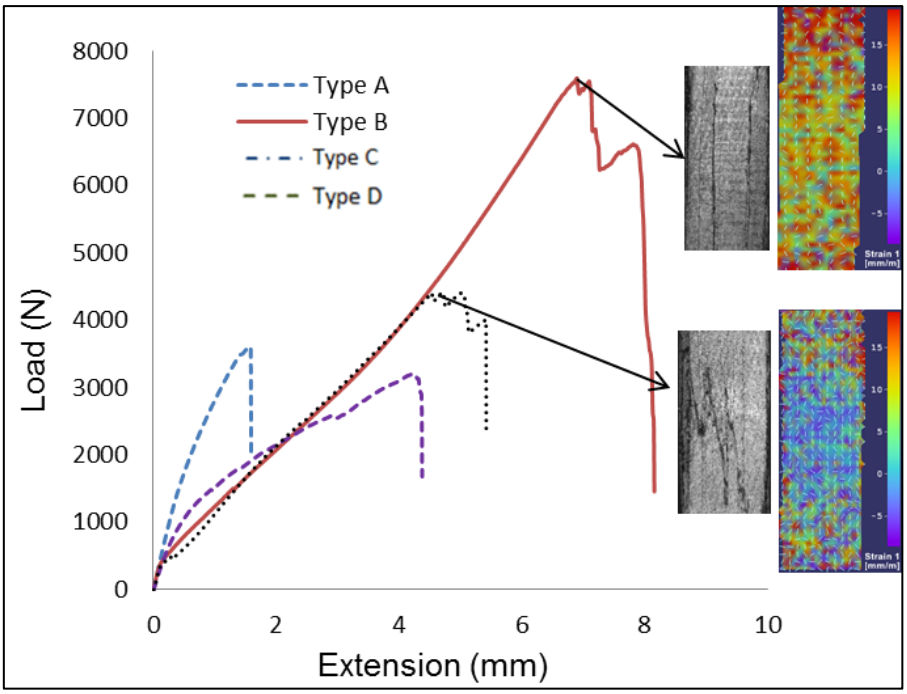

Figure 56. Tension load-elongation curves (macro-scale) for flax/tannin composites.

The macro failure modes of flax/tannin composites were indicated from post-load-displacement behaviour and recorded DIC images. Figure 56 shows the load-extension curves for different tannin composites. After the maximum force, the loads applied on the flax mat composite (type A) dropped dramatically, whereas the composite types (B and C) still behaved load-carrying capacity. The first load drop of composites may be due to the combination of failure of tannin resins and the first delamination. However, for the load-re-increase, it was very likely that the progress of specimen delamination was not in a continuous fashion but rather in an abrupt and irregular way. Unlike non-woven flax composites, woven fabric composites showed more than one propagating crack. Examples of type B and C composite were shown in Figure 56, where matrix cracks occurred at different locations, leading to two longitudinal crack propagation routes for type B and the Z-like failure pattern for type C, respectively. The crack of tannin resins induced the delamination of layers, followed by fibre breakage and longitudinal matrix crack. It can be seen from Figure 57 that fabric layers (type B) were completely separated and type A was

fractured into two pieces. The interactive failure criteria like Von Mises approach is preferably used for isotropic composites [177] as below:

$$(\frac{\sigma_x}{X})^2 + (\frac{\sigma_y}{Y})^2 - \frac{\sigma_x \sigma_y}{X^2} + \left(\frac{\tau_{xy}}{S}\right)^2 = K \qquad (4.14)$$

Where σ_x, σ_y, and τ_{xy} are respectively the applied stress on the longitudinal, transvers and shear direction. X, Y, Z are the related the strength properties. A crack will be initiated within a ply when the value of k is smaller than 1.

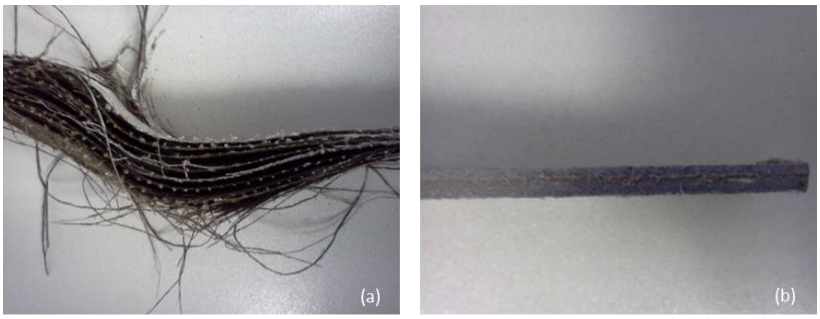

Figure 57. Tested samples during tension (a) delamination; (b) fracture.

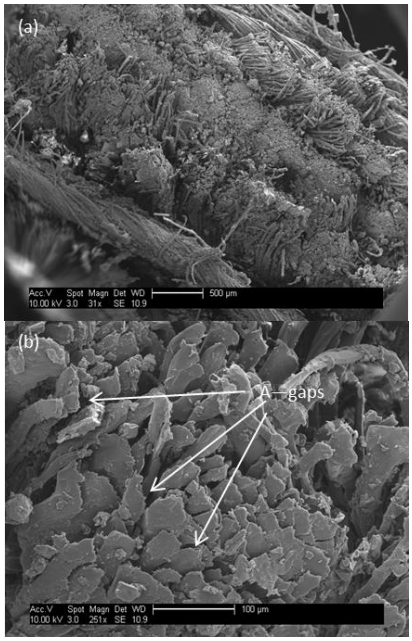

Figure 58. SEM micrographs of a cut non-fractured sample: (a) cross-section of the delaminated sample, (b) magnified graph.

To further understand the tensile failure mechanisms, SEM micrographs for tensile surfaces of flax/tannin composites are shown in Figure 58 and Figure 59. SEM is an important characterisation method for composite technology (e.g.

failure mechanism) as reported in the literature [107; 126]. As discussed previously, composites B, C and D showed delamination behaviour without fracture during tensile testing. A woven sample was cut into a specimen and investigated by SEM. Figure 58(a) clearly shows the separation of fibre layers upon testing. It indicates the poor wettability between these fabric layers. Some noticeable gaps between matrix and fibres were indicated by 'A' in Figure 58(b). These empty gaps indicating the poor interface contact between fibres can also account for the weak load transfer and unexpected performance. Based on the research [82], chemical treatments like alkali treatment to enhance the fibre/matrix interfacial adhesion by purifying the fibre surface can be used for improving the possibility for chemical bonding [82]. An advanced approach for the problems is nano-scale fibres leading to remarkable fibre dispersion, hence good intermolecular interactions [186].

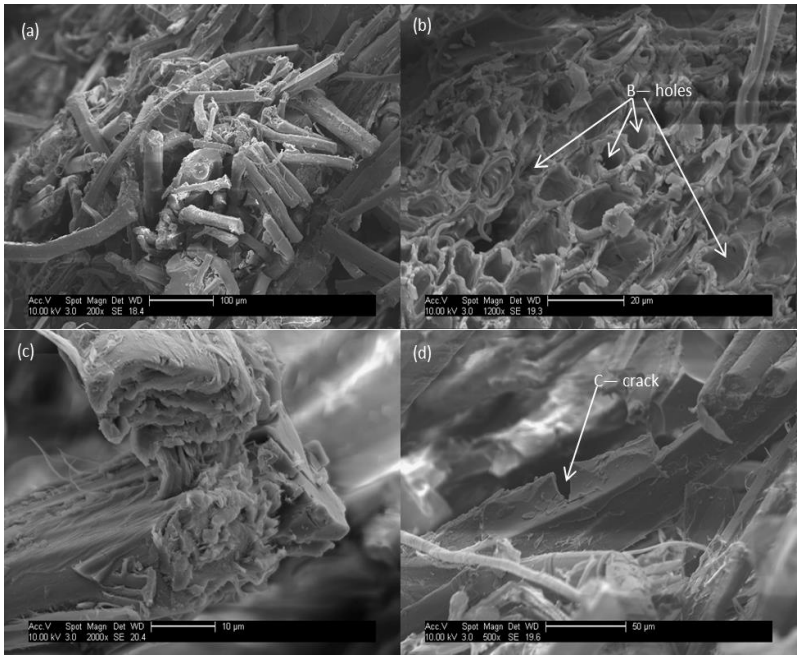

Figure 59. SEM micrographs of tensile fractured composites: (a) fracture area; (b) fibre pull-out, (c) fibre breakage, (d) brittle failure of resin matrix.

Figure 59 is the cross-sectional micrographs of tensile fracture surface of non-woven flax/tannin composites. From Figure 59 (a), the bonding quality between fibre layers was better than that of non-fracture specimen. Figure 59 (b) shows the holes (indicated by 'B') after fibre pull-out. The fibre breakage shown in

Figure 59 (c) was caused by the applied stress. Symbol ‘C’ in Figure 59 (d)) points to a small crack within the tannin resins adjacent to fibres. This crack may be initiated at the end of failure and did not continue to propagate without enough energy.

4.3.5 Effects of fibre configurations on flexural properties

Two important properties, flexural strength and flexural modulus, were calculated. The flexural properties reflect the laminate stiffness and dimensional stability, which are partially controlled by the nature of fibre fabrics, such as out of plane properties. In general, the occurrence of an initial crack during bending depends on the tension surface stress, which increases with increase in the maximum stress of compressive layers and is related to the number of fibre yarns in the area.

The flexural strength of flax/tannin composite in different laminate lay-up angles and perform types are shown in Figure 60. From the strength results, it can be observed that nonwoven flax mat reinforced tannin composites exhibited the highest flexural strength of 97 MPa than woven samples. There are three reasons that can explain the phenomenon: (1) non-woven flax mat showed a better bending resistance due to its relatively low cross-sectional applied stress resulting from the higher areal weight (600-1200 g/m^2) of the thicker flax mat; (2) Compared to the woven samples, the non-woven flax mat /tannin laminates had a better wettability, resulting in good stress transfer and energy absorption, leading to higher flexural strength; (3) The waviness of flax fibres caused by the woven fabric architecture significantly reduces the compressive properties, to which the flexural strength is very sensitive. The literature [80; 104] on this topic indicates that the high areal weight reinforcement can be considered as some external layers resulting in more number of fibres in the bridging area. The SEM micrographs and the tensile results provide good evidence for the relatively good fabric adhesion and wettability of the flax mat/tannin composites (type A). In addition, it has been reported that the degree of straightness of fibres and the misalignment greatly influence the compressive strength and the bucking behaviours [187]. The combination of different parameters, such as

fibre characteristics, cure time, pre-treatment etc., between nonwoven and woven flax composites could contribute to the final different bending performance. As illustrated in Figure 60, there was no obvious lay-up angle influence in the flexural strength of sequentially stacked fabric-reinforced composites, having a similar strength value of around 60 MPa. In other words, the compressive layers in all the composites under three-point bending showed almost the same stress resistance, giving rise to the similar maximum stress on the tension axial and resulted flexural strength.

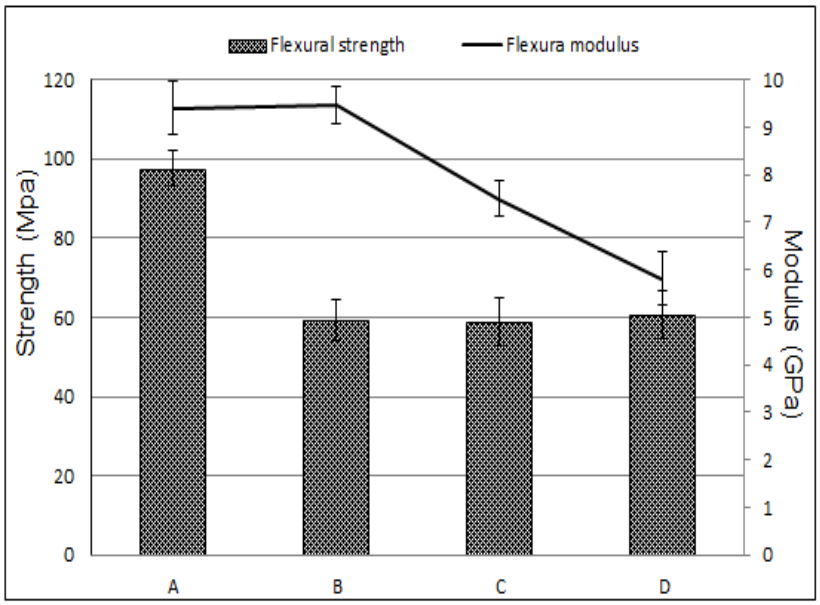

Figure 60. Flexural strength and modulus of the nonwoven and woven flax composites.

Nonwoven and UD woven flax laminates had the highest flexural modulus values of 9.4 GPa and 9.3 GPa, respectively. The high areal weight of nonwoven flax mat and the good wettability accounts for the high flexural modulus of nonwoven flax reinforced tannin composites. Compared to the [0, +45°, 90°, -45°]$_2$ composites (type D, 5.8 GPa), the flexural modulus of the UD flax fabric reinforced composites (type B) increased 63.1 % and that of the [0, 90°]$_4$ composites (type C) increased 29.1 %. This is expected because the inherent stiffness of the woven fabric corresponding to the different lay-up angles affects the flexural modulus of laminates. The UD directional flax fabric preformed the highest modulus in the tension/compressive direction and thus contributes to the highest overall flexural modulus. In the woven flax composites

with eight fabric layers, the flexural modulus depends on the number of the UD (0°) flax fabrics in the flexural modulus trend: UD> $[0, 90°]_4$>$[0, +45°, 90°, -45°]_2$.

The load-displacement curves of non-woven flax mat reinforced tannin-based composites (type A) are shown in Figure 61. The force dropped down dramatically in an almost straight line after the maximum load, corresponding to the brittle failure mode with little delamination and fibre fibrillation. Figure 62 (a) shows the crack on the tensile side and propagated through the sample thickness. However, with increasing displacement, the curve showed a slow decrease of load due to the presence of delamination (see in Figure 62 (b)), which was also confirmed in Yan's investigations [82].

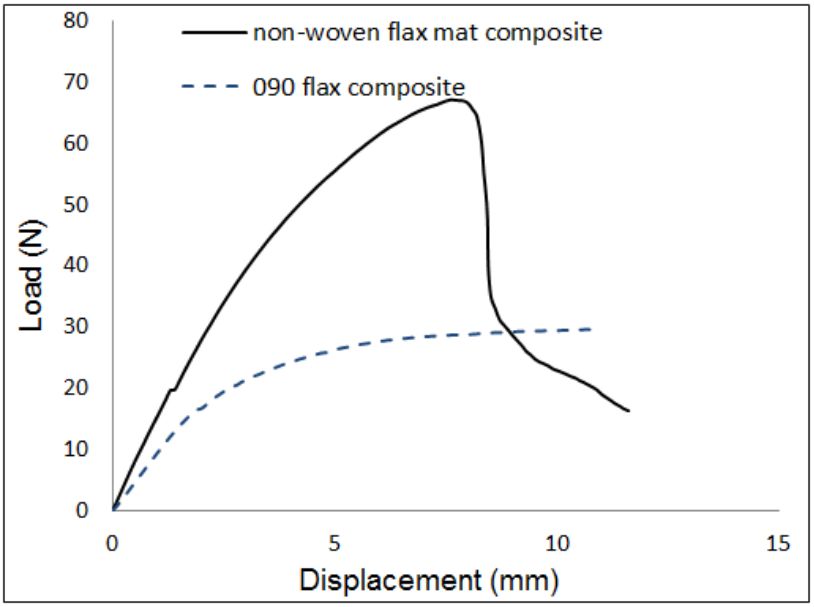

Figure 61. Flexural load-displacement curves of the selected flax/tannin composites.

The curve of $[0, 90]_4$ composites was represented as the typical load-displacement curve with three basic zones of woven fabric laminates (Figure 61). The linear relationship between load and displacement was shown in first region, followed by a non-linear response. From the literature [3], this phenomenon is the consequence of the re-orientation of the micro-fibrils along the tensile direction and the arrangement of the strongest part in the cell wall for re-crystallization. Then a load plateau with an increasing displacement was displayed in the third region without fracture failure. The flexural failure in the $[0, 90]_4$ composites was the mechanism of delamination accompanied with

catastrophic laminar damage as evidenced in Figure 62 (c) and Figure 62 (d). As discussed before, the load was still carried and transferred through the bridging fibres in the delaminated samples after the maximum force. In fact, all the woven fabric composites during tests represented the same separation phenomenon of layers with no crack propagation (as shown in Figure 62 (a)), in line with literature [82]. Compared to the non-woven flax tannin composites, the typical delamination during loading indicates the lack of bonding between flax layers and tannin resins in the woven fabric reinforced composites.

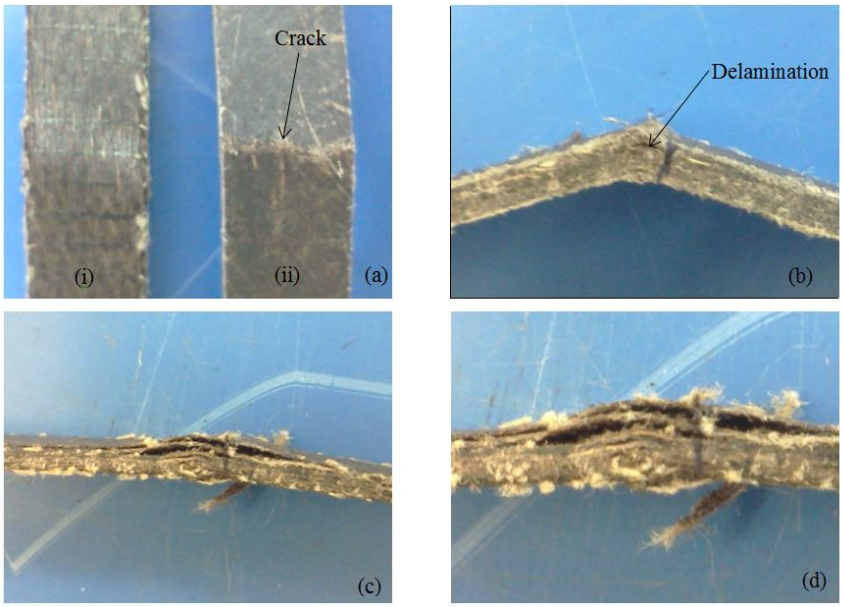

Figure 62. Flexural failure of composite samples during three point bending: (a) i- UD flax composite with no crack on the tension surface; ii-crack failure of nonwoven flax mat composite; (b) side section of non-woven composite without breaking into two piece; (c) the delamination of $[0, 90]_4$ composite after bending; (d) buckling of the layers away from each other (magnification of the delaminated $[0, 90]_4$ composite.

4.3.6 Effects of fibre configurations on impact properties

The basic impact behaviour of the flax fibre tannin matrix composites was analysed from Figure 63 showing force versus vertical impactor displacement curves for different composite systems. The maximum force represents the maximum capacity of materials to carry load and is generally marked as the occurrence of the first failure of laminates [188]. The composite $[0, +45°, 90°, -45°]_4$ (type D) had the highest maximum force of 1123 N. It is attributed to the

homogenised properties in this configuration, displaying higher failure threshold force. From the point of view of the fibre direction distribution, the short fibre nonwoven flax/tannin composite (type A) also enhanced the damage resistance more than the UD (0°) composite (type B) and the composite $[0, 90°]_4$ (type C).

Composite A displayed classic behaviour of perforation, in which there was a continuous monotonic increment of z displacement with constant force. The other evidence is the damage image of sample A with a hole after impact (Figure 64 (a)). At the saturation instant, the energy dissipation by system was switched from 'internal' fragmentation to friction between the dart surface and the perforation hole. In consequence, the velocity decreased linearly with increasing dart displacement after saturation point at the displacement equal to 15.3 mm (as seen in Figure 65) plotted directly from the recorded impact data.

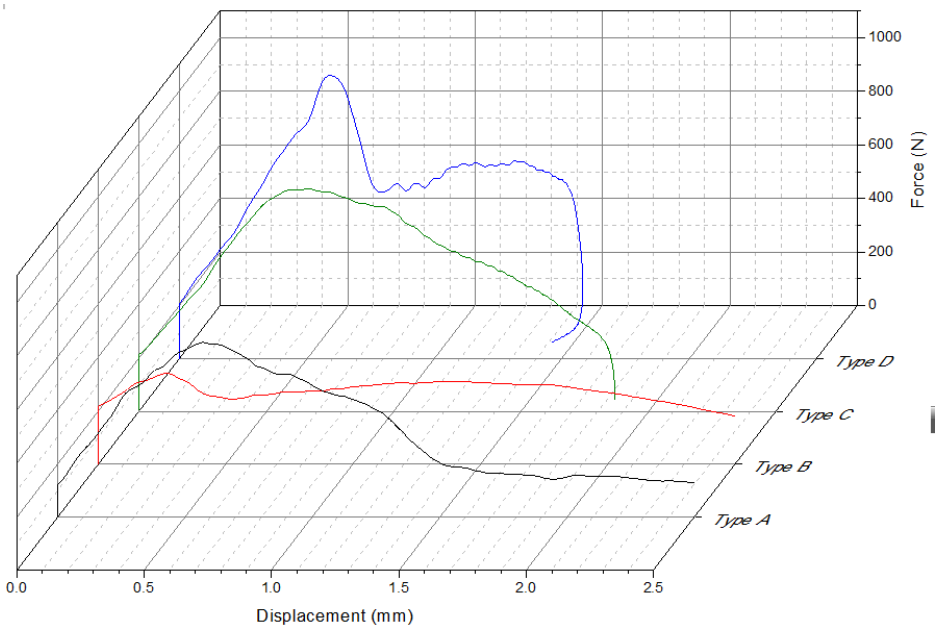

Figure 63. Impact force-displacement curves for different composites.

In addition, the UD (0°) composite (type B) showed a similar impact performance to the nonwoven flax composite (type A). For composite B, a crack propagated through the whole sample (Figure 64 (b)) and broke it into two pieces. This is due to the horizontal weak interfacial phase in UD (0°) composites (composite B). Crack was initiated and then the weak transverse phases allowed crack propagation along the longitudinal direction. For type C,

the dart stopped without rebounding while reaching the maximum penetration displacement of 18.7mm as seen in Figure 65.

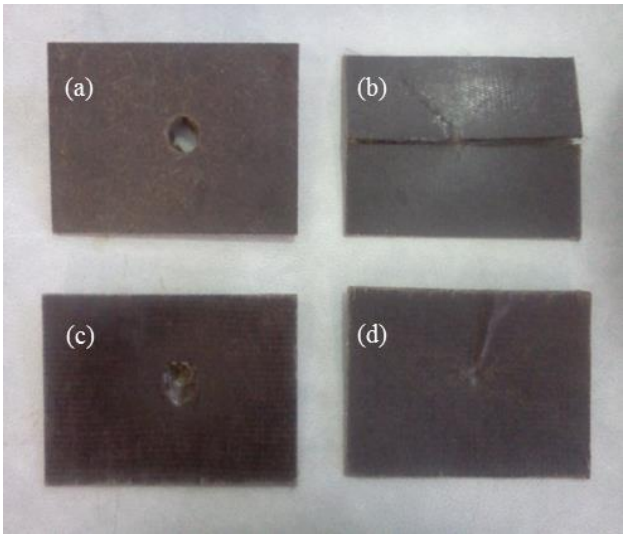

Figure 64. Examined samples after impact test: (a) Flax mat; (b) 100 %UD flax; (c) $[0, 90°]_4$; (d) $[0, +45°, 90°, -45°]_2$.

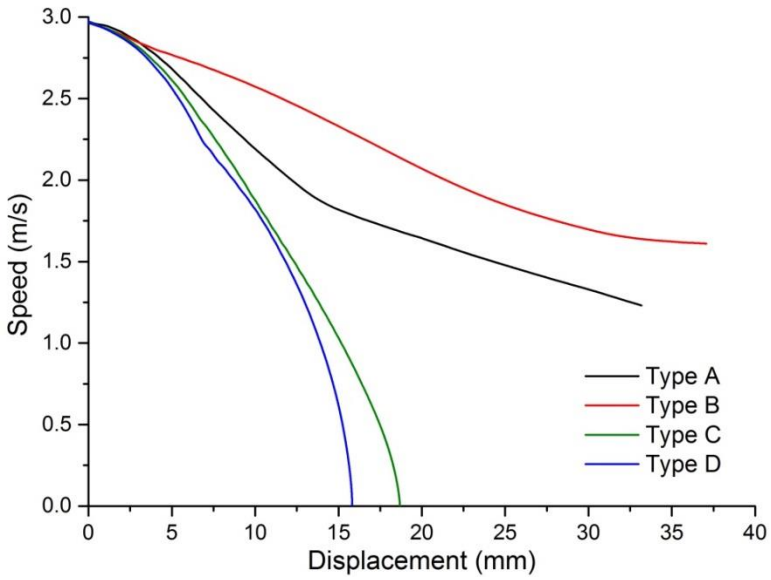

Figure 65. Speed-displacement curves for composite A and B.

There was no exchange residual energy with dart due to lack of rebound for composite C. However, the end curve of composite D folded towards decreasing displacement, which is a strong evidence of rebound. The amount of elastic energy stored by the specimen was released from the ‘fold’ point to the end and no further energy dissipation occurred. The energy absorption of type

D composite decreased after the peak value as release energy in Figure 66. The fibre fabric layup of $[0, +45°, 90°, -45°]_4$ offered good stress transfer and even mechanical properties in various directions. This fabric arrangement showed the best impact resistance implied by the presence of rebound.

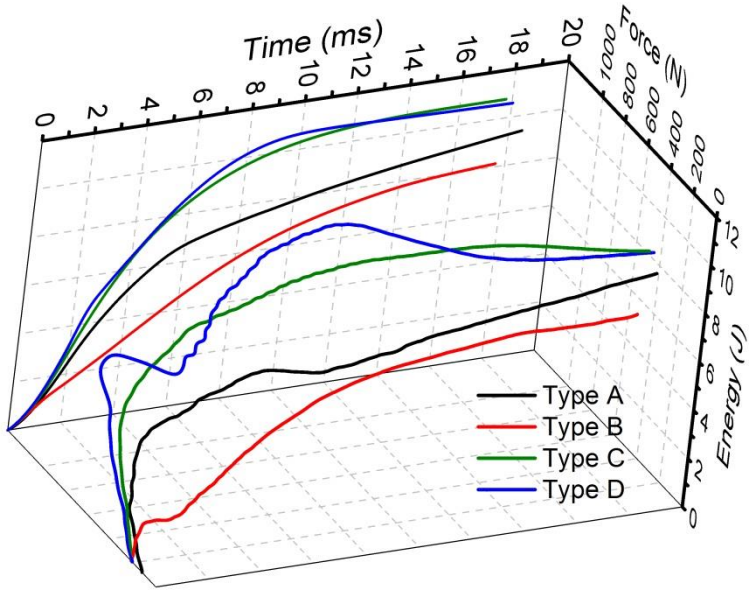

Figure 66. 3D-time-force-energy for flax/tannin composites.

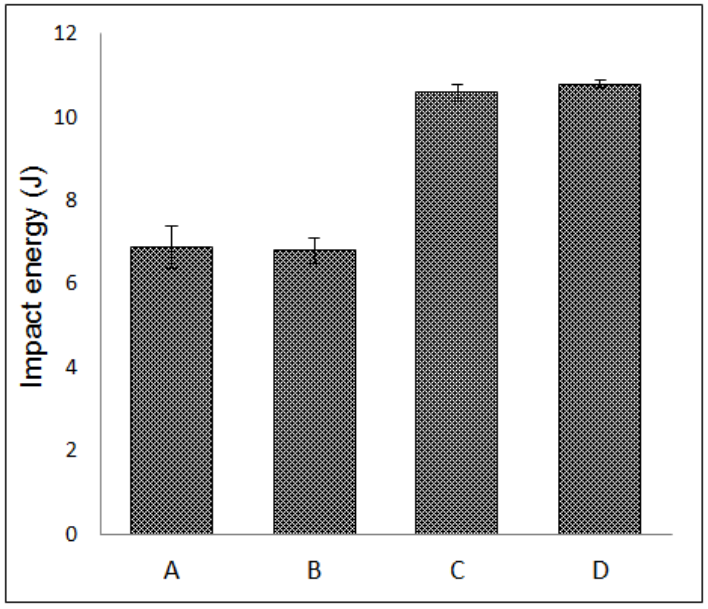

Figure 67. Impact energy for different composite types.

The trend of impact energy of test specimens is: C>D>A>B (Figure 67). The impact energy was determined as saturation energy for perforation case, and as

final absorbed energy for rebound case. The composites A and B exhibited much lower impact energy (6.9 and 6.8 J, respectively) than the composites C and D since the specimens A and B were carried out in the perforation case. For composite A and B, a certain amount of energy was dissipated by friction, but not absorbed by samples. The impact energy of type D (10.6 J) was slightly lower than the one of type C (10.8 J). This slight difference is accredited to the energy released back to rebound dart during the impact tests of composite D.

4.4 Conclusions

The effect of fibre configurations on mechanical performances of flax/tannin composites was investigated. The UD (0°) composites (type B) showed the highest tensile strength of up to 140 MPa and elastic modulus of 9.6 GPa. The initial storage modulus of the composites showed strong agreement with the tensile properties. The glass transition temperature of composites was around 60 °C. It was found that failure mechanisms for the tensile test included fibre pull-out, fibre breakage and brittle tannin failure. The non-woven flax mat reinforced composites presented much higher flexural properties than the woven fabric composites. In addition, the $[0, +45°, 90°, -45°]_2$ composite (type D) displayed good impact performance due to the even distribution of stiffness and strength. The investigations suggest that the fabric arrangement could be properly tailored to balance tensile properties and impact resistance. Also, with further surface treatment (e.g. alkali treatment) to improve fibre/matrix adhesion, flax/tannin composite will possibly show an improvement in mechanical properties.

Chapter 5. Influence of surface treatments on properties of nonwoven flax mat/tannin composites

5.1 Introduction

One of the limitations for natural fibre composites is that the hydrophilic property of natural fibres leads to not only the high water sensitivity of final composites but also the poor fibre/hydrophobic matrix interface quality, influencing the mechanical performances. The direct applied load on the composites is transferred from the matrix to the adjacent stronger fibres which carry the load to improve properties. It is therefore that a strong fibre/matrix interface makes sure the effective load distribution within the composites with good mechanical improvement. On the contrary, a weak interface even reduces the reinforcement efficiency, impairing mechanical properties of the composites, due to the ineffective load transfer.

To improve the interface quality, adequate surface modifications, mainly chemical treatments (e.g. mercerization, acetylation, silane treatment, and other fibre pre-treatments) are commonly used for natural cellulose fibres to improve the composite performances [81]. Alkali treatment or mercerization is a common method to produce high quality fibres. It causes the breaking down of the fibre bundles in to smaller fibres, which results in the development of a rough fibre surface topography and better fibre-matrix adhesion. It also increases the number of possible reactive sites on fibre surface and hence can be used as pre-treatment for other modifications, like acetylation and silane treatments. In a recent investigation [82], a 21.9 % and 16.1 % improvement in tensile and flexural strength of flax/epoxy composites was observed after alkali treatment of 5 $_{wt}$% NaOH for 30 min. As an example of the acetylation modification, butanetetracarboxylic acid (BTCA) can act as a cross-linker between cellulose hydroxyl groups in the fibre cell preventing fibres from swelling and thus increasing the fibre stability [164]. Silane is a common coupling agent used to let glass fibres adhere better to polymer matrix, stabilising the composite material. For reacting with silane coupling agent, thermoset resins like epoxies are more reactive than thermoplastics like PP. This is due to the liquid flow

property of resins bearing organofunctionalities to form 3D (three dimensional) strong polymer networks after curing with proper hardeners. As stated in the literature review, by applying silane treatment on flax fibres, the interfacial properties of the final composites could be enhanced. Research activities in the use of laccase in various application areas have recently been reviewed by Kudanga et al. [189]. The laccase-catalysed modification can be used to tailor the properties of various lignocellulosic materials, including flax fibre materials based on the application needs [190]. Natural phenols, such as syringaldehyde, acetosyringone and p-coumaric acid, dodecyl gallate-(Doga), in combination with laccase treatment, were developed recently to graft on the flax fibres and offered the antimicrobial properties [191; 192].

The water sensitivity plays an important role in degradation and decrease of mechanical properties of composites; hence it cannot be neglected [122]. Assarar and his co-workers [121] reported how the water ageing influenced the flax and glass epoxy composites with 11 unidirectional plies. A 30 % decrease of young's modules of flax fibre composites in the first 10 days showed a much worse result from water ageing, in comparison with the 9 % modulus decrease of glass composites even at the saturation time. Stamboulis and his co-workers [108] reported that moisture content affected stiffness of flax/PP composites more than tensile strength. The stiffness increased somehow at low moisture content due to the filled interfacial gap by swelling flax fibres, while it decreased significantly after 7 $_{wt}$% moisture content. A study of moisture absorption and environmental durability of flax (Green and Duralin)/PP composites was conducted by Stamboulis and his co-workers [108]. Green flax/PP composites were clearly more sensitive to water than Durbin flax ones, meanwhile the addition of MA (maleic-anhydride)-PP lowered the initial water uptake rate with little effect on the maximum moisture content.

The effects of production parameters on properties of flax/tannin composites have been studied by Sauget et al. [193]. With respect to the investigation of manufacturing techniques for nonwoven flax/tannin composites, the best mechanical result was obtained by curing at 130°C for 35 min. In chapter 4, the 12 unidirectional (UD) flax layers/tannin composites showed highest tensile

strength up to 140 MPa while non-woven flax/tannin composites exhibited low tensile strength around 50 MPa. The SEM images of the fractured surface suggested that an improvement on flax/tannin adhesion could potentially increase the mechanical properties.

However the effective fibre modifications for flax/tannin composites are not established yet due to the lack of study in this field. Hence in this study, the author has successfully prepared tannin composites through compression moulding (130 °C/35 min/1.5 MPa), with untreated and chemically treated non-woven flax mats (alkali, acetylation, silane and enzymatic treatment). The effect of fibre treatments on mechanical property was obtained through tension testing incorporated with digital image correlation (DIC) method, three point bending tests and low velocity impact tests. Dynamic mechanical properties and water resistance of flax/tannin composites with different surface treatments were also analysed.

5.2 Methodology

5.2.1 Materials

Table 17. Untreated and treated non-woven flax mat tannin composites.

Matrix	Fibre type	Modification	Treatment details
Tannin resin	Untreated	-	-
	NaOH-treated	Mercerization	5 $_{wt}$% NaOH purification
	BTCA-treated	Acetylation	Alkali+BTCA
	APS-treated	Silane treatment	Alkali +APS
	LD-treated	Enzyme	Benzenediol+dodecyl gallate

The flax fibres used as reinforcement in tannin composites were provided by Ecotechnilin Ltd in the form of non-woven fibre mats with areal weight of 600 g/mm^2 and average thickness of 3 mm. The same fibre mats with different treatments as discussed in Chapter 4 were supplied by VTT, Finland (Table 17). The Retan MD® mimosa tannin (0.4 g/cm^3) mainly extracted from black wattle was purchased from the SCRD, France. The hexamethylenetetramine

(hexamine, >99.0%) used as hardener for resin preparation was purchased from Sigma-Aldrich.

5.2.2 Aqueous resin preparation

The tannin resins prior to composite manufacturing were prepared using aqueous tannin and the 33 $_{wt}$% hexamine/water solution (12:1, w/w). First, the tannin powders were dissolved into water with weight ratio of 5:7 by using a magnetic stirrer. About 0.2 $_{wt}$% de-foaming agent on resin mass was added into water before mixing. The required tannins were added in a few steps to minimize the solid precipitation. The stirring was maintained for 20-30 minutes to ensure the complete dissolution and homogenous distribution. After that, the weighted hexamine solution was added, and the temperature was adjusted to 40 °C with continuously stirring for 10 minutes. The final tannin resin solution had a solid content of about 41%.

5.2.3 Composite manufacturing

Non-woven flax mats (200×300 mm) were manually impregnated using an impregnation tool pack (from Easycomposite Ltd), including a 100 mg digital scale, laminating brushes and a plastic finned roller designed for chopped strand matting etc. The applied resin solutions for each layers was about 2.5 times than the weight to give a calculated 50 $_{wt}$% fibre ratio in the final composites. The impregnation was done by spreading and squeezing resin carefully on both sides of the mats. The impregnated fibre mats were then left in room temperature to dry overnight.

Prior to the stacking stage, water was sprayed on both side of the mats to adjust the overall moisture content to 20 % (Figure 68), based on the previous study by Sauget et al. [193]. Three fibre mats were stacked between two aluminium mould plates (300×300 mm) to form composites by compression moulding (Figure 68). The compression moulding was done by a 40 Ton Press (shown in Figure 68) with the molding cycle: (1) pre-heating of mould at 130°C; (2) maturation time before applying pressure:15 s; (3) 15 ton for 30 s and then 9 ton for 34 min. The moulding cycle was determined to get a fibre mass fraction

between 50 % and 55 % while respecting the 2.5 mm thickness. Four composite plates were prepared for each composite type.

Figure 68. Overview of composites manufacturing (a) water content adjustment; (b) aluminium plate mould; (c) compression machine; (d) examples of composites.

5.2.4 Characterisation and tests

All the composites were stored for three days to ensure the completion of post cure of tannin resins. The panels were cut to the testing size by a CNC milling

machine using 2 mm carbide drill at feed rate of 400 MPM. Details on optimized machining parameters are shown in Appendix 4.

5.2.4.1 SEM characterization

Single fibres were extracted from the treated and untreated flax mats, and then were examined using a XL30 SFEG analytical high resolution scanning electron microscopy (SEM), supplied by FEI for fibre morphology analysis

5.2.4.2 Mechanical testing

Similar to the experiments in Chapter 4, mechanical tests (in Appendix 2), including tension (DIC method), three-point bending and falling weight impact testing and dynamic mechanical testing, were carried out on the manufactured non-woven flax/tannin composites with different chemical treatments. The tensile specimens were glued with aluminium tabs to avoid stress concentration (Appendix 5).

In addition, shear properties of the composites were obtained based on the ASTM D7078. A V-notched specimen was clamped between two pairs of loading rails, along with digital image correlation set-up (as seen in Figure 69). When loaded in tension, the rails introduce shear forces into the specimen through the cross section. The specimens had the cross-notch width of 31 mm and thickness of around 2.5 mm. The cross-head speed of 2 mm/min was applied during the tests.

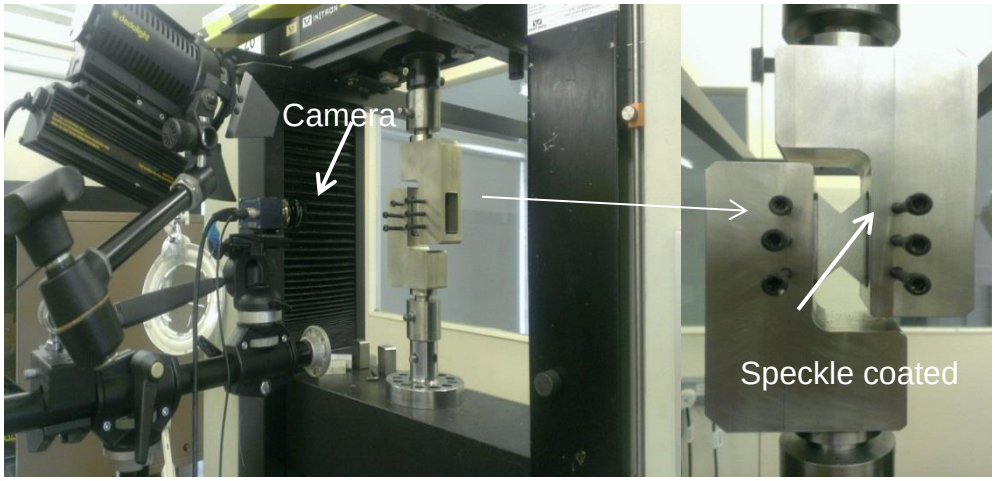

Figure 69. Shear tests method and sample location with DIC method.

5.2.4.3 Water immersion

The effect of treatments on water absorption of flax/tannin composites was investigated in accordance with ASTM D5229. Three specimens (150×100 mm) per composite type were pre-dried in an oven of 60 °C for 24 hours, and measured as the initial weight with value close to the nearest 0.1 mg after cooling them to room temperature. Then the specimens were immersed in a sealed de-ionised water bath at 25 °C to conduct the water absorption tests. After the first immersion for 2 h, the specimens were taken out from water and gently blotted with clean dry paper to remove the surface excess water. The samples were then immediately weighed and re-immersed, followed by the same procedure at different time intervals of 24, 72, 192, 336, 504 up to 672 h exposure until a saturation point was reached. The water content was calculated by following:

$$M_t = \frac{W_t - W_0}{W_0} \times 100\% \qquad (5.1)$$

Where W_t is the weight of the wet composite specimen at time t and W_0 is the mass of dried specimen, M_t the moisture content at time t.

5.3 Results and discussion

5.3.1 SEM investigations

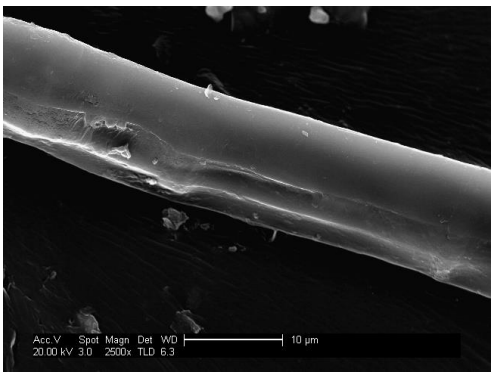

Figure 70. The SEM morphology of untreated single flax fibre.

The scanning electron micrographs (SEM) clearly show differences in the surface morphology of the flax fibres depending on the applied fibre surface

modifications, including 5 $_{wt}$% NaOH, BTCA, APS and LD. Scanning was synchronized with microscopic beam to maintain the small size over large distance (to the specimen). The magnification of the images was set at 2500 for the unmodified flax fibre and 5000 for modified types. Figure 70 and Figure 71 provide details about the surface characteristics of flax fibres with and without chemical treatment.

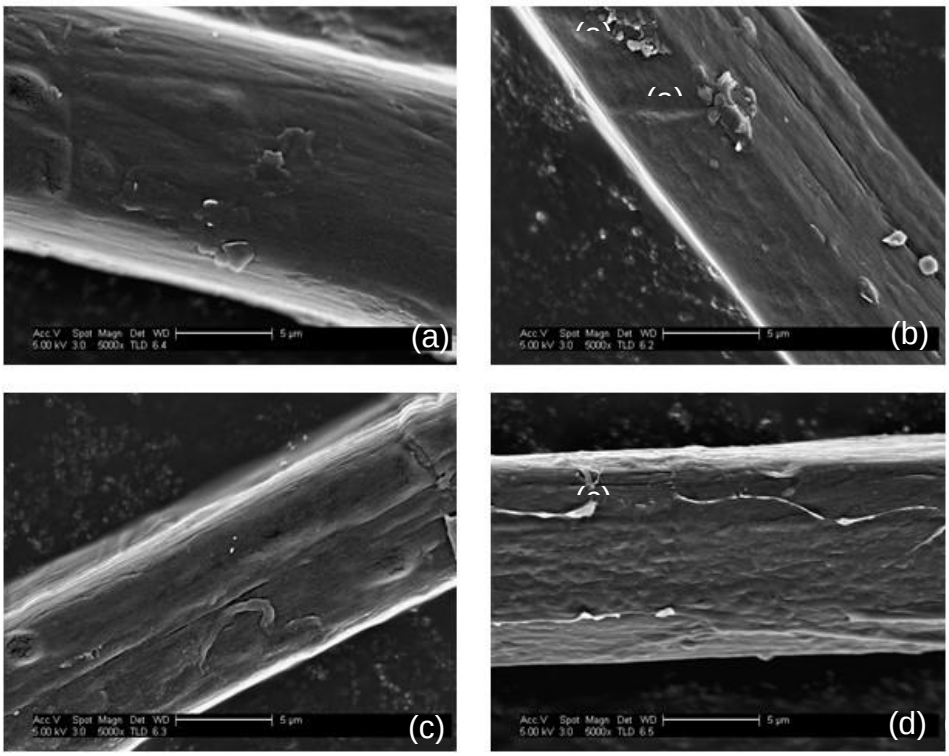

Figure 71. SEM morphologies of treated flax fibres: (a) 5% NaOH treated; (b) BTCA treated; (c) APS treated; (d) LD treated.

Figure 70 shows the original surface topography of the supplied flax fibres from the untreated flax mat. The neat fibre structure was not clear and partially covered by attached substances, such as fibre waxes and fats. A very effective procedure to purify the flax fibres is alkalization using NaOH, resulting in the removal of wax, the primary cell wall and other additives [83]. It can be seen from Figure 71 (a) that the resulting fibre surfaces became more structured with obvious striations. The dissolution of materials (lignin, hemicellulos etc.) on the primary cell wall gives a rougher fibre surface, exposing more inter-fibrils for better fibre/matrix wettability. This shows strong agreement with FTIR analysis

in Chapter 3. However there were still residual granular particles corresponding to lignin on the surface. The knuckle–swellings and disclamation as present in the raw fibres can still be found after NaOH-treatment. It has been reported that the higher NaOH concentration (10 $_{wt}$%) may start the conversion of the crystalline form from cellulose I to cellulose II, which causes deeper and broader striation [82]. The surface features of fibres are also clearly visible for other two modifications (BTCA and APS). More structure of raw fibre cell wall on the three treatments was exposed on the fibre surface than that of the NaOH-treated flax fibre to increase the roughness, revealing potential for fibre/matrix adhesion improvement. Another thing noted for LD fibre was the thin layer with many small protrusions, which were considered as the grafted hydrophobic Doga compounds. All the modifications resulted in uncovering the fibre fibrils with different amount of residual fibre additives sticking on the surface. In conclusion, the rougher fibre surfaces have a potential to improve the fibre/matrix adhesion.

5.3.2 Effect of fibre treatment on dynamic mechanical properties

Dynamic mechanical analysis done in the experiments studied the effect of fibre surface treatments on the temperature dependency of viscoelastic properties of flax/tannin composites. Figure 72 and Figure 73 show the curves corresponding to storage (E’), loss modulus (E’’) and tanδ (ratio of E’’/E’) with the increase of temperature to 200°C, and the dynamic characteristics (shown in Table 18) were determined based on these figures.

From Table 18, the initial storage modulus of composites varies quite a lot as a result of different fibre treatment techniques employed. The initial storage modulus at 30 °C for untreated composites was 4.2 GPa, much lower than that of treated samples. The BTCA and APS treated composites showed highest initial storage modulus around 5.4 GPa. In addition, NaOH and LD types respectively exhibited 23.8 % and 9.5 % increase in storage modulus at 30°C, compared to untreated composites. Each chemical modification had a significant improvement with different levels on the interfacial bonding due to the rougher fibre surface topography after partially or completely removing the

non-cellulose lignin during processing. The rougher fibre gives rise to the larger fibre/matrix contact surface, improving the load transfer, while the rearranged or re-oriented fibrils can lead to a better stress/load carrying ability along the fibre axis. The reduced fibre length/diameter ratio could enhance the fibre reinforcement. As time increased, the storage modulus decreased gradually with a slight glass transition period and almost maintained the same value trend, as an example of the storage modulus at 80 °C for flax/tannin composites. After 130-140 °C, the modulus dropped greatly (the highest degree for APS) possibly due to the onset of material degradation.

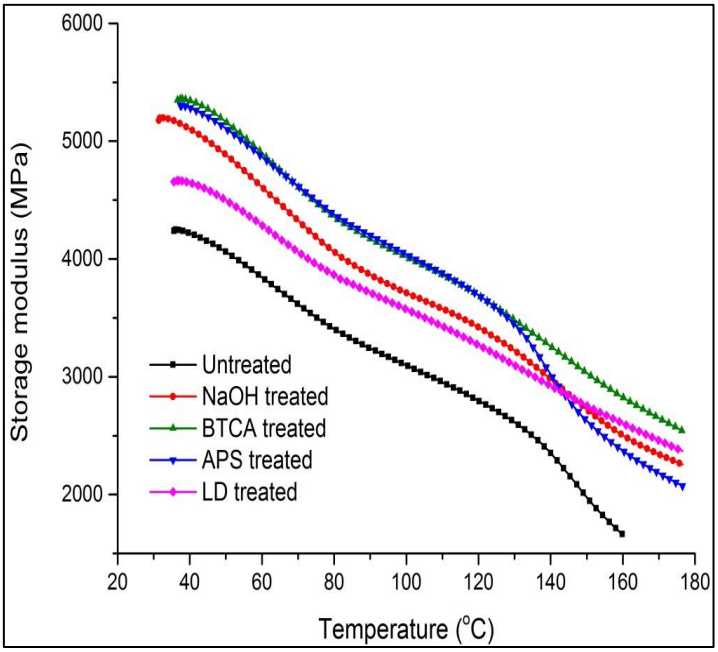

Figure 72. Variation of storage modulus of flax/tannin composites with different treatments as a function of temperature.

Table 18. Dynamic mechanical properties of flax/tannin composites.

Type	E' at 30 °C (GPa)	E' at 80 °C (GPa)	E'' at 30 °C (MPa)	T_g (°C)
Untreated	4.26	3.42	158.18	70.02
NaOH	5.24	4.05	205.31	71.15
BTCA	5.45	4.35	215.38	70.76
APS	5.42	4.37	194.83	71.08
LD	4.61	3.86	177.74	70.70

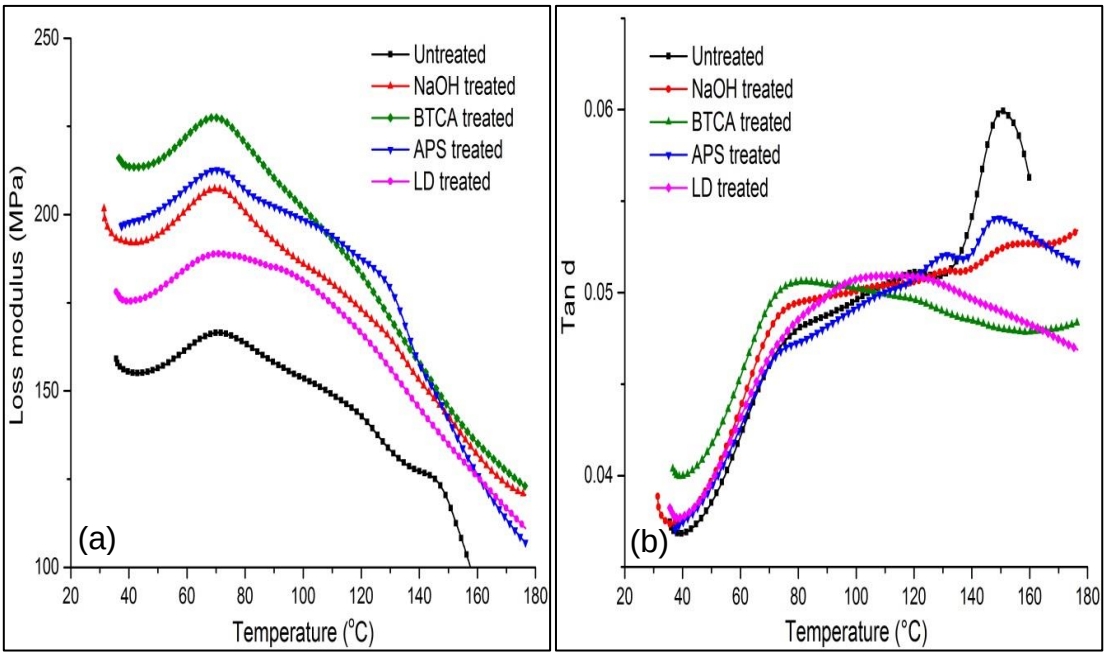

Figure 73. Variation of loss modulus (a) and tanδ (b) as a function of temperature for flax/tannin composites with different treatments.

The variation of loss modulus and tanδ of flax/tannin composites with surface treatments was shown in Figure 73. The glass transition temperature of flax tannin composites was determined at loss modulus peak (Figure 73 (a)), but not from the tan δ peaks (Figure 73 (b)). The T_g of untreated composites was observed at 70.02 °C, while the T_g for modified composites was not significantly altered in the range of 70-71°C. The similarity of T_g revealed that the surface treatments had little change on the mobility of amorphous chain segments in the tannin resins. However, the magnitude of loss modulus value of flax/tannin composites increased after application of the chemical treatment. This is attributed to the increased ability to absorb energy, resulting from more adhered flax fibres. Tanδ is an important damping factor for dynamic behaviour of materials. There was a damping peak at about 77 °C corresponding to glass transition temperature for each composites type. An extra tanδ peak was located at 151.02 °C for untreated composites. The reason has not been determined but possibly was resin degradation inducting molecular relaxation. APS and NaOH types also showed the damping peak with a lower magnitude at the temperature close to 150 °C.

5.3.3 Effect of treatments on tensile properties of flax/tannin

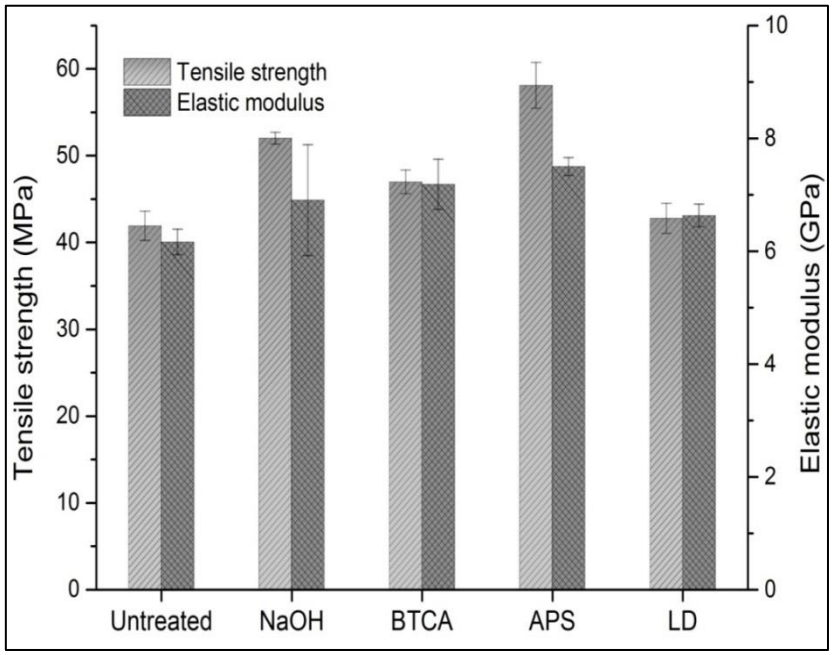

Figure 74. Tension properties of untreated and treated composites.

The effects of fibre pre-treatments on tensile properties (e.g tensile strength and tensile modulus obtained from Figure 74) of nonwoven flax/tannin composites are shown in Figure 74. The untreated composites had a similar tensile strength around 41.9 MPa to the previously tensile results of flax/tannin composites reported by Sauget and his co-workers [193]. It is clear that every fibre modification had a positive effect on tensile strength at certain level. Pure NaOH treated composites increased 24.1 % in the tensile strength of 52.0 MPa in the comparison to untreated composites. The improved roughness of fibre surface by alkaline treatment (Figure 71) results in the better flax/tannin wettability, interfacial adhesion and consequently sufficient stress transfer. The extra introduction of silane couple agent (APS) after NaOH purification enhanced the tensile strength to 58.1 MPa with about 38.6 % improvement. When the fibres were impregnated with resins, silane linkages were formed between fibre surface and resin at elevated temperature so as to further improve the interfacial adhesion strength. However the alkaline-esterification (BTCA) leads to a lesser degree of strength enhancement at 47.0 MPa. After the NaOH purification as the first stage, the additional APS treatment provided better

fibre/matrix adhesion compared to BTCA treatment, which resulted in a lower tensile strength than pure NaOH treated composites. This is probably owing to the decrease of fibre strength, caused by the severe dissolution of hemicellulose after added BTCA modifications. This negative result to some extent countered the fibre/matrix adhesion improvement by esterification influence, reducing the reinforcing effect of flax fibres. It was observed that LD treated flax/tannin composites showed a slightly higher tensile strength of 42.8 MPa than the untreated composites. It demonstrates that enzyme-LD modification still needs development to suit this novel flax/tannin composite. Based on the results of Young's modulus, it can be considered that APS treated composites, which showed the best results in tensile strength, exhibited the highest tensile modulus of 7.5 GPa among all the samples. Similarly, untreated composites had the lowest modulus values of 6.1 GPa. The modulus of BTCA composites (7.2 GPa) was slightly higher than NaOH type (6.9 GPa).

Failure initiation strength

Non-interactive (e.g. maximum stress criteria [194]) and interactive approaches (e.g. Tsai-Wu [195] and Puck criteria [196]) are commonly adopted by industries to predict the failure of composite laminates. The former method ignores the normal stress and shear stress interaction, while the latter requires experimental data to determine the parameters with physical understanding. The in-plane failure prediction of laminates has been successfully applied in UD laminates with 'ply by ply' failure analysis [197]. For laminates like multi-axis layers with homogenised properties, Lausten et al. [198] and Leong et al. [199] recently provided an alternative way to simplify the failure analysis to derive the initial failure, called failure initiation strength. Traditionally for engineering composites, it is assumed that only linear elastic behaviour occurs before the micro-cracks initiation causing non-linear transition. However, the plasticity of matrix or fibres may also lead to nonlinear behaviour in practical problems. This approach takes this effect of damage and plasticity interactions and is based on the numerical differentiation of stress-strain curves with smoothly declining

tangent. Contributed from both elastic (ε_e) and plastic (ε_p) deformation, the strain (ε) could be expressed as:

$$\varepsilon = \frac{\sigma}{E} + a \times \ln\left[1 - \left(\frac{\sigma}{\sigma_0}\right)^m\right] \quad (5.2)$$

Where ε_e is derived from Hooke's law simply using applied stress (σ) and elastic modulus (E); ε_p is a function of three parameters, a (the scale parameter for plastic deformation), σ_0 (the horizontal asymptote value) and m (strain-hardening parameter). As introduced by Christensen [200], when the third derivative of a stress-strain curve reaches zero, referring to the peak of 2nd derivative value, the onset of failure strength (S_i) and associated strain as the nonlinear to linear transition point are obtained accordingly:

$$\frac{d^3\sigma}{d^3\varepsilon} = 0 \quad (5.3)$$

Since the non-woven flax mats exhibited a plastic-like deformation under tension (see in Chapter 3), the above theory and calculation could be applied on the non-woven flax/tannin composites with quasi-homogenised properties. Combing the universal global optimisation (UGO) and Levenberg-Marquardt (LM), curve fitting was based on the RSS (residual of sum of square) method by uisng 1stOpt software, a professional nonlinear curve fitting software:

$$Min.RSS = \sum_{i=1}^{n} (\varepsilon - \varepsilon_i)^2 \quad (5.4)$$

Where ε is the practical input strain value, ε_i is calculated strain value. An example of building regression code is seen below:

```
Algorithm=UGO [100];

RegType=0;

Variables x, y;

Parameters E [40,200], a [-10, 0], A, m;

DataFile "C:\tesion-FT-untreated.xls [test01 [B4:C674]]";

MinFunction Sum(i=1:671)((X[i]/E+a*ln(1-(x[i]/A)^m)-y[i])^2);
```

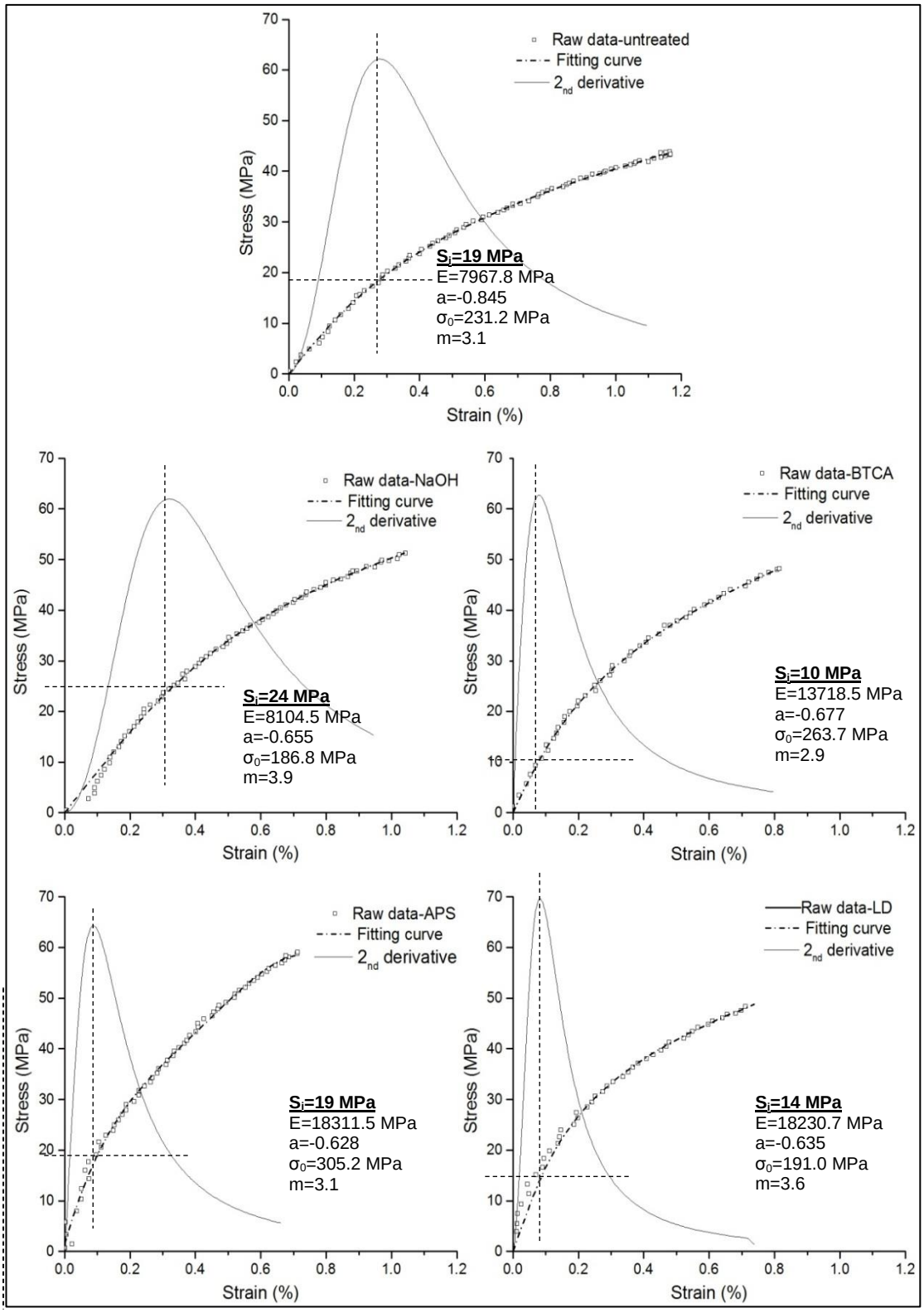

Figure 75. Example of computation of tensile failure initiation for flax/tannin.

Figure 75 shows the stress-strain curves, together with the failure initiation strength and corresponding parameters for flax/tannin composites with different

treatments. Non-linear relationships were observed for all composites almost from the beginning of the curves, without any visible transition point. The onset of failure, tracked by using normal prediction failure method, can occur very early. It is nevertheless, the plasticity of the fibre mats has to be considered. The re-alignment and deformation of short flax fibres will induce micro-cracks in tannin resins, as tannin resins have a great extent of internal stress for brittle failure (Chapter 4). The better the fibre/matrix adhesion, the more load transferred to flax fibres, and hence higher the total applied stress required for resin crack initiation. The NaOH treated composites had the highest initial failure strength of 24 MPa among the composites. The APS treated composites showed the same initial failure strength of 19 MPa as untreated composites, although the APS treatment significantly improved the tensile strength by 36 %. The application of BTCA treatment largely decreased the failure strength down by 50 % to 10 MPa. The modulus obtained from this method is much higher than the chord modulus (strain range: 0.0015 to 0.0045), but still in line with the trend (APS>LD>BTCA>NaOH>untreated). The nonlinear behaviour dominates the strain range for chord modulus calculation, hence engineering chord modulus differs greatly from tangential modulus, which changed significantly in the range and was used for the initial failure strength prediction. It has to be noted that this prediction method is conservative due to lack of verification, but this robustly-determined value can still encapsulate the effect of treatments on the real initial failure with the concern on plastic deformation.

DIC-failure analysis

The advantage of using DIC method not only gives accurate micro-scale strain through full-field analysis, but also reflected precise progress of strain change all through the testing to failure [198]. The principle strain in the area for untreated composites changed from 0.001 and 0.003, which was used to calculate the chord elastic modulus. Figure 76 showed the principle strain distribution from 13 s to 40 s for flax/tannin composite with different treatment. In the same time-scale of 27s, the presence of much lower strain change was observed for all treated samples, which means that the composite

microstructure had a superior strain resistance to untreated ones as a result of less interface adhere strength between untreated fibres and tannin resins. The micro-heterogeneity of strain filed indicates the strain localisation, attributed to the inhomogeneous composite with high fibre weight content over 50 %, also investigated by Ramire et al. [176]. The fibre agglomeration can happen during impregnation at low resin content, resulting in a large number of flaws.

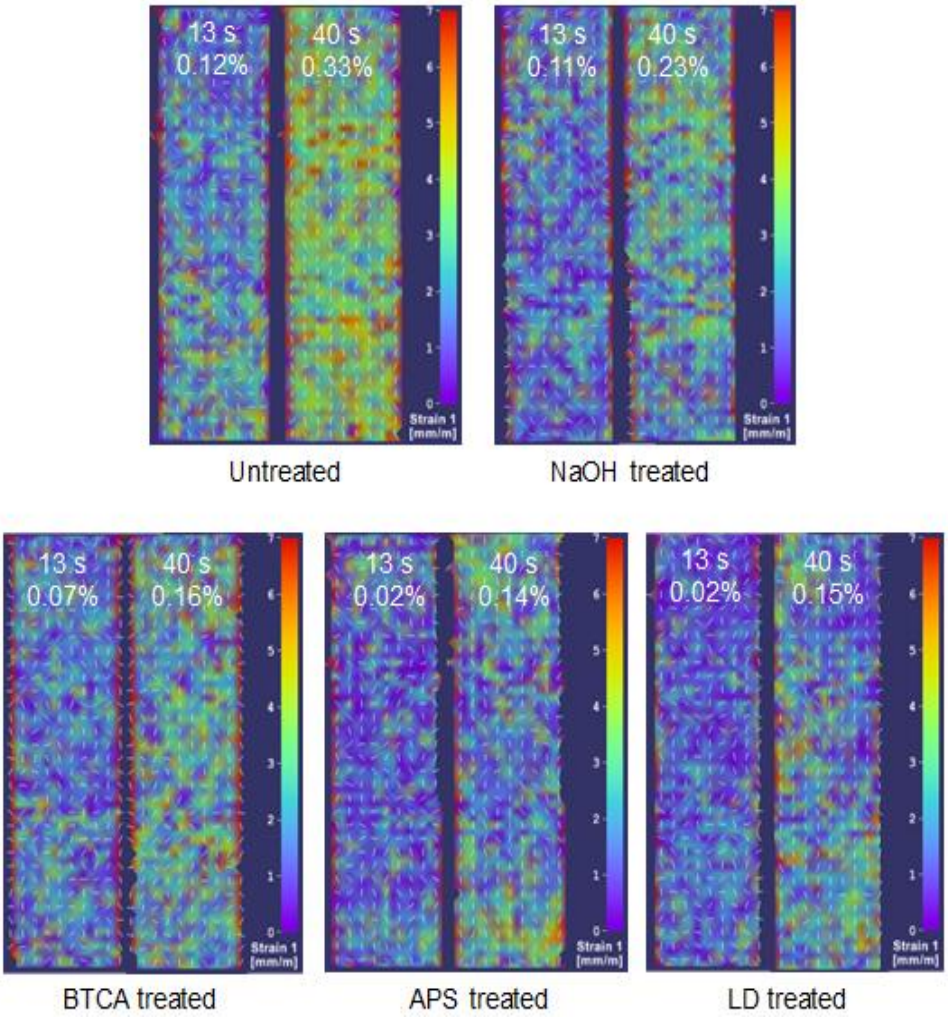

Figure 76. Strain distribution and localisation of flax/tannin composite at 13 and 40 s.

The flax tannin composites behaved similar to the chopped strand matt laminates (CSM) [29; 30]. The resin cracked first between fibres and then propagated through the transverse direction. The damage areas spread into large regions, together with re-alignment of fibres in the load direction (Figure 77 and Figure 78).

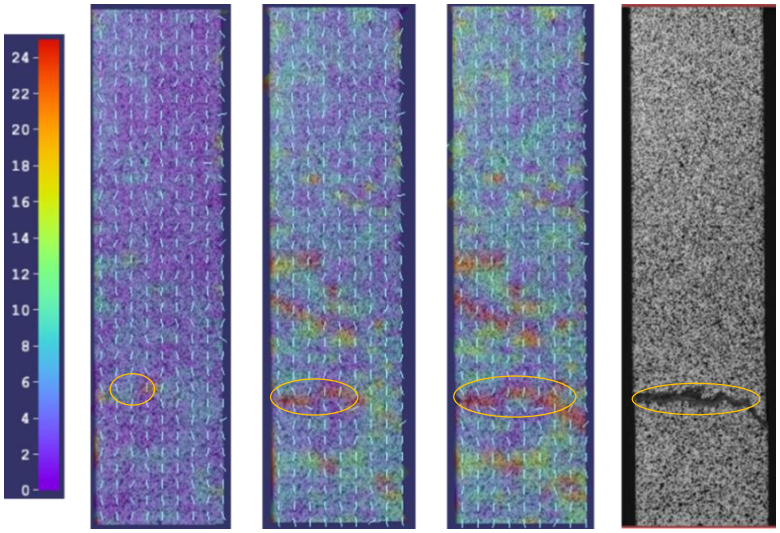

Figure 77. Representative failure progress monitored by strain change for nonwoven flax mat/tannin composites.

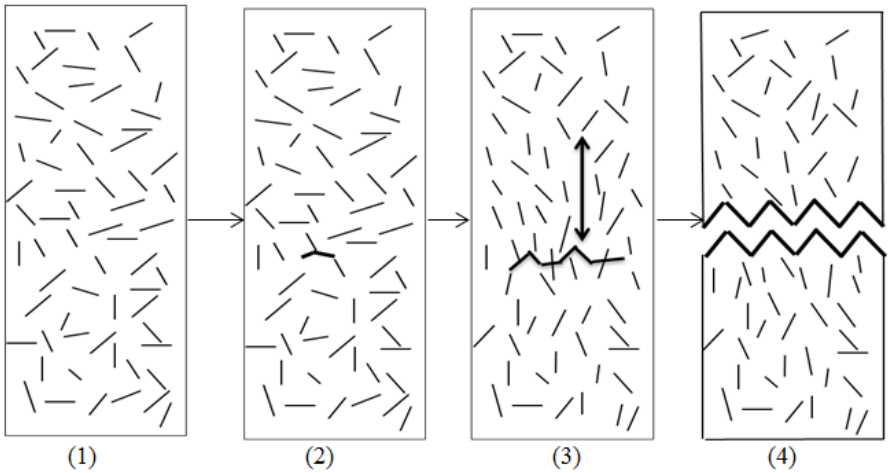

Figure 78. Typical failure stages of tensile fracture for flax/tannin composites: (1) no-crack; (2) fibre orientation and crack initiation; (3) crack propagation; (4) failure.

5.3.4 Effect of treatments on shear properties of flax/tannin

The shear strain has to be measured at the pure shearing location which is difficult to determine prior to the tests [201]. The shear strength is simply determined from the ultimate load and cross sectional area. The shear strain is indicated by normal strain at +45° and -45° using the following equation:

$$\gamma_i = |\varepsilon_{+45}| + |\varepsilon_{-45}| \quad (5.5)$$

Where γ_i is the engineering shear strain at the data points, ε_{+45} and ε_{-45} is the normal strain at +45° and -45° direction over the selected area under shear

stress (as shown in Figure 79). The shear chord modulus of elasticity was calculated using the engineering shear strain range (4000 με) with the starting strain point at the strain of 0.15 %-0.25 %.

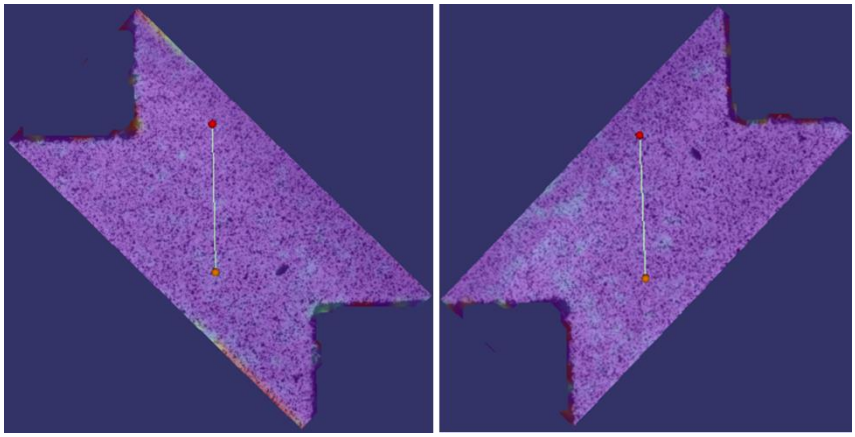

Figure 79. Image analysis of shear strain at +45° and -45°.

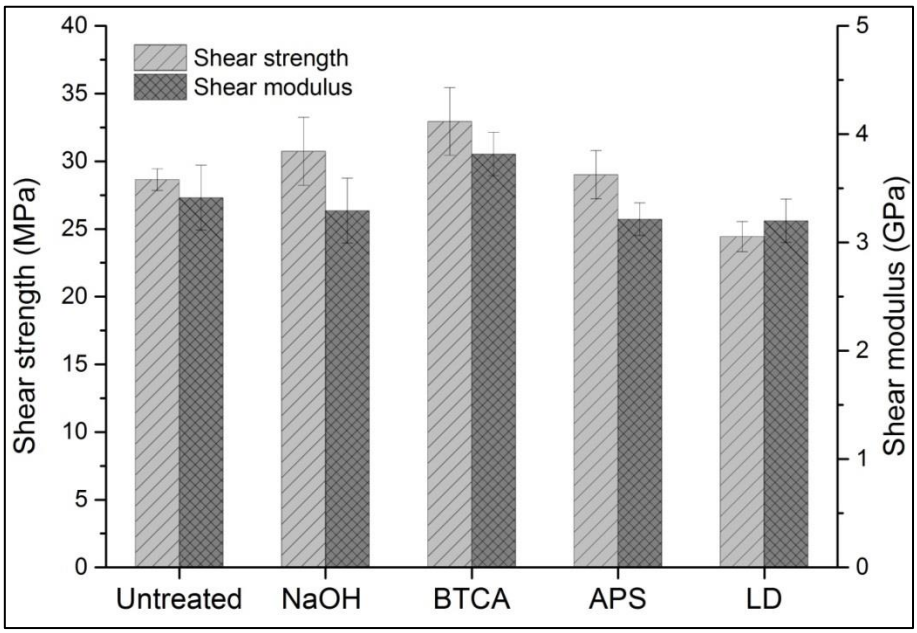

Figure 80. Comparison of shear properties of flax/tannin composites with treatments.

The shear properties (shear strength and shear modulus) are displayed in Figure 80. Comparing to untreated composites (28.6 MPa), NaOH modification increased the shear strength up to 30.7 MPa. BTCA treated composites showed the highest shear strength of 32.9 MPa (about 15% increase) among all the composites. It suggested that the mercerisation followed by the BTCA treatment gave the best result to improve the shear strength for flax/tannin composites.

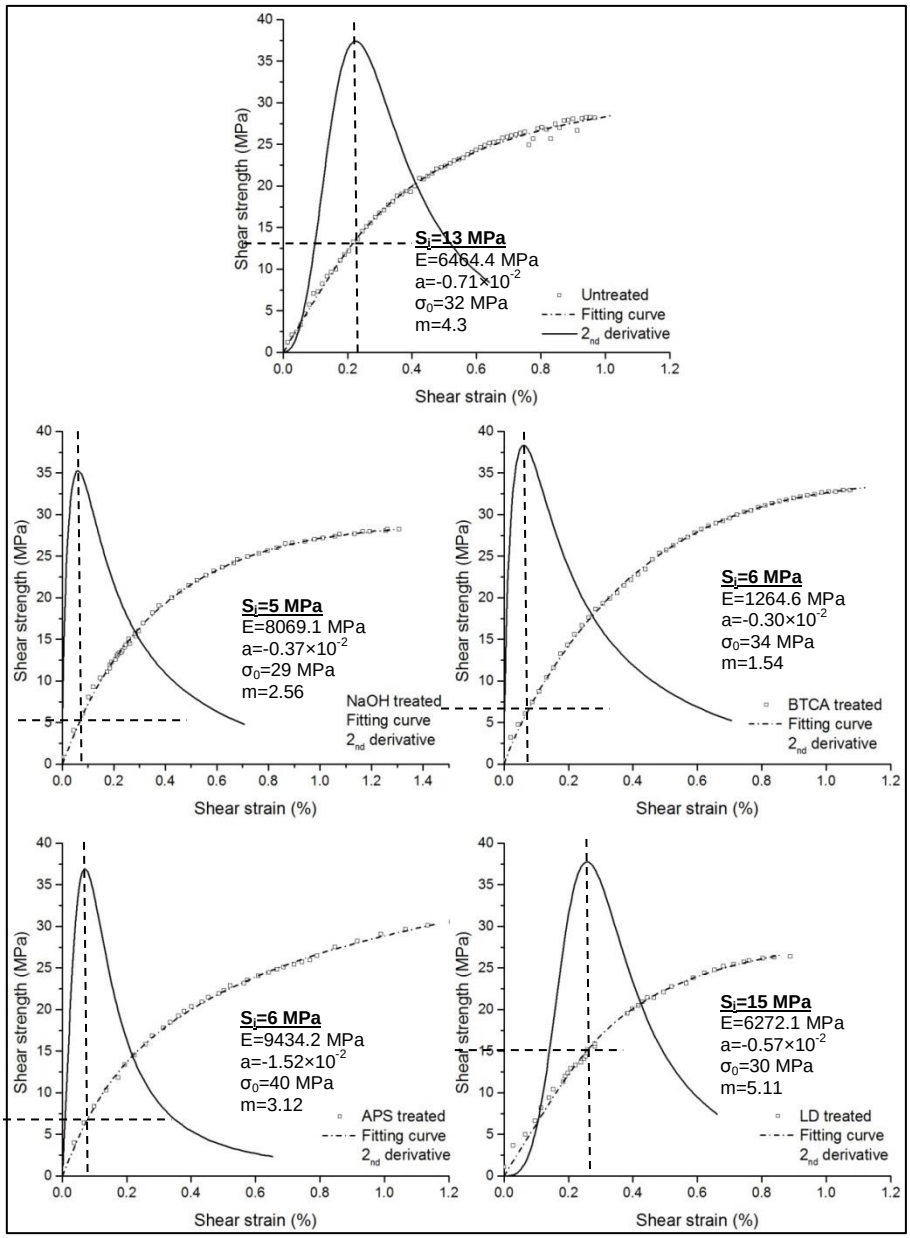

Figure 81. Example of computation of shear failure initiation for flax/tannin composites.

The strength change of less than 1 MPa after the APS treatment was not taken into consideration, while the LD composite type showed reduced shear strength, possibly attributed to decrease in fibre shear strength. The latter is possibly due to that the decrease of fibre properties, overweighing the increase of flax/matrix wettability in terms of shear strength. It was noted that NaOH and APS treated composites exhibited lower shear modulus of 3.29 and 3.21 GPa than untreated composites (3.41 GPa). These two treatments seemed to slightly decrease the modulus but retained or increased the shear strength.

Similar to the tension computation estimation, the initiation failure strength for shearing testing were determined in Figure 81. The untreated composites exhibited 13 MPa as failure initiation strength over treated composites, including NaOH, BTCA and APS types, except for LD composites presenting the highest value of 15 MPa. It seems that the decrease of the initial failure strength is related to the improved interfacial adhesion, resulting in increase in shear strength. Unlike in the tension case, when the fibre/matrix shear interfacial strength was improved by the three treatments to different extent, more load was introduced to the resin (not fibres) for the ease of occurrence of micro-cracks. Again, the computationally-determined modulus was not comply with the engineering chord modulus due to the high degree of curve tangent change.

An example of shear failure of flax/tannin composites is shown in Figure 82. It was observed that after the maximum stress point, there was no sudden brittle failure, but a gradual sample failure. The crack initiated from the upper and lower notch designed for stress concentration. Then the crack propagated slowly through the area under shear force as seen in Figure 82. Flax fibres bridged the crack surfaces to keep the load carrying capability, increasing the shear toughness and showing good resistance to crack growth in shear loading. The crack growth was not in a straight line possibly due to the plastic deformation of flax fibres.

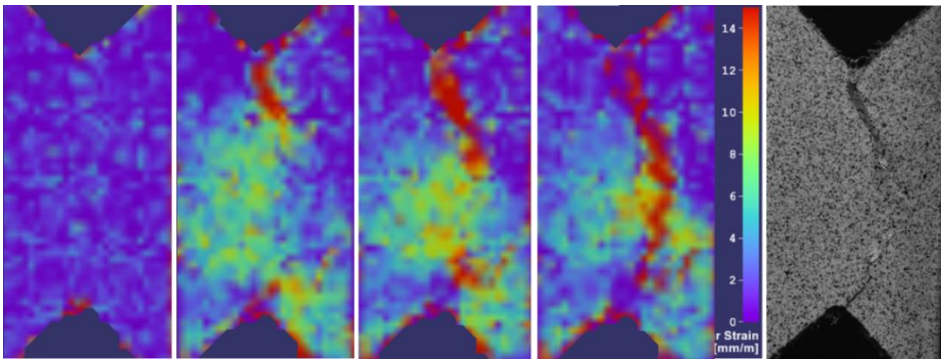

Figure 82. Example of shear strain field up to failure for flax/tannin composites.

5.3.5 Effect of treatments on flexural properties of flax/tannin

The quasi-static loading was applied on the composite specimens through three-point bending test to detect the material stiffness and dimensional

stability. The bending material undergoes the maximum tension stress on the bottom surface, and the force gradually transit through the thickness to the maximum compression stress on the upper material. As a result, the maximum flexural stress occurs at the mid-plane of sample and cracks are normally initiated on the tension surface.

Table 19. Flexural properties of untreated and treated flax/tannin composites.

Material	Flexural strength (MPa)			Flexural modulus (GPa)			Failure strain (%)		
	$\bar{X}$	S	CV	$\bar{X}$	S	CV	$\bar{X}$	S	CV
Untreated	61.27	4.1	6.2	6.12	0.3	5.2	2.49	0.2	9.2
NaOH treated	65.53	4.9	7.3	6.60	0.4	6.4	1.87	0.2	11.8
BTCA treated	71.73	4.8	6.9	6.52	0.6	9.1	2.07	0.2	9.3
APS treated	63.47	4.1	6.8	6.16	0.2	4.0	2.31	0.06	2.4
LD treated	51.88	1.1	2.2	5.48	0.3	6.1	1.82	0.1	5.9

***** $\bar{X}$-average, S-standard deviation. CV-coefficient of variation (%)

The flexural properties with static analysis are summarized in Table 19. According to the results, the application of NaOH-BTCA treatment on flax fibres significantly improved the flexural strength by 14.6 % and flexural modulus by 6.3 % of the flax tannin composites. NaOH and APS treated composites showed 6.5 % and 3.4 % increase of flexural strength, respectively. As discussed previously, the modifications improved the fibre roughness, allowing sufficient contact between fibres and tannin resins so as to enhance the interfacial adhesion and the stress transfer. However, the flexural strength and modulus of LD treated samples was about 18.2 % and 11.7 %, respectively, less than that of untreated composites. The decrease in fibre strength and modulus after LD modifications may account for the paradoxical results when compared to ‘better’ fibre-matrix adhesion. It has been proved in Chapter 3 that during fibre treatments, the removal of fibre components can cause reduction in the fibre mechanical properties. This indicates the difference in degree of effects of fibre treatments at various loading and testing conditions. The different property trends (tensile and flexural) of alkaline and silane treated

henequen fibre/HDPE composites were found by Herrera-Franco [202] as well. Li and his colleagues [167] also observed the increased tensile strength (6.7 %) and decreased flexural modulus (-6.1 %) for treated sisal/PLA composites in comparison to the untreated composites. Another observation was that all the treatments reduced the failure strain by up to 26.9 % due to the improvement in fibre/matrix interfacial adhesion, lowering the molecular/fibre mobility.

Table 20. Computed 'flexural failure initiation strength' of flax/tannin.

Type	E (MPa)	a (10^{-2})	σ_0 (MPa)	m	S_i (MPa)
Untreated	6423.8	-0.72	65.2	2.9	21
NaOH	8027.6	-0.42	68.3	2.7	25
BTCA	8011.1	-0.63	82.5	3.1	33
APS	6797.1	-0.74	70.0	3.2	26
LD	6695.4	-0.46	53.4	2.4	10

Typical predictions of initiation flexural failure strength by stress-strain curves of flax/tannin composite for each treatment are shown in Table 20. The highest failure initiation of 33 MPa was obtained for BTCA treated composites, which also exhibited the best flexural properties. Compared to the untreated composites with 21 MPa as initial failure strength, LD treatment leads to over 50 % decrease, showing strong agreement with its reduced flexural strength and modulus. NaOH and APS treated composites showed similar improvement of around 20 % in failure initiation strength. The predicted modulus for all composites was relative close to the chord flexural modulus, indicating good material stiffness under bending condition. The composites showed gradual fall-off in load capacity after their ultimate flexural strength. This is due to the pulling-out flax fibres carrying the load to slow the crack propagation.

5.3.6 Effect of treatments on impact properties of flax/tannin

The low velocity impact tests can simulate the actual loading issues on materials and hence are very useful for problem finding and solving in real world. The input energy (L_e) introduced by dart falling action is equal to the

energy dissipated by the whole system (L_w) as seen in the energy balance equation below [203]:

$$mgh = L_e = \frac{1}{2}mv^2 = L_w = L_{we} + L_{wi} \quad (5.6)$$

Where m the dart weight, v the contacting velocity, h the height, g the standard gravity (9.8 m/s^2), L_e the input energy equal to kinetic energy ($\frac{1}{2}mv^2$)and gravitational potential energy (mgh), L_{we} is the external energy dissipation, such as friction etc., L_{wi} refers to the internally dissipated energy by material elastic/plastic deformation or fragmentation.

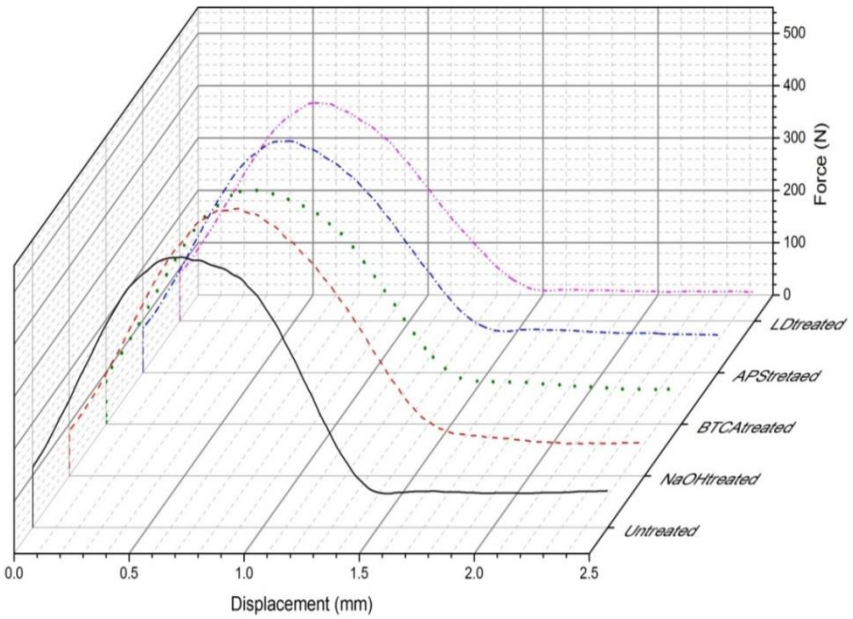

Figure 83. Waterfall description of impact force-displacement for flax/tannin composites with different treatments.

Table 21. Impact characteristics of flax/tannin composites.

Sample	Peak force (N)	Failure energy (J)	Impact energy (J)	Saturation (ms)
Untreated	515±33	2.52±0.1	4.80±0.12	4.7±0.1
NaOH	510±23	2.52±0.1	4.86±0.16	5.1±0.2
BTCA	446±22	1.91±0.2	4.31±0.22	4.9±0.1
APS	510±32	2.23±0.2	4.58±0.25	5.0±0.2
LD	416±30	1.64±0.2	3.68±0.15	4.5±0.1

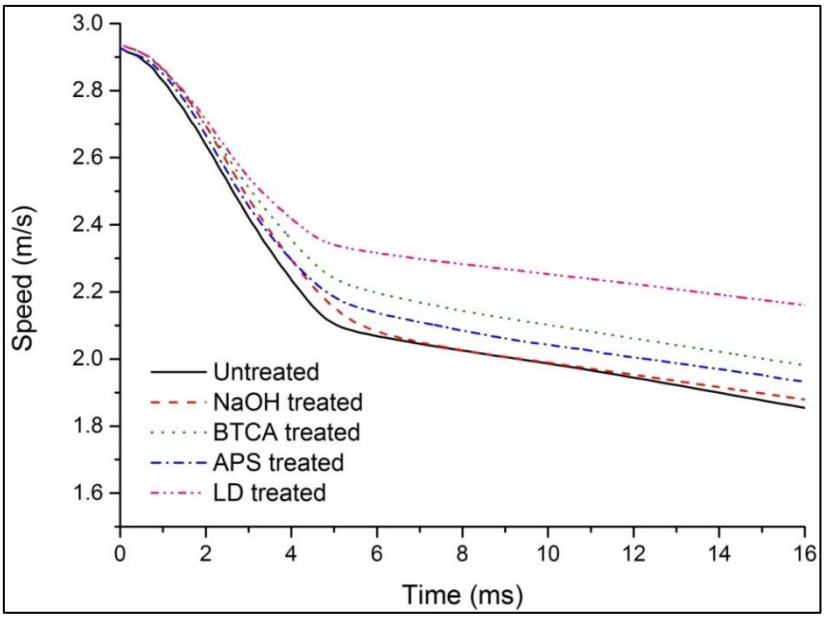

Figure 84. Speed change as a function of time during impact tests.

Figure 83 shows the typical load versus displacement curves average-smoothed (Savitzky-Golay method) by Origin software to minimize sample oscillation effect. The load increased with increasing displacement towards the peak force after which visible failure occurred. Then the load capability reduced dramatically to saturation point, followed by a force plateau (around 100 N) with continuous growth of displacement, indicating perforation situation during the impact testing. The other evidence is the velocity-displacement relationship (Figure 84). The velocity-decrease gradient changes to a lower value after the transition of energy dissipation mechanism mainly from L_{wi} by failure to L_{we} by friction. Belingardi and Vadori [203] also pointed out that the saturation instant can be defined at the transition time after which the velocity changes slowly. According to Table 21, the crack initiation and damage failure till the saturation took place in a very small timescale of 4-5 ms. The longest time elapsed to saturation was 5.1ms for NaOH treated composites while untreated composites had the shortest time of 4.7 ms. This indicates that the saturation time is probably influenced by the flax/tannin interfacial adhesion. The displacement at the saturation point was approximately 1.2-1.3 mm (Figure 84), even less than the composite average thickness of 2.5 mm. Clearly, the cracks propagated very fast through the thickness before the real dart perforation, resulting in total

collapse. The load-displacement trend of flax/tannin composites is very similar to that of non-woven hemp/polyester composite found by Thakal et al. [204] who also described the influence of impact load level into four stages. Stage 1 shows sudden load increase related to the in-plane stiffness of composites, followed by matrix damage in stage 2. The matrix cracking progress in stage 3 leads to fibre/matrix interfacial debonding, and finally, fibre breakage, delamination and perforation occurred in stage 4.

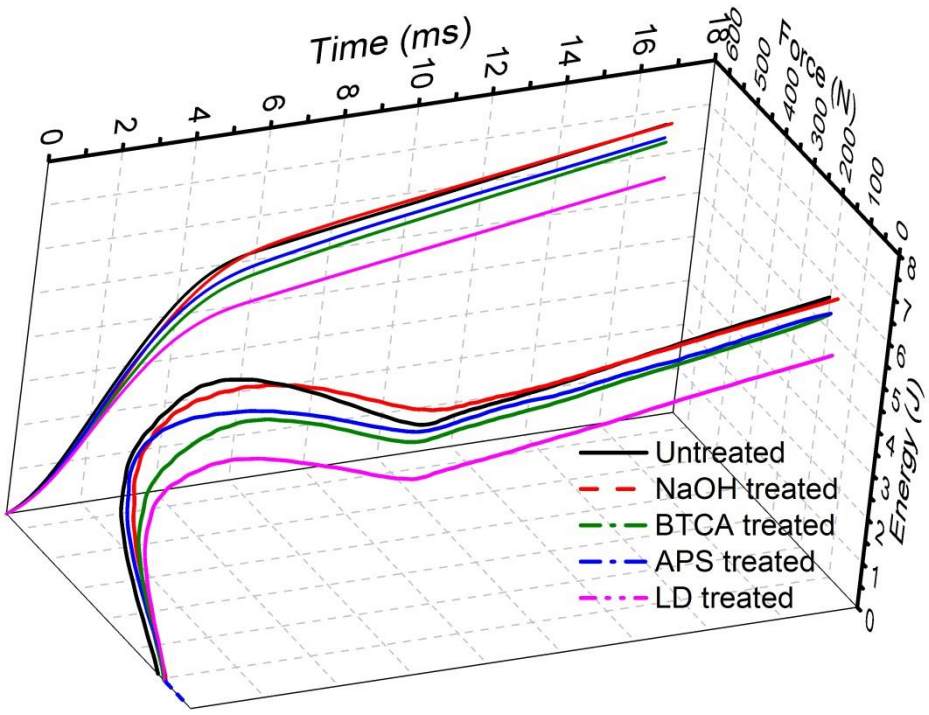

Figure 85. 3D description of time-force-energy for flax/tannin composites.

The threshold force for visible damage and the associated failure energy are shown in Table 21. The peak force trend does not correspond to that of elastic modulus, which normally is proportional to threshold force [205]. This is possibly due to the influence of different degree of surface imperfections of each composite type. The force peak of untreated composites (515 N) is only 5 N higher than that of APS and NaOH treated composites (510 N).LD treated composites (414N) showed 18% force reduction compared to untreated samples. On the basis of failure of fibre composites, the energy of damage propagation is due to three mechanisms of energy-absorption: frictional pull-out

energy during crack growth, interfacial short fibre/matrix debonding in the non-woven mats and the laminate delamination by matrix crack. The composite absorbed energy for crack growth and debonding until the peak force. The visual damage can rapidly reduce the load carrying capability [204]. NaOH and untreated composites showed the same failure energy of 2.52 J, 20 % and 30 % respectively higher than APS and BTCA treated composites. The lowest energy (1.64 J) was dissipated by LD to generate unrecoverable damage, showing agreement with its lowest flexural results.

The 3D time-force energy curves for untreated and treated flax/tannin composites were plotted in Figure 85. The time-force curves were similar to displacement-force curves due to the fact that there was no rebound case allowed force 'fold back' in force-displacement curves. The XZ projection of the 3D curves (Time-energy) reflected the effect of fibre treatment on energy dissipation progress. The absorbed energy could be measured as the area under force-displacement curves, and also be analysed by calculating the kinetic energy change. It can be seen from Figure 85 that the energy increased almost linearly with a gradient change at the transition time around 4-5 ms. The energy dissipated by the system before the transition was defined as the impact energy used for crack initiation and propagation. The following energy increment is mainly contributed by the friction between the dart surface and the sample edge in the perforation hole. The total input energy from the dart was about 10.26 J. As seen in Table 21, the best case for saturation energy is about 4.78 J (46.8 % of the total energy) found for NaOH treated composites. Untreated flax/tannin composites absorbed almost the same energy of 4.86 J, which is about 47.4 % energy absorption percentage. Although APS treated flax composites had comparable peak force to untreated composites, the impact energy of 4.58 J for APS samples showed a slight decrease around 7.0 %, compared to untreated ones. The BTCA and LD treated nonwoven flax/tannin composites had the impact energy before perforation is 4.31 J and 3.68 J, respectively, which is 42 % and 35.9 % of the total energy. This impact energy trend could also be distinguished from the residual velocity in Figure 84. The residual velocity at the saturation point followed the trend:

NaOH<untreated<APS<BTCA<LD. The lower residual velocity suggests higher energy dissipation due to material fragmentation.

5.3.7 Effects of treatments on water absorption of flax/tannin

As cellulosic materials, flax fibres have high hydrophilicity, leading to the importance of study in water sensitivity of flax reinforced composites. At the initial water absorption stage, the absorbed water remains in the inter-fibirillar space of cellulosic structure and causes cracks and micro voids [130]. Especially for flax reinforced bio-matrix composites, the reduction of mechanical properties on account of water immersion or moisture exposure is still the issue. The most common model for the water absorption prediction is expressed as Fickian's law [84; 206]

$$\frac{\partial_c}{\partial_t} = D_z \frac{\partial^2 c}{\partial_z{}^2} \tag{5.7}$$

Where c is the specimen moisture volumetric concentration, t the time, D_z the diffusion coefficient through-thickness direction. Coupling with the temperature (T) and time (t) effects, the moisture absorption can be expressed by the following equation:

$$G(T,t) = 1 - \frac{8}{\pi^2} \sum_{j=0}^{\infty} \frac{\exp\left[-(2j+1)^2 \pi^2 \left(\frac{D_z(T)t}{h^2}\right)\right]}{(2j+1)^2} \tag{5.8}$$

which is approximated by:

$$G(T,t) = 1 - \exp\left[-7.3\left(\frac{D_z(T)t}{h^2}\right)^{0.75}\right] \tag{5.9}$$

Where G presents the moisture absorption, h the thickness of materials, j the summation index. The initial curve slope has a proportional relationship with diffusion coefficient. For values M_t/M_m lower than 0.6 approximately, the initial part of the W_t-square t curve can be correlated by:

$$\text{Slope} = \frac{M_2 - M_1}{\sqrt{t_2} - \sqrt{t_1}} = \frac{4M_m}{h\sqrt{\pi}}\sqrt{D} \tag{5.10}$$

Where M_m is the maximum absorption value, M_2 and M_1 are the moisture content, t_2 and t_1 are the corresponding time, D is the diffusion coefficient in dimensions of [length^2 time^{-1}].

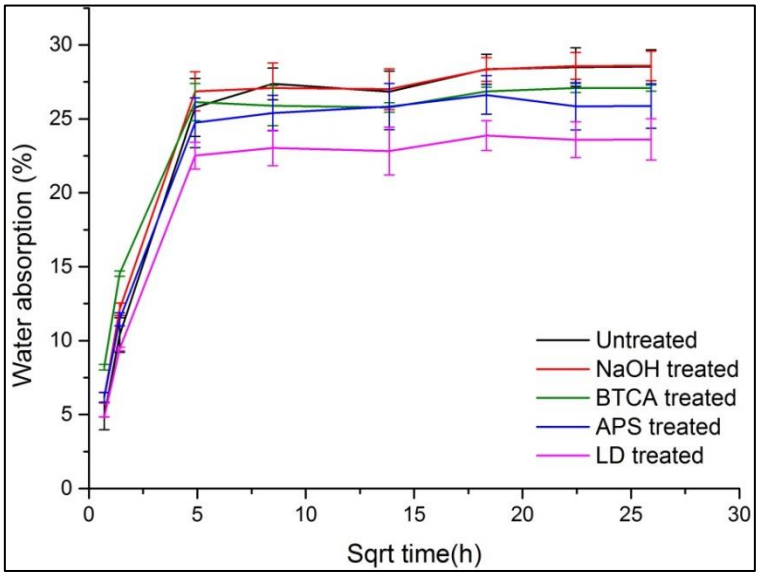

Figure 86. Average moisture uptake of flax composites at 100% of relative humidity.

Figure 86 shows moisture content resulting from the water absorption tests on the tannin composites reinforced with unmodified and modified non-woven flax fibre mats. It was obvious that the moisture content of flax fibre composites increased with increasing immersion time and eventually achieved the maximum values at the equilibrium state. The curves started with a linear initial part to achieve an equilibrium plateau, which cprresponds to Fickian behaviour (Fick's second law of diffusion). All the tested specimens exhibited fast water uptake for the first three days, and then slowly approached the saturation stage. The flax fibres containing many –OH groups in flax/tannin composites were able to easily combine with water, resulting in swelling, plasticizing and even degradation. In addition, the micro-voids or gaps, caused by the incompatibility between hydrophobic tannin resins and hydrophilic flax fibres, in the interfacial region could be filled with permeated water.

The surface treatments may influence the hydrophilicity and the surface adhesion, consequently leading to the various moisture absorption results, such as maximum moisture content (M_m) and diffusion efficiency (D), thickness swelling, as seen in Table 22 and Figure 87. At the 100% relative humidity level,

Table 22. Water absorption properties of flax/tannin composites with surface treatments.

Composite	As-received moisture (%)	Water content (2h-%)	Water content (24h-%)	Maximum moisture (%)	Thickness swelling (%)	Diffusivity ($10^{-3}cm^2/s$)
Untreated	4.50±0.21	10.38±0.41	25.77±1.45	28.52±1.82	15.30±0.51	0.043
NaOH treated	4.68±0.32	12.12±0.16	26.86±1.25	28.58±0.45	17.23±1.52	0.036
BTCA treated	4.18±0.19	14.54±0.13	26.13±1.51	27.08±0.53	17.57±1.32	0.031
APS treated	4.28±0.42	11.44±0.15	24.73±1.35	25.86±1.46	16.16±1.36	0.036
LD treated	4.17±0.33	9.43.±0.52	22.51±0.98	23.61±1.23	16.79±0.81	0.036

the NaOH-only composites almost sustained the maximum water content, whereas the other treated composites absorbed respectively less moisture than untreated composites. LD treated showed the lowest maximum moisture content of 23.6 % after water immersion. The grafted Doga chemical produced a hydrophobic layer on the fibre surface (see in SEM images), accounting for the improvement in water resistance. APS and BTCA treatments also introduced hydrophobic chemical groups on flax fibres, account for their 3 $_{wt}$% and 1 $_{wt}$% moisture reductions. The rougher fibre topography after alkali treatment may increase micro-voids due to the removal of interfibrillar matrix material, such as lignin and pectin. The rate at which moisture diffuses into or out of any solid through a cross section unit is determined as diffusivity D, also called flux, which is obtained through Fick's second law. Untreated and BTCA treated flax/tannin composites displayed the highest (4.3×10^{-3} cm^2/s) and lowest (3.1×10^{-3} cm^2/s) diffusion coefficient, respectively. The other three composite types (NAOH, APS and LD treated) had the similar diffusivity values about 3.6×10^{-3} cm^2/s. In terms of the thickness swelling, all the samples showed a very good dimensional stability, indicated by the relatively low thickness swell between 15-16 %. Clearly the surface treatments had little effect on the fibre swelling, largely controlling the thickness swelling.

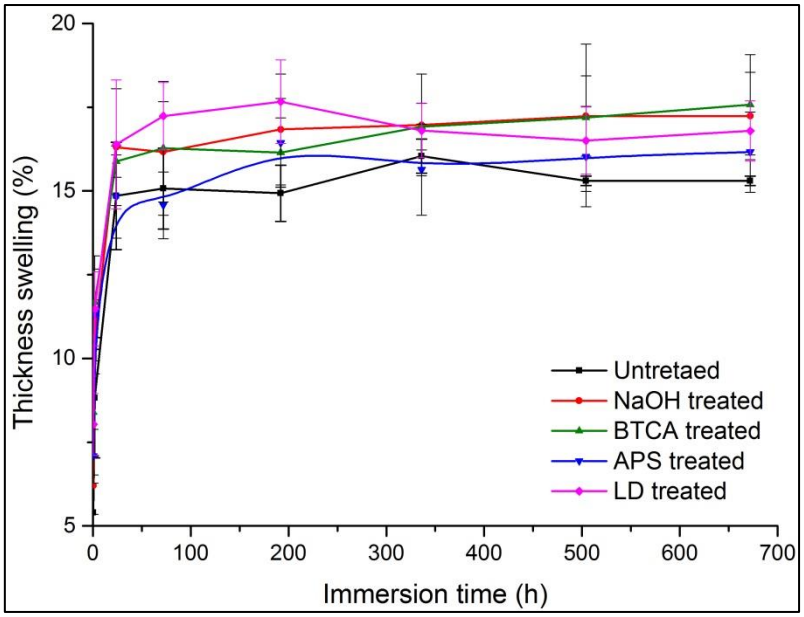

Figure 87. Thickness swelling of flax composites at 100% of relative humidity.

5.4 Conclusions

Mimosa tannin extracted from wattle trees were used with pre-treated flax to prepare flax/tannin composite for potential vehicle applications. These pre-treatments were found to improve the mechanical properties of flax/tannin composites to different levels. The storage modulus at 30 °C increased after treatments, indicating improved fibre/matrix adhesion. There was almost no influence on glass transition temperature at around 70 °C. The most significant influence of the applied treatments was seen in tensile properties, where APS treatment resulted in a 36.8 % increase in tensile strength, together with a highest tensile modulus of 7.5 GPa. A 14.6 % and 6.3 % increase in flexural strength and modulus respectively was observed in BTCA treated composites, which also showed best shear strength (35 MPa). Analysis of failure initiation analysis also reflected the improvement by surface treatment, but with different trend of failure onset value. Comparing to load-bearing properties, the impact performance of flax/tannin composites was much less affected by fibre modifications; however NaOH treatment still slightly increased the saturation energy to 4.86 J. With respect to water sensitivity, only 15-16% thickness swell of composites indicates their relatively good dimensional stability, although their maximum moisture content was over 20%. Consequently, for applications with various loading and environmental conditions, a proper fibre treatment has to be considered for non-woven flax/tannin composites to maximize the final enhancement effects.

Chapter 6. Influence of treatments on properties of hybrid flax/supersap bio-epoxy composites

6.1 Introduction

In addition to the tannin resins investigated in the previous two chapters, the vegetable oil-derived renewable epoxy resin is also a potential substitute of petroleum-based resin for flax composites. Their mechanical performance together with the environmental resistance make bio-epoxy/flax composites suitable for load-bearing parts such as vehicle body panels, crash elements and body trims body chasis [105; 136-139]. Adhekunle et al. [102] manufactured flax/bio-thermoset (methacrylated soybean oil and methyacrylic anhydride modified soybean oil) composites with different fibre stacking sequences and lay-up angles, leading to the maximum tensile strength of 119 MPa and Young's modulus of 14 GPa. A flexural strength of 201 MPa and modulus of 24 GPa was also achieved. Flax yarn and flax woven fabric reinforced soy protein concentrated resins (SPC) were prepared by Huang and Netravali [70]. Flax yarn composites showed the highest tensile strength of 298 MPa and flexural strength of 117 MPa. Table 23 shows some published mechanical properties of synthetic and bio-thermoset composites reinforced by flax fibres.

Table 23. Examples of mechanical properties of flax-thermoset composites.

Fibre/ Matrix	Processing	Tensile strength	Tensile modulus	Flexural strength	Ref
Flax/$(MSO)_a$	Compression	50-120 MPa	6-15 GPa	180 MPa	[102]
Flax/$(MMSO)_b$	Compression	50-120 MPa	7-15 GPa	201 MPa	[102]
Flax yarn/SPC_c	Pultrusion	298 MPa	4.3 GPa	117 MPa	[70]
Arctic flax/epoxy	Resin transfer	280 MPa	40 GPa	-	[103]
Flax/ epoxy	Compression	280 MPa	32 GPa	250 MPa	[105]

*a-Methacrylated soybean oil, b-methacrylic anhydride-modified soybean oil.c-soy protein concentrated

Currently, the woven flax fabrics are used in thermoset composites to give outstanding mechanical properties; but with extremely high cost and processing difficulties compared to non-woven flax mats. Avril et al. [207] have investigated

the optimisation of pine oil-derived epoxy/flax composites with respect to fibre configurations (non-woven thick mat, unidirectional-UD fabrics and balanced fabrics). The UD flax fabric composites (12 UD layers) showed highest tensile strength of 220 MPa and low impact resistance, while the nonwoven mat composites (2 layers) had the tensile strength of about 90 MPa. Work done in Chapter 3 suggested that flax fabric lay-up arrangement could be properly tailored to balance the tension and impact properties. Additionally as discussed previously, one of the main limitations for the flax composites is that the hydrophilic property of flax, leading to the poor interfacial adhesion with the nonpolar hydrophobic polymer matrix and difficulties in mixing, which influence the mechanical properties [180; 208]. To date, the surface treatments on flax fibres have been studied for matrix-rich composites and not for fibre-rich composites, which may differ due to fibre agglomeration.

Also as for vehicle industries, the environmental durability of materials (temperature, water sensitivity, UV degradation etc.) plays a very important role in the practical use range. Lots of studies regarding on the environmental resistance were done on flax reinforced composites based on synthetic polymers (PP, epoxy etc.) [87]. The storage modulus of flax/PP composites was found to increase at rubbery plateau after using zein as a coating on flax fibre due to improved mechanical stability [47]. Green flax/PP composites (18% max. moisture content) were more sensitive to water than Durbin flax/PP composites (12.8%), meanwhile the MA (maleic-anhydride)-PP/Duralin flax composites presented a lowest initial diffusivity of 5×10^{-3} cm^2/s [108].

Currently, the high cost of woven fibre fabrics and the low mechanical properties of bio-resin/flax composites limit their use in structural applications. The surface compatibility between pine oil-derived epoxy and flax fibres still remains a challenge and is yet to be solved. To investigate flax bio-composites with both economic advantages and acceptable properties (mechanical and environmental resistance) for structural applications, the author has studied flax/supersap bio-epoxy composites (FE) with a hybrid fibre configuration (nonwoven/UD flax fabrics). The non-woven flax mats were modified by alkali, acetylation, silane and enzymatic treatment prior to the composite preparation.

Tension, flexural, shear and impact properties of composites were obtained through adequate experiments to determine the influence of surface treatments on the mechanical performance. The effects of fibre pre-treatments on environmental resistance of FE composites were studied by conducting dynamic mechanical analysis (DMA), water absorption measurements and tensile tests after ageing conditioning (UV and Xenon conditioning).

6.2 Methodology

6.2.1 Materials

Table 24 below presents a qualitative evaluation of the main natural fibres laminates, following 3 criteria and with the perspective of composite manufacturing: mechanical performance, cost and processability.

Table 24. Qualitative evaluation of constituents for composites manufacturing.

	Flax non-woven mat	Flax balanced fabric	Flax UD
Mechanical performance	–	+	++
Cost	++	–	– –
Processability	++	+	–

An optimised fibre configuration was hence decided for bio-epoxy based composites for property balance and economic advantages. SuperSap 100/1000 epoxy resin containing 40 % pine oil derived bio-epoxy was supplied by Entropy. The details of UD and non-woven (NW) mats were described in chapter 2. The hybrid composites were made as below and seen in Table 25:

$$NW_1\ [UD]_5\ NW_1$$

The flax/supersap composites were manufactured by compression moulding at Mahytec, France (Table 25). The average thickness and fibre mass ratio were respectively 2.9 mm and 55-60 $_{wt}$%. The specimens were machined into the required specimen size for further characterisation (Figure 88).

Table 25. The hybrid flax reinforced bio-epoxy composites with treatments.

Matrix type	Fibre type		
		Configuration	Treatment
Supersap bio-epoxy	UD fabric	*Provided material* 5 internal layers	Untreated
	Non-woven mat	*Investigating factor* 2 (top and bottom)	Untreated 5 % NaOH Alkali + BTCA Alkali + APS Laccase-Doga (LD)

* BTCA- Butanetetracarboxylic acid, APS- Amiopropyltriethoxysilane, Laccase-Benzenediol, Doga-dodecyl gallate.

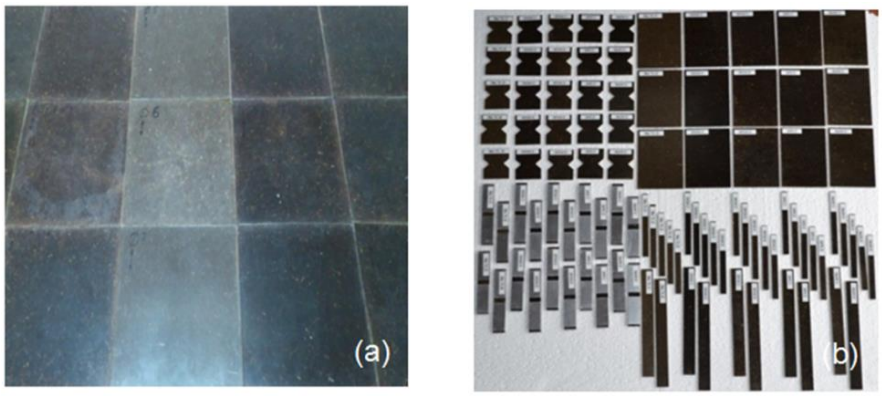

Figure 88. (a) Composites plates; (b) Machined specimens for testing

6.2.2 Pure bio-resin formation

The cured epoxy was prepared in a proper glass mould as seen in Chapter 4 for tannin resin preparation. The epoxy/hardener ratio is 1:2 by volume as suggested by the data sheets. Before pouring epoxy mixture into mould, the material was vacuumed at 500 bar for 20 mins to reduce the dissolved air. The curing cycle was 90°C for 2 hours.

6.2.3 Preparation of composites (provided by MahyTec)

A study regarding on curing cycle, pressure, maturation etc. was carried out to reduce surface porosity for homogeneity. Both non-woven and UD layers were

carefully impregnated and then stacked in the designed positions. The laminates were produced using a 270×270mm aluminium mould. The optimal parameters were identified as follows:

- Pre-heating of mould and oven : 80°C
- Maturation time of the resin before applying pressure : 15min
- Consolidation pressure : 30 bar
- Curing cycle : 2hrs at 90°C

6.2.4 Characterisation and tests

6.2.4.1 Mechanical testing

Similar to flax/tannin composites in Chapter 5, mechanical properties of flax/bio-epoxy composites, including tension, flexural, shear, damage resistance, were investigated through tensile testing(DIC), three-point bending, shear testing and falling weight impact testing, respectively (as described in Appendix 1). By comparing untreated and treated composites, the fibre surface treatment for this particular composite could be optimised.

6.2.4.2 Environmental resistance analysis

DSC analysis was done on both epoxy resin and untreated composites to determine the extent of curing and possible degradation, seperately. The treated FE composites were excluded since generally chemical fibre surface treatments have little effect on the curing characteristics. Dynamic mechanical analysis (DMA) was conducted for both cured resin and final composites to analyse the influence of fibre addition and treatments on the thermo-mechanical properties of the composite. Water sensitivity of the composites was measured through water absorption tests, in accordance to ASTM D5229.

The UV and Xenon Arc light weathering based on ISO 4892-3 and ISO 4892-2 was performed at VTT on FE composites. The UV ageing conditioning was done by using UVB-313 in the temperature range of -15 to 25 °C cycles for 552 h (23 days) in QUV Accelerated weathering tester and freezer. Similarly, samples were exposed to artificial weathering for 500 h with Xenon Arc light in

the apparatus Q-Sun Xe-3-HS and Q-SUN Xenon test Chamber XE-3-H/HSB/HS. The tensile properties of the composites before and after light conditioning were determined according to ASTM D3039. An Instron 5/100 5500R machine was used to obtain accurate traction properties of coupon specimens (25×250 mm). Four specimens per test were at the cross head speed of 2 mm/min with the load cell of 100 KN.

6.3 Results and discussion

Part 1-mechanical properties

6.3.1 Effect of treatments on tensile properties of hybrid FE

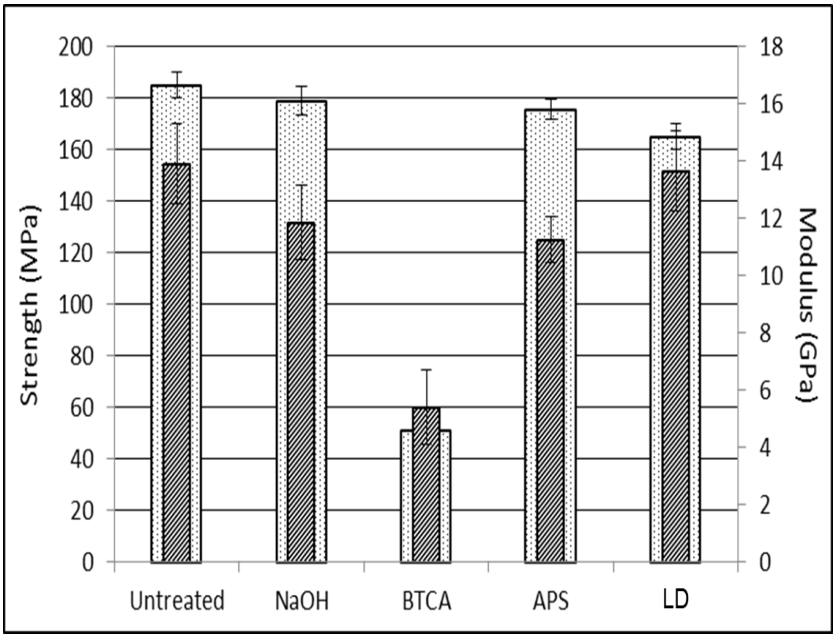

Figure 89. Tensile strength and modulus of hybrid FE composites.

The tensile properties of flax/supersap composites were compared through different treatments (non-treated, NaOH, BTCA, APS and Laccase-Doga). Tensile strength and Young's modulus are shown in Figure 89. The untreated flax/supersap composites exhibited tensile strength and tensile modulus of up to 185 MPa and 14 GPa, respectively. The NaOH treated composites displayed the tensile strength of about 178 MPa, less than 10 MPa reductions in tensile strength. The average tensile strength was observed to be at 175 MPa and 165 MPa for APS and Doga treated composites, respectively. Over 70% reduction

of tensile strength was found for the BTCA treated flax/supersap laminates (51 MPa) compared to untreated composites (185 MPa). Clearly, these chemical treatments have no significant improvement in ultimate tensile strength of the composites although they do have positive effect on flax/supersap wettability as discussed in Chapter 3. The modulus of the elasticity follows the trend: untreated>Doga>APS>NaOH>BTCA. The BTCA treated flax/supersap composites showed the lowest modulus of 5.4 GPa.

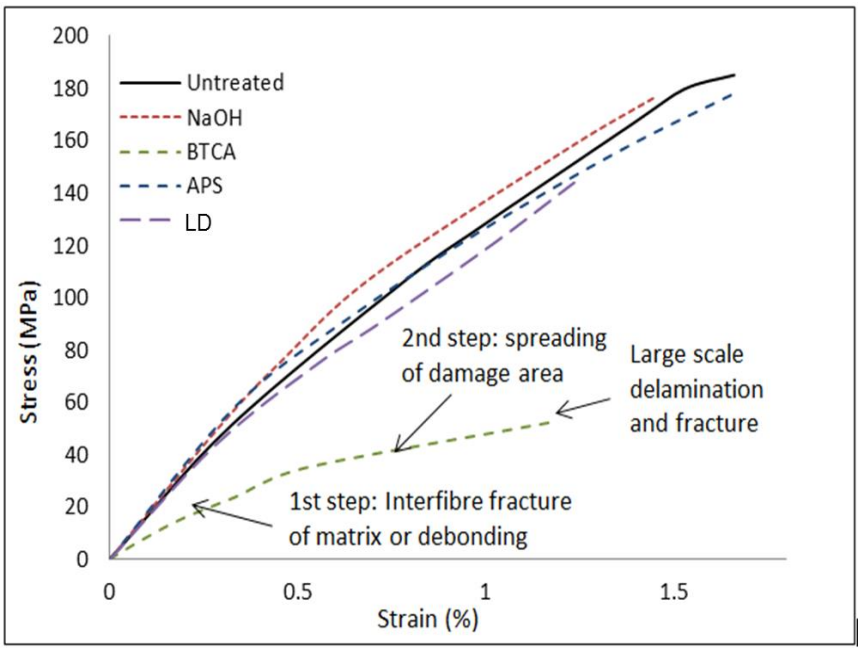

Figure 90. Stress-strain curves of hybrid FE composites.

NaOH treatment was able to maintain the tensile properties at an acceptable level; however the BTCA treatment highly decreased the tensile properties of the composites. The dissolution of hemicellulose during the treatment increased the fibre/matrix adhesion due to the rougher fibre surface; nevertheless the lack of inner matrix (hemicellulose) could possibly give rise to the tensile property reduction of flax fibres themselves. A few papers [25; 81; 82; 82] showed the chemical treatments only benefit the properties of bio-epoxy composites with the high matrix content. As the matrix ratio decreases below 50 $_{wt}$%, the fibre properties will contribute more to the composites due to the lack of resin to wet the flax fibres. The selected BTCA treatment may result in the most severe damage of microstructure of flax fibres, hence the insufficient load transfer. The

NaOH, APS and Laccase Doga treatments, resulted in dissimilar failure mechanisms of fibre/matrix adhesion, but showed similar effects on the tensile properties.

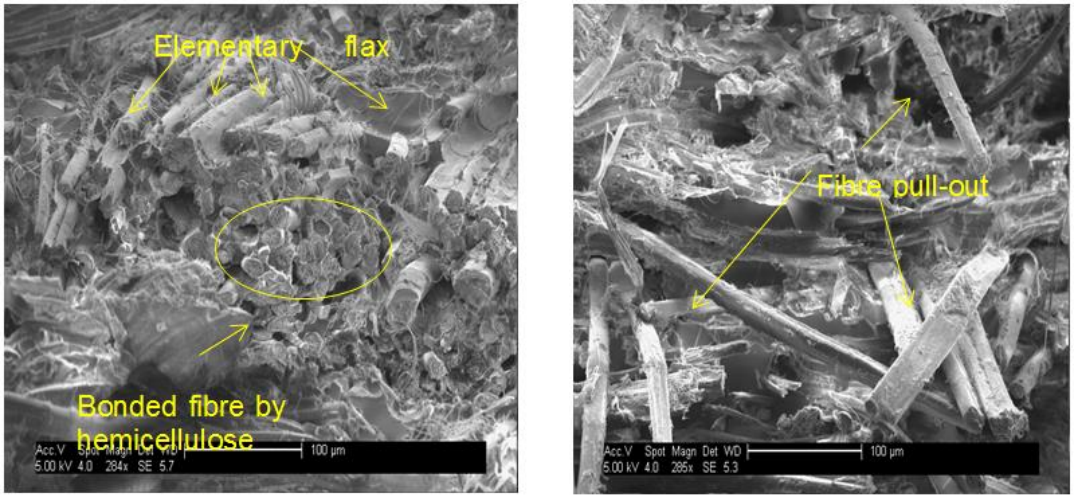

Figure 91. SEM micrographs of cross-sectional area of neat composites.

Figure 90 shows the representative stress-strain curves obtained from the tension tests of flax/supersap composites with chemical treatments. A quasi-linear behaviour was observed for flax/supersap composites, with no clear yield point or transition area. All the curves showed a continuously increasing stress with corresponding increase in strain up to a sudden brittle failure point, after which the force dropped dramatically. The failure progress for non-woven fibre mat reinforced composites in tension has been reported in literature [116; 209].

The failure started at the existing cracks or weak sites between the fibres. A substantial reduction of stiffness took place through a series of steps, causing a decrease in the initial slope of the stress/strain curve. Untreated and APS specimens showed the highest elongation up to 1.7 % at the breaking point, while the BTCA composites showed the lowest modulus and breaking elongation at approximately 1.2 %. It should however be noted that the NaOH treated composites had a lower decrease in stiffness than untreated specimens. The increase in fibre/matrix adhesion after NaOH treatment may result in relatively difficult fibre re-orientation and crack propagation.

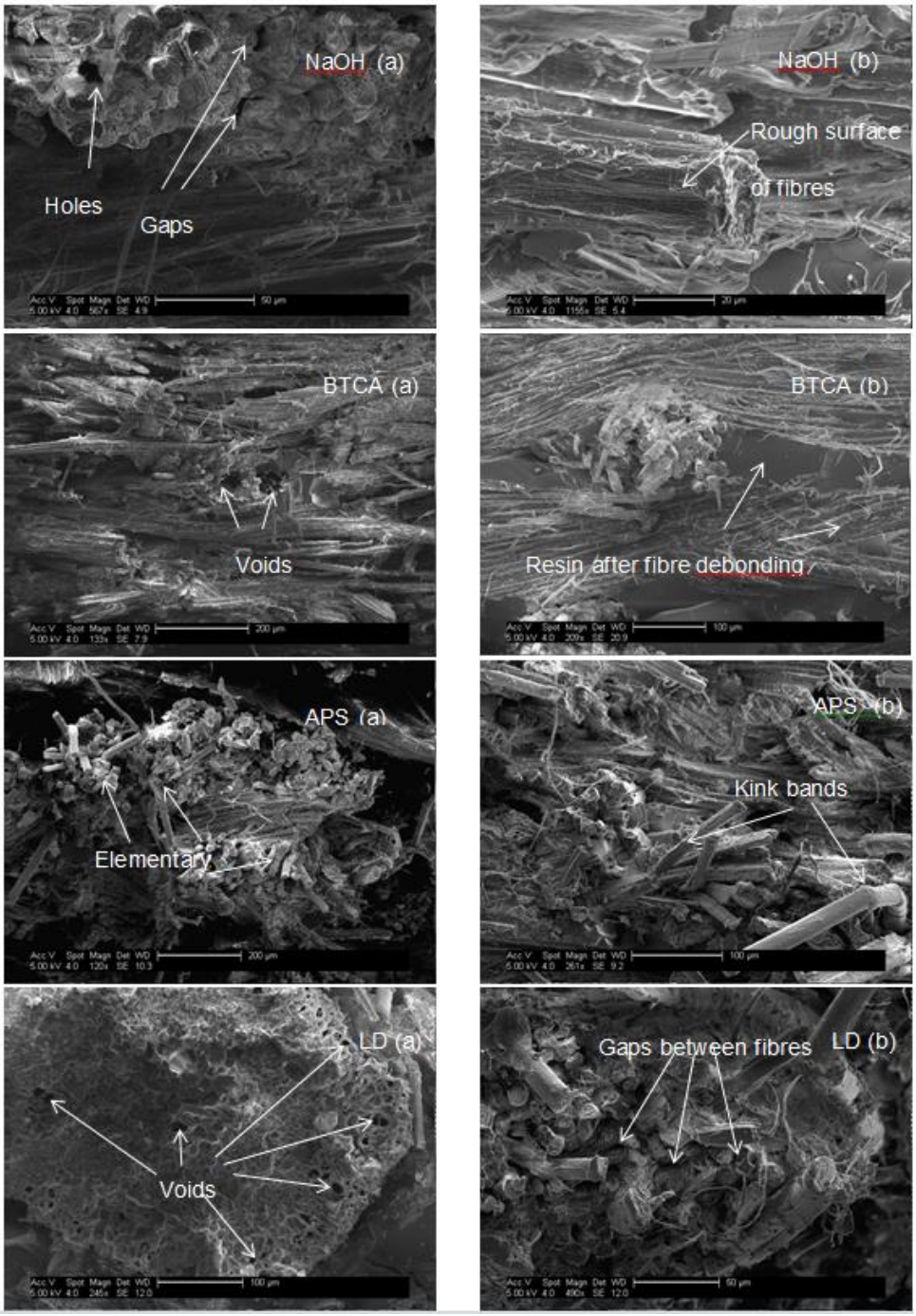

Figure 92. SEM images of fracture surface of composites with treatments.

Figure 91 shows the SEM images of the fracture surface of the untreated flax/supersap composites after tensile tests. As seen from Figure 91 (a), the elementary flax fibres were tightly held by the lignin and hemicellulose as inter-febrile matrix to form technical fibre, consisting of 10 to 40 elementary fibres. Fibre pull-out, fibre breakage and resin cracks were all observed in the

specimens. Extensive debonding and fibre-pull out were found at edge between the technical fibre/fibre bundles. This suggests weak interfacial strength between the fibre surface and bio-epoxy resins but a good inner-fibre bonding. The SEM cross-section photographs of composites with different treatments are shown in Figure 92. The visible holes and gaps were observed in all specimens with treatments. The holes could be caused by the fibre pull-out during tests or were there beforehand. Both explanations indicate poor adhesion with less load transfers between the elementary fibres.

6.3.2 Effect of treatments on shear properties of hybrid FE

Table 26. Shear properties of hybrid FE composites with treatments.

Hybrid FE Composite	Ultimate strength (MPa)	Shear modulus (GPa)	Break elongation (%)
Untreated	56.84±2.2	6.64±0.7	2.22±0.5
NaOH treated	45.80±3.2	4.15±0.6	2.42±0.6
BTCA treated	49.29±2.6	6.52±1.2	3.20±0.6
APS treated	51.55±2.5	3.64±0.9	3.73±0.9
LD treated	42.43±1.7	4.82±0.7	2.40±0.8

The effect of fibre treatment on shear properties is indicated from the testing results in Table 26. In terms of the ultimate strength, untreated FE specimens exhibited highest value up to 57 MPa. As discussed previously, the chemical treatments may lead to the lack of hemicellulose matrix in the inner fibril structure, causing insufficient load transfer between elementary fibres. The LD treatment gives rise to the lowest shear strength of around 42 MPa, 25 % reduction from the strength of non-treated hybrid FE composites. It was noticed that BTCA specimens showed comparable shear strength (50 MPa, 10% less than untreated ones) whereas the lowest tensile strength among the composites. The BTCA treatment (applied on the NW flax mats) greatly deteriorated the fibre properties (as seen in Chapter 3). However, the untreated UD fabrics, the middles layers, may mainly contribute the composite performances during shear tests.

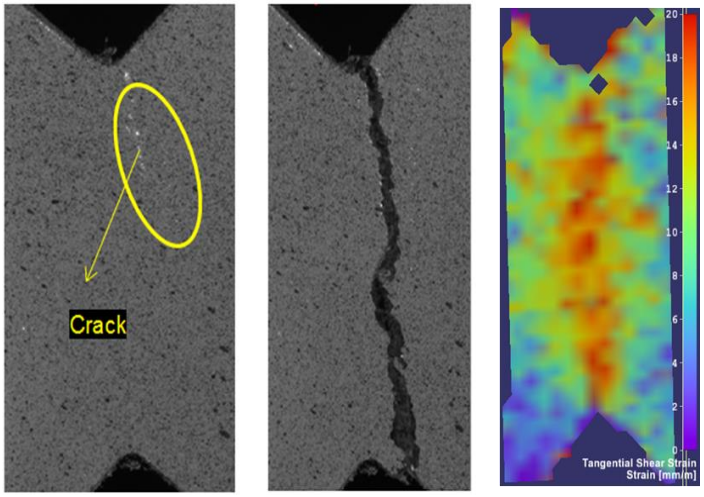

Figure 93. Failure progress of LD specimens: (a) crack occurring; (b) crack occurring; (c) Shear strain distribution at failure.

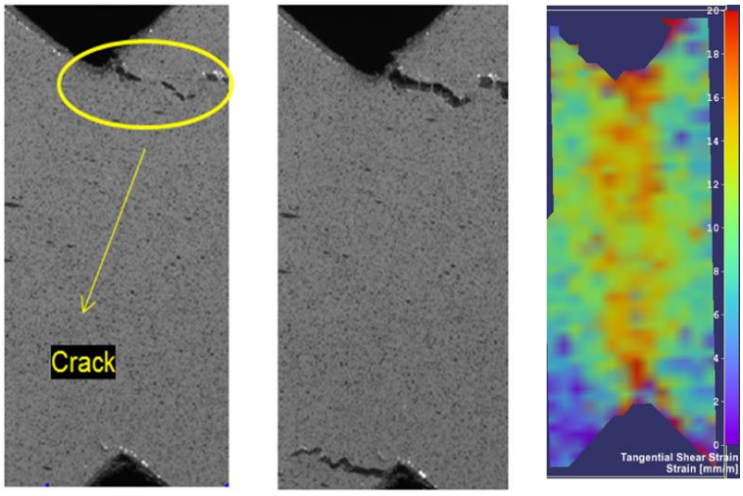

Figure 94. Failure progress of BTCA specimens:(a) upper notch failure; (b) crack propagation and lower notch failure; (c) shear strain distribution at failure.

It has been observed that LD specimens showed a brittle-like failure after the ultimate load while the other composites had a tougher behaviour. It was demonstrated by the failure progress image recorded by the digital camera (Figure 93 and Figure 94), where examples of BTCA and LD composites were displayed. For LD treated composites, the crack occurred at the upper notch root, and then propagated very quickly through longitudinal area with high shear strain. A completely different failure mode was exhibited for BTCA composites: (i) slight twisting of specimen; (ii) a visible crack occurring at the upper notch root; (iii) crack propagation in the transverse fabric direction (much slower); (iv)

crack observed at the lower notch root. The specimen kept transferring the load through the area with low shear strain (see in Figure 94).

6.3.3 Effect of treatments on flexural properties of hybrid FE

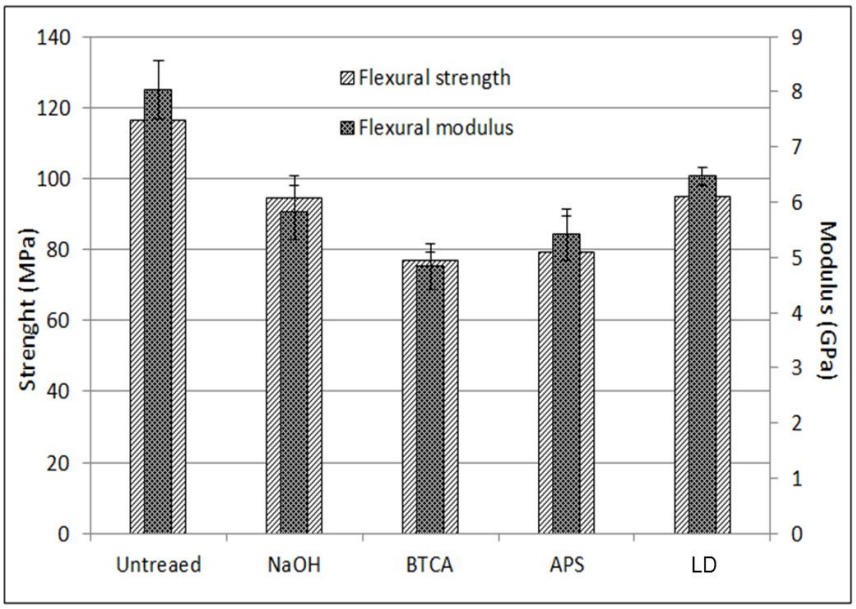

Figure 95. Flexural properties of hybrid FE composites.

The flexural properties (strength and modulus) of flax/supersap composites with different surface treatments are shown in Figure 95. With respect to the flexural strength, the neat flax/supersap laminates exhibited the highest value of around 125 MPa, followed by strength of around 100 MPa for NaOH and LD treated composites. As shown in the previous discussion on tensile properties, the unmodified FE composites had the highest tensile strength, consequently resulting in the highest force peak at the outer surface of specimen during bending, and hence the highest flexural strength. Although, the chemical treatments can improve the flax/matrix compatibility; the loss of inner matrix (e.g. hemicellulose) probably reduces the strength of the fibre itself, resulting in a weaker composite. The BTCA composites presented the lowest flexural strength of 79 MPa, showing agreement with the tensile test results. However, APS treated composites were observed with almost the same strength reduction around 36% compared to the BTCA FE composites. The APS treatment maybe leads to decrease in compression properties, influencing the compression layer in bending and further reducing the flexural strength. As the

flexural strength declined due to the possible decline in fibre strength, the highest flexural modulus was found to be about 8.04 GPa for neat composites. The trend shows agreement with previous tension modulus with negative effect resulting from the fibre surface treatments. The flexural modulus greatly dropped to around 40% (to 4.8 GPa) for BTCA treated composites, which also exhibited the lowest tensile modulus.

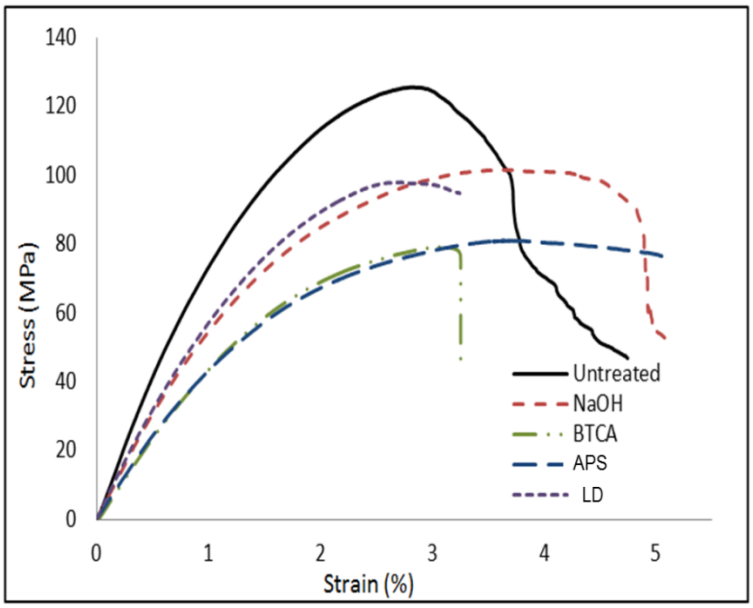

Figure 96. Stress-strain curves for representative FE composites during bending.

The stress-strain curves of chemical treated-flax reinforced supersap bio-epoxy composites are shown Figure 96. All the curves showed two basic zones of fabric laminates prior to the maximum stress. The linear part of the curve was used to measure the flexural modulus. The following second region showed the non-linear relationship resulting from the visco-elastic nature of polymers. From the literature [3], this phenomenon is the consequence of the re-orientation of the micro-fibrils along the tensile direction and re-crystallization. The failure of untreated BTCA composites was more brittle with dramatic force drop. The cracks happened at the bottom surface and propagated though the NW layer towards the laminate UD core. A yield-like deformation was found for the other composites due to the fact that the tension force was carried by the middle UD fabric layer without crack propagation. The no-crack phenomenon was also observed in woven flax fabric/tannin composites.

6.3.4 Effect of treatments on impact properties of hybrid FE

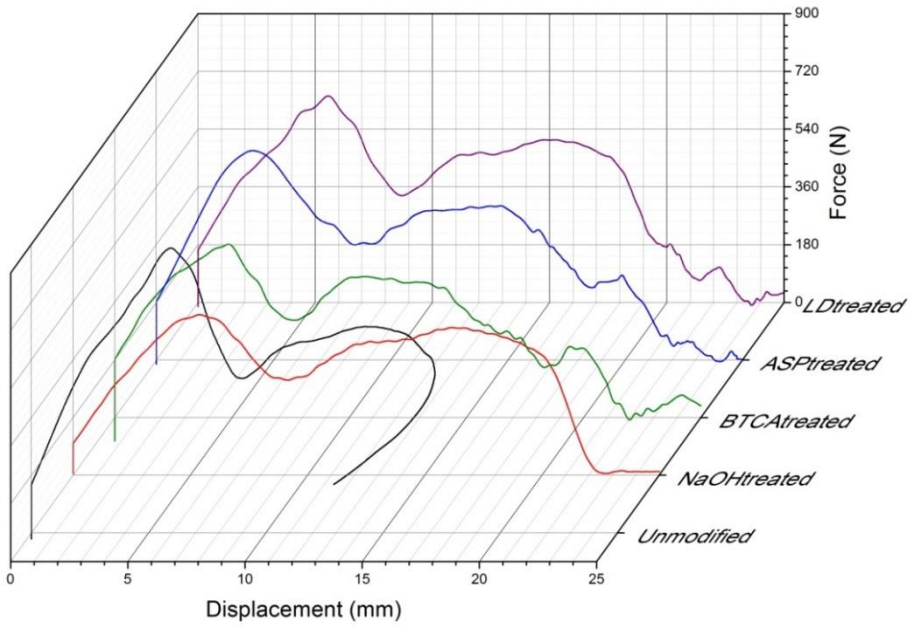

Figure 97. Force versus displacement of FE composites under impact.

From Figure 97, it can be seen that the untreated composite specimens showed a very typical ‘impactor-rebound’ phenomenon, indicated by the curve folding back on itself with decreasing displacement, while the treated specimens performed ‘perforation’ impact cases. For untreated neat composites, the impactor rebounded upwards at the displacement of 17 mm due to the energy released from the elastic deformation during impacting. For the treated composites, the velocity reached a plateau after the saturation point around 20 mm. The breakage force is contributed by the outer non-woven layers, and the following energy absorption is mainly due to the ‘internal’ fragmentation of UD core. According to previous investigations on flax/tannin composites, the non-woven flax mat layer will have higher threshold forces while UD flax fabric laminates could show more energy absorption for creation of indentation and crack propagation. As seen in the Figure 98, the tested specimens were broken along the longitudinal direction into two pieces. The cracks propagated evenly through the non-woven laminate from the bottom and then transferred to the rapid transverse crack and delamination when they came across the stiffer UD laminates in longitudinal direction. For the non-woven/UD flax design in the flax

reinforced supersap bio-epoxy composites, the outer non-woven layers improved the impact shock (high threshold force), while the inner UD flax core was capable of offering reasonable fragmentation energy dissipation rather than fibre debonding and delamination.

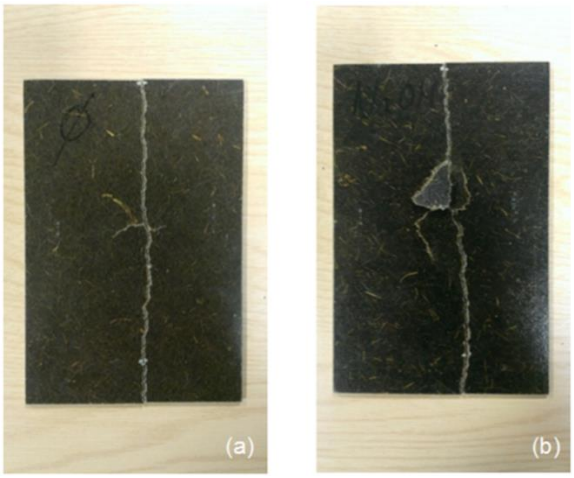

Figure 98. Damage of hybrid FE composites (a) typical damage (b) the worst case.

Table 27. Energy-absorbing characteristics of FE composites for impact tests.

Sample	Peak force (N)	Energy at peak force (J)	Total energy (J)	Released energy (J)
Untreated	887±64	3.3±0.2	9.1±0.2	1.8±0.2
NaOH	497±87	1.7±0.1	8.3±0.3	NA
BTCA	538±42	1.9±0.1	7.7±0.6	NA
APS	664±54	2.6±0.4	8.9±0.1	NA
LD	643±34	2.4±0.5	9.2±0.2	NA

The force-time curves were also plotted with the energy absorption, calculated as the area under the force-displacement curves (Figure 97). Similarly, there was a quasi-constant force ongoing part after the failure force peak for the composites. As seen from corresponding energy-time curves, the energy required after failure point to break the samples (e.g. crack propagation) cannot be ignored. When the force approached to zero the energy absorption became constant. The energy of the treated composites (NaOH, BTCA, APS and LD) increased with time, followed by an energy plateau. Nevertheless, due to the rebound performances, the unmodified composites took all the potential energy

and then released around 10 % back to the impactor (Table 27) with final absorbed energy of 9.14 J. NaOH, APS and LD treated composites absorbed energy of 8.34 J, 8.99 J and 9.28 J in average, respectively. The BTCA treated composites had the lowest energy absorption of 7.70 J, in accordance with the lowest mechanical properties (tensile, flexural and shear).

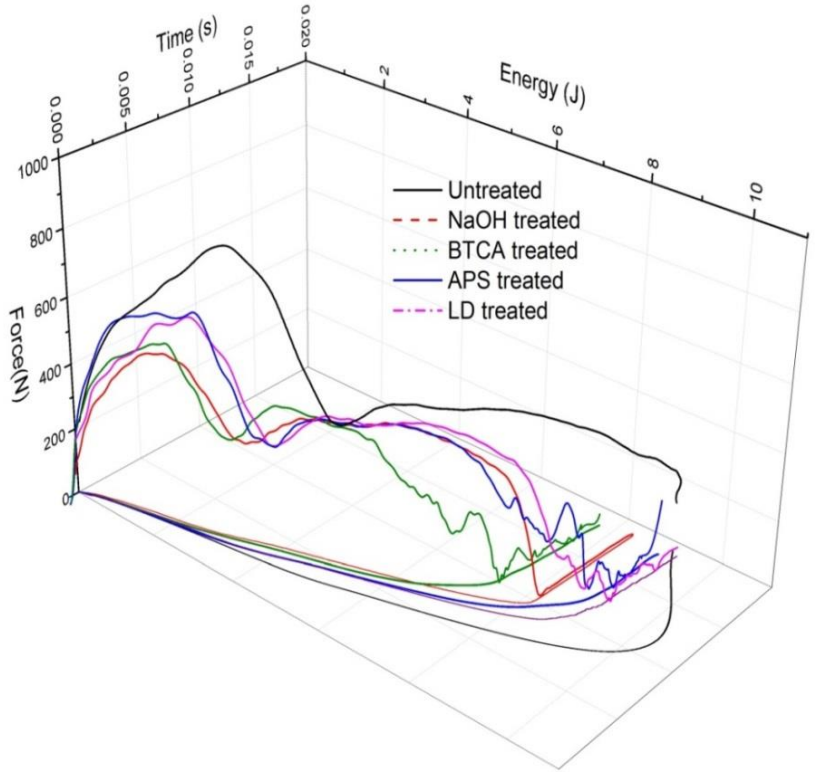

Figure 99. 3D curves of force-time-energy of FE composites.

The threshold force (maximum load) and the required failure energy are shown in Table 27. The peak force trend (untreated>LD>APS>NaOH>BTCA) is same as the trend observed for composite elastic modulus. For simplicity as given by Davesi [205], the threshold force value is proportional to the equivalent in-plane modulus which is associated with the elastic modulus:

$$F_p = \frac{8\pi^2 E h^3 G_{II}}{9(1-V^2)} \tag{6.1}$$

Where F_p is the peak load, E for the in-plane modulus of composites, h for the composite thickness, G_{II} is the strain energy release rate. The total energy was much higher (up to 4 times) than the absorbed energy at maximum load. Thus it

is difficult to explain the fracture principle of the composites by linear elastic fracture mechanism (LEFM). Untreated composites required highest kinetic energy of 3.3 J for the occurrence of the failure. Very small energy values below 2 J at peak force were found for NaOH and BTCA composites, demonstrating their sensitivity to damage at a certain energy level.

Part 2-environmental resistance

6.3.5 Differential Scanning Calorimetry (DSC)

For DSC measurement, when the sample undergoes a physical transformation, more or less heat will flow to the sample to maintain the same temperature as reference (exothermic or endothermic). An endothermic or exothermic process within the materials results in a significant deviations in the difference between the two heart flows. A flat or shallow baseline is shown up when there is slight difference of heat flow between samples and references to required temperature, especially for a thermodyanamic chemical process. The enthalpies of the transition can be calculated by the integration of the corresponded transition peak as ΔH=KA, Where ΔH is the specific reaction enthalpy, A the area under the curve, K the calorimetric constant value.

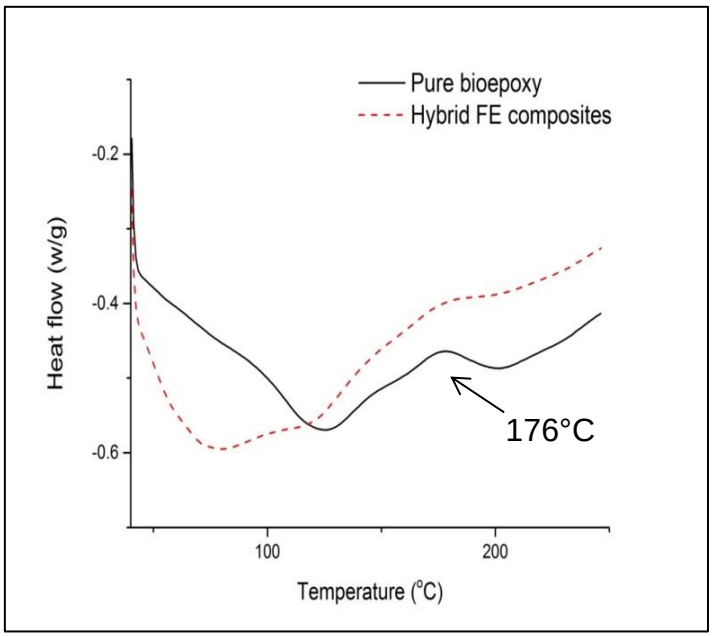

Figure 100. DSC curves of pure epoxy and flax/supersap composites.

The thermal changes in pure supersap bio-epoxy and flax reinforced composites were measured as a function of temperature (Figure 100). The heat flow decreased with temperature from the beginning point due to the enthalpy relaxation from the previous thermal history. For pure epoxy resins, the theoretical baseline shift, resulting from the glass transition in the amorphous area of the resin, was overlapped with an endothermic peak. An exothermic peak was found around 176 °C that corresponds to the extra curing reaction. It was confirmed that that the bio-epoxy resin had not completely cured.

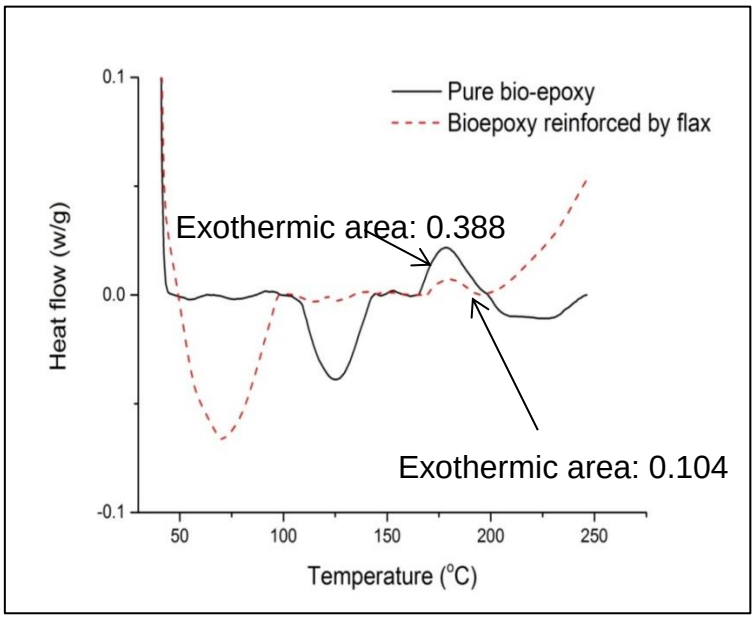

Figure 101. DSC curves after baseline subtraction for further comparison.

To magnify the curve significance between supersap epoxy and composites, the origin DSC curves were re-plotted after baseline subtraction (Figure 101). The glass transition change was hence eliminated after this modification. An initial large endotherm progress (before 100 °C) was observed for flax reinforced supersap bio-epoxy composites. This is attributed to the loss of water absorbed by flax fibres. Although the hydroxyl groups of cellulosic fibres attract water, epoxy resin is water-resistant material [84; 161]. The endotherm behaviour of bio-epoxy in the temperature range between 100 and 150 °C almost disappeared for the flax reinforced epoxy specimen, suggesting differences in thermal hysteresis for the two studied materials. The incomplete cure of flax/epoxy composites was also reflected by the exothermic peak at the

same temperature (177 °C) as bio-epoxy resins. Compared to pure bio-epoxy, the flax/supersap bio-epoxy composites had a higher curing degree due to the smaller peak area responsible for less curing energy. The compression heating procedure for composites was also able to accelerate the cure of epoxy resins. The enthalpy required for the completion of curing for flax composites is almost three times than the one of pure epoxy. Furthermore, the degradation of pure epoxy was identified at 230 °C, after which heat flow increased as a result of exothermic reactions. The flax/supersap bio-epoxy composites showed an earlier degradation initiation at 200 °C, on account of the onset of degradation of flax fibres. The literature [73; 74] in this area of research reported similar degradation temperature for flax fibres at 203 °C.

6.3.6 Effect of treatments on thermal-mechanical properties

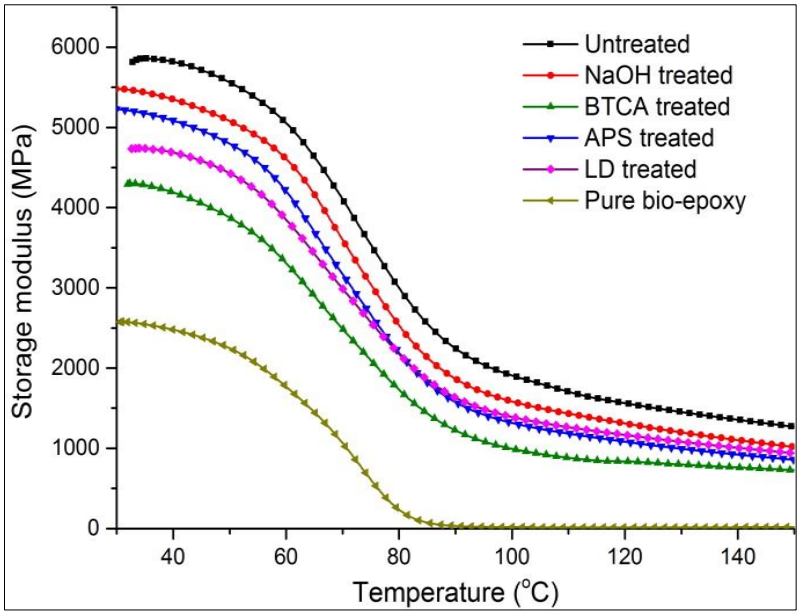

Figure 102. Variation of storage modulus of resin and FE composites.

The storage modulus of pure supersap epoxy and composites subjected to the same temperature increase (30 °C to 150 °C) is shown in Figure 102. Clearly, the addition of flax fibres significantly improved the storage modulus of bio-epoxy resins. The initial storage modulus is related to the load bearing capacity of a material and is analogous to the flexural modulus (E) [210]. As seen in Table 28, the trend of the storage modulus of FE composites shows strong

agreement (Untreated>LD>NaOH>APS>BTCA) with the flexural modulus, indicating the effect of fibre surface treatments on the dynamic stiffness of composites. The incorporation of chemical treatments leads to a noticeable decrease in modulus of neat composites. The decrease in fibre strength caused by the loss of inter-fibrils matrix (e.g. hemicellulose) during treatments possibly result in less constrains on segmental flexibility, hence reduced interfacial strength. The highest decrease of stiffness was observed for BTCA composites with nearly 26.9 % and 39.9 % decrease for storage and flexural modulus, respectively.

Table 28. Flexural and storage modulus of FE composites.

Composite	Flexural modulus (GPa)	SD	Storage modulus (GPa)
Untreated	8.04	0.52	5.81
NaOH treated	5.82	0.49	5.23
BTCA treated	4.83	0.41	4.29
APS treated	5.41	0.47	4.73
LD treated	6.46	0.17	5.48

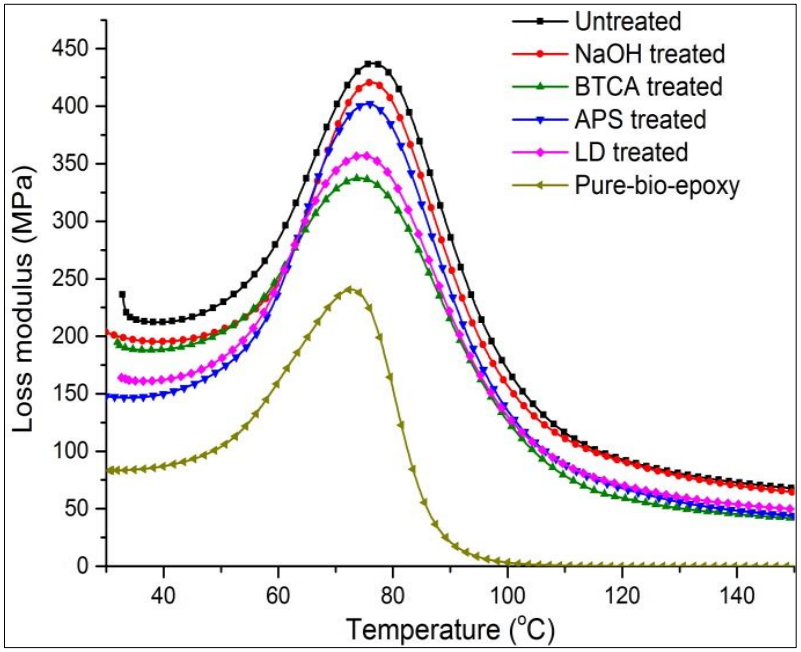

Figure 103. Effect of treatments on loss modulus of resin and FE composites.

It is clear from Figure 102 that the storage modulus decreased with a significant fall in the temperature range of approximate 60 to 90 °C due to the glass transition phenomena of bio-epoxy. After the glass transition point, the polymer chain segments are able to move and hence molecules turn into rubbery state with little elastic [177]. All the chemical treatments lead to a shift of T_g at 60 °C to slight lower values (e.g. 53 °C for BTCA treated composites). Surface treatments make the stiffer resin adjacent to the fibre/matrix interface and larger gradient of modulus. The transition region is therefore enlarged.

Table 29. Thermal-mechanical properties of untreated and treated composites.

Testing material	T_g (loss) (°C)	T_g (Tanδ) (°C)	Max E'' (MPa)	Max Tanδ	B
Pure bio-epoxy	72.74	84.83	241	0.834	0
Untreated	77.32	82.43	430	0.144	1.69
NaOH treated	75.28	81.29	400	0.176	1.61
BTCA treated	75.49	82.00	337	0.188	1.58
APS treated	76.79	81.87	356	0.155	1.66
LD treatd	75.55	82.30	420	0.161	1.64

Loss modulus, which represents the capability of energy dissipation within a material with viscous motions as heat, of FE composites and resin is shown in Figure 103. An α relaxation peak of epoxy resin was obtained at 72 °C, associated with the glass transition. Compared with pure epoxy, all the composites showed an increase in T_g (75 to 77 °C) as seen in Table 29 due to fibre reinforcement effects. A β relaxation peak may indicate changes in chain segments caused by reorientation in crystalline phase [211]. The non-observation of β transition in flax/supersap composites possibly is the evidence of the absence of crystallinity in flax fibres. The T_g as α relaxation peak shifted slightly to a comparatively lower temperature (75-76 °C) detected in all treated composites (NaOH, BTCA, APS and LD treated). It has been widely reported that using proper fibre coupling methods, the improvement of interfacial fibre/matrix can cause the increase of glass transition temperature of composites [94]. However in the present investigation, the treatments had a

slight effect of increasing T_g through better interfacial adhesion. This primarily is attributed to the compensation of decrease in fibre strength, leading to fewer constraints on segmental flexibility. For the same reason, the highest and lowest loss modulus were found in untreated and BTCA treated composites with the maximum and minimum viscous dissipation, respectively.

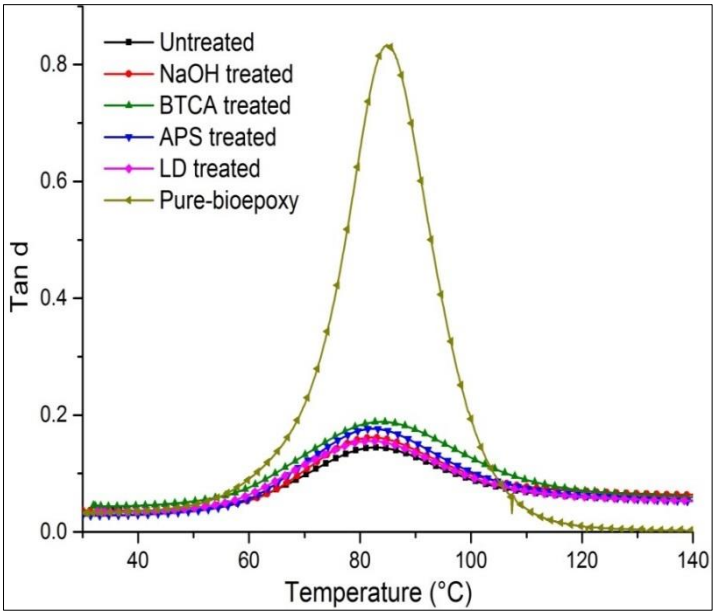

Figure 104. Effect of treatments on tan δ of resin and FE composites.

The damping of a material to loss mechanical energy into heat measured as a ratio of storage (elastic) and loss (viscous) modulus, called tanδ. In comparison to the untreated composites, an increased magnitude of tanδ peak was observed in treated flax/supersap composites. The untreated fibres can carry more stress when compared to treated fibres (Chapter 3). It will tend to dissipate less energy with lower magnitude of damping peak in comparison to treated composites. The magnitude of tanδ was also reported by Gupta [212] to reflect impact properties of materials. As in the previous study, the untreated composites showed a rebound case subjected to the falling weight impact, while the treated composites broke longitudinally. The untreated FE composites had better damping property, thus dissipating more energy by internal friction.

The bonding properties between flax and fibres could also be indicated quantitatively. According to the following equation, the bonding properties for various treated flax composites could be assessed by [47]:

$$B = \frac{1 - \frac{\tan\delta_c}{\tan\delta_m}}{V_f} \quad (6.2)$$

Where B is a parameter used to indicate the interfacial bonding strength, $\tan\delta_c$ for composites and $\tan\delta_m$ for pure matrix. V_f is the fibre volume fraction which could be calculated from composite volume (V_c), composite weight (M_c), fibre weight ratio (W_f) and resin density (ρ_m):

$$V_f = \frac{V_c - \frac{M_c \times (1 - W_f)}{\rho_m}}{V_c} \quad (6.3)$$

The lower value of B parameter indicates lower interfacial strength. From the results summarised in Table 29, B value decreased after all the treatments, possibly owing to the loss of inner fibre strength.

6.3.7 Effect of treatment on water absorption properties

Figure 105 shows the curves of water uptake against (time)$^{1/2}$of hybrid flax/ supersap bio-epoxy composites (unmodified, NaOH, BTCA, APS and LD) immersed in de-ionised water at room temperature (25 °C). The initial curve slope has a proportional relationship with diffusion coefficient (D_z) which can be calculated as:

$$D_z = \pi \left(\frac{h}{4M_m}\right)^2 \left(\frac{M_2 - M_1}{\sqrt{t_2} - \sqrt{t_1}}\right) \quad (6.4)$$

Where

M_m is the maximum water absorption,

$\left(\frac{M_2 - M_1}{\sqrt{t_2} - \sqrt{t_1}}\right)$ is the linear slope of the plotted curve.

The time accurate to hours to achieve 99.99% equilibrium can also be approximately predicted at a given temperature:

$$t_{max}(T) = \frac{0.93h^2}{D_z(T)} \quad (6.5)$$

Table 30. Summarised water absorption properties of FE composites with and without treatments.

Composite	As-received moisture (%)	Water content (2h %)	Water content (24h %)	Maximum moisture (%)	Thickness swelling (%)	Diffusivity ($10^{-3}cm^2/s$)
Untreated	1.02±0.12	2.57±1.17	9.19±1.96	17.86±1.15	24.54±1.85	0.028
NaOH treated	1.03±0.22	2.79±0.42	9.27±1.32	17.91±0.82	21.20±1.59	0.028
BTCA treated	1.01±0.08	2.38±0.18	9.83±1.25	19.02±0.33	27.05±1.52	0.025
APS treated	0.98±0.17	2.17±0.43	8.2±1.68	17.71±1.56	22.36±2.05	0.022
LD treated	0.97±0.11	1.86±0.12	8.15±1.50	17.87±1.52	23.53±0.99	0.024

The water absorption of all the composites increased with the immersion time until equilibrium state with saturated moisture content. It is clear from Figure 105, water molecules were absorbed very rapidly in the first 1 week, and then the absorption rate slowed and followed Fickian diffusion to approach saturation after 2 weeks. The maximum water content at the equilibrium state for untreated, NaOH, APS and LD treated flax reinforced supersap bio-epoxy composites, immersed at 25 °C for 672 (4 weeks) is 17.86, 17.91, 19.02, 17.71, 17.87 % respectively. Except the BTCA treated specimens, that absorbed 2 % more water, the maximum water uptake of all treated composites was not very dissimilar, with less than 0.2 $_{wt}$% variation. The BTCA modification slightly increased the moisture sensitivity of flax/ supersap bio-epoxy composites.

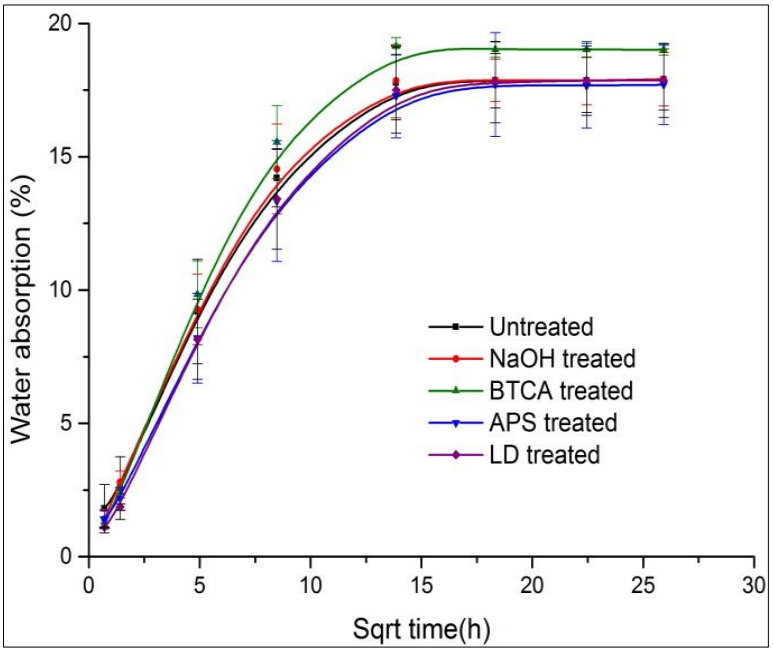

Figure 105. Water content versus time root of FE composites.

It has been widely reported that the water absorption behaviour of natural cellulosic fibre reinforced composites primarily depends on several significant factors, such as the existence of polar groups in fibres for water-reacted hydrogen boning, the composite porosity, lumen size and fibre matrix adhesion [23; 108; 206]. The non-woven fibre composite exhibited lower water absorption compared to woven composites due to less void content of chopped mat composites. A study done on natural fibre reinforced synthetic epoxy

composites indicated that the pure EFB (oil palm empty fruit bunches) fibre mat/ epoxy composites exhibited saturated water absorption of 22 %, much higher than the jute fibre mat/supersap composites (less than 10 %) [213]. The water resistance of flax/supersap composites is attributed to the hydrophobic epoxy matrix. However, the large fibre content (57 $_{wt}$%) of non-woven mats could easily introduce micro-voids to trap water due to fibre agglomeration.

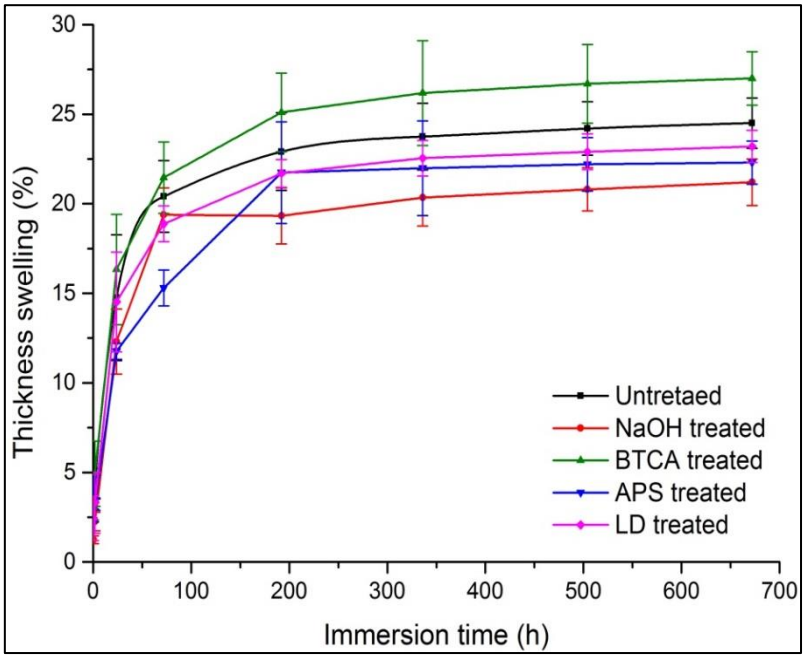

Figure 106. Thickness swelling behaviour of FE composites.

The associated diffusivity and saturation time for hybrid flax/supersap bio-epoxy composites are summarised in Table 30. The unmodified FE composites had a diffusive coefficient value and predicted saturation time of 0.028 and 769 h, respectively. The lowest diffusion coefficient value of 0.022 was obtained for APS composites, which had the highest water absorption and saturation time. Following a Fickian diffusion process, water molecules were initially attracted by hydroxyl groups of natural fibres, which damaged the fibre/matrix interface, offering micro-channels for further water permeation. BTCA and LD treated composites displayed respectively lower diffusion coefficient of 0.025 and 0.024 compared to untreated FE composites.

The fibre swell and the water filled in the fibre/matrix surface are the main reasons for the dimensional changes of natural fibre reinforced composites. It

has been demonstrated by Jawaid [213] and Nourbakhsh [214] that the linear expansion in thickness is the most likely and noteworthy change in dimension. Figure 106 shows the thickness swelling behaviours of hybrid flax/supersap composites with treatments. As water immersion time increased, the thickness percentage increased, similar to the water absorption/time behaviour. As discussed, water was absorbed in the hydrophilic fibre cell walls to swell of flax fibres and hence the thickness of FE composites. The stress caused by fibre swelling leads to micro-cracking and subsequent loss of epoxy resin in the form of particles. As shown in Figure 107, flax fibres were clearly exposed on the composite surface after water conditioning. The NaOH treated flax/supersap composites showed the lowest rate of thickness swelling (21.2 %) among all the composites. Thickness swelling for the BTCA treated FE composites was the highest with the value of 27.1 %. The unmodified FE composites had a middle-level thickness swelling of 24.5 %. A decreased thickness swellling was also found for other two treatments (APS and LD).

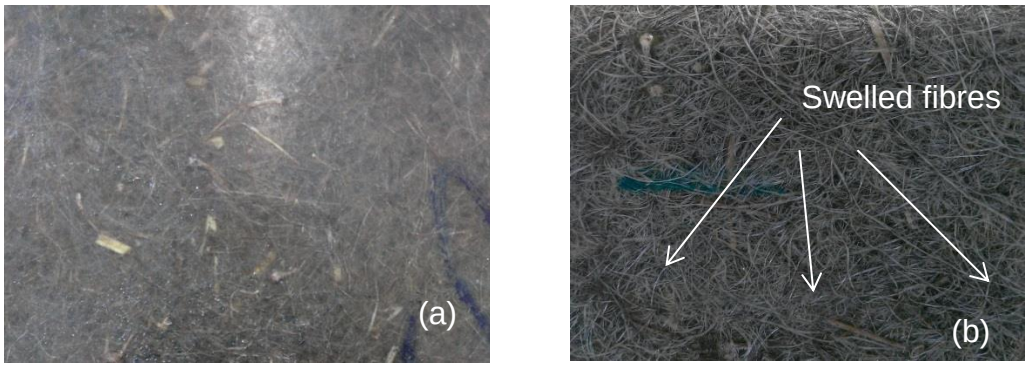

Figure 107. Surface change by water immersion (a) before; (b) after.

6.3.8 Effect of treatment on UV and Xenon ageing properties

All the samples not only showed visible changes in colour and colour intensity on the sample surface, but also slight distortion of the samples after the test procedure. Visual changes in the samples can be seen in Figure 108. Big changes were observed after 500 h time of Xenon exposure. A small layer of the epoxy resin was degraded off from the surface and also fibres were changed so that there was only white cellulose left on the surface forming a hairy surface for the composite. The composites with modified flax mats seem

to restrict the changes caused by weathering (visually) a bit better than composite without flax modification. Compared to Xenon exposure, the UV-B used in this test was less effective in degrading the material surface.

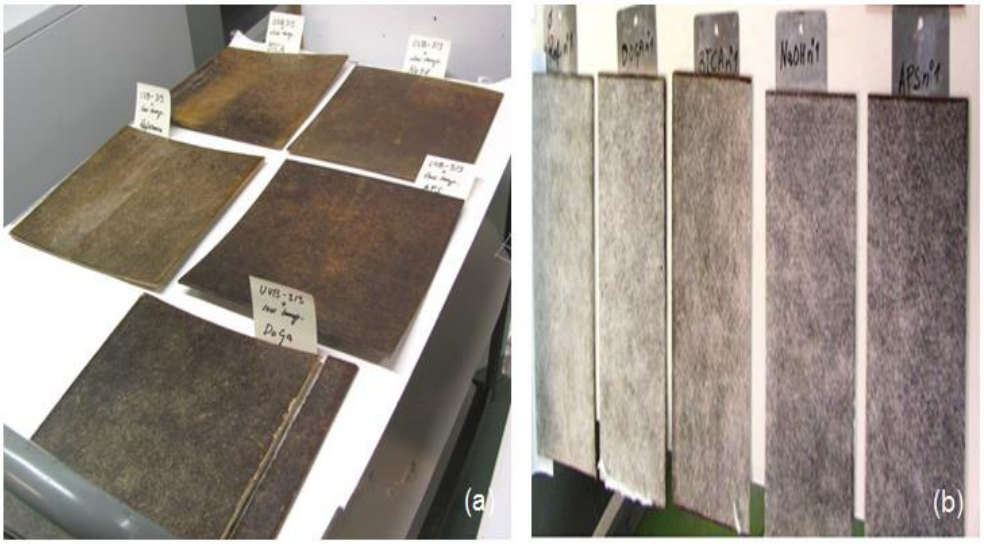

Figure 108. Flax/supersap bio-epoxy composites samples with and without treatments after ageing condition: (a) UV radiation for 552 h; (b) Xenon light for 500h.

Table 31. Tension properties of hybrid flax/supersap bio-epoxy composites with different treatments in weathering conditions.

Sample	Tensile strength (MPa)			Tensile modulus (GPa)		
	Normal	UV	Xenon	Normal	UV	Xenon
Untreated	185.4±8.5	185.4±7.8	172.2±8.1	13.9±0.4	14.0±0.3	8.8±0.4
NaOH	178.5±6.4	146.9±6.4	169.8±6.5	11.9±0.5	10.5±0.4	11.8±0.5
BTCA	51.7±6.1	40.2±5.8	45.9±6.2	6.4±0.6	5.4±0.2	6.0±0.2
APS	175.4±6.2	157.3±8.2	175.1±6.2	11.3±0.4	9.8±0.5	11.5±0.6
LD	164.5±5.7	157.1±7.0	160.3±5.6	13.7±0.4	13.7±0.2	11.9±0.3

The tensile properties of the composites after freeze+UV cycle conditions are shown in the Table 31. It is apparent that the ageing condition had only visual effects on the tensile properties of untreated composites as they retained (almost) the same strength (185 MPa) and tensile modulus (14 GPa). The tension strength of NaOH treated composites dropped around 18% from 178

MPa to 147 MPa. LD treated composites showed similar tensile modulus of 13.67 GPa with a slight 8MPa decrease in tensile strength after ageing.

For the 500 h Xenon-exposure condition, APS type had the best mechanical-property resistance. It retained the tensile strength and modulus at 175 MPa and 11 GPa, respectively. All treated composites have very good mechanical-property resistance to the 500h exposure condition with less than or about 10 % decrease of tensile properties. The NaOH treated composites exhibited almost the same tensile modulus of 11.8 GPa after Xenon conditioning. However the tension strength and modulus of untreated composites decreased 7 % and 36 % respectively after ageing.

6.4 Conclusions

The untreated composites (tensile, shear and flexural strength of around 185 MPa, 57 and 125 MPa, respectively) show a good potential to be used in vehicle applications. Pure NaOH treatment is the most promising one. NaOH composites maintained the tensile strength of around 180 MPa, and improved the fracture toughness and flexural strength. However, BTCA treatments decreased the tensile strength. With regards to the impact resistance, LD treated flax/supersap composites had a slightly higher energy absorption than untreated composites. The improvement in fibre/matrix wettability may not be able to compensate the reduction of fibre strength (due to the removal of interfibrillar matrix by general treatments). Also the low resin content and untreated UD layer core could also account for the ‘not so significant’ effect of treatments.

This chapter also suggests that the applied treatments for fibre/supersap bio-epoxy composites (57 $_{wt}$% fibre ratio) significantly can improve Xenon ageing resistance, but with little change on UV ageing and water absorption results. The environmental resistance of novel hybrid flax/supersap composites with different treatments was investigated for potential use in auto interior and exterior trims applications. The fibre treatments had little effect on glass transition temperature around 75°C. The saturated water absorption content of untreated and treated FE composites were at about 17.8 %. However, the

maximum thickness swelling ratio of NaOH treated composites was 3 % less than untreated ones, indicating better dimensional stability. For UV and Xenon ageing, the composites with modified flax mats showed less visual changes, which was a bit better than composite without flax modification. With respect to the tensile properties, the untreated composites had the best performance after UV exposure, while for Xenon exposure; the four treated composites (NaOH, BTCA, APS and LD) showed much better resistance.

Chapter 7. Impact response of fully renewable bio-sandwiches based on flax bio-composites

7.1 Introduction

Sandwich composites (Figure 109 (a)) are normally made by skin materials-outer low-density composite plates combined with core materials like polymer foams and honey comb materials. As a light weight structure, sandwich composites with proper design could maintain the low structural weight and keep high structure stiffness and strength against various loading conditions, such as traction, bending, compression etc. [215; 216]. In order to reduce the energy consumption, these structures have been used in a wide range of applications, including aircrafts, sports cars, and helmets and so on [217; 218]. An innovative example of composite-made sandwich structures in vehicle applications is shown in Figure 109 (b): an Aptera electric car with sandwich-made body panels.

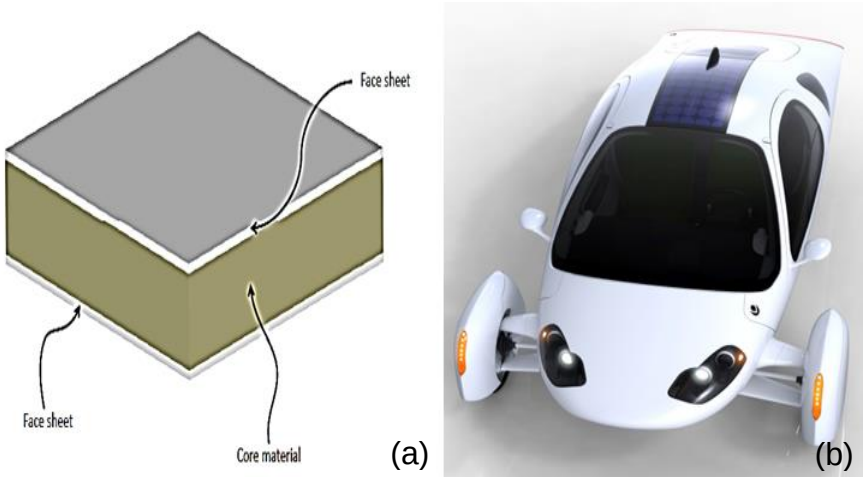

Figure 109. (a) Schematic drawing of a sandwich plate and (b) Aptera electric car.

For a sandwich application with certain impact load, such as accidental tool drops, bird strikes, and ballistic loading etc., the impact energy must be dissipated properly for the protection purpose [219-221]. Hence the improved impact resistance is one of the major consideration with the development of composite sandwich structures. Under a low-velocity impact on sandwiches, it is very dangerous to have damage, no matter visible or not, undetected and un-

analysed. The description of the damage initiation and propagation model towards collapse is important to understand the damage causes and further enhance the impact properties.

Many studies [222-225] have shown that the impact characteristics of sandwiches depend on properties of materials (facing sheet, core foams and their relationships etc.) and shape of the structure. The thick core material with low density can carry shear stresses from transverse loading, while the composite face sheets usually resist tension and compression when subject to impact. The outstanding performance in the core crush and face sheet failure could give rise to good energy absorption efficiency [226; 227]. Thermoset based composites reinforced by carbon or glass fibres are utilised as strong and stiff sandwich skins. To offer the acceptable impact characteristics, commercial core materials are foams (expanded thermoset and thermoplastic foams), balsa and honeycombs. The density and modulus of the core materials highly influence the impact response of the final sandwich structures.

The responses of sandwich structures with foam core and composite skins under low to high velocity loading have been investigated for many years [228-230]. Failure modes of these sandwich panels could be normally identified into three groups: (1) face sheet buckling; (2) core crush with sheet failure; (3) debonding between face sheets and core [231-233]. A quasi-elastic deflection occurs during an initial impact moment, followed by the irreversible damage formation (e.g. indentation) after certain load [234]. According to the modified Herzian law, the contact force (F) produced on the composite skins at impact loading could be given as a function of vertical impact displacement (a) [235]:

$$F = ka^{1.5} \tag{7.1}$$

$$k = \frac{3}{4} \times \frac{R^{0.5}}{\frac{1-v^2}{E_i} + \frac{1}{E_c}} \tag{7.2}$$

Where R is the radius of the semi-spherical impact dart, v the Posson's ratio of the dart materials, while E_i and E_c are the elastic modulus of the dart material and the composite plate, respectively. Nevertheless, the impact behaviours of

sandwich composites are seen to be strongly influenced by velocity change of the projectile objects [236-238]. Ghelli and his co-workers [239] characterised the falling weight impact damage of sandwich panels (glass fibre composite skins with rigid PVC foam) and observed the effect of strain rate on the performance of sandwiches. The falling weight impact showed improved resistance to penetration, compared to the equivalent quasi-static indentation (the same impactor moving displacement). Due to the viscos-elastic nature of polymers, sandwiches will behave differently at different strain rate ($\dot{\varepsilon}$) as:

$$\dot{\varepsilon} = \frac{d}{dt}\varepsilon = v/L \tag{7.3}$$

Where v is the impact dart velocity, and L the sandwich thickness. The maximum peak load, energy absorption and even the damping properties could vary a lot at different impact velocities.

Lots of attention has been found on synthetic fibre composite based sandwiches [218; 220; 226], but few on natural fibre composite-face sheets and bio-degradable foam core. Given the increasing environmental concerns and strict regulations, the introduction of new bio-composites sandwiches could be very interesting for future development so as to reduce the foot print and offer other environmental benefits. Ude et al. [226] produced bio-composite (woven natural silk fibre/epoxy) sandwich panels with different core configurations (foam, coremat and honey comb). It was found that among all core materials, the foam-type sandwiches exhibited the best energy absorption capability. The bio-composites made of natural fibres and bio-resins have a potential to replace the synthetic composites due to low cost, good mechanical properties and environmental advantages. Bio-foams normally are bio-degradable foams with competitive physical or mechanical performances to general synthetic foams [240-242]. Table 32 shows the physical and thermal properites of PLA based bio-foams compared to EPS (expanded polystyrene). In addition to the properties, the PLA foam has CO_2 emission less than 1000 kg per 1 ton production; about 2 to 3 times lower than other commonly used foamed polymers like EPS, PP, PET etc.

Table 32. Property comparison between PLA bio-foam and EPS [240-242].

Property	Unit	PLA foam		EPS	
		Density kg/m^3	value	Density, kg/m^3	value
Thermal conductivity	mW/mK	35	34	30	33
Compressive strength	kPa	40	200	30	200
Compressive modulus	MPa	40	4.0		
C-value (for drop test)		35	2.5		2.4
Bending strength	kPa	36	300	30	300
Youngs modulus	MPa	25	3.2	35	3.2
Shear strength	kPa	35	150-200		
Shear modulus	MPa	35	2.7		

There is no reported work on the impact properties of fully renewable sandwich panels made by bio-composites sheets and bio-foams. Therefore, by taking environmental advantage of the bio-resourced flax/tannin (FT) and flax/supersap bio-epoxy (FE) composites, the bio-sandwich structures with commercial bio-degradable foam cores (bio-PS and PLA) were fabricated to analysis impact behaviours using falling weight impact tests. The impact velocity was designed from low speed of 3 m/s to relatively high speed of 7 m/s. The objectives in this research work are to produce the light weight bio-sandwich structures suitable for vehicle applications and to characterise the impact response of the sandwiches.

7.2 Methodology

7.2.1 Materials and fabrication of sandwich panels

PLA and bio-PS foams were purchased from Foam Board, UK and Synbra, Netherland, respectively (Table 33).. BioFoam® from Synbra is a 100% bio-based PLA foam made from Synterra® PLA and is physically and mechanically

comparable to EPS (expanded polystyrene). Bio-PS foams were in the form of 5 mm thick board, and PLA foam had the thickness of 100 mm. Nonwoven FT and hybrid FE composites were compression moulded in ENSTIB and MahyTec, respectively as seen in the previous chapters. The fibre weight fraction was about 50 $_{wt}$% with average 2.5 mm for FT composite, and 57 $_{wt}$% with average thickness 3 mm for FE composites. The glue selected for the application is Loctite Hysol 3430, a typical two component-based adhesive. By mixing the components properly, the resin cures very fast at room temperature. This adhesive is designed to provide gap filling properties and high structural boning strength for a range of substrates (woods, epoxies, polymers etc.), even for poorly filling and rough surface.

Table 33. Prepared bio-sandwich structures for characterisation

Face sheets	Foam core	Foam density	Glue
Nonwoven flax/tannin (FT)	PLA	35 kg/m^3	Loctite hysol
Nonwoven flax/tannin (FT)	Bio-PS	28.8 kg/m^3	3430 epoxy
Hybrid flax/epoxy (FT)	Bio-PS	28.8 kg/m^3	adhesive

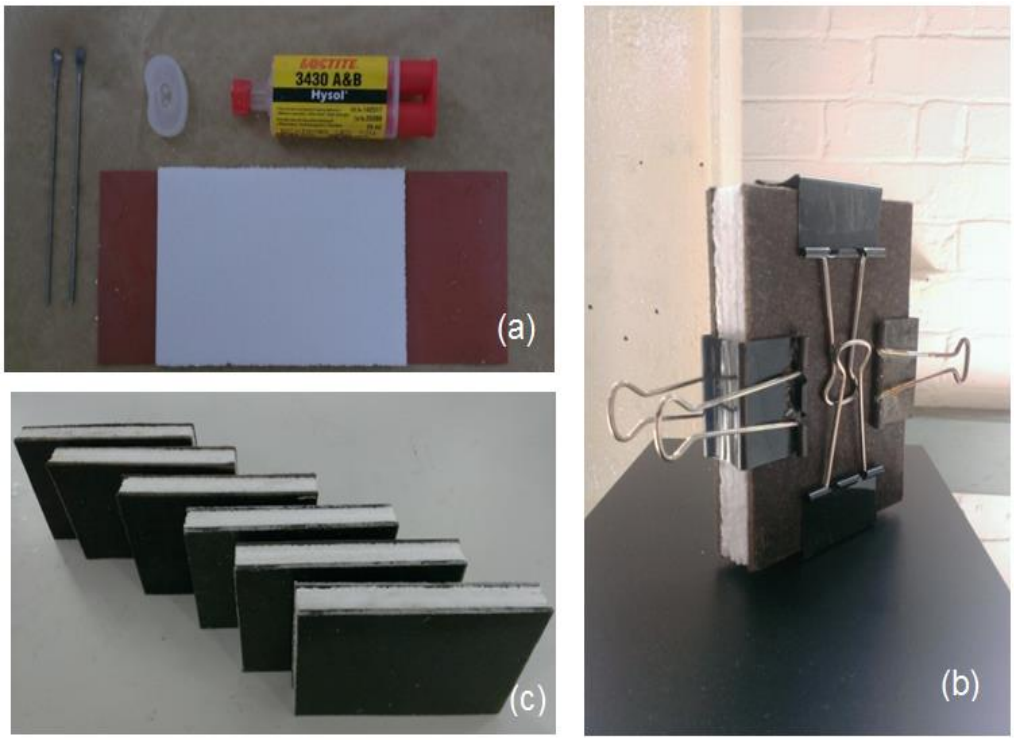

Figure 110. Sandwich preparation (a) bonding; (b) clamping (c) final sandwich.

The composite sheets (150×100 mm) were bonded on the top and bottom faces of 20 mm thick foam cores (see Figure 110) with same surface area. Four bio-PS sheets (5 mm thick) were attached by glue prior to the sandwich preparation to make 20 mm thick PS foam, while the PLA foams were directly cut into 20 mm thickness. The first stage in sandwich fabrication was to pre-treat and polish the composite face plates. They were degreased using acetone for 2 min. The surfaces were then dried and the adhesive was applied evenly on the sheet surface using a glue gun (as shown in Figure 110 (a)). The composite sheets were applied on both sides of the foam and then were allowed to cure for 24 hours in a press. To ensure the even distribution of pressure across the adhered surface and full contact between adhesive and face sheets, the sandwich structures were clamped (Figure 110 (b)).

7.2.2 Microscopy analysis

Scanning electronic microscopy were performed at 5 V using a XL30 SFEG analytical high resolution scanning electron microscopy (SEM), supplied by FEI. Image J software was used to analyse cells' geometry of both PLA and bio-PS foams to provide the information for understanding the effect of foam types. Three-plane (XY, YZ and XZ plane) investigation was applied on each foam.

7.2.3 Compression analysis on foams

The compressive properties of core materials directly influence the impact damage resistance of resultant sandwiches [243], hence compression tests according to ASTM D1621 were conducted on an Instron 5/100 5500R machine for both PLA and bio-PS polymer foams. A 5 KN load cell was used at the crosshead speed of 2.5 mm/min. Five foam specimens (50×50×20 mm) were tested for each sample.

7.2.4 Falling weight impact testing

A total dropping mass of 2.280 kg was determined for the falling weight impact tests, which is in line with the previous impact testing experiments on composites. The diameter of the semi-spherical impact dart (made of steel) is

about 20 mm. Impact response of bio-foam sandwiches (bio-PS and PLA foam) with face sheets of flax/tannin and flax/supersap composites were evaluated. Three specimens were tested for each set at speed of 3, 5 and 7 m/s with different potential energy 10.26, 28.5 and 55.86 J, respectively. In addition, the failure and post-failure moments of the bio-sandwiches were filmed through high speed camera so as to further assess the impact resistance (as shown in Figure 111). The results of sandwiches were measured with the average of three specimens. Transient data, including time, load, velocity and displacement, was collected for each sample. The data was recorded in terms of force, velocity as a function of time and dart displacement. In order to eliminate and minimise the unwanted load oscillation caused from machine noise, the load-related plots were carefully smoothed through Zavitzky-Golay method using Origin lab software.

Figure 111. Drop tower impact test co-operated with high speed camera.

7.3 Results and discussion

7.3.1 Foam structure analysis

The impact energy dissipation by polymer foams largely depends on the compression behaviours, regardless of the strain rate. Since polymer foam cells

normally grow unevenly in three directions, the selection of loading plane (Figure 112) is crucial to optimise the impact and compression performances. The geometric properties of PLA and bio-PS foams were analysed through SEM shown in Figure 113. Table 34 shows the foam properties such as cell size and anisotropy obtained by using the Image J.

Table 34. Morphology properties of PLA and bio-PS polymer foams.

Direction	Mean cell size (mm^2)	Principle cell dimension (L, mm)		Shape anisotropy L_{max}/L_{min}
		PLA foam		
3D	0.06	NA		Isotropy
		Bio-PS foam		
XY	0.06	0.41	0.35	1.17
YZ	0.04	0.35	0.33	1.06
ZX	0.03	0.27	0.23	1.15

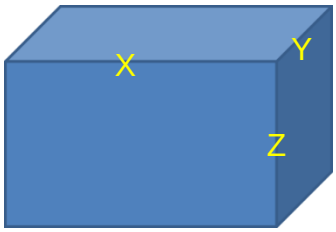

Figure 112. Test surface of the bio-foams based on the 3D directions.

The SEM images show the differences between PLA and PS foams. A bulk PLA foam ball consisted of many small foam cells packed and squeezed together. Clearly through the micrographs, the cell size measurement had limitations in all the directions. The foam cell was much smaller at the contacting edge between foam balls. However, the mean size of foam cells located in the middle area could still be approximately measured as 0.06 mm^2. PLA foam was considered as isotropic material due to the assumption of the even foam growth distribution in manufacturing. PS foams showed more anisotropic property with different cell sizes. The principle cell dimension (L) was calculated by the following equations:

$$L = \frac{1.5}{N} \tag{7.4}$$

Where N is the number of cells per length of straight line drawn parallel to the principle directions on each plane. By loading at different directions, the foam may present the best compressive strength under loading at XY plane as a result of higher cell density than XZ and YZ plane.

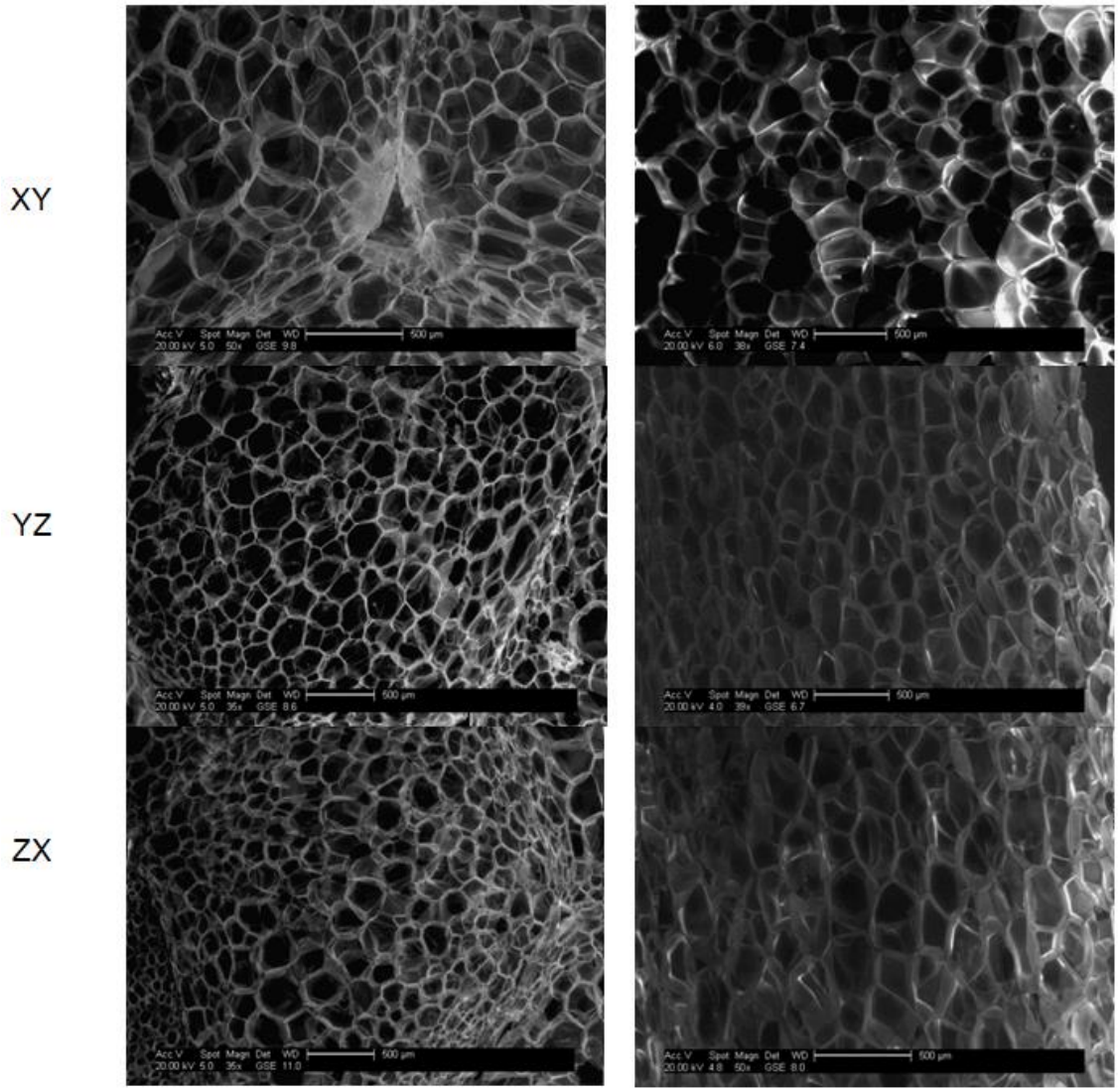

Figure 113. Cell structure of PLA (left column) and bio-PS foam (right column) through SEM investigation at three planes.

7.3.2 Compressive properties of bio-foams

Figure 114 shows the averaged curves of load-deflection relationships of PLA and bio-PS foams under compression testing. It was noted that the 'zero-deformation' point was established by carefully extending the quasi-linear load-deformation portion to the zero load line. All the characteristics, such as strain,

modulus, strength at certain strain, were measured from this point (as $X_{0\text{-}PLA}$ and $X_{0\text{-}PS}$ in Figure 114). The compressive modulus (E_c) was calculated using the slope of the straight load-deflection line (K) as below:

$$E_c = K \times \frac{H}{A} \tag{7.5}$$

Where H is the origin specimen height, and A is the initial cross sectional area. Based on the results (Table 35), the PLA foams exhibited much higher compressive modulus than the bio-PS foams, indicating good stiffness. There was a transition period (between 2-2.5 mm) observed for PLA foams, after which load increased gradually with increasing deflection/strain. This may be correlated to the yield behaviour of PLA foam cells without catastrophic collapse. It can be seen from Table 35 that bio-PS had lower stress at 10% deformation than PLA foam but almost the same stress at 20% deformation. This is due to the more elastic performance of bio-PS foam, indicated by the consistence compressive modulus. The compressive characteristics of PLA and bio-PS foams suggest that the bio-PS form-based sandwiches may result in less resistance to deflection at a low energy input, but will approach the level of PLA sandwiches with increasing total energy input.

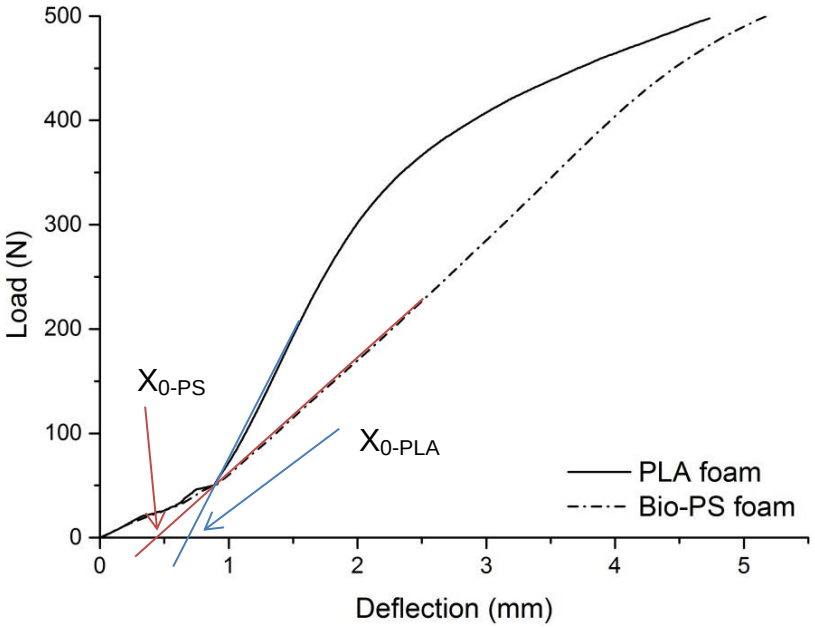

Figure 114. Compression load-deflection curves for bio-foams.

Table 35. Compressive properties of bio-foams.

Foam type	Zero strain	Compressive modulus	Stress at 10% deformation	Stress at 20% deformation
PLA	3.5 %	1.88±0.22 MPa	145.1±6.2 KPa	198.7±5.6 KPa
Bio-PS	2.1 %	0.82±0.19 MPa	87.7±6.6 KPa	180.1±9.3 KPa

7.3.3 Influence of foams and face sheets on impact response (3 m/s)

The impact responses of sandwiches with different foam cores and face sheets were obtained at 3 m/s (total potential energy of 10.26 J). Figure 115 illustrates the load and speed versus displacement plots of representative sandwich specimens. The load and absorbed energy versus time plots for the investigated materials are shown in Figure 116. The characteristic properties are summarised in Table 36.

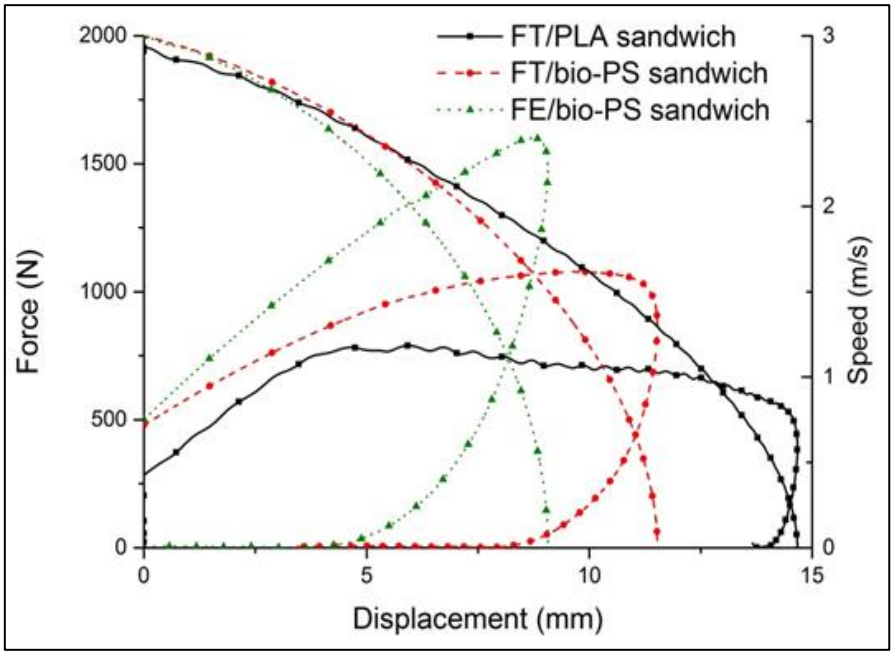

Figure 115. Comparison of load and speed vs displacement plotted for three different bio- sandwiches (3 m/s).

In this investigation, the average peak load of the specimens at 3m/s, as shown in Figure 115, was 782, 1076 and 1600 N for FT/PLA, FT/bio-PS and FE/bio-PS sandwich samples, respectively. Load increased almost linearly with

Table 36. Average impact parameters for sandwich samples impacted at 3, 5 and 7 m/s.

Sandwiches	Peak load (N)	Deflection at peak load (mm)	Time to max load (ms)	Total time (ms)	Energy to peak load (J)	Total energy absorbed (J)
			3 m/s (10.3J)			
FT/PLA	780±152	8.7±1.2	1.9±0.4	13.9±1.3	3.2±0.2	9.6±0.3
FT/bio-PS	1031±180	11.2±1.3	4.5±0.3	12.5±1.6	8.6±1.2	9.6±0.3
FE/bio-PS	1600±123	4.7±0.6	4.2±0.4	10.5±1.8	9.8±0.5	8.4±0.2
			5 m/s (28.5 J)			
FT/PLA	863±134	9.2±2.2	1.7±0.5	16.9±1.9	5.0±0.4	27.3±0.4
FT/bio-PS	1129±120	10.8±1.5	2.3±0.7	14.2±.1.4	9.3±0.2	28.5±0.2
FE/bio-PS	2145±110	17.3±0.7	5.1±0.2	12.4±.1.6	26.1±0.8	26.1±0.5
			7 m/s (55.9 J)			
FT/PLA	796±130	9.3±1.8	1.4±0.6	12.5±1.7	5.6±0.7	30.9±1.8
FT/bio-PS	959±110	10.6±0.9	1.5±0.5	12.5±1.8	8.5±0.6	35.8±1.2
FE/bio-PS	1620±86	12.1±0.6	1.8±0.7	13.4±1.4	13.9±0.5	52.7±1.2

displacement up to an initial load peak. The threshold force for the sample damage is normally indicated at the initial load peak [188]. It was seen that FE/bio-PS samples had the highest peak load with low defection, as a function of the sample stiffness. This is because the hybrid flax/supersap composite sheet performs higher tension and bending strength than non-woven flax/tannin composites. The FT/PLA samples displayed higher stiffness as indicated by the lower deflection to peak load, compared to FT/bio-PS sandwiches. At 3m/s, for all types of sandwiches, there was no indication of sharp drops in load with increasing displacement, which means no severe material failure (as shown in Figure 116-3 m/s).

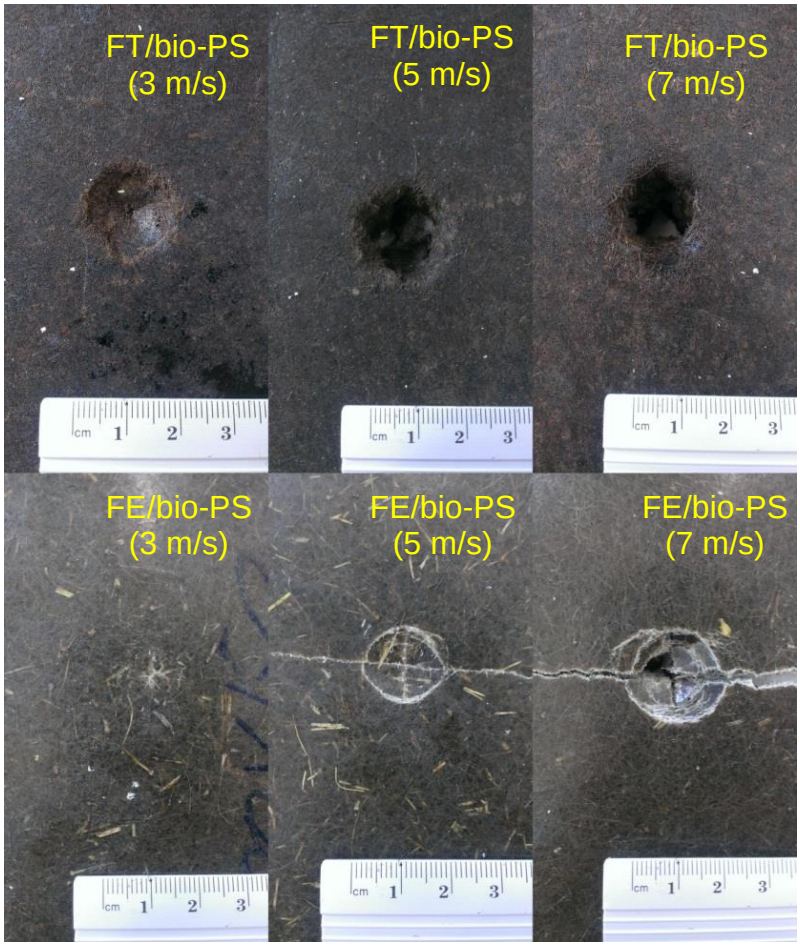

Figure 116. Comparison of damage area on the top skin surface of sandwiches.

All the sandwiches varied with foam and face sheet types exhibited the rebound phenomenon at low velocity (3 m/s). After the rebound point, which can be

referred as the ultimate dart movement, the load decreased with decreasing the impactor displacement. All the potential energy was dissipated by sandwich, and then a certain amount of energy was released from the elastic deformation to drive the dart bound up. The ultimate dart movement could be determined at velocity of 0 m/s through the speed versus displacement curves (Figure 116). For all cases of sandwiches, speed starting from 3 m/s decreased non-linearly to zero where the rebound took place.

The displacement of the dart in the reverse/opposite direction is a reflection of the elastic response/deformation of the sample. FT/PLA, FT/bio-PS and FE/bio-PS sandwiches showed the opposite movement of 0.6, 3.2 and 4.6 mm, respectively. In terms of foam types, bio-PS foam core had better elastic response, resulting in larger dart displacement (in opposite direction) after impact, than PLA foams used in sandwiches with flax/tannin face sheets. This is due to the relatively denser cell structure of PS foams, providing better elastic response, compared to PLA foam consisting of closed cells. As discussed in previous chapter, a rebound case was found in FE composites but not FT composites at similar energy level. This accounts for the difference in elastic rebound between FE/bio-PS and FT/bio-PS sandwiches, absorbing energy of 8.4 J and 9.6 J, respectively.

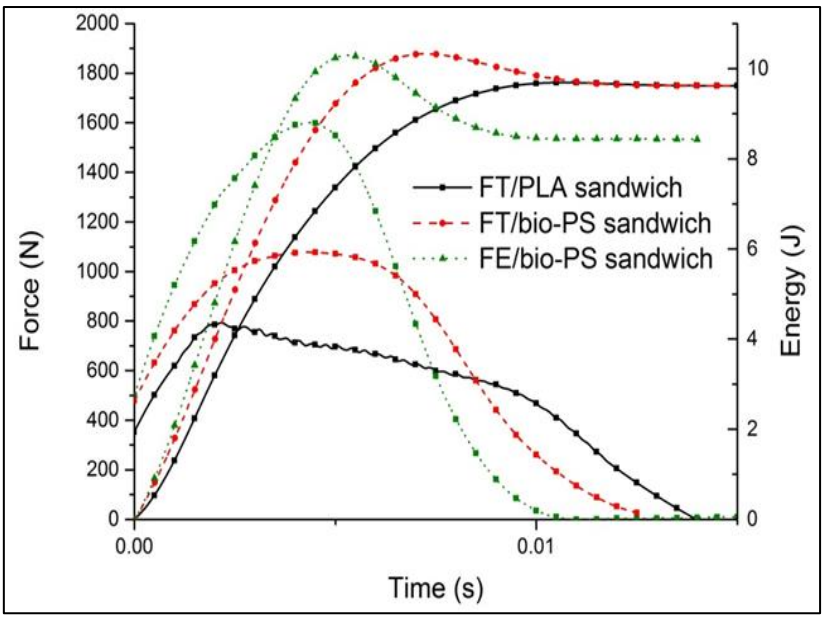

Figure 117. Load and energy versus time plots for bio-sandwiches impacted at 3 m/s.

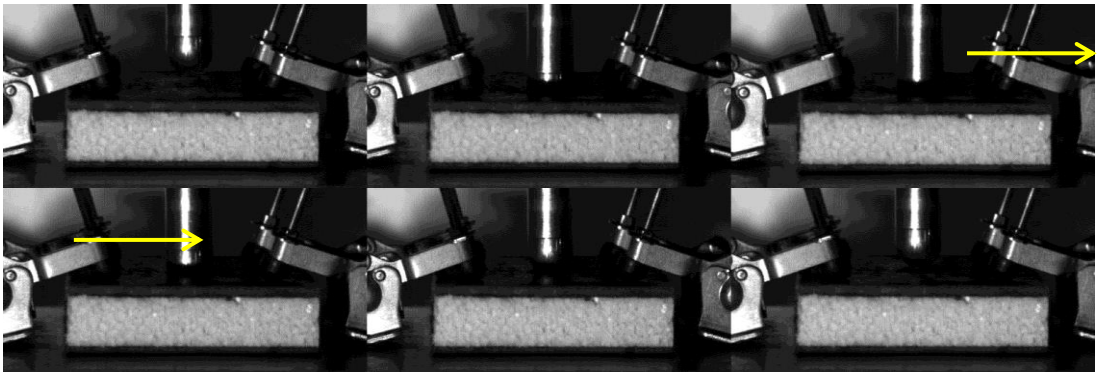

Figure 118. Impact response moment of FT/PLA sandwiches at 3 m/s.

The load and energy versus time plots for sandwich samples (FT/PLA, FT/bio-PS and FE/bio-PS) at 10.26 J (3 m/s) are shown in Figure 117. In comparison with FT/bio-PS sandwiches, the shorter time (2.1 ms) to the load peak of the FT/PLA sample is also due to the higher stiffness of PLA foam than bio-PS foam. In the study of the effect of face sheets, FT/bio-PS samples had a wider load-time peak than FE/bio-PS samples. This is attributed to the greater extent of damage sustained (i.e. plastic deformation) by the FT/bio-PS samples to dissipate energy. With the lowest level of striker rebound, there was almost no energy release for FT/PLA sandwiches, giving the final energy at 9.64 J. Since the FT/bio-PS samples achieved the same energy intake (9.64J) after 0.62 J was released, there was no significant effect of bio-foam types on the energy absorption. As a result of the energy loss of 1.82 J, FE face sheets give rise to the lowest total energy intake of 8.44 J under impacting at 3 m/s. The more energy release indicates better protection capability, but may result in damage to outer-system caused by the rebound situation.

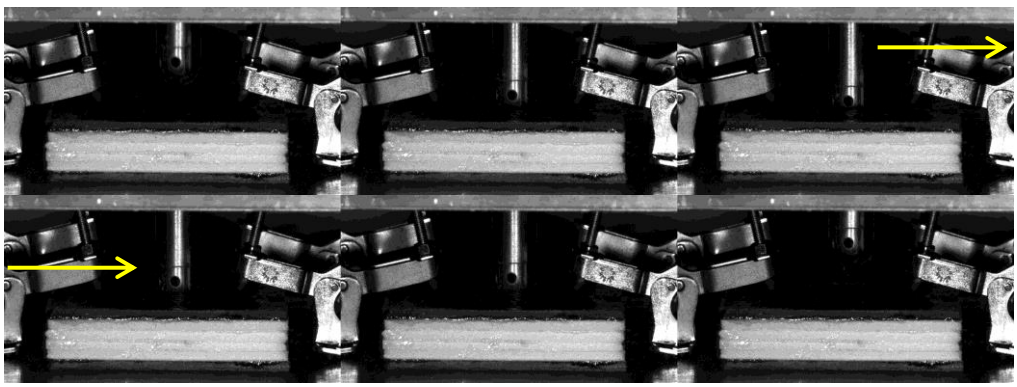

Figure 119. Impact response moment of FT/bio-PS sandwiches at 3 m/s.

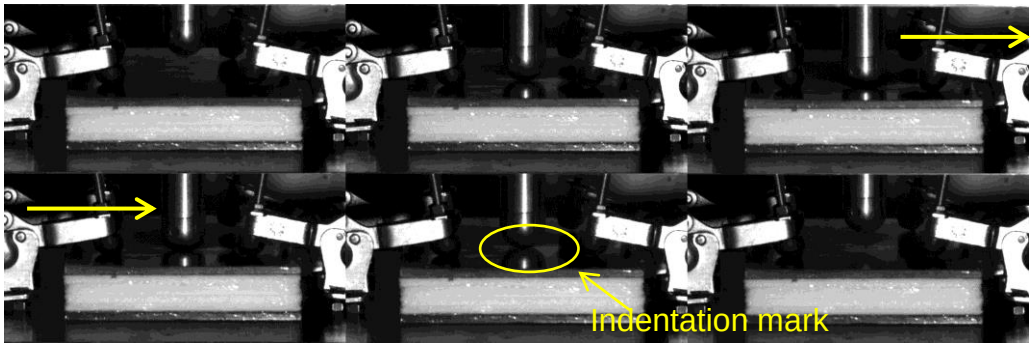

Figure 120. Impact response moment of FE/bio-PS sandwiches at 3 m/s.

In order to have better understanding of material responses, the impact moments are shown in Figure 118 to Figure 120 for each material at 3 m/s. In case of the flax/tannin face sheets, the sandwiches performed similarly in the recorded video for both bio-PS and bio-PLA foam cores. There was no visual elastic deformation but circular damage observed on flax/tannin face sheets. Due to stretching and bending, the top FT fact sheets yielded and the foam underneath absorbed most of the rest energy after the failure of face sheet. In contrast, it is quite noticeable from Figure 120 that the FE/bio-PS composites showed a great extent of deformation recovery at 3 m/s. Comparing to the big damage area (about 20 mm diameter) introduced by the striker tip on the FT/bio-PS sandwich, an almost invisible damage was found in the FE/bio-PS sample (shown in Figure 116).

7.3.4 Influence of foams and face sheets on impact response (5 m/s)

With increasing velocity to 5 m/s, the most noticeable thing for FT (flax/tannin) face sheet sandwiches (bio-PS and PLA foam based separately) is two load drops without dart rebound in the transient response plots (Figure 121 and Figure 122). The first peak load was 963 and 1128 N for FT/PLA and FT/bio-PS samples, respectively. The load dropped due to the failure of the top face sheet and foams under the impact region. The decrease in the load continued up to the point of perforation through the face sheet. After the first load drop, it again increased as the load was picked up by the rest of the foam and the bottom sheet. Mohan [244] and Hurso [227] have observed similar impact response of sandwich materials under falling weight impact tests. The second load peak

showed very close force value as compared to first peak for both FT based sandwiches. More loads were transferred to the strong back face sheet when approaching the bottom layer. FT/bio-PLA samples had longer ultimate displacement above 40 mm than FT/bio-PS sandwiches, indicating the low resistance of PLA foam to penetration. In the previous section (Figure 114), it was observed that under compression, initially, the foams exhibit a linear response, followed by a large plateau where they deflect a lot under the action of slightly higher loads, followed by (at high deflections) an exponential load response to small deflections. Since the speed continued to decrease, the energy dissipated after the perforation is not only determined by the friction but also through the indentation enlarge and foam damage. FT/PLA sandwiches absorbed the kinetic energy of 27.28 J (95.7%) through the deformation and penetration of face sheet, followed by foam damage. 100% of the potential energy (28.5 J) was fully absorbed by FT/bio-PS sandwiches (see in Table 36).

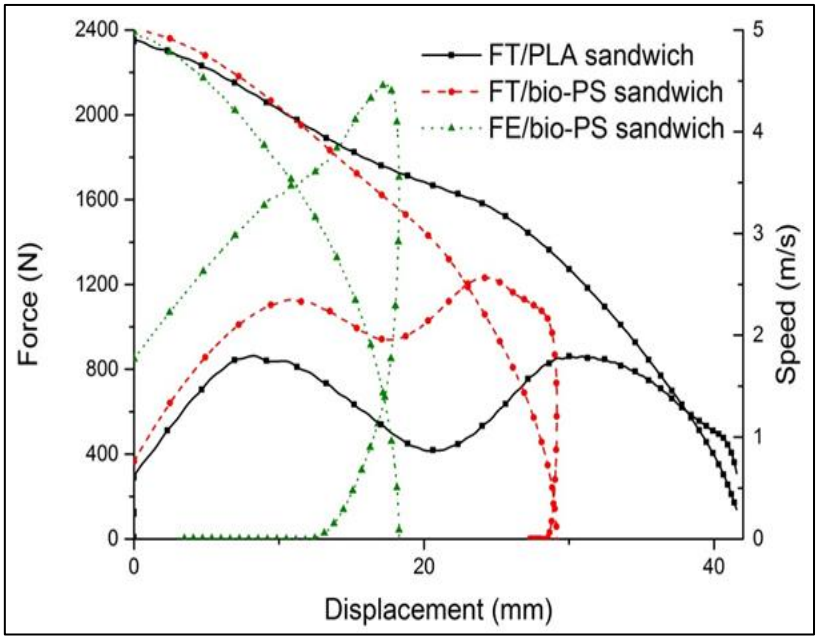

Figure 121. Load and speed versus displacement response at 5 m/s.

Effect of face sheets (FE and FT composites) on the impact response of sandwiches at 5 m/s (28.5 J) was also evaluated. It is clear from Figure 121 that FE/bio-PS got first initial load peak at 2137 N at the time and displacement of 5 ms and 17 mm, respectively. The increased peak force of FE/bio-PS

sandwiches is due to the stronger FE composites than FT as face sheets. Similar to the impact behaviour at 3 m/s, the FE/bio-PS samples also showed the dart-rebound situation as the load-displacement curve folded back after displacement of 18 mm where velocity turned negative. At the displacement of about 29 mm, the force and velocity together dropped to zero value, displaying the case of striker stop and onset of rebound. Due to the energy-release (about 2.4 J) response of FE (flax/supersap), the FE/bio-PS had lower energy absorption of 91.6% (26.1J) and lower damage degree than FT/bio-PS sandwiches (Figure 122).

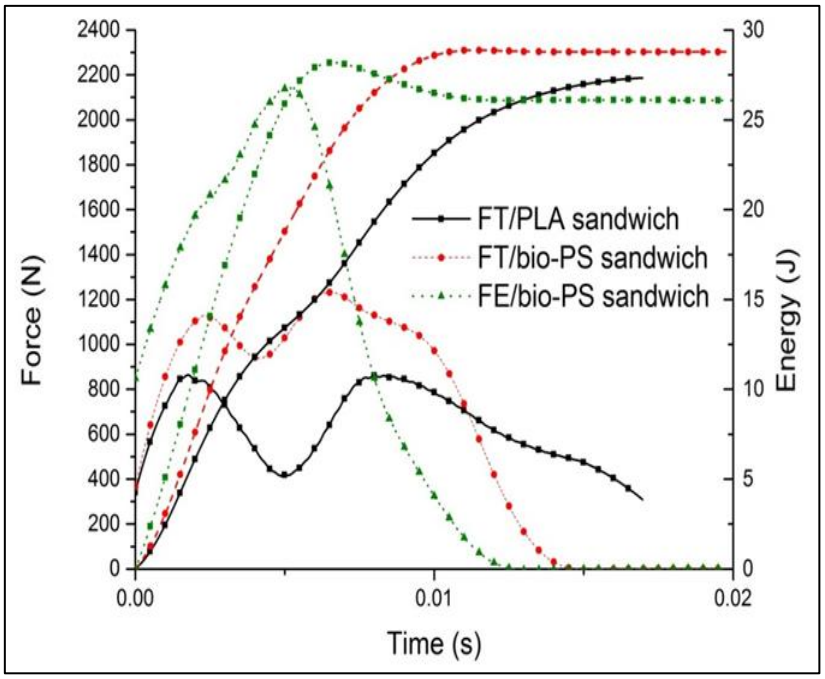

Figure 122. Load and energy versus time plots for bio-sandwiches impacted at 5 m/s.

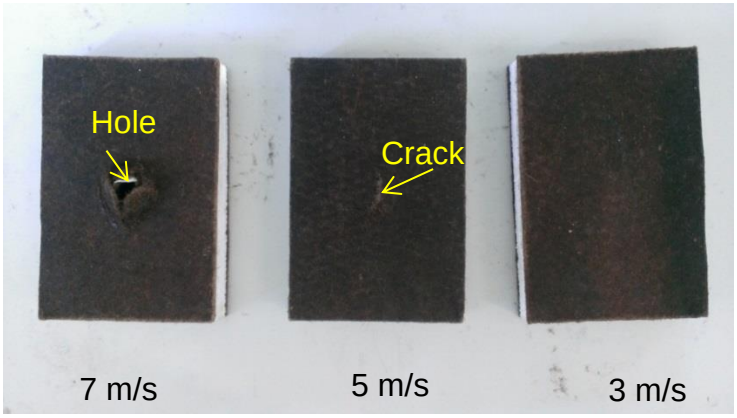

Figure 123. Back sheet of FT/bio-PS sandwiches after impacting at different velocity.

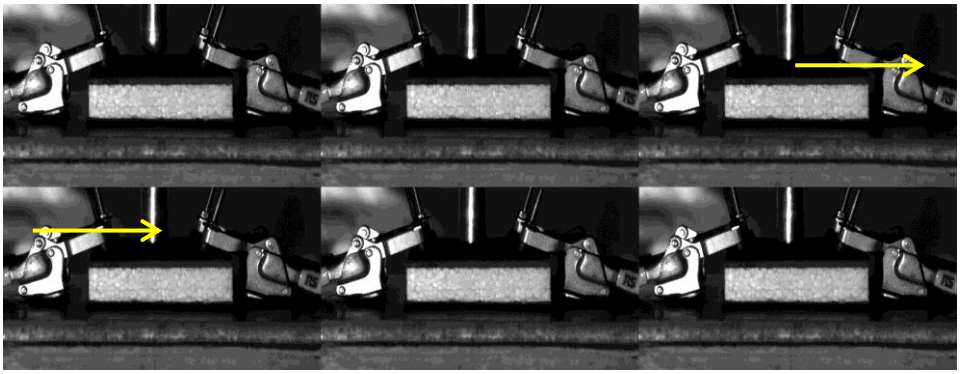

Figure 124. Impact response moment of FT/PLA sandwiches at 5 m/s.

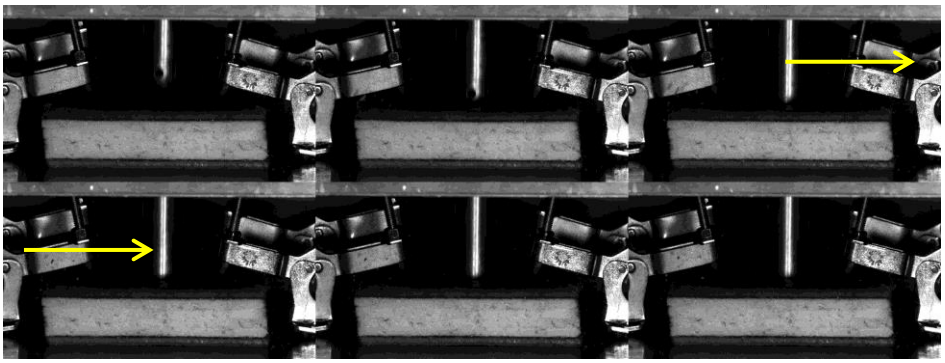

Figure 125. Impact response moment of FT/bio-PS sandwiches at 5 m/s.

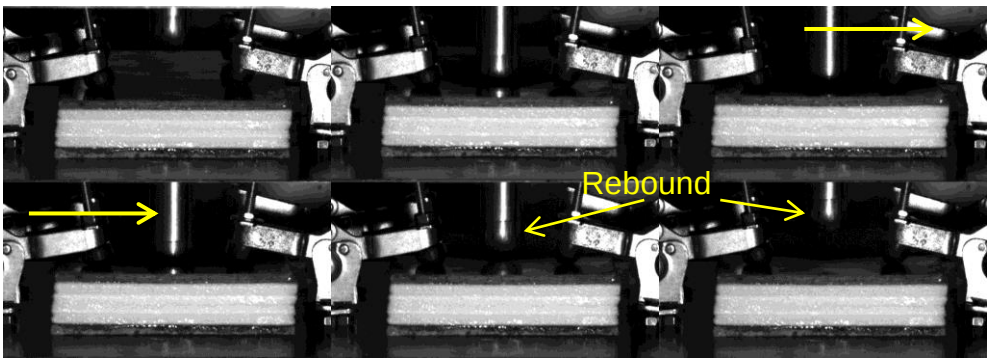

Figure 126. Impact response moment of FE/bio-PS sandwiches at 5 m/s.

The impact moments of sandwiches with different bio-foams and face sheets were recorded. For the FT based sandwiches, the dart went down directly into the sandwiches and then finally stopped (Figure 124 and Figure 125). The FT sandwich with bio-PS foam was penetrated less than FT/PLA with fully perforation. The striker still punched through the top sheet of FT/bio-PS and just damaged the bottom sheet with a visible crack absorbing the residual energy (Figure 123). For FE/bio-PS sandwiches, the striker rebounded backwards

unlike the saturation case in FT/bio-PS composites (Figure 126). It was also noticed that a crack occurred together with elastic bending deformation. An indent with cross cracks was found on the face sheet as well (as seen in Figure 116). The long crack was aligned almost parallel to the UD fabric fibre direction of FE composite face sheets. A crossed crack got initiated at the impacting centre and then the crack propagated more easily along the UD fibre direction.

7.3.5 Influence of foams and face sheets on impact response (7 m/s)

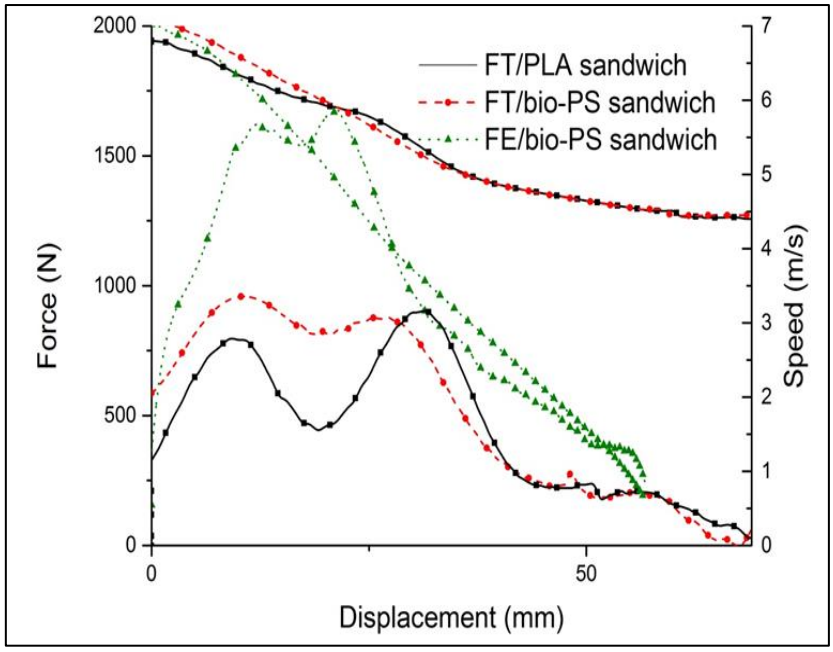

Figure 127. Load and speed versus displacement of sandwiches impacted at 7 m/s.

According to Figure 127 presenting the force and speed versus displacement plots, a similar impact response was found for FT (flax/tannin) based composites with PLA and bio-PS foams. For both sandwiches, the load increased to an initial peak, then dropped and gained to a second load peak due to the property variations through the 3-layer sandwiches (face sheet-foam-face sheet) as discussed previously. The threshold force for failure is about 792 and 958 N respectively for FT/PLA and FT/bio-PS samples. It can be seen that after the second peak, load gradually dropped to a plateau with almost constant force of 220 N. The perforation of both sandwiches by impactor accounts for this phenomenon. The evidence is shown in Figure 128 and Figure 129,

showing continuous dart penetration for FT based composites at the speed of 7 m/s. During the post-perforation stage, the impact parameters like load and energy dissipation are dominated by the internal friction, which remained load resistance for some time and kept absorbing energy. The velocity decreased rapidly to 4.5 m/s, followed by a gradual slope change. After the perforation, which absorbed most of the energy, the remaining energy of the impactor was not able to dissipate just by way of friction. As a consequence, the dart eventually hit the obstacle under the sample clamping jig.

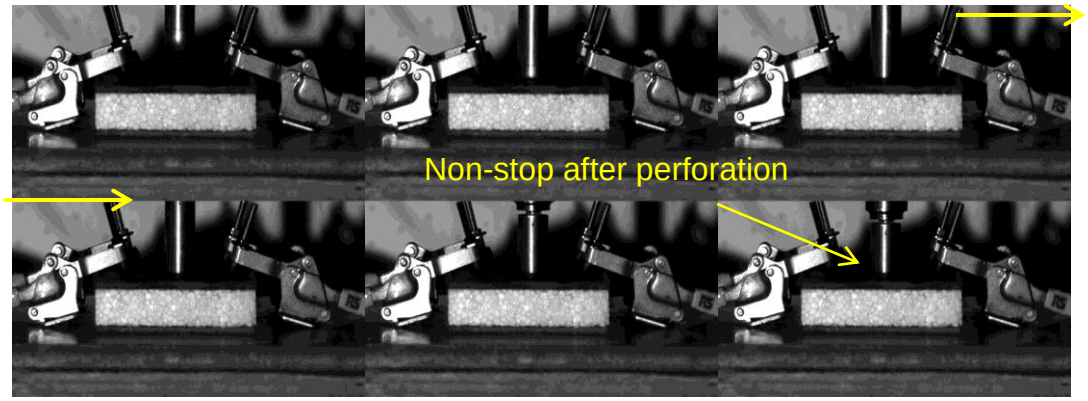

Figure 128. Impact response moment of FT/PLA sandwiches at 7 m/s.

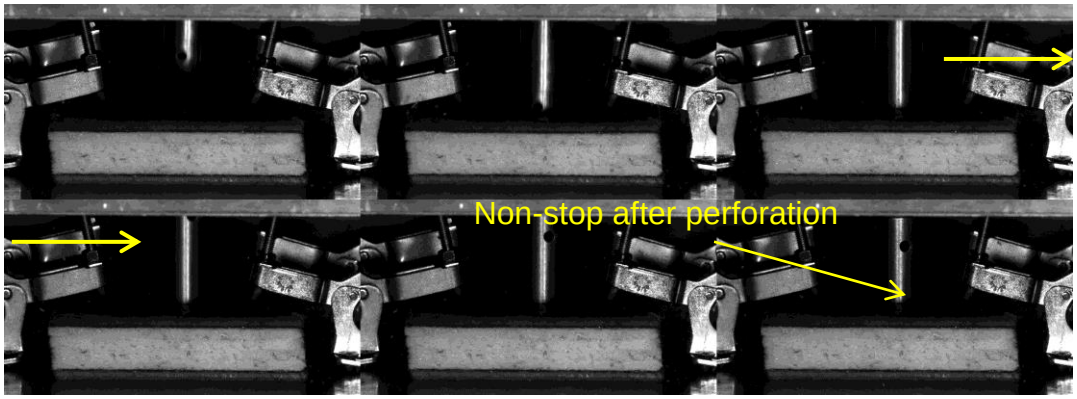

Figure 129. Impact response moment of FT/bio-PS sandwiches at 7 m/s.

At the high speed level (7 m/s) corresponding to total energy of 55.86 J, the FE/bio-PS samples performed much better than FT/bio-PS sandwiches (Figure 131). Similar to FT sandwiches, a load increase was observed after the initial force drop for FE/bio-PS samples, indicating that the top sheet was punched through, and then the bottom face sheet, together with the bio-PS foam, resisted the load. Also, as shown in Figure 130, the FE sample exhibited

debonding at the interface and between the core and top face sheets and this contributed to the load drop in the load-time/displacement response. The initial and second peak loads for FE/bio-PS sandwiches were 1600 and 1674 N, respectively, which were much higher than ones of FT/bio-PS sample. FE/bio-PS showed the highest energy absorption of 52.7 J through indentation at the point of impact, core damage beneath the top face sheet and debonding.

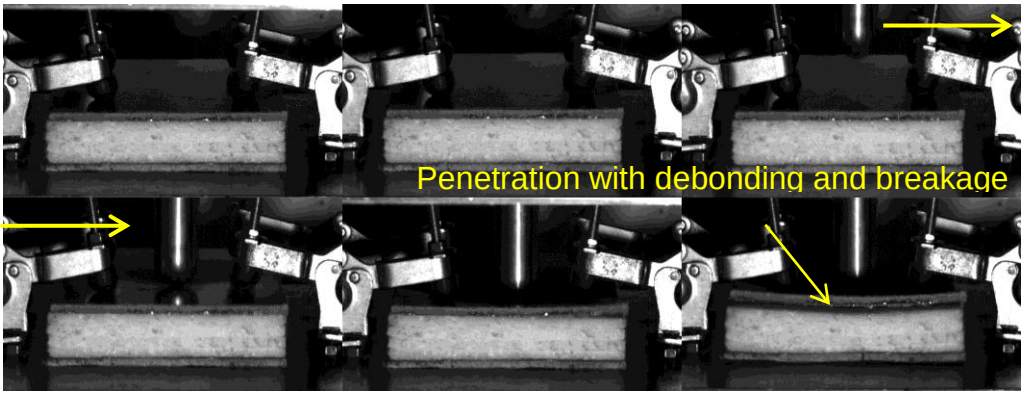

Figure 130. Impact response moment of FE/bio-PS sandwiches at 7 m/s.

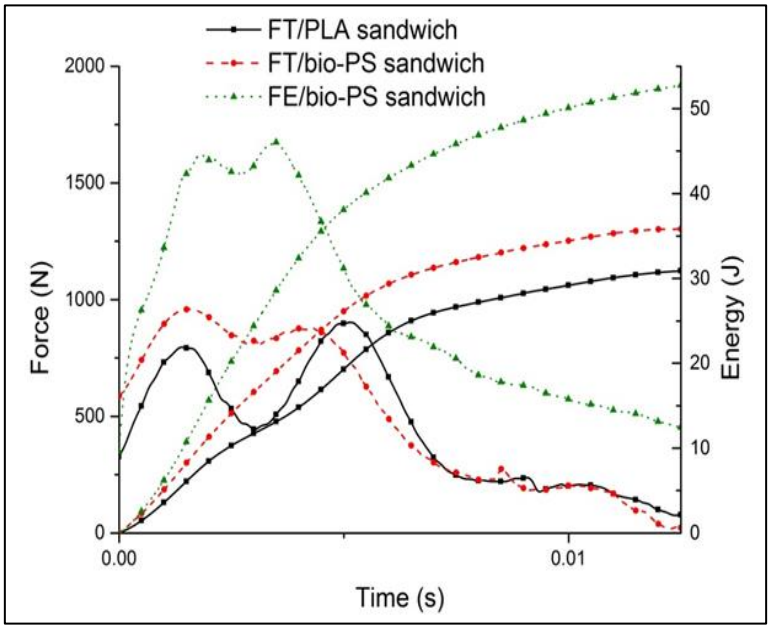

Figure 131. Load and energy versus time of sandwiches impacted at 7 m/s.

7.4 Conclusions

Falling weight impact tests with different velocities were carried out on renewable sandwich materials (FT/PLA, FT/bio-PS and FE/bio-PS). The

material stiffness is responsible for initial peak load value as the failure threshold. FE face sheet offers higher stiffness than FT sheets, resulting in higher failure loads and better damage resistance for FE/bio-PS sandwiches at all the speed level (3, 5 and 7 m/s). At 3 m/s, both FT based sample had rebound situations with energy absorption over 90 %, however FE sandwiches showed higher energy release with the mean energy absorption about 82 %. By increasing the velocity to 5 m/s, FT/bio-PS samples absorbed a little bit more energy than FT/PLA samples as a result of the better resistance to penetration for PS foam. Both FT based samples absorbed over 95 % energy, whereas a rebound case was observed in FE/bio-PS composites (about 7.5 % energy release) with uneven crack propagation caused by the weak transvers strength of FE face sheets. The effect of foams and face sheets on energy absorption at the high speed of 7 m/s was signified. Bio-PS foam based FT sandwiches absorbed over 4 J more than PLA foam based FT sandwiches. It is worth pointing out that FE based sandwiches (PS foam) had a significant improvement in the average energy absorption (94%), compared to the FT samples (PS foam) with only 60% energy absorption. It can be concluded that FE/bio-PS sandwiches provide better impact resistance, especially for high strain-rate impact.

Chapter 8. Conclusions and future work

8.1 Conclusions of the thesis

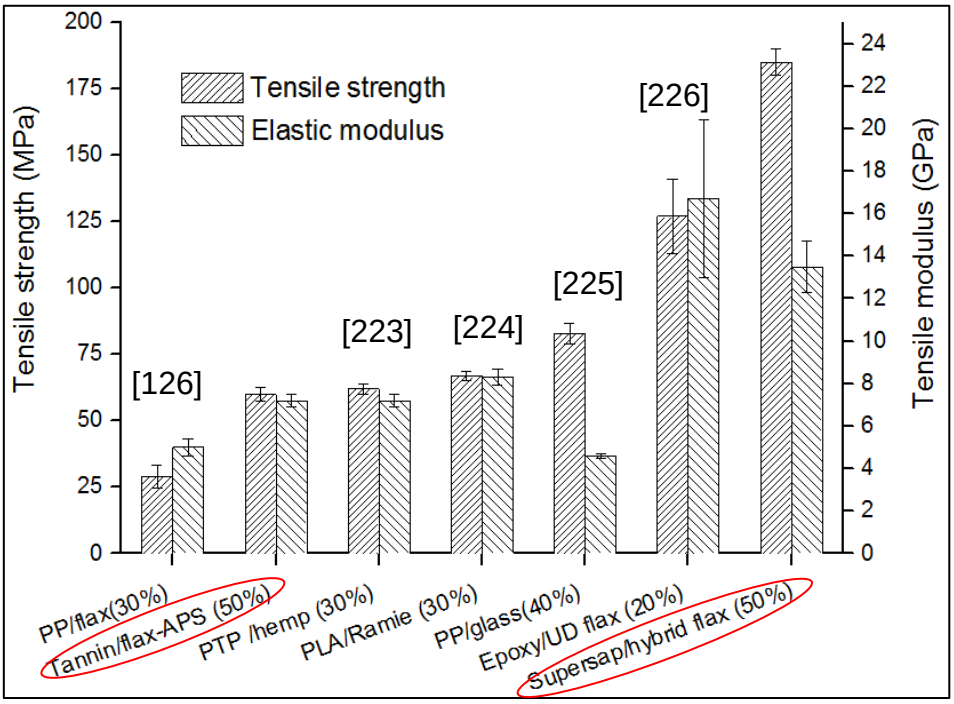

Figure 132. Literature comparison of tensile properties for natural composites (fibre content in weight fraction).

This work provides engineers an early stage of development on the studied composites but could be beneficial for other natural fibre/bio-matrix composites. Flax reinforced tannins and supersap bio-epoxy composites have good intrinsic properties that make them attractive to use in structural and non-structural components. Three factors are mostly considered for automotive candidate materials: mechanical performance, physical performance and cost/weight. Figure 132 shows the tensile property assessment of these composites compared to the literature and other very recent innovations. NW flax/tannin composites with APS treatments can reach up to 60 MPa for tensile strength and 7 GPa for elastic modulus, similar to the current thermoplastic based composites (flax/PP, glass/PP etc. as seen in Figure 132). Hybrid flax/supersap composites (no fibre treatments) also display competitive mechanical performances (tensile strength of 185 MPa and flexural strength of 125 MPa) with ecological benefits. Other assessed factors like density, weight and

production method, are summarised in Table 37. The flax/supersap composites have a renewable content over 65 $_{wt}$%, while the flax/tannin composites increase the renewable content approaching 100 $_{wt}$%. The high bio-content in these composites indicates the low raw-material production energy (hence low cost) compared to synthetic polymer based composites. In addition, both of the two novel flax composites contain flax fibre over 50 $_{wt}$%, accounting for the composite light weight (high specific properties) due to the much lower density of flax fibres than glass fibres.

Table 37. Other properties of the novel flax composites compared to literature.

Species	Density ($g.cm^3$)	Specific modulus ($GPa/g.cm^3$)	Specific strength ($MPa/g.cm^3$)	Cost	Process method
NW flax/tannin	0.75	Up to 9.6	Up to 80	+++	Compression
Hybrid flax/supersap	1.3-1.4	10.8	154.2	++	Compression
PLA/flax [131]	1.3-1.4	6.4	10.7	-	Twin-screw
PP/flax [131]	1.10	7.3	50.9	+	Compression
PP/jute [245]	1.2	4.8	39.9	++	Injection
UPE/hemp [246]	NA	3.3	23	-	RTM
Epoxy/flax [247]	1.3	11.5	161	-	Compression
PP/glass [248]	1.2	3.8	69	--	Compression

The studied flax/bio-matrix composites also have some limitations in applications. They are found sensitive to temperature, moisture and light ageing. Those parameters have detrimental effects on their mechanical performances. The glass transition temperature (T_g) of flax/tannin composites and flax/supersap composites were observed around 70 °C and 75 °C, respectively. The results overperform some recent developed natural composites, such as flax/epoxydized soil bean oil (57 °C) [26], flax/acrodur epoxy (66 °C) [249] and hemp/epoxydized soli bean oil (65 °C) [26]. However the temperature resistance of these composites may still be weak in high-temperature-environment applications like oil tank and gear box etc. With

respect to the moisture uptake, flax/tannin composites showed much higher water sensitivity (maximum moisture of 23 $_{wt}$%) than flax/supersap composites (17 $_{wt}$%). Assara and his co-workers [121] reported a water uptake of only 15 $_{wt}$% of their produced flax (38 $_{vf}$%)/epoxy composites. Regarding on the light ageing properties, untreated flax/supersap composites had the best mechanical performance after UV. After fibre modifications, the resistance to Xenon ageing of composites increased. It is therefore that flax/tannin composites can be used for interior non-structural and semi-structural applications in vehicels, while flax/supersap composites have a potential for exterior structural applications.

8.2 Suggestions to the future work

The flax fibre fabrics, nonwoven mats and supersap epoxy are commercial products/formulations; however, the technology of tannin resin still needs improvement. A high level of water presents and is created in pure tannin cured with hexamine, same for the composites. This is due to the tannin/hexamine curing mechanism. The presence of moisture leads to variable degree of curing and performance of the composites. Also the extent of internal stress due to warping in tannin resin restricts the ability for fibre/resin adhesion and to transfer sufficient load to flax fibres, together with surface voids affecting water sensitivity. Consequently, the tannin curing formation could be further optimised in hardener types, water content, curing cycle and possibly by addition or particulate reinforcements (nano-particles etc.), so as to improve the material performance for structural applications and environmental conditioning.

Unlike thin fibre fabrics, thick flax mats are relatively difficult for resin impregnation as a result of the non-woven fibre configuration. For bio-epoxy resin, high viscose epoxy resin (designed for compression moulding) does not perform very well in wetting the fibre mats. Application at higher temperature or replacement of low viscosity resin may be an option to solve the problem. Tannin resin is in the aqueous form and hence is easily absorbed by hydrophilic flax fibres. It is however, difficult to control the resin content and distribution to fully wet the thick mats, since the fibre mats can easily absorb too much resin

just in a small area. Both bio-epoxy and tannin resin, need technical changes for fast and low cost manufacturing of non-woven flax mats.

For a sandwich structure, the fracture analysis and damage tolerance is very important to better understand the sandwich performance under impact. In addition, the preparation of bio-sandwiches could be simplified by proper techniques, such as 3D resin infusion. Feasibility studies need to be performed on manufacturing complex components (like seat; box; crush cones etc.) made by flax/tannin or flax/supersap composites. A lot of effort is required to optimise the design, manufacturing techniques and related production parameters to meet the product requirements.

In order to have an efficient development, simulation could be applied all through the above three-level directions from materials to products. The first step is to build proper material-level (mainly mechanical and environmental degradation properties) models for flax reinforced bio-composites. Since natural composites, especially for flax/tannin composites, behave differently from normal synthetic composites, a modified model/theory is needed for best validation. Based on this, a real product performance can hence be properly estimated to further accelerate the whole progress picture.

REFERENCES

[1] Tomas, G. S. (2012)*, Renewable materials for automotive applications*, available at: http://www.ienica.net/fibresseminar/schuh.pdf (accessed November/26th).

[2] Fan, J., Nassiopoulos, E., Brighton, J., De Larminat, A. and Njuguna, J. (2011), "New structural biocomposites for car applications", *Society of Plastics Engineers - EUROTEC 2011 Conference Proceedings,* .

[3] Mohanty, A. K., Misra, M. and Hinrichsen, G. (2000), "Biofibres, biodegradable polymers and biocomposites: An overview", *Macromolecular Materials and Engineering,* vol. 276-277, no. 1, pp. 1-24.

[4] Peroni, I. (2009), "Natural fibres and composites: Research development and production", *International Journal of Materials and Product Technology,* vol. 36, no. 1-4, pp. 396-416.

[5] Ganji, M. and Tabarsa, T., (2011), *A novel phenol - Based composite production: Features and characterization*.

[6] Khalil, H. P. S. A., Tehrani, M. A., Davoudpour, Y., Bhat, A. H., Jawaid, M. and Hassan, A. (2013), "Natural fiber reinforced poly(vinyl chloride) composites: A review", *Journal of Reinforced Plastics and Composites,* vol. 32, no. 5, pp. 330-356.

[7] John, M. J. and Thomas, S. (2008), "Biofibres and biocomposites", *Carbohydrate Polymers,* vol. 71, no. 3, pp. 343-364.

[8] Njuguna, J., Pena, I., Zhu, H., Rocks, S. A., Blazquez, M. and Desai, S. A. (2010), "Opportunities and Environmental Health Challenges Facing Integration of Polymer NanoComposites Technologies for Automotive Applications", *International Journal of Polymers and Technologies,* vol. 2, pp. 117-226.

[9] Puglia, D., Biagiotti, J. and Kenny, J. M. (2004), "A review on natural fibre-based composites - Part II: Application of natural reinforcements in composite materials for automotive industry", *Journal of Natural Fibers,* vol. 1, no. 3, pp. 23-65.

[10] Pizzi, A., Kueny, R., Lecoanet, F., Massetau, B., Carpentier, D., Krebs, A., Loiseau, F., Molina, S. and Ragoubi, M. (2009), "High resin content natural matrix-natural fibre biocomposites", *Industrial Crops and Products,* vol. 30, no. 2, pp. 235-240.

[11] Chabba, S. and Netravali, A. N. (2005), "'Green' composites part 2: Characterization of flax yarn and glutaraldehyde/poly(vinyl alcohol) modified soy protein concentrate composites", *Journal of Materials Science,* vol. 40, no. 23, pp. 6275-6282.

[12] Kumar, R. and Anandjiwala, R. D. (2012), "Flax-fabric-reinforced arylated soy protein composites: Brittle-matrix behavior", *Journal of Applied Polymer Science,* vol. 124, no. 4, pp. 3132-3141.

[13] Liu, Z., Erhan, S. Z., Akin, D. E., Barton, F. E., Onwulata, C. and McKeon, T. A. (2008), "Modified flax fibers reinforced soy-based composites: Mechanical properties and water absorption behavior", *Composite Interfaces,* vol. 15, no. 2-3, pp. 207-220.

[14] Liu, Z. and Erhan, S. Z. (2008), ""Green" composites and nanocomposites from soybean oil", *Materials Science and Engineering A,* vol. 483-484, no. 1-2 C, pp. 708-711.

[15] Liu, Z., Erhan, S. Z., Akin, D. E. and Barton, F. E. (2006), ""Green" composites from renewable resources: Preparation of epoxidized soybean oil and flax fiber composites", *Journal of Agricultural and Food Chemistry,* vol. 54, no. 6, pp. 2134-2137.

[16] Hollaway, L. C. and Head, P. R. (2001), "Chapter 2 - Advanced polymer composite materials and their components", in *Advanced Polymer*

Composites and Polymers in the Civil Infrastructure, Elsevier Science Ltd, Oxford, pp. 7-35.

[17] Hollaway, L. C. and Head, P. R. (2001), "Chapter 3 - Manufacture and properties of advanced polymer composites relevant to civil engineering", in *Advanced Polymer Composites and Polymers in the Civil Infrastructure,* Elsevier Science Ltd, Oxford, pp. 37-88.

[18] Barbero, E. J. (1999), *Introduction to composite materials design,* Taylor and Francis, Philadelphia ; London.

[19] Harris, B. and Institute of Materials (Great Britain) (1999), *Engineering composite materials,* 2nd ed, IOM, London.

[20] Dittenber, D. B. and Rao, H. V. S. G. (2011), "Critical review of recent publications on use of natural composites in infrastructure", .

[21] Pandey, J. K., Ahn, S. H., Lee, C. S., Mohanty, A. K. and Misra, M. (2010), "Recent Advances in the Application of Natural Fiber Based Composites", *Macromolecular Materials and Engineering,* vol. 295, no. 11, pp. 975-989.

[22] Dakka, S. M. (2003), "TG/DTA/MS of poly(methyl methacrylate). The effect of particle size", *Journal of Thermal Analysis and Calorimetry,* vol. 74, no. 3, pp. 729-734.

[23] Cheung, H., Ho, M., Lau, K., Cardona, F. and Hui, D. (2009), "Natural fibre-reinforced composites for bioengineering and environmental engineering applications", *Composites Part B: Engineering,* vol. 40, no. 7, pp. 655-663.

[24] Raquez, J., Deléglise, M., Lacrampe, M. and Krawczak, P. (2010), "Thermosetting (bio)materials derived from renewable resources: A critical review", *Progress in Polymer Science (Oxford),* vol. 35, no. 4, pp. 487-509.

[25] Chabba, S. and Netravali, A. N. (2005), "'Green' composites part 1: Characterization of flax fabric and glutaraldehyde modified soy protein concentrate composites", *Journal of Materials Science,* vol. 40, no. 23, pp. 6263-6273.

[26] O'Donnell, A., Dweib, M. A. and Wool, R. P. (2004), "Natural fiber composites with plant oil-based resin", *Composites Science and Technology,* vol. 64, no. 9, pp. 1135-1145.

[27] Takada, Y., Shinbo, K., Someya, Y. and Shibata, M. (2009), "Preparation and properties of bio-based epoxy montomorillonite nanocomposites derived from polyglycerol polyglycidyl ether and ε-polylysine", *Journal of Applied Polymer Science,* vol. 113, no. 1, pp. 479-484.

[28] Panthapulakkal, S. and Sain, M. (2007), "Injection-molded short hemp fiber/glass fiber-reinforced polypropylene hybrid composites -mechanical, water absorption and thermal properties", *Journal of Applied Polymer Science,* vol. 103, no. 4, pp. 2432-2441.

[29] Mohanty, A. K., Tummala, P., Liu, W., Misra, M., Mulukutla, P. V. and Drzal, L. T. (2005), "Injection molded biocomposites from soy protein based bioplastic and short industrial hemp fiber", *Journal of Polymers and the Environment,* vol. 13, no. 3, pp. 279-285.

[30] Mehta, G., Drzal, L. T., Mohanty, A. K. and Misra, M. (2006), "Effect of fiber surface treatment on the properties of biocomposites from nonwoven industrial hemp fiber mats and unsaturated polyester resin", *Journal of Applied Polymer Science,* vol. 99, no. 3, pp. 1055-1068.

[31] Yu, L., Dean, K. and Li, L. (2006), "Polymer blends and composites from renewable resources", *Progress in Polymer Science (Oxford),* vol. 31, no. 6, pp. 576-602.

[32] Nabi Saheb, D. and Jog, J. P. (1999), "Natural fiber polymer composites: A review", *Advances in Polymer Technology,* vol. 18, no. 4, pp. 351-363.

[33] Holbery, J. and Houston, D., (2006), *Natural-fiber-reinforced polymer composites in automotive applications*, Springer Boston.

[34] Sparnins, E. (2009), *Mechanical properties of flax fibers and their composites* (Doctor thesis), Luleå University of Technology, .

[35] Summerscales, J., Dissanayake, N. P. J., Virk, A. S. and Hall, W. (2010), "A review of bast fibres and their composites. Part 1 - Fibres as reinforcements", *Composites Part A: Applied Science and Manufacturing,* vol. 41, no. 10, pp. 1329-1335.

[36] Anandjiwala, R. D. and Blouw, S. (2007), "Composites from bast fibres - Prospects and potential in the changing market environment", *Journal of Natural Fibers,* vol. 4, no. 2, pp. 91-901.

[37] Cao, Y., Wu, Y. and Goda, K. (2008), "Research and development of bast fiber-reinforced composites", *Cailiao Yanjiu Xuebao/Chinese Journal of Materials Research,* vol. 22, no. 1, pp. 10-17.

[38] Symington, M. C., Banks, W. M., West, O. D. and Pethrick, R. A. (2009), "Tensile testing of cellulose based natural fibers for structural composite applications", *Journal of Composite Materials,* vol. 43, no. 9, pp. 1083-1108.

[39] Xie, Y., Hill, C. A. S., Xiao, Z., Militz, H. and Mai, C. (2010), "Silane coupling agents used for natural fiber/polymer composites: A review", *Composites Part A: Applied Science and Manufacturing,* vol. 41, no. 7, pp. 806-819.

[40] Rosa, M. F., Chiou, B. -., Medeiros, E. S., Wood, D. F., Mattoso, L. H. C., Orts, W. J. and Imam, S. H. (2009), "Biodegradable composites based on starch/EVOH/glycerol blends and coconut fibers", *Journal of Applied Polymer Science,* vol. 111, no. 2, pp. 612-618.

[41] Wambua, P., Vangrimde, B., Lomov, S. and Verpoest, I. (2007), "The response of natural fibre composites to ballistic impact by fragment simulating projectiles", *Composite Structures,* vol. 77, no. 2, pp. 232-240.

[42] Mishra, S., Naik, J. B. and Patil, Y. P. (2004), "Studies on swelling properties of wood/polymer composites based on agro-waste and novolac", *Advances in Polymer Technology,* vol. 23, no. 1, pp. 46-50.

[43] Behzad, T. and Sain, M. (2005), "Cure simulation of hemp fiber acrylic based composites during sheet molding process", *Polymers and Polymer Composites,* vol. 13, no. 3, pp. 235-244.

[44] Ragoubi, M., Bienaimé, D., Molina, S., George, B. and Merlin, A. (2010), "Impact of corona treated hemp fibres onto mechanical properties of polypropylene composites made thereof", *Industrial Crops and Products,* vol. 31, no. 2, pp. 344-349.

[45] Van de Velde, K. and Kiekens, P. (2001), "Thermoplastic polymers: overview of several properties and their consequences in flax fibre reinforced composites", *Polymer Testing,* vol. 20, no. 8, pp. 885-893.

[46] Wang, B., Panigrahi, S., Tabil, L. and Crerar, W. (2007), "Pre-treatment of flax fibers for use in rotationally molded biocomposites", *Journal of Reinforced Plastics and Composites,* vol. 26, no. 5, pp. 447-463.

[47] John, M. J. and Anandjiwala, R. D. (2009), "Chemical modification of flax reinforced polypropylene composites", *Composites Part A: Applied Science and Manufacturing,* vol. 40, no. 4, pp. 442-448.

[48] Kaith, B. S., Singha, A. S., Kumar, S. and Kalia, S. (2008), "Mercerization of flax fiber improves the mechanical properties of fiber-reinforced composites", *International Journal of Polymeric Materials,* vol. 57, no. 1, pp. 54-72.

[49] De Rosa, I. M., Santulli, C. and Sarasini, F. (2010), "Mechanical and thermal characterization of epoxy composites reinforced with random and quasi-unidirectional untreated Phormium tenax leaf fibers", *Materials and Design,* vol. 31, no. 5, pp. 2397-2405.

[50] Thygesen, A., Thomsen, A. B., Daniel, G. and Lilholt, H. (2007), "Comparison of composites made from fungal defibrated hemp with composites of traditional hemp yarn", *Industrial Crops and Products,* vol. 25, no. 2, pp. 147-159.

[51] La Rosa, A. D., Recca, G., Summerscales, J., Latteri, A., Cozzo, G. and Cicala, G. (2014), "Bio-based versus traditional polymer composites. A life cycle assessment perspective", *Journal of Cleaner Production,* vol. 74, pp. 135-144.

[52] Patel, M., Bastioli, C., Marini, L. and Würdinger, E. (2005), "Life-cycle Assessment of Bio-based Polymers and Natural Fiber Composites", in *Biopolymers Online,* Wiley-VCH Verlag GmbH & Co. KGaA, .

[53] Timmis, A. J., Hodzic, A., Koh, L., Bonner, M., Soutis, C., Schäfer, A. W. and Dray, L. (2014), "Environmental impact assessment of aviation emission reduction through the implementation of composite materials", *International Journal of Life Cycle Assessment,* .

[54] Guo, M., author, Murphy, R. and Imperial College, London, degree granting institution. (2010.), *Life cycle assessment (LCA) of light-weight eco-composites* (Ph.D. thesis), Imperial College London, .

[55] Corvasce, F. (1999), "Environment friendly tire concepts using a biopolymeric filler derived from starch", *Bioplastic Conference,* 24.6.

[56] Gerngross, T. U. (1999), "Can biotechnology move us toward a sustainable society?", *Nature biotechnology,* vol. 17, no. 6, pp. 541-544.

[57] Gerngross, T.U. and Slater, S.C., (0816), *How green are green plastics?*.

[58] Hakala, S., Virtanen, Y., Meinander, K. and Tanner, T., (1997), *Life-cycle assessment, comparison of biopolymer and traditional diaper systems*.

[59] Wötzel, K., Wirth, R. and Flake, M. (1999), "Life cycle studies on hemp fibre reinforced components and ABS for automotive parts", *Die Angewandte Makromolekulare Chemie,* vol. 272, no. 1, pp. 121-127.

[60] Corbière-Nicollier, T., Gfeller Laban, B., Lundquist, L., Leterrier, Y., Månson, J. -. E. and Jolliet, O. (2001), "Life cycle assessment of biofibres replacing glass fibres as reinforcement in plastics", *Resources, Conservation and Recycling,* vol. 33, no. 4, pp. 267-287.

[61] Kosbar, L. L., Gelorme, J. D., Japp, R. M. and Fotorny, W. T. (2000), "Introducing Biobased Materials into the Electronics Industry", *Journal of Industrial Ecology,* vol. 4, no. 3, pp. 93-105.

[62] Diener, J. and Siehler, U. (1999), "Ökologischer Vergleich von NMT- und GMT-Bauteilen", *Die Angewandte Makromolekulare Chemie,* vol. 272, no. 1, pp. 1-4.

[63] Dissanayake, P. J. (2011), *Life cycle assessment of flax fibres for the reinforcement of polymer matrix composites* (PhD thesis), University of Plymouth, Plymouth.

[64] Wambua, P., Ivens, J. and Verpoest, I. (2003), "Natural fibres: can they replace glass in fibre reinforced plastics?", *Composites Science and Technology,* vol. 63, no. 9, pp. 1259-1264.

[65] Peng, X., Fan, M., Hartley, J. and Al-Zubaidy, M. (2012), "Properties of natural fiber composites made by pultrusion process", *Journal of Composite Materials,* vol. 46, no. 2, pp. 237-246.

[66] Scandola, M. and ZIni, E. (2003), *Flax fibres as polymer composite reinforcement*, available at:

http://www.ienica.net/italyseminar/fibres/scandolapresentation.pdf. (accessed 03/2012).

[67] Bos, H. L. (2004), *The potential of Flax Fibre as Reinforcement for composite Materials* (PhD thesis), Eindhoven University, Eindhoven.

[68] Mikhalovska, L. I., Gun'Ko, V. M., Rugal, A. A., Oranska, O. I., Gornikov, Y. I., Morvan, C., Follain, N., Domas, C., Pakhlov, E. M. and Mikhalovsky, S. V. (2012), "Cottonised flax fibres vs. cotton fibres: Structural, textural and adsorption characteristics", *RSC Advances,* vol. 2, no. 5, pp. 2032-2042.

[69] Laine, L. and Rozite, L. (2010)*, State of Art: Eco-efficient composite materials*, available at: http://www.ketek.fi/anacompo/STATE%20OF%20THE%20ART.pdf (accessed 03/2012).

[70] Huang, X. and Netravali, A. (2007), "Characterization of flax fiber reinforced soy protein resin based green composites modified with nano-clay particles", *Composites Science and Technology,* vol. 67, no. 10, pp. 2005-2014.

[71] Snoeck, D. and De Belie, N. (2012), "Mechanical and self-healing properties of cementitious composites reinforced with flax and cottonised flax, and compared with polyvinyl alcohol fibres", *Biosystems Engineering,* vol. 111, no. 4, pp. 325-335.

[72] Baley, C., Perrot, Y., Busnel, F., Guezenoc, H. and Davies, P. (2006), "Transverse tensile behaviour of unidirectional plies reinforced with flax fibres", *Materials Letters,* vol. 60, no. 24, pp. 2984-2987.

[73] Van De Velde, K. and Kiekens, P. (2002), "Thermal degradation of flax: The determination of kinetic parameters with thermogravimetric analysis", *Journal of Applied Polymer Science,* vol. 83, no. 12, pp. 2634-2643.

[74] Gassan, J. and Bledzki, A. K. (2001), "Thermal degradation of flax and jute fibers", *Journal of Applied Polymer Science,* vol. 82, no. 6, pp. 1417-1422.

[75] Stamboulis, A., Baillie, C. A. and Peijs, T. (2001), "Effects of environmental conditions on mechanical and physical properties of flax fibers", *Composites Part A: Applied Science and Manufacturing,* vol. 32, no. 8, pp. 1105-1115.

[76] Hughes, M., Carpenter, J. and Hill, C. (2007), "Deformation and fracture behaviour of flax fibre reinforced thermosetting polymer matrix composites", *Journal of Materials Science,* vol. 42, no. 7, pp. 2499-2511.

[77] Jähn, A., Schröder, M. W., Füting, M., Schenzel, K. and Diepenbrock, W. (2002), "Characterization of alkali treated flax fibres by means of FT Raman spectroscopy and environmental scanning electron microscopy", *Spectrochimica Acta - Part A: Molecular and Biomolecular Spectroscopy,* vol. 58, no. 10, pp. 2271-2279.

[78] Cantero, G., Arbelaiz, A., Llano-Ponte, R. and Mondragon, I. (2003), "Effects of fibre treatment on wettability and mechanical behaviour of flax/polypropylene composites", *Composites Science and Technology,* vol. 63, no. 9, pp. 1247-1254.

[79] Kaith, B. S. and Kalia, S. (2007), "Grafting of flax fiber (Linum usitatissimum) with vinyl monomers for enhancement of properties of flax-phenolic composites", *Polymer Journal,* vol. 39, no. 12, pp. 1319-1327.

[80] Di Bella, G., Fiore, V. and Valenza, A. (2010), "Effect of areal weight and chemical treatment on the mechanical properties of bidirectional flax fabrics reinforced composites", *Materials and Design,* vol. 31, no. 9, pp. 4098-4103.

[81] Van de Weyenberg, I., Ivens, J., De Coster, A., Kino, B., Baetens, E. and Verpoest, I. (2003), "Influence of processing and chemical treatment of flax

fibres on their composites", *Composites Science and Technology,* vol. 63, no. 9, pp. 1241-1246.

[82] Yan, L., Chouw, N. and Yuan, X. (2012), "Improving the mechanical properties of natural fibre fabric reinforced epoxy composites by alkali treatment", *Journal of Reinforced Plastics and Composites,* vol. 31, no. 6, pp. 425-437.

[83] Van de Weyenberg, I., Chi Truong, T., Vangrimde, B. and Verpoest, I. (2006), "Improving the properties of UD flax fibre reinforced composites by applying an alkaline fibre treatment", *Composites Part A: Applied Science and Manufacturing,* vol. 37, no. 9, pp. 1368-1376.

[84] Alix, S., Lebrun, L., Morvan, C. and Marais, S. (2011), "Study of water behaviour of chemically treated flax fibres-based composites: A way to approach the hydric interface", *Composites Science and Technology,* vol. 71, no. 6, pp. 893-899.

[85] Bledzki, A. K., Fink, H. and Specht, K. (2004), "Unidirectional hemp and flax EP- and PP-composites: Influence of defined fiber treatments", *Journal of Applied Polymer Science,* vol. 93, no. 5, pp. 2150-2156.

[86] Singha, A. S. and Rana, A. K. (2012), "Effect of Aminopropyltriethoxysilane (APS) Treatment on Properties of Mercerized Lignocellulosic Grewia optiva Fiber", *Journal of Polymers and the Environment,* , pp. 1-10.

[87] John, M. J. and Anandjiwala, R. D. (2008), "Recent developments in chemical modification and characterization of natural fiber-reinforced composites", *Polymer Composites,* vol. 29, no. 2, pp. 187-207.

[88] Bledzki, A. K., Mamun, A. A., Lucka-Gabor, M. and Gutowski, V. S. (2008), "The effects of acetylation on properties of flax fibre and its polypropylene composites", *Express Polymer Letters,* vol. 2, no. 6, pp. 413-422.

[89] Guduri, B. R., Semosa, H. and Meng, Y. Z. (2009), "Green composites from woven flax fiber and bio-copolyester", *ICCM International Conferences on Composite Materials,* .

[90] Grönqvist, S., Buchert, J., Rantanen, K., Viikari, L. and Suurnäkki, A. (2003), "Activity of laccase on unbleached and bleached thermomechanical pulp", *Enzyme and microbial technology,* vol. 32, no. 3-4, pp. 439-445.

[91] Grönqvist, S., Viikari, L., Niku-Paavola, M., Orlandi, M., Canevali, C. and Buchert, J. (2005), "Oxidation of milled wood lignin with laccase, tyrosinase and horseradish peroxidase", *Applied Microbiology and Biotechnology,* vol. 67, no. 4, pp. 489-494.

[92] Garcia-Ubasart, J., Colom, J. F., Vila, C., Hernández, N. G., Blanca Roncero, M. and Vidal, T. (2012), "A new procedure for the hydrophobization of cellulose fibre using laccase and a hydrophobic phenolic compound", *Bioresource technology,* vol. 112, pp. 341-344.

[93] Garcia-Ubasart, J., Esteban, A., Vila, C., Roncero, M. B., Colom, J. F. and Vidal, T. (2011), "Enzymatic treatments of pulp using laccase and hydrophobic compounds", *Bioresource technology,* vol. 102, no. 3, pp. 2799-2803.

[94] Wang, B., Tabil, L. and Panigrahi, S. (2008), "Effects of chemical treatments on mechanical and physical properties of flax fiber-reinforced composites", *Science and Engineering of Composite Materials,* vol. 15, no. 1, pp. 43-57.

[95] Hebeish, A., Abou-Zeid, N. Y., Waly, A. and Higazy, A. (1988), "Chemical modification of flax cellulose via etherification, esterification and crosslinking reactions", .

[96] George, J., Ivens, J. and Verpoest, I. (1999), "Mechanical properties of flax fibre reinforced epoxy composites", *Angewandte Makromolekulare Chemie,* vol. 272, pp. 41-45.

[97] Duchemin, B., Thuault, A., Vicente, A., Rigaud, B., Fernandez, C. and Eve, S. (2012), "Ultrastructure of cellulose crystallites in flax textile fibres", *Cellulose,* vol. 19, no. 6, pp. 1837-1854.

[98] Zafeiropoulos, N. E., Vickers, P. E., Baillie, C. A. and Watts, J. F. (2003), "An experimental investigation of modified and unmodified flax fibres with XPS, ToF-SIMS and ATR-FTIR", *Journal of Materials Science,* vol. 38, no. 19, pp. 3903-3914.

[99] Nigam, V., Soni, H., Saroop, M., Verma, G. L., Bhattacharya, A. S. and Setua, D. K. (2012), "Thermal, morphological, and X-ray study of polymer-clay nanocomposites", *Journal of Applied Polymer Science,* vol. 124, no. 4, pp. 3236-3244.

[100] Bismarck, A., Aranberri-Askargorta, I., Springer, J., Lampke, T., Wielage, B., Stamboulis, A., Shenderovich, I. and Limbach, H. -. (2002), "Surface characterization of flax, hemp and cellulose fibers; Surface properties and the water uptake behavior", *Polymer Composites,* vol. 23, no. 5, pp. 872-894.

[101] Garside, P. and Wyeth, P. (2004), "Identification of Cellulosic Fibres by FTIR Spectroscopy: Thread and Single Fibre Analysis by Attenuated Total Reflectance", *Studies in Conservation,* vol. 48, no. 4, pp. 269-275.

[102] Adekunle, K., Cho, S., Ketzscher, R. and Skrifvars, M. (2012), "Mechanical properties of natural fiber hybrid composites based on renewable thermoset resins derived from soybean oil, for use in technical applications", *Journal of Applied Polymer Science,* vol. 124, no. 6, pp. 4530-4541.

[103] Oksman, K. (2001), "High quality flax fibre composites manufactured by the resin transfer moulding process", *Journal of Reinforced Plastics and Composites,* vol. 20, no. 7, pp. 621-627.

[104] Muralidhar, B. A., Giridev, V. R. and Raghunathan, K. (2012), "Flexural and impact properties of flax woven, knitted and sequentially stacked knitted/woven preform reinforced epoxy composites", *Journal of Reinforced Plastics and Composites,* vol. 31, no. 6, pp. 379-388.

[105] Adekunle, K., Cho, S., Patzelt, C., Blomfeldt, T. and Skrifvars, M. (2011), "Impact and flexural properties of flax fabrics and Lyocell fiber-reinforced bio-based thermoset", *Journal of Reinforced Plastics and Composites,* vol. 30, no. 8, pp. 685-697.

[106] Åkesson, D., Skrifvars, M., Seppälä, J. and Turunen, M. (2011), "Thermoset lactic acid-based resin as a matrix for flax fibers", *Journal of Applied Polymer Science,* vol. 119, no. 5, pp. 3004-3009.

[107] Bax, B. and Müssig, J. (2008), "Impact and tensile properties of PLA/Cordenka and PLA/flax composites", *Composites Science and Technology,* vol. 68, no. 7–8, pp. 1601-1607.

[108] Stamboulis, A., Baillie, C. A., Garkhail, S. K., Van Melick, H. G. H. and Peijs, T. (2000), "Environmental durability of flax fibres and their composites based on polypropylene matrix", *Applied Composite Materials,* vol. 7, no. 5-6, pp. 273-294.

[109] Bos, H. L., Müssig, J. and van den Oever, M. J. A. (2006), "Mechanical properties of short-flax-fibre reinforced compounds", *Composites Part A: Applied Science and Manufacturing,* vol. 37, no. 10, pp. 1591-1604.

[110] Huang, G. and Liu, L. (2008), "Research on properties of thermoplastic composites reinforced by flax fabrics", *Materials and Design,* vol. 29, no. 5, pp. 1075-1079.

[111] Peijs, T., Garkhail, S., Heijenrath, R., Van Den Oever, M. and Bos, H. (1998), "Thermoplastic composites based on flax fibres and polypropylene: Influence of fibre length and fibre volume fraction on mechanical properties", *Macromolecular Symposia,* vol. 127, pp. 193-203.

[112] Andersons, J., Sparniņš, E. and Joffe, R. (2006), "Stiffness and strength of flax fiber/polymer matrix composites", *Polymer Composites,* vol. 27, no. 2, pp. 221-229.

[113] Van de Velde, K. and Kiekens, P. (2003), "Effect of material and process parameters on the mechanical properties of unidirectional and multidirectional flax/polypropylene composites", *Composite Structures,* vol. 62, no. 3-4, pp. 443-448.

[114] Arbelaiz, A., Fernández, B., Valea, A. and Mondragon, I. (2006), "Mechanical properties of short flax fibre bundle/poly(ε{lunate}-caprolactone) composites: Influence of matrix modification and fibre content", *Carbohydrate Polymers,* vol. 64, no. 2, pp. 224-232.

[115] Arbelaiz, A., Fernández, B., Ramos, J. A., Retegi, A., Llano-Ponte, R. and Mondragon, I. (2005), "Mechanical properties of short flax fibre bundle/polypropylene composites: Influence of matrix/fibre modification, fibre content, water uptake and recycling", *Composites Science and Technology,* vol. 65, no. 10, pp. 1582-1592.

[116] Garkhail, S. K., Heijenrath, R. W. H. and Peijs, T. (2000), "Mechanical properties of natural-fibre-mat-reinforced thermoplastics based on flax fibres and polypropylene", *Applied Composite Materials,* vol. 7, no. 5-6, pp. 351-372.

[117] Modniks, J. and Andersons, J. (2010), "Modeling elastic properties of short flax fiber-reinforced composites by orientation averaging", *Computational Materials Science,* vol. 50, no. 2, pp. 595-599.

[118] Andersons, J., Joffe, R., Spārniņš, E. and Weichert, D. (2011), "Modeling the effect of reinforcement discontinuity on the tensile strength of UD flax fiber composites", *Journal of Materials Science,* vol. 46, no. 15, pp. 5104-5110.

[119] Van Den Oever, M. J. A., Bos, H. L. and Van Kemenade, M. J. J. M. (2000), "Influence of the physical structure of flax fibres on the mechanical properties of flax fibre reinforced polypropylene composites", *Applied Composite Materials,* vol. 7, no. 5-6, pp. 387-402.

[120] Bos, H. L., Molenveld, K., Teunissen, W., Van Wingerde, A. M. and Van Delft, D. R. V. (2004), "Compressive behaviour of unidirectional flax fibre reinforced composites", *Journal of Materials Science,* vol. 39, no. 6, pp. 2159-2168.

[121] Assarar, M., Scida, D., El Mahi, A., Poilâne, C. and Ayad, R. (2011), "Influence of water ageing on mechanical properties and damage events of two reinforced composite materials: Flax-fibres and glass-fibres", *Materials and Design,* vol. 32, no. 2, pp. 788-795.

[122] Sgriccia, N., Hawley, M. C. and Misra, M. (2008), "Characterization of natural fiber surfaces and natural fiber composites", *Composites Part A: Applied Science and Manufacturing,* vol. 39, no. 10, pp. 1632-1637.

[123] Liang, S., Gning, P. B. and Guillaumat, L. (2012), "A comparative study of fatigue behaviour of flax/epoxy and glass/epoxy composites", *Composites Science and Technology,* vol. 72, no. 5, pp. 535-543.

[124] Yan, L. and Chouw, N. (2013), "Crashworthiness characteristics of flax fibre reinforced epoxy tubes for energy absorption application", *Materials and Design,* vol. 51, pp. 629-640.

[125] Muralidhar, B. A. (2013), "Tensile and compressive behaviour of multilayer flax-rib knitted preform reinforced epoxy composites", *Materials and Design,* vol. 49, pp. 400-405.

[126] Hughes, M., Carpenter, J. and Hill, C. (2007), "Deformation and fracture behaviour of flax fibre reinforced thermosetting polymer matrix composites", *Journal of Materials Science,* vol. 42, no. 7, pp. 2499-2511.

[127] Muralidhar, B. A. (2013), "Study of flax hybrid preforms reinforced epoxy composites", *Materials and Design,* vol. 52, pp. 835-840.

[128] Muralidhar, B. A. (2013), "Tensile and compressive properties of flax-plain weave preform reinforced epoxy composites", *Journal of Reinforced Plastics and Composites,* vol. 32, no. 3, pp. 207-213.

[129] Liu, Q. and Hughes, M. (2008), "The fracture behaviour and toughness of woven flax fibre reinforced epoxy composites", *Composites Part A: Applied Science and Manufacturing,* vol. 39, no. 10, pp. 1644-1652.

[130] Newman, R. H. (2009), "Auto-accelerative water damage in an epoxy composite reinforced with plain-weave flax fabric", *Composites Part A: Applied Science and Manufacturing,* vol. 40, no. 10, pp. 1615-1620.

[131] Oksman, K., Skrifvars, M. and Selin, J. (2003), "Natural fibres as reinforcement in polylactic acid (PLA) composites", *Composites Science and Technology,* vol. 63, no. 9, pp. 1317-1324.

[132] Graupner, N., Herrmann, A. S. and Müssig, J. (2009), "Natural and man-made cellulose fibre-reinforced poly(lactic acid) (PLA) composites: An overview about mechanical characteristics and application areas", *Composites Part A: Applied Science and Manufacturing,* vol. 40, no. 6–7, pp. 810-821.

[133] Avella, M., Buzarovska, A., Errico, M. E., Gentile, G. and Grozdanov, A. (2009), "Eco-Challenges of Bio-Based Polymer Composites", *Materials,* vol. 2, no. 3, pp. 911-925.

[134] Bax, B. and Müssig, J. (2008), "Impact and tensile properties of PLA/Cordenka and PLA/flax composites", *Composites Science and Technology,* vol. 68, no. 7–8, pp. 1601-1607.

[135] Le Duigou, A., Davies, P. and Baley, C. (2010), "Interfacial bonding of Flax fibre/Poly(l-lactide) bio-composites", *Composites Science and Technology,* vol. 70, no. 2, pp. 231-239.

[136] Adekunle, K., Cho, S., Ketzscher, R. and Skrifvars, M. (2012), "Mechanical properties of natural fiber hybrid composites based on renewable thermoset resins derived from soybean oil, for use in technical applications", *Journal of Applied Polymer Science,* vol. 124, no. 6, pp. 4530-4541.

[137] Lincoln, J. D., Shapiro, A. A., Earthman, J. C., Saphores, J. M. and Ogunseitan, O. A. (2008), "Design and evaluation of bioepoxy-flax composites for printed circuit boards", *IEEE Transactions on Electronics Packaging Manufacturing,* vol. 31, no. 3, pp. 211-220.

[138] Berger, C., Bledzki, A. K., Heim, H. and Böttcher, A. (2011), "Fiber-reinforced epoxy composites made from renewable resources", *International SAMPE Technical Conference.*

[139] Felline, F., Pappadà, S., Gennaro, R. and Passaro, A. (2013), "Resin transfer moulding of composite panels with bio-based resins", *SAMPE Journal,* vol. 49, no. 3, pp. 20-24.

[140] Barbosa Jr., V., Ramires, E. C., Razera, I. A. T. and Frollini, E. (2010), "Biobased composites from tannin–phenolic polymers reinforced with coir fibers", *Industrial Crops and Products,* vol. 32, no. 3, pp. 305-312.

[141] Pizzi, A. and Mittal, K. L. (2003), *Handbook of adhesive technology,* 2nd ed, Marcel Dekker, New York.

[142] Pizzi, A. (1983), *Wood adhesives : chemistry and technology,* Dekker, New York.

[143] Pizzi, A. (1994), *Advanced wood adhesives technology,* Dekker, New York.

[144] Pichelin, F., Kamoun, C. and Pizzi, A. (1999), "Hexamine hardener behaviour: Effects on wood glueing, tannin and other wood adhesives", *Holz als Roh - und Werkstoff,* vol. 57, no. 5, pp. 305-307.

[145] Bisanda, E. T. N., Ogola, W. O. and Tesha, J. V. (2003), "Characterisation of tannin resin blends for particle board applications", *Cement and Concrete Composites,* vol. 25, no. 6, pp. 593-598.

[146] Ndazi, B., Tesha, J. V., Karlsson, S. and Bisanda, E. T. N. (2006), "Production of rice husks composites with Acacia mimosa tannin-based resin", *Journal of Materials Science,* vol. 41, no. 21, pp. 6978-6983.

[147] Saiah, R., Sreekumar, P. A., Gopalakrishnan, P., Leblanc, N., Gattin, R. and Saiter, J. M. (2009), "Fabrication and characterization of 100% green composite: Thermoplastic based on wheat flour reinforced by flax fibers", *Polymer Composites,* vol. 30, no. 11, pp. 1595-1600.

[148] Andersons, J. and Joffe, R. (2011), "Estimation of the tensile strength of an oriented flax fiber-reinforced polymer composite", *Composites Part A: Applied Science and Manufacturing,* vol. 42, no. 9, pp. 1229-1235.

[149] Eichhorn, S. J., Dufresne, A., Aranguren, M., Marcovich, N. E., Capadona, J. R., Rowan, S. J., Weder, C., Thielemans, W., Roman, M., Renneckar, S., Gindl, W., Veigel, S., Keckes, J., Yano, H., Abe, K., Nogi, M., Nakagaito, A. N., Mangalam, A., Simonsen, J., Benight, A. S., Bismarck, A., Berglund, L. A. and Peijs, T. (2010), "Review: Current international research into cellulose nanofibres and nanocomposites", *Journal of Materials Science,* vol. 45, no. 1, pp. 1-33.

[150] Bhatnagar, A. and Sain, M. (2005), "Processing of cellulose nanofiber-reinforced composites", *Journal of Reinforced Plastics and Composites,* vol. 24, no. 12, pp. 1259-1268.

[151] Hrabalova, M., Schwanninger, M., Wimmer, R., Gregorova, A., Zimmermann, T. and Mundigler, N. (2011), "Fibrillation of flax and wheat

straw cellulose: Effects on thermal, morphological, and viscoelastic properties of poly(vinylalcohol)/fibre composites", *BioResources,* vol. 6, no. 2, pp. 1631-1647.

[152] Qua, E. H., Hornsby, P. R., Sharma, H. S. S., Lyons, G. and Mccall, R. D. (2009), "Preparation and characterization of Poly(vinyl alcohol) nanocomposites made from cellulose nanofibers", *Journal of Applied Polymer Science,* vol. 113, no. 4, pp. 2238-2247.

[153] Bunsell, A. R. (2005), *Fundamentals of fibre reinforced composite materials,* Institute of Physics Publishing, Bristol.

[154] Pethrick, R. A. (2010), *Polymer science and technology : for scientists and engineers,* Whittles, Dunbeath.

[155] Charlet, K. and Béakou, A. (2011), "Mechanical properties of interfaces within a flax bundle Part I: Experimental analysis", *International Journal of Adhesion and Adhesives,* vol. 31, no. 8, pp. 875-881.

[156] Romhány, G., Karger-Kocsis, J. and Czigány, T. (2003), "Tensile Fracture and Failure Behavior of Technical Flax Fibers", *Journal of Applied Polymer Science,* vol. 90, no. 13, pp. 3638-3645.

[157] Andersons, J., Sparniņš, E., Joffe, R. and Wallström, L. (2005), "Strength distribution of elementary flax fibres", *Composites Science and Technology,* vol. 65, no. 3-4, pp. 693-702.

[158] Ahmad, F., Choi, H. S. and Park, M. K. (2014), "A review: Natural fiber composites selection in view of mechanical, light weight, and economic properties", *Macromolecular Materials and Engineering,* .

[159] Lefeuvre, A., Bourmaud, A., Morvan, C. and Baley, C. (2014), "Tensile properties of elementary fibres of flax and glass: Analysis of reproducibility and scattering", *Materials Letters,* vol. 130, pp. 289-291.

[160] Pielichowski, K. and Njuguna, J. (2005), *Thermal degradation of polymeric materials,* Rapra Technology, Shawbury.

[161] Zhu, J., Zhu, H., Njuguna, J. and Abhyankar, H. (2013), "Recent development of flax fibres and their reinforced composites based on different polymeric matrices", *Materials,* vol. 6, no. 11, pp. 5171-5198.

[162] Kalia, S., Kaith, B. S. and Kaur, I. (2009), "Pretreatments of natural fibers and their application as reinforcing material in polymer composites?A review", *Polymer Engineering & Science,* vol. 49, no. 7, pp. 1253-1272.

[163] George, J., Sreekala, M. S. and Thomas, S. (2001), "A review on interface modification and characterization of natural fiber reinforced plastic composites", *Polymer Engineering and Science,* vol. 41, no. 9, pp. 1471-1485.

[164] Li, X., Tabil, L. and Panigrahi, S. (2007), "Chemical Treatments of Natural Fiber for Use in Natural Fiber-Reinforced Composites: A Review", *Journal of Polymers and the Environment,* vol. 15, no. 1, pp. 25-33.

[165] Zhu, X. and Cheng, J. (2003), "Kinetic parameters of thermal degradation of polymers", *Journal of Dong Hua University (English Edition),* vol. 20, no. 1, pp. 54-57.

[166] El-Sabbagh, A., Steuernagel, L. and Ziegmann, G. (2013), "Low combustible polypropylene/flax/magnesium hydroxide composites: mechanical, flame retardation characterization and recycling effect", *Journal of Reinforced Plastics and Composites,* .

[167] *Effect of Sisal Fiber Surface Treatment on Properties of Sisal Fiber Reinforced Polylactide Composites*(2011), .

[168] Zhou, L. M., Yeung, K. W., Yuen, C. W. M. and Zhou, X. (2004), "Characterization of ramie yarn treated with sodium hydroxide and

crosslinked by 1,2,3,4-butanetetracarboxylic acid", *Journal of Applied Polymer Science,* vol. 91, no. 3, pp. 1857-1864.

[169] Kim, H., Kim, H. and Cho, D. (2009), "Thermal analysis of hydrolysis and degradation of biodegradable polymer and bio-composites", *Journal of Thermal Analysis and Calorimetry,* vol. 96, no. 1, pp. 211-218.

[170] Hornsby, P. R., Hinrichsen, E. and Tarverdi, K. (1997), "Preparation and properties of polypropylene composites reinforced with wheat and flax straw fibres: Part I Fibre characterization", *Journal of Materials Science,* vol. 32, no. 2, pp. 443-449.

[171] Rudnik, E. (2007), "Thermal properties of biocomposites", *Journal of Thermal Analysis and Calorimetry,* vol. 88, no. 2, pp. 495-498.

[172] Zhou, L. M., Yeung, K. W., Yuen, C. W. M. and Zhou, X. (2005), "Effect of NaOH mercerisation on the crosslinking of ramie fabric using 1, 2, 3, 4-butanetetracarboxylic acid - Reaction kinetics", *Journal of the Textile Institute,* vol. 96, no. 4, pp. 213-220.

[173] Xie, Y., Hill, C. A. S., Xiao, Z., Militz, H. and Mai, C. (2010), "Silane coupling agents used for natural fiber/polymer composites: A review", *Composites Part A: Applied Science and Manufacturing,* vol. 41, no. 7, pp. 806-819.

[174] Erasmus, E. and Anandjiwala, R. (2009), "Studies on enhancement of mechanical properties and interfacial adhesion of flax reinforced polypropylene composites", *Journal of Thermoplastic Composite Materials,* vol. 22, no. 5, pp. 485-502.

[175] Shah, D. U., Schubel, P. J., Licence, P. and Clifford, M. J. (2012), "Hydroxyethylcellulose surface treatment of natural fibres: The new 'twist' in yarn preparation and optimization for composites applicability", *Journal of Materials Science,* vol. 47, no. 6, pp. 2700-2711.

[176] Ramires, E. C. and Frollini, E. (2012), "Tannin–phenolic resins: Synthesis, characterization, and application as matrix in biobased composites reinforced with sisal fibers", *Composites Part B: Engineering,* vol. 43, no. 7, pp. 2851-2860.

[177] Birley, A. W. (1992), *Physics of plastics : processing, properties, and materials engineering,* Hanser Publishers; Oxford University Press distributor, Munich ; New York; New York.

[178] Soden, P. D., Hinton, M. J. and Kaddour, A. S. (2004), "Chapter 2.1 - Lamina properties, lay-up configurations and loading conditions for a range of fibre reinforced composite laminates", in Hinton, M. J., Kaddour, A. S. and Soden, P. D. (eds.) *Failure Criteria in Fibre-Reinforced-Polymer Composites,* Elsevier, Oxford, pp. 30-51.

[179] Staab, G. H. (1999), "6 - Laminate Analysis", in Staab, G. H. (ed.) *Laminar Composites,* Butterworth-Heinemann, Woburn, pp. 191-282.

[180] Zhu, J., Njuguna, J., Abhyankar, H., Zhu, H., Perreux, D., Thiebaud, F., Chapelle, D., Pizzi, A., Sauget, A., de Larminat, A. and Nicollin, A. (2013), "Effect of fibre configurations on mechanical properties of flax/tannin composites", *Industrial Crops and Products,* vol. 50, no. 0, pp. 68-76.

[181] Gaugler, M. and Grigsby, W. J. (2009), "Thermal degradation of condensed tannins from radiata pine bark", *Journal of Wood Chemistry and Technology,* vol. 29, no. 4, pp. 305-321.

[182] Vázquez, G., Santos, J., Freire, M. S., Antorrena, G. and González-Álvarez, J. (2012), "DSC and DMA study of chestnut shell tannins for their application as wood adhesives without formaldehyde emission", *Journal of Thermal Analysis and Calorimetry,* , pp. 1-7.

[183] De, S. K. and White, J. R. (1996), *Short fibre-polymer composites,* Woodhead, Cambridge.

[184] Seyler, R. J. (1994), *Assignment of the glass transition,* .

[185] Wang, R., Wang, J. and Wu, L. (2002), "Prediction for elastic properties of plain weave fabric composites", *Fuhe Cailiao Xuebao/Acta Materiae Compositae Sinica,* vol. 19, no. 1, pp. 90-94.

[186] James Njuguna, Francesco Silva and Sophia Sachse, *Nanocomposites for Vehicle Structural Applications*, INTECH Open Access Publisher.

[187] Avery, D. P., Samborsky, D. D., Mandell, J. F. and Cairns, D. S. (2004), "Compression strength of carbon fiber laminates containing flaws with fiber waviness", *Collection of ASME Wind Energy Symposium Technical Papers AIAA Aerospace Sciences Meeting and Exhibit,* pp. 54.

[188] Belingardi, G. and Vadori, R. (2002), "Low velocity impact tests of laminate glass-fiber-epoxy matrix composite material plates", *International Journal of Impact Engineering,* vol. 27, no. 2, pp. 213-229.

[189] Kudanga, T., Nyanhongo, G. S., Guebitz, G. M. and Burton, S. (2011), "Potential applications of laccase-mediated coupling and grafting reactions: A review", *Enzyme and microbial technology,* vol. 48, no. 3, pp. 195-208.

[190] Kim, S. and Cavaco-Paulo, A. (2012), "Laccase-catalysed protein-flavonoid conjugates for flax fibre modification", *Applied Microbiology and Biotechnology,* vol. 93, no. 2, pp. 585-600.

[191] Aracri, E., Fillat, A., Colom, J. F., Gutiérrez, A., del Río, J. C., Martínez, T. T. and Vidal, T. (2010), "Enzymatic grafting of simple phenols on flax and sisal pulp fibres using laccases", *Bioresource technology,* vol. 101, no. 21, pp. 8211-8216.

[192] Fillat, A., Gallardo, O., Vidal, T., Pastor, F. I. J., Díaz, P. and Roncero, M. B. (2012), "Enzymatic grafting of natural phenols to flax fibres: Development of antimicrobial properties", *Carbohydrate Polymers,* vol. 87, no. 1, pp. 146-152.

[193] Sauget, A., Nicollin, A. and Pizzi, A. (2013), "Fabrication and mechanical analysis of mimosa tannin and commercial flax fibers biocomposites", *Journal of Adhesion Science and Technology,* vol. 27, no. 20, pp. 2204-2218.

[194] Tsai, S. W. (1984), "A Survey of Macroscopic Failure Criteria for Composite Materials", *Journal of Reinforced Plastics and Composites,* vol. 3, no. 1, pp. 40-62.

[195] Tsai, S. W. and Wu, E. M. (1971), "A General Theory of Strength for Anisotropic Materials", *Journal of Composite Materials,* vol. 5, no. 1, pp. 58-80.

[196] Puck, A. and Schürmann, H. (2002), "Failure analysis of FRP laminates by means of physically based phenomenological models", *Composites Science and Technology,* vol. 62, no. 12-13 SPECIAL ISSUE, pp. 1633-1662.

[197] Gibson, R. F. (2012), *Principles of composite material mechanics,* 3rd ed, CRC, Boca Raton, Fla.

[198] Laustsen, S., Lund, E., Kühlmeier, L. and Thomsen, O. T. (2014), "Interfibre Failure Characterisation of Unidirectional and Triax Glass Fibre Non-Crimp Fabric Reinforced Epoxy Laminates", *Applied Composite Materials,* .

[199] Leong, M., Overgaard, L. C. T., Daniel, I. M., Lund, E. and Thomsen, O. T. (2013), "Interlaminar/interfiber failure of unidirectional glass fiber reinforced composites used for wind turbine blades", *Journal of Composite Materials,* vol. 47, no. 3, pp. 353-368.

[200] Christensen, R. M. (2008), "Observations on the definition of yield stress", *Acta Mechanica,* vol. 196, no. 3-4, pp. 239-244.

[201] Makeev, A., He, Y. and Schreier, H. (2013), "Short-beam shear method for assessment of stress-strain curves for fibre-reinforced polymer matrix composite materials", *Strain,* vol. 49, no. 5, pp. 440-450.

[202] Herrera-Franco, P. J. and Valadez-González, A. (2005), "A study of the mechanical properties of short natural-fiber reinforced composites", *Composites Part B: Engineering,* vol. 36, no. 8, pp. 597-608.

[203] Belingardi, G. and Vadori, R. (2002), "Low velocity impact tests of laminate glass-fiber-epoxy matrix composite material plates", *International Journal of Impact Engineering,* vol. 27, no. 2, pp. 213-229.

[204] Dhakal, H. N., Zhang, Z. Y., Richardson, M. O. W. and Errajhi, O. A. Z. (2007), "The low velocity impact response of non-woven hemp fibre reinforced unsaturated polyester composites", *Composite Structures,* vol. 81, no. 4, pp. 559-567.

[205] Davies, G. A. O., Hitchings, D. and Ankersen, J. (2006), "Predicting delamination and debonding in modern aerospace composite structures", *Composites Science and Technology,* vol. 66, no. 6, pp. 846-854.

[206] Takemura, K., (2010), *Effect of water absorption on mechanical properties of hemp fiber reinforced composite*.

[207] Avril, C., Bailly, P. A., Njuguna, J., Nassiopoulos, E. and Larminat, D. A. (2012), "Development of flax-reinforced bio-composites for high-load bearing automotive parts", *European Conference on composite materials (ECCM),* 24-28, June, Venice, Italy, .

[208] Zhu, J., Abhyankar, H. and Njuguna, J. (2013), "Effect of fibre treatment on water absorption and tensile properties of flax/tannin composites", *ICMR2013,* September, Cranfield, UK, .

[209] Lee, N. and Jang, J. (1999), "Effect of fibre content on the mechanical properties of glass fibre mat/polypropylene composites", *Composites Part A: Applied Science and Manufacturing,* vol. 30, no. 6, pp. 815-822.

[210] Ismail, H., Shuhelmy, S. and Edyham, M. R. (2002), "The effects of a silane coupling agent on curing characteristics and mechanical properties of bamboo fibre filled natural rubber composites", *European Polymer Journal,* vol. 38, no. 1, pp. 39-47.

[211] Mohanty, S. and Nayak, S. K. (2010), "Short bamboo fiber-reinforced HDPE composites: Influence of fiber content and modification on strength of the composite", *Journal of Reinforced Plastics and Composites,* vol. 29, no. 14, pp. 2199-2210.

[212] Gupta, S., Raju Mantena, P. and Al-Ostaz, A. (2010), "Dynamic mechanical and impact property correlation of nanoclay and graphite platelet reinforced vinyl ester nanocomposites", *Journal of Reinforced Plastics and Composites,* vol. 29, no. 13, pp. 2037-2047.

[213] Jawaid, M., Abdul Khalil, H. P. S., Noorunnisa Khanam, P. and Abu Bakar, A. (2011), "Hybrid Composites Made from Oil Palm Empty Fruit Bunches/Jute Fibres: Water Absorption, Thickness Swelling and Density Behaviours", *Journal of Polymers and the Environment,* vol. 19, no. 1, pp. 106-109.

[214] Nourbakhsh, A., Kokta, B. V., Ashori, A. and Jahan-Latibari, A. (2008), "Effect of a novel coupling agent, polybutadiene isocyanate, on mechanical properties of wood-fiber polypropylene composites", *Journal of Reinforced Plastics and Composites,* vol. 27, no. 16-17, pp. 1679-1687.

[215] Ueng, C. E. S. (2003), "Sandwich Composites", in Meyers, R. A. (ed.) *Encyclopedia of Physical Science and Technology (Third Edition),* Academic Press, New York, pp. 407-412.

[216] Uddin, N., Mousa, M. A. and Fouad, F. H. (2013), "10 - Impact behavior of hybrid fiber-reinforced polymer (FRP)/autoclave aerated concrete (AAC) panels for structural applications", in Uddin, N. (ed.) *Developments in Fiber-Reinforced Polymer (FRP) Composites for Civil Engineering,* Woodhead Publishing, , pp. 247-271.

[217] Mills, N. (2007), "Chapter 18 - Sandwich panel case study", in Mills, N. (ed.) *Polymer Foams Handbook,* Butterworth-Heinemann, Oxford, pp. 425-447.

[218] Dweib, M. A., Hu, B., O'Donnell, A., Shenton, H. W. and Wool, R. P. (2004), "All natural composite sandwich beams for structural applications", *Composite Structures,* vol. 63, no. 2, pp. 147-157.

[219] Vijayasimha Reddy, B. G., Sharma, K. V. and Yella Reddy, T. (2014), "Deformation and impact energy absorption of cellular sandwich panels", *Materials & Design,* vol. 61, no. 0, pp. 217-227.

[220] Arteiro, A., Reis, A. L. M. A., Nóvoa, P. J. R. O., Silva, L. F. M., Zupan, M. and Marques, A. T. (2013), "Low velocity impact and flexural performance of sandwich structures with cork and polymer foam cores", *Ciência & Tecnologia dos Materiais,* vol. 25, no. 2, pp. 79-84.

[221] Cheeseman, B. A. and Bogetti, T. A. (2003), "Ballistic impact into fabric and compliant composite laminates", *Composite Structures,* vol. 61, no. 1-2, pp. 161-173.

[222] Feng, D. and Aymerich, F. (2013), "Damage prediction in composite sandwich panels subjected to low-velocity impact", *Composites Part A: Applied Science and Manufacturing,* vol. 52, no. 0, pp. 12-22.

[223] Zhou, J., Hassan, M. Z., Guan, Z. and Cantwell, W. J. (2012), "The low velocity impact response of foam-based sandwich panels", *Composites Science and Technology,* vol. 72, no. 14, pp. 1781-1790.

[224] Ivañez, I., Barbero, E. and Sanchez-Saez, S. (2014), "Analytical study of the low-velocity impact response of composite sandwich beams", *Composite Structures,* vol. 111, no. 0, pp. 459-467.

[225] Sun, Z., Jeyaraman, J., Shi, S., Sun, S., Hu, X. and Chen, H. (2014), "Processing and property of carbon-fiber aluminum-foam sandwich with aramid-fiber composite adhesive joints", *Journal of Adhesion Science and Technology,* .

[226] Ude, A. U., Ariffin, A. K. and Azhari, C. H. (2013), "Impact damage characteristics in reinforced woven natural silk/epoxy composite face-sheet and sandwich foam, coremat and honeycomb materials", *International Journal of Impact Engineering,* vol. 58, no. 0, pp. 31-38.

[227] Hosur, M. V., Bhuiyan, A. and Jeelani, S. (2009), "Impact response of nanophased foam core/braided face sheet sandwich composites", *Society for Experimental Mechanics - SEM Annual Conference and Exposition on Experimental and Applied Mechanics 2009,* Vol. 3, pp. 1535.

[228] Sharma, S. C., Murthy, H. N. N. and Krishna, M. (2004), "Low-velocity impact response of polyurethane foam composite sandwich structures", *Journal of Reinforced Plastics and Composites,* vol. 23, no. 17, pp. 1869-1882.

[229] Kepler, J. (2004), "Impact penetration of sandwich panels at different velocities - An experimental parameter study: Part II - Interpretation of results and modeling", *Journal of Sandwich Structures and Materials,* vol. 6, no. 5, pp. 379-397.

[230] HAN, M. S. and CHO, J. U. (2014), "Impact damage behavior of sandwich composite with aluminum foam core", *Transactions of Nonferrous Metals Society of China,* vol. 24, Supplement 1, no. 0, pp. s42-s46.

[231] Akil Hazizan, M. and Cantwell, W. J. (2002), "The low velocity impact response of foam-based sandwich structures", *Composites Part B: Engineering,* vol. 33, no. 3, pp. 193-204.

[232] "Low-velocity impact response of foam-core sandwich composites : Nemes, J.A. and Simmonds, K.E. Journal of Composite Materials Vol 26 No 4 (1992) pp 500–519", (1992), *Composites,* vol. 23, no. 6, pp. 462.

[233] Edgren, F., Asp, L. E. and Bull, P. H. (2004), "Compressive failure of impacted NCF composite sandwich panels - Characterisation of the failure process", *Journal of Composite Materials,* vol. 38, no. 6, pp. 495-514.

[234] Benevolenski, O. I., Karger-Kocsis, J., Mieck, K. -. and Reubmann, T. (2000), "Instrumented Perforation Impact Response of Polypropylene Composites with Hybrid Reinforcement Flax/Glass and Flax/Cellulose Fibers", *Journal of Thermoplastic Composite Materials,* vol. 13, no. 6, pp. 481-496.

[235] Yang, S. H. (1981), *Indentation Law for Composite Laminates,* 19820007250, NASA, United States.

[236] Kolopp, A., Rivallant, S. and Bouvet, C. (2013), "Experimental study of sandwich structures as armour against medium-velocity impacts", *International Journal of Impact Engineering,* vol. 61, no. 0, pp. 24-35.

[237] Goldsmith, W., Wang, G. -., Li, K. and Crane, D. (1997), "Perforation of cellular sandwich plates", *International Journal of Impact Engineering,* vol. 19, no. 5-6, pp. 361-379.

[238] Iqbal, M. A. and Gupta, N. K. (2008), "Energy absorption characteristics of aluminum plates subjected to projectile impact", *Latin American Journal of Solids and Structures,* vol. 5, no. 4, pp. 259-287.

[239] Ghelli, D., D'Ubaldo, O., Santulli, C., Nisini, E. and Minak, G. (2012), "Falling Weight Impact and Indentation Damage Characterisation of

Sandwich Panels for Marine Applications", *Open Journal of Composite Materials,* vol. 2, no. 1, pp. 8-14.

[240] Niaounakis, M. (2015), "Chapter 9 - Foaming and Foamed Products", in Niaounakis, M. (ed.) *Biopolymers: Processing and Products,* William Andrew Publishing, Oxford, pp. 327-359.

[241] Nik Pauzi, N. N. P., A. Majid, R., Dzulkifli, M. H. and Yahya, M. Y. (2014), "Development of rigid bio-based polyurethane foam reinforced with nanoclay", *Composites Part B: Engineering,* vol. 67, no. 0, pp. 521-526.

[242] Shogren, R. L., Petrovic, Z., Liu, Z. and Erhan, S. Z. (2004), "Biodegradation behavior of some vegetable oil-based polymers", *Journal of Polymers and the Environment,* vol. 12, no. 3, pp. 173-178.

[243] Tagarielli, V. L., Deshpande, V. S. and Fleck, N. A. (2007), "The dynamic response of composite sandwich beams to transverse impact", *International Journal of Solids and Structures,* vol. 44, no. 7–8, pp. 2442-2457.

[244] Mohan, K., Yip, T. H., Idapalapati, S. and Chen, Z. (2011), "Impact response of aluminum foam core sandwich structures", *Materials Science and Engineering A,* vol. 529, no. 1, pp. 94-101.

[245] Bledzki, A. K., Jaszkiewicz, A. and Scherzer, D. (2009), "Mechanical properties of PLA composites with man-made cellulose and abaca fibres", *Composites Part A: Applied Science and Manufacturing,* vol. 40, no. 4, pp. 404-412.

[246] Mehta, G., Mohanty, A. K., Misra, M. and Drzal, L. T. (2004), "Effect of novel sizing on the mechanical and morphological characteristics of natural fiber reinforced unsaturated polyester resin based bio-composites", *Journal of Materials Science,* vol. 39, no. 8, pp. 2961-2964.

[247] Charlet, K., Baley, C., Morvan, C., Jernot, J. P., Gomina, M. and Bréard, J. (2007), "Characteristics of Hermès flax fibres as a function of their location in the stem and properties of the derived unidirectional composites", *Composites Part A: Applied Science and Manufacturing,* vol. 38, no. 8, pp. 1912-1921.

[248] Granta Design Limited, (2010), *materials selection software*, CES EduPack Ver.6.2.0 ed., Cambridge.

[249] Cherif, Z. E., Poliane, C., Momayez, L. and Chen, J. (2012), "Flax/epoxy prepreg: effect of processing parameters on mechanical properties", *Materials technology,* vol. 100, pp. 459-466.

[250] Makeev, A., Seon, G., Cline, J. and Shonkwiler, B. (2014), "In quest of methods for measuring 3D mechanical properties of composites", *Composites Science and Technology,* vol. 100, pp. 105-112.

[251] Lee, D. and Tippur, H. V. (2009), "Stress-wave induced fracture of unidirectional composites: An experimental study using digital image correlation method", *12th International Conference on Fracture 2009, ICF-12,* Vol. 3, pp. 1875.

[252] Allaer, K., De Baere, I., Lava, P., Van Paepegem, W. and Degrieck, J. (2014), "On the in-plane mechanical properties of stainless steel fibre reinforced ductile composites", *Composites Science and Technology,* vol. 100, pp. 34-43.

[253] Maksymenko, O. P., Frankevych, L. F. and Sakharuk, O. M. (2013), "Determination of the moduli of elasticity of materials by the method of digital image correlation", *Materials Science,* vol. 48, no. 6, pp. 825-831.

[254] Brown, E. N. and Liu, C. (2007), "Applying digital image correlation to unidirectional composite iosipescu shear test specimens", *Proceedings of the SEM Annual Conference and Exposition on Experimental and Applied Mechanics 2007,* Vol. 1, pp. 301.

[255] Canal, L. P., González, C., Molina-Aldareguía, J. M., Segurado, J. and Llorca, J. (2012), "Application of digital image correlation at the microscale in fiber-reinforced composites", *Composites Part A: Applied Science and Manufacturing,* vol. 43, no. 10, pp. 1630-1638.

APPENDICES

Apendix 1. Statistical analysis

1. General statistics

Considering numerous sample data obtained in the investigations, general statistical method was applied for small sample groups, such as mechanical testing group etc. Data distribution characteristics could be calculated as below:

$$\bar{X} = \frac{\sum_{i=1}^{n} X_i}{n} \qquad (A1.1)$$

$$S_{n-1} \sqrt{= \frac{\sum_{i=1}^{n} X_i^2 - n\bar{X}^2}{n-1}} \qquad (A1.2)$$

$$CV = 100 \times \frac{S_{n-1}}{\bar{X}} \qquad (A1.3)$$

Where n is the specimen numbers, X_i is the measured property as single data. $\bar{X}$ is sample average, S_{n-1} the standard deviation (square root of sample variance), CV the sample coefficient of variation, presenting the significance of sample difference in S_{n-1}.

2. Weibull statistics

The strength of any flax fibres (bundle) component is principally dependent on the weak interphase location and flaw distribution. A simple analogy is a length of chain which is only as strong as its weakest link. This means that no two supposedly identical chains will have the same strength, the same way for the flax fibre strength. Thus to model the fibre strength we need a statistical model which gives emphasis to the extreme value of c. The weibull statistics usually for ceramic failure strength therefore adopted for flax fibres. A two parameter weibull distribution is:

$$P_f = 1 - \exp\left[-V\left(\frac{\sigma}{\sigma_m}\right)^m\right] \qquad (A1.4)$$

Where

$P_f(V)$ is the probability of failure for a sample of volume V,

σ is the applied stress,

σ_m is a normalizing constant, normally the sample mean

m is the weilbull modulus, a dimensionless parameter.

From the equation, we see:

$$\ln\left(\frac{1}{1-P_f\,(V)}\right) = \mathrm{V}(\frac{\sigma}{\sigma_m})^m \qquad (A1.5)$$

hence

$$\ln\left[\ln\left(\frac{1}{1-P_f\,(V)}\right)\right] = \mathrm{mln}\sigma - mln\sigma_m + lnV \qquad (A1.6)$$

The m could be measured as the slope from plotting the above equation. M is a figure merit for the reproducibility or reliability of strength values in a range of samples. The higher the m value the better the reliability of the components.

To calculate a value for m:

i. Test N samples (N as large as possible; at least 20)
ii. Ranke in ascending order of σ_f, i.e……..i…….N (strongest)
iii. The probability of failure, $P_f = \frac{i}{(N+1)}$ at $(\sigma_f)_i$.
iv. Therefore, the probability of survival, $P_s = \left(1 - P_f\right) = \left[\frac{(N+1)-i}{(N+1)}\right]$.
v. We then need to calculate σ_m and then $\frac{\sigma_f}{\sigma_m}$.
vi. The we can either plot P_s versus $\frac{\sigma_f}{\sigma_m}$ on lnln versus in graph paper, the slope is –m, or calculate $\mathrm{lnln}(\frac{1}{P_s})$ and $\ln(\frac{\sigma_f}{\sigma_m})$ and plot on standard graph paper, the slope is m.

The obtained plots and m value are shown in Chapter 3, the related parameters in calculation are displayed in below Tables.

Table 1-1. Weibull calculations for flax bundle (UD) at 40 mm gauge.

X	Ascending number	X/Xmean	Ln X/Xm	Pf	Ps	1/ps	lnln 1/ps
190	1	0.791996665	-0.2332	0.047619	0.952381	1.05	-3.02023
215	2	0.896206753	-0.10958	0.095238	0.904762	1.105263	-2.30175
220	3	0.91704877	-0.08659	0.142857	0.857143	1.166667	-1.86982
225	4	0.937890788	-0.06412	0.190476	0.809524	1.235294	-1.55443
227	5	0.946227595	-0.05527	0.238095	0.761905	1.3125	-1.3022
228	6	0.950395998	-0.05088	0.285714	0.714286	1.4	-1.08924
230	7	0.958732805	-0.04214	0.333333	0.666667	1.5	-0.90272
233	8	0.971238016	-0.02918	0.380952	0.619048	1.615385	-0.73486
237	9	0.98791163	-0.01216	0.428571	0.571429	1.75	-0.5805
245	10	1.021258858	0.021036	0.47619	0.52381	1.909091	-0.43599
245	11	1.021258858	0.021036	0.52381	0.47619	2.1	-0.29849
246	12	1.025427261	0.025109	0.571429	0.428571	2.333333	-0.1657
249	13	1.037932472	0.037231	0.619048	0.380952	2.625	-0.03554
250	14	1.042100875	0.041239	0.666667	0.333333	3	0.094048
254	15	1.058774489	0.057112	0.714286	0.285714	3.5	0.225351
255	16	1.062942893	0.061041	0.761905	0.238095	4.2	0.361224
256	17	1.067111296	0.064955	0.809524	0.190476	5.25	0.50575
260	18	1.08378491	0.080459	0.857143	0.142857	7	0.66573
265	19	1.104626928	0.099508	0.904762	0.095238	10.5	0.855
268	20	1.117132138	0.110765	0.952381	0.047619	21	1.113344

Table 1-2. Weibull calculations for flax bundle (Balance) at 40 mm gauge.

X	Ascending number	X/Xmean	Ln X/Xm	Pf	Ps	1/ps	lnln 1/ps
145	1	0.885225885	-0.12191	0.047619	0.952381	1.05	-3.02023
146	2	0.891330891	-0.11504	0.095238	0.904762	1.105263	-2.30175
149	3	0.90964591	-0.0947	0.142857	0.857143	1.166667	-1.86982
150	4	0.915750916	-0.08801	0.190476	0.809524	1.235294	-1.55443
153	5	0.934065934	-0.06821	0.238095	0.761905	1.3125	-1.3022
156	6	0.952380952	-0.04879	0.285714	0.714286	1.4	-1.08924
159	7	0.970695971	-0.02974	0.333333	0.666667	1.5	-0.90272
159	8	0.970695971	-0.02974	0.380952	0.619048	1.615385	-0.73486
160	9	0.976800977	-0.02347	0.428571	0.571429	1.75	-0.5805
163	10	0.995115995	-0.0049	0.47619	0.52381	1.909091	-0.43599
164	11	1.001221001	0.00122	0.52381	0.47619	2.1	-0.29849
165	12	1.007326007	0.007299	0.571429	0.428571	2.333333	-0.1657
169	13	1.031746032	0.031253	0.619048	0.380952	2.625	-0.03554
170	14	1.037851038	0.037152	0.666667	0.333333	3	0.094048
173	15	1.056166056	0.054645	0.714286	0.285714	3.5	0.225351
175	16	1.068376068	0.06614	0.761905	0.238095	4.2	0.361224
175	17	1.068376068	0.06614	0.809524	0.190476	5.25	0.50575
179	18	1.092796093	0.08874	0.857143	0.142857	7	0.66573
180	19	1.098901099	0.094311	0.904762	0.095238	10.5	0.855
186	20	1.135531136	0.127101	0.952381	0.047619	21	1.113344

Table 1-3. Weibull calculations for flax bundle (UD) at 75 mm gauge.

X	Ascending number	X/Xmean	Ln X/Xm	Pf	Ps	1/ps	lnln 1/ps
170	1	0.863821138	-0.14639	0.047619	0.952381	1.05	-3.02023
174	2	0.884146341	-0.12313	0.095238	0.904762	1.105263	-2.30175
175	3	0.889227642	-0.1174	0.142857	0.857143	1.166667	-1.86982
180	4	0.914634146	-0.08923	0.190476	0.809524	1.235294	-1.55443
184	5	0.93495935	-0.06725	0.238095	0.761905	1.3125	-1.3022
185	6	0.94004065	-0.06183	0.285714	0.714286	1.4	-1.08924
186	7	0.945121951	-0.05644	0.333333	0.666667	1.5	-0.90272
187	8	0.950203252	-0.05108	0.380952	0.619048	1.615385	-0.73486
188	9	0.955284553	-0.04575	0.428571	0.571429	1.75	-0.5805
190	10	0.965447154	-0.03516	0.47619	0.52381	1.909091	-0.43599
197	11	1.00101626	0.001016	0.52381	0.47619	2.1	-0.29849
198	12	1.006097561	0.006079	0.571429	0.428571	2.333333	-0.1657
205	13	1.041666667	0.040822	0.619048	0.380952	2.625	-0.03554
207	14	1.051829268	0.050531	0.666667	0.333333	3	0.094048
213	15	1.082317073	0.079104	0.714286	0.285714	3.5	0.225351
213	16	1.082317073	0.079104	0.761905	0.238095	4.2	0.361224
214	17	1.087398374	0.083788	0.809524	0.190476	5.25	0.50575
220	18	1.117886179	0.11144	0.857143	0.142857	7	0.66573
222	19	1.12804878	0.120489	0.904762	0.095238	10.5	0.855
228	20	1.158536585	0.147158	0.952381	0.047619	21	1.113344

Table 1-4. Weibull calculations for flax bundle (Balance) at 75 mm gauge.

X	Ascending number	X/Xmean	Ln X/Xm	Pf	Ps	1/ps	lnln 1/ps
145	1	0.848946136	-0.16376	0.047619	0.952381	1.05	-3.02023
148	2	0.866510539	-0.14328	0.095238	0.904762	1.105263	-2.30175
152	3	0.889929742	-0.11661	0.142857	0.857143	1.166667	-1.86982
153	4	0.895784543	-0.11006	0.190476	0.809524	1.235294	-1.55443
158	5	0.925058548	-0.0779	0.238095	0.761905	1.3125	-1.3022
159	6	0.930913349	-0.07159	0.285714	0.714286	1.4	-1.08924
161	7	0.942622951	-0.05909	0.333333	0.666667	1.5	-0.90272
163	8	0.954332553	-0.04674	0.380952	0.619048	1.615385	-0.73486
164	9	0.960187354	-0.04063	0.428571	0.571429	1.75	-0.5805
168	10	0.983606557	-0.01653	0.47619	0.52381	1.909091	-0.43599
170	11	0.995316159	-0.00469	0.52381	0.47619	2.1	-0.29849
172	12	1.007025761	0.007001	0.571429	0.428571	2.333333	-0.1657
172	13	1.007025761	0.007001	0.619048	0.380952	2.625	-0.03554
180	14	1.053864169	0.052464	0.666667	0.333333	3	0.094048
180	15	1.053864169	0.052464	0.714286	0.285714	3.5	0.225351
188	16	1.100702576	0.095949	0.761905	0.238095	4.2	0.361224
192	17	1.12412178	0.117002	0.809524	0.190476	5.25	0.50575
195	18	1.141686183	0.132506	0.857143	0.142857	7	0.66573
196	19	1.147540984	0.137621	0.904762	0.095238	10.5	0.855
200	20	1.170960187	0.157824	0.952381	0.047619	21	1.113344

Apendix 2. Mechanical testing campaign

1. Test matrix

Table 2-1. Quasi-static mechanical tests.

	Tensile	Shear	3-point bending
Standard	ASTM D3039	ASTM D7078	ASTM D7264
Outcome	Tensile Strength Tensile strain Tensile modulus Stress-strain	Shear strength Shear modulus Stress-strain	Flexural strength Flexural modulus Flexural stress-strain
Sample Geometry	250x25 mm	V-notched (see drawing)	Rectangular coupons 154x13 mm
Standard test speed	2 mm/min	2 mm/min	1 mm/min
Samples per test	3-5	3-5	3-5

Table 2-2. Dynamic mechanical tests.

	DMA	Drop-weight impact
Standard	-	ASTM D7136
Outcome	Storage modulus Loss modulus Tanδ Glass transition	Damage resistance Impact response
Sample Geometry	35×12 mm	100×150 mm
Standard test speed	1 Hz	3 m/s
Testing condition	Room T to 250°C	Room temperature
Samples per test	2	3

2. Test details

Tensile

Standard: ASTM 3039

Sample's Thickness: 2.5-3 mm

Properties extracted: Tensile Strength, tensile strain, tensile modulus, Stress-strain curve

Quantity per test: 3-5 for each material

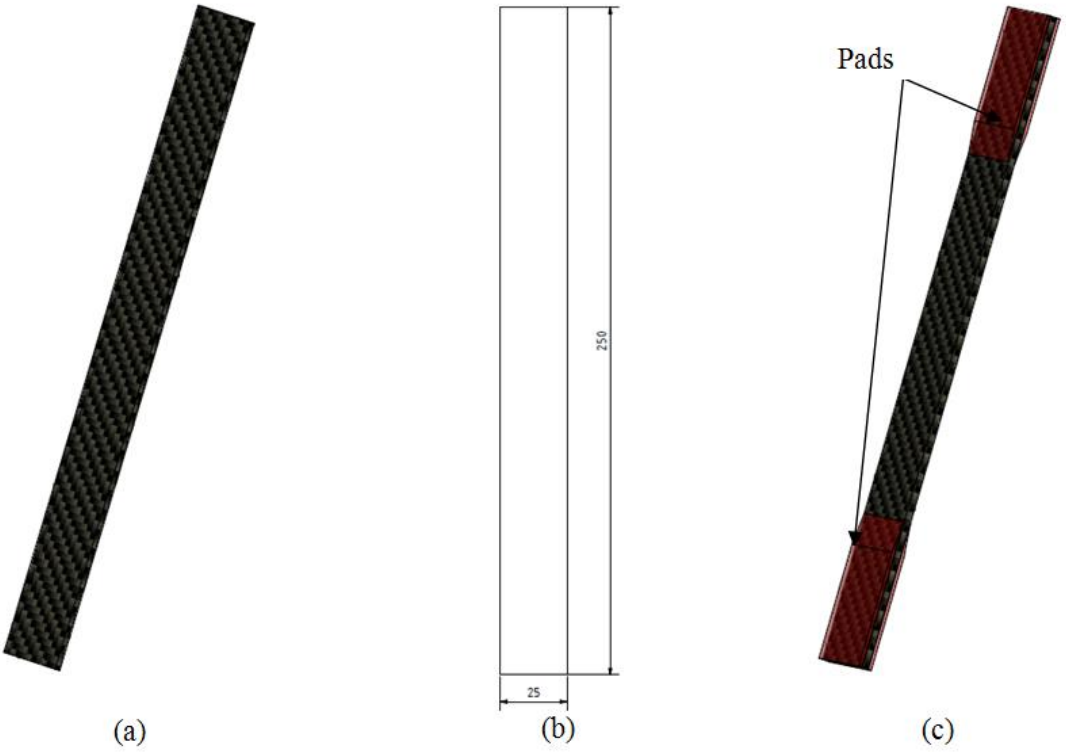

Figure 2-1. (a) Sample geometry, (b) Drawing and dimensions, (c) Assembly of the samples with the pads for the tensile tests.

Shear

Standard: ASTM 7078

Sample's Thickness: 2.5-3 mm

Properties extracted: Shear strength, shear modulus, stress-strain curve

Quantity per test: 3-5 for each material

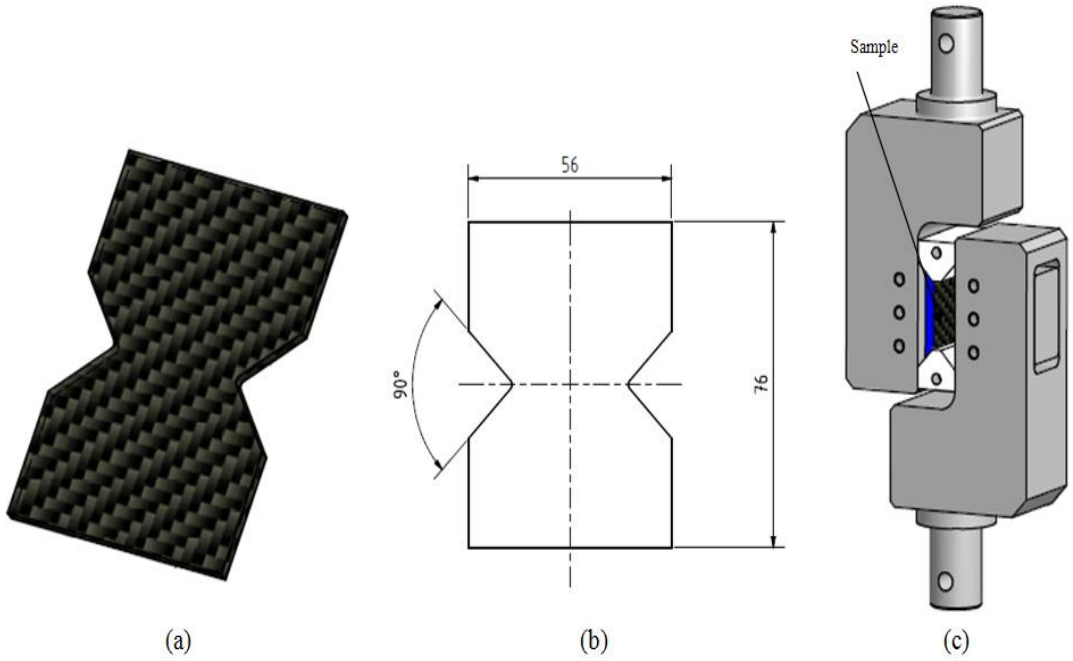

Figure 2-2. (a) Sample geometry, (b) Drawing and dimensions, (c) Assembly of the samples in the testing fixture for the shear tests.

Three point bending tests

Standard: ASTM 7264

Sample's Thickness: 2.5-3 mm

Properties extracted: Flexural strength, flexural modulus, stress-strain curve

Quantity per test: 3-5 for each material

Figure 2-3. (a) Sample geometry, (b) Drawing and dimensions for the 3-point bending tests.

Drop weight impact tests

Standard: ASTM 7136

Sample's Thickness: 2.5-3 mm

Properties extracted: Damage resistance, impact energy etc.

Quantity per test: 3 for each material

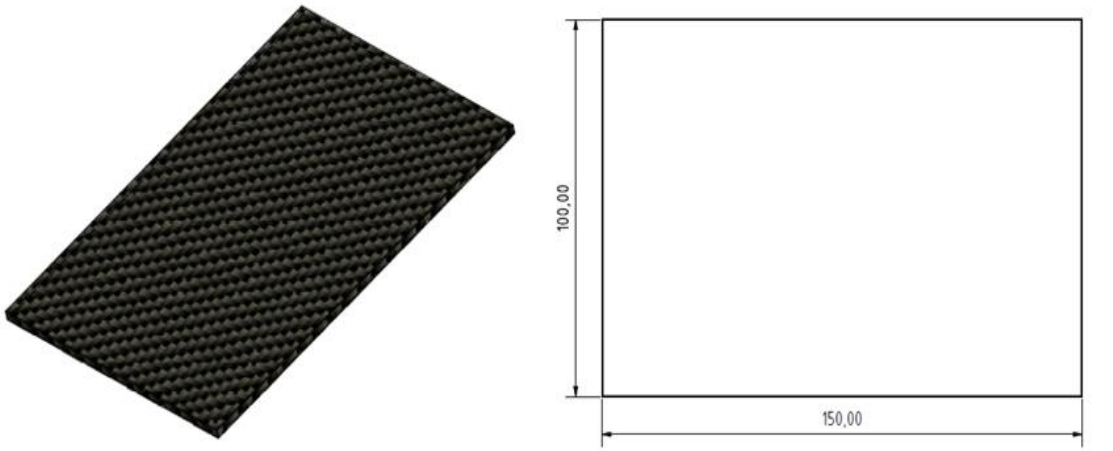

Figure 2-4. (a) Sample geometry, (b) Drawing and dimensions.

Apendix 3. Digital image correlation (DIC)

The digital image correlation, DIC, is a developed method suitable for the precise measurement of material or component deformation on whole surface [250; 251]. To date, more and more scientist and engineers choose to use DIC to understand and develop products [252; 253]. DIC has been successfully applied for various applications, such as determination of material properties, failure mechanics and simulation validation etc. [254; 255].

Figure 3-1 shows a micro-scale stochastic pattern on the testing surface, on which many black dots are distributed on the white-base background. The speckle pattern on the testing project is the fundamental mechanism for digital image correlation. The speckles move together with the object surface and hence can present the deformation and movement of the material body (Figure 3-1). The correlation method refers to the pattern matching. The subset of pixels on target is defined to handle and analyse the intensity of the pixel data. Through complex calculations based on snapshots, the displacement over the object surface could then be obtained.

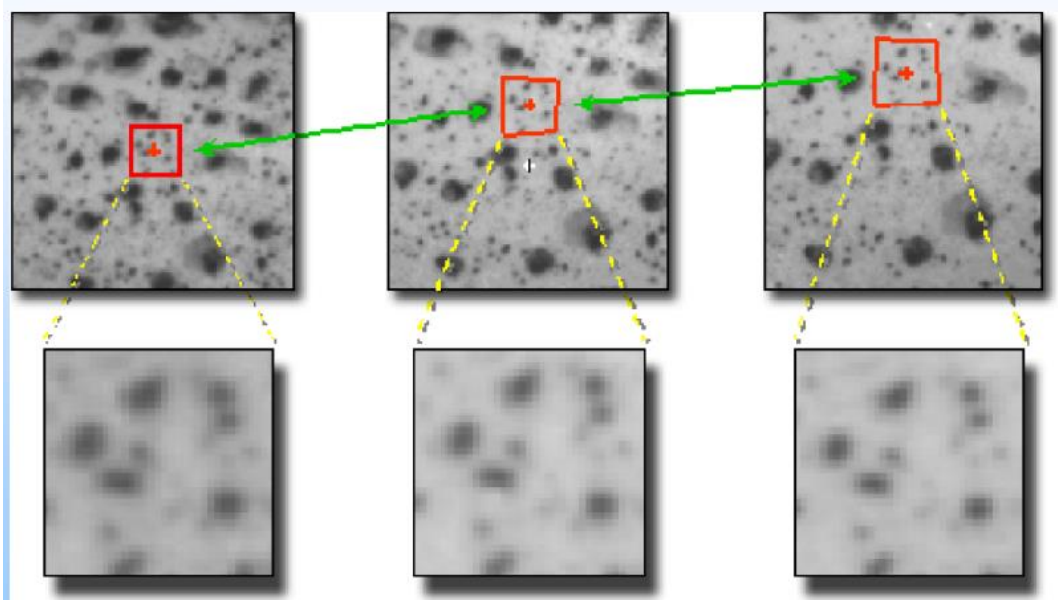

Figure 3-1. Image correlation of facets [250; 251].

Figure 3-2. shows the deformation of a point (P), the displacement can be expressed as:

$$\Delta X_q = X_q - X_p \tag{A3.1}$$

$$\Delta Y_q = Y_q - Y_p \tag{A3.2}$$

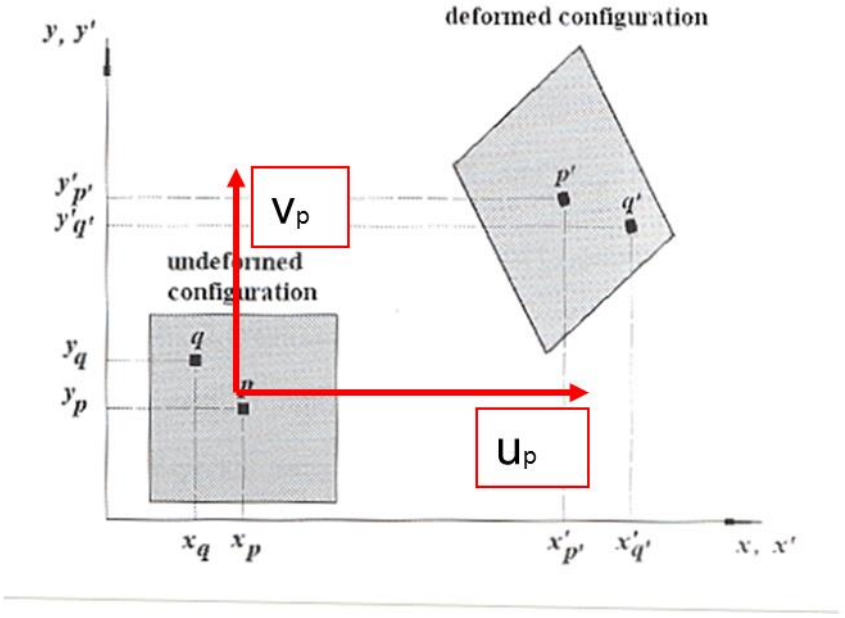

Figure 3-2. 2D in-plane deformation [252; 253].

Then the position of any point can be defined by correlation functions:

$$X'_{q'} = X_q + u_p + \frac{\partial u_p}{\partial X}\Delta X_q + \frac{\partial u_p}{\partial Y}\Delta Y_q \tag{A3.3}$$

$$Y'_{q'} = Y_q + v_p + \frac{\partial v_p}{\partial Y}\Delta Y_q + \frac{\partial v_p}{\partial X}\Delta X_q \tag{A3.4}$$

Use the above equation to solve for displacement vector:

$$\overrightarrow{V_p} = \left[u_p\ v_p\ \frac{\partial u_p}{\partial X}\ \frac{\partial u_p}{\partial Y}\ \frac{\partial v_p}{\partial Y}\ \frac{\partial v_p}{\partial X}\right]^T \tag{A3.5}$$

To best use DIC method, it is important to make the pattern, depending on the size requirement of speckles. For small speckles, carbon particles are sprayed after applying white paint. Black paint spraying and brushing are used for moderate and large speckles, respectively. Fluorescent paint is applied for very high resolution when requested.

Using DIC method has a lot of advantages: (1) simple preparation of the specimen; (2) ordinary white light required; (3) no requirement on specimen size due to the magnification of recorded images; (4) ability to obtain large strain and movement from the view of the camera.

The disadvantages of DIC are: (1) sensitive to light fluctuation; (2) difficulty in measuring out-plain strain; (2) tedious calibration process; (4) challenging mathematics.

Apendix 4. Composite machining

Due to the novelty of flax reinforced tannin based bio-composites, it is also very important to select the best technology to machining these investigated bio-materials. Machining challenges for composites normally include surface quality (e.g. fibre pull-out, uncut fibres, and delamination) and rapid tool wear. Factors like drill design, tooling material, speed and feed rate have a directly effect on the material performances during machining. A CNC (computer numerical controlled) milling machine shown in Figure 4-1 was used to understand and optimise the machining parameters.

Figure 4-1. The CNC machine for composite machining.

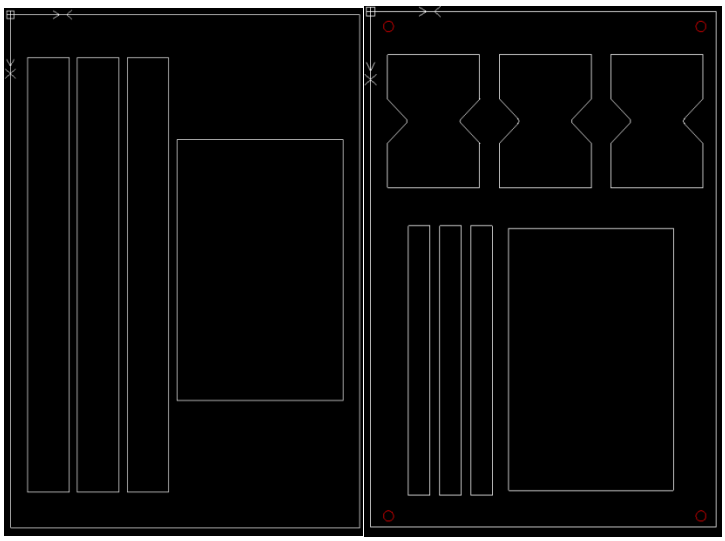

Figure 4-2. The drawing pattern designed by Draftsight.

Figure 4-3 shows the example pattern to produce required specimens in a 20×30 cm composite plate for mechanical tests (tension, shear, flexural, impact). The optimised processing parameters for flax/tannin composites are shown in Figure 4-3. From the practical operation, the feed rate was determined at 400 SFM (121 m/min) with depth increment of 1 mm to a final value of -3.5 mm for a nice cutting edge and precise size. 3 mm carbide drill was selected. As an example, a requested 76x56 mm in Hourglass shape was delivered with 76.01 by 56.00 mm.

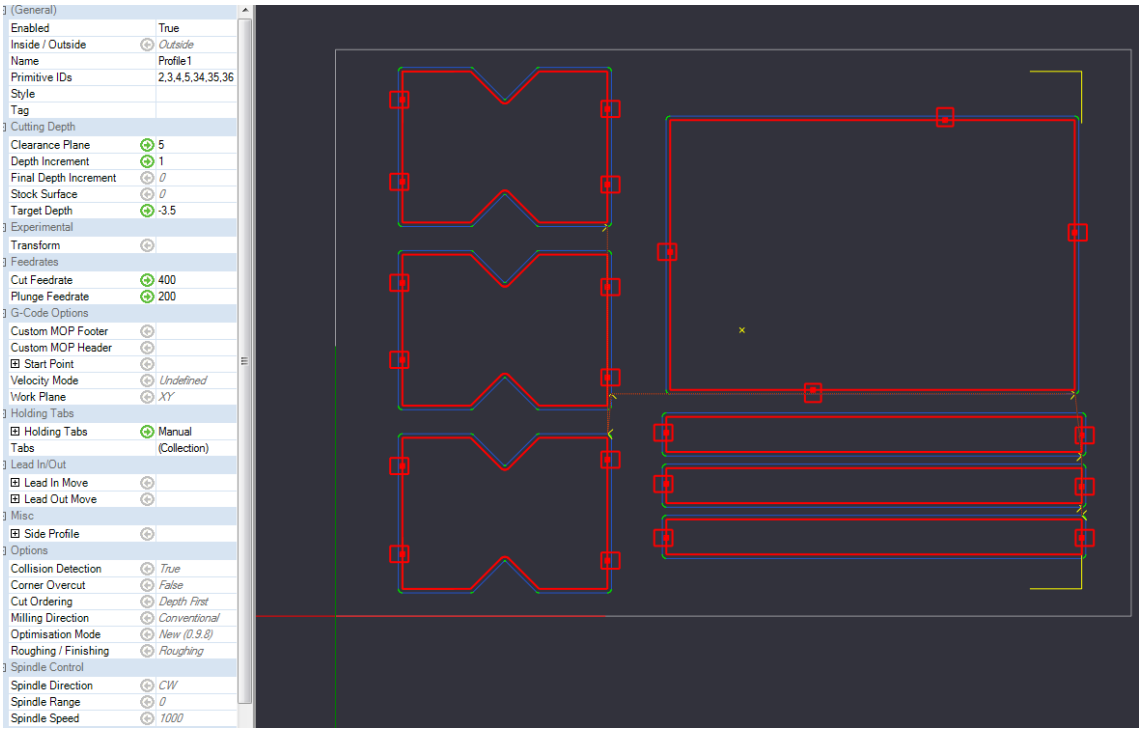

Figure 4-3. Optimised tooling path and machining parameters.

An example of generated G-code is seen below:

```
G21 G90  G40
G0 Z5.0
T3 M6
G17
M3 S1000
G0 X275.8856 Y10.0669
G0 Z1.0
G1 F200.0 Z-1.0
G1 F400.0 Y35.0669
G3 X274.3856 Y36.5669 I-1.5 J0.0
G1 X24.3856
G3 X22.8856 Y35.0669 I0.0 J-1.5
```

```
G1 Y10.0669
G3 X24.3856 Y8.5669 I1.5 J0.0
G1 X274.3856
G3 X275.8856 Y10.0669 I0.0 J1.5
G0 Z5.0
G0 X274.4606 Y38.5474
G0 Z1.0
G1 F200.0 Z-1.0
G3 F400.0 X275.8856 Y40.0455 I-0.075 J1.4981
G1 Y65.0455
G3 X274.3856 Y66.5455 I-1.5 J0.0
G1 X24.3856
G3 X22.8856 Y65.0455 I0.0 J-1.5
G1 Y40.0455
G3 X24.3856 Y38.5455 I1.5 J0.0
G1 X274.3856
G3 X274.4606 Y38.5474 I0.0 J1.5
G1 F200.0 X274.4179 Y36.5666
G1 Z-2.0
G3 F400.0 X274.3856 Y36.5669 I-0.0323 J-1.4997
G1 X24.3856
G3 X22.8856 Y35.0669 I0.0 J-1.5
G1 Y26.0
G1 Y24.5 Z-1.5
G1 Y21.5
G1 Y20.0 Z-2.0
G1 Y10.0669
G3 X24.3856 Y8.5669 I1.5 J0.0
G1 X274.3856
G3 X275.8856 Y10.0669 I0.0 J1.5
G1 Y21.0
G1 Y22.5 Z-1.5
G1 Y25.5
G1 Y27.0 Z-2.0
G1 Y35.0669
G3 X274.4179 Y36.5666 I-1.5 J0.0
G0 Z5.0
G0 X274.3871 Y68.5669
G0 Z1.0
G1 F200.0 Z-1.0
G3 F400.0 X275.8856 Y70.0669 I-0.0014 J1.5
G1 Y95.0669
G3 X274.3856 Y96.5669 I-1.5 J0.0
G1 X24.3856
G3 X22.8856 Y95.0669 I0.0 J-1.5
G1 Y70.0669
G3 X24.3856 Y68.5669 I1.5 J0.0
G1 X274.3856
```

G3 X274.3871 I0.0 J1.5
G1 F200.0 X274.3862 Y66.5455
G1 Z-2.0
G3 F400.0 X274.3856 I-0.0006 J-1.5
G1 X24.3856
G3 X22.8856 Y65.0455 I0.0 J-1.5
G1 Y57.0
G1 Y55.5 Z-1.5
G1 Y52.5
G1 Y51.0 Z-2.0
G1 Y40.0455
G3 X24.3856 Y38.5455 I1.5 J0.0
G1 X274.3856
G3 X275.8856 Y40.0455 I0.0 J1.5
G1 Y48.0
G1 Y49.5 Z-1.5
G1 Y52.5
G1 Y54.0 Z-2.0
G1 Y65.0455
G3 X274.3862 Y66.5455 I-1.5 J0.0
G0 Z5.0
G0 X274.3856 Y36.5669
G0 Z-1.0
G1 F200.0 Z-3.0
G1 F400.0 X24.3856
G3 X22.8856 Y35.0669 I0.0 J-1.5
G1 Y26.0
G1 Y24.5 Z-1.5
G1 Y21.5
G1 Y20.0 Z-3.0
G1 Y10.0669
G3 X24.3856 Y8.5669 I1.5 J0.0
G1 X274.3856
G3 X275.8856 Y10.0669 I0.0 J1.5
G1 Y21.0
G1 Y22.5 Z-1.5
G1 Y25.5
G1 Y27.0 Z-3.0
G1 Y35.0669
G3 X274.3856 Y36.5669 I-1.5 J0.0
G0 Z5.0
G0 X222.6947 Y98.9048
G0 Z1.0
G1 F200.0 Z-1.0
G3 F400.0 X223.2372 Y100.0595 I-0.9575 J1.1547
G1 Y200.0595
G3 X221.7372 Y201.5595 I-1.5 J0.0
G1 X71.7372

```
G3 X70.2372 Y200.0595 I0.0 J-1.5
G1 Y100.0595
G3 X71.7372 Y98.5595 I1.5 J0.0
G1 X221.7372
G3 X222.6947 Y98.9048 I0.0 J1.5
G1 F200.0 Z-2.0
G3 F400.0 X223.2372 Y100.0595 I-0.9575 J1.1547
G1 Y138.7262
G1 Y140.2262 Z-1.5
G1 Y143.2262
G1 Y144.7262 Z-2.0
G1 Y200.0595
G3 X221.7372 Y201.5595 I-1.5 J0.0
G1 X180.0
G1 X178.5 Z-1.5
G1 X175.5
G1 X174.0 Z-2.0
G1 X71.7372
G3 X70.2372 Y200.0595 I0.0 J-1.5
G1 Y161.3928
G1 Y159.8928 Z-1.5
G1 Y156.8928
G1 Y155.3928 Z-2.0
G1 Y100.0595
G3 X71.7372 Y98.5595 I1.5 J0.0
G1 X126.0
G1 X127.5 Z-1.5
G1 X130.5
G1 X132.0 Z-2.0
G1 X221.7372
G3 X222.6947 Y98.9048 I0.0 J1.5
G0 Z5.0
G0 Y96.5669
G0 Z0.0
G1 F200.0 Z-2.0
G1 F400.0 X132.0
G1 X130.5 Z-1.5
G1 X127.5
G1 X126.0 Z-2.0
G1 X24.3856
G3 X22.8856 Y95.0669 I0.0 J-1.5
G1 Y86.0
G1 Y84.5 Z-1.5
G1 Y81.5
G1 Y80.0 Z-2.0
G1 Y70.0669
G3 X24.3856 Y68.5669 I1.5 J0.0
G1 X274.3856
```

G3 X275.8856 Y70.0669 I0.0 J1.5
G1 Y81.0
G1 Y82.5 Z-1.5
G1 Y85.5
G1 Y87.0 Z-2.0
G1 Y95.0669
G3 X274.3856 Y96.5669 I-1.5 J0.0
G1 X222.6947
G1 F200.0 Z-3.0
G1 F400.0 X132.0
G1 X130.5 Z-1.5
G1 X127.5
G1 X126.0 Z-3.0
G1 X24.3856
G3 X22.8856 Y95.0669 I0.0 J-1.5
G1 Y86.0
G1 Y84.5 Z-1.5
G1 Y81.5
G1 Y80.0 Z-3.0
G1 Y70.0669
G3 X24.3856 Y68.5669 I1.5 J0.0
G1 X274.3856
G3 X275.8856 Y70.0669 I0.0 J1.5
G1 Y81.0
G1 Y82.5 Z-1.5
G1 Y85.5
G1 Y87.0 Z-3.0
G1 Y95.0669
G3 X274.3856 Y96.5669 I-1.5 J0.0
G1 X222.6947
G0 Z5.0
G0 X222.1338 Y98.6129
G0 Z-1.0
G1 F200.0 Z-3.0
G3 F400.0 X223.2372 Y100.0595 I-0.3966 J1.4466
G1 Y138.7262
G1 Y140.2262 Z-1.5
G1 Y143.2262
G1 Y144.7262 Z-3.0
G1 Y200.0595
G3 X221.7372 Y201.5595 I-1.5 J0.0
G1 X180.0
G1 X178.5 Z-1.5
G1 X175.5
G1 X174.0 Z-3.0
G1 X71.7372
G3 X70.2372 Y200.0595 I0.0 J-1.5
G1 Y161.3928

```
G1 Y159.8928 Z-1.5
G1 Y156.8928
G1 Y155.3928 Z-3.0
G1 Y100.0595
G3 X71.7372 Y98.5595 I1.5 J0.0
G1 X126.0
G1 X127.5 Z-1.5
G1 X130.5
G1 X132.0 Z-3.0
G1 X221.7372
G3 X222.1338 Y98.6129 I0.0 J1.5
G1 F200.0 Z-3.5
G3 F400.0 X223.2372 Y100.0595 I-0.3966 J1.4466
G1 Y138.7262
G1 Y140.2262 Z-1.5
G1 Y143.2262
G1 Y144.7262 Z-3.5
G1 Y200.0595
G3 X221.7372 Y201.5595 I-1.5 J0.0
G1 X180.0
G1 X178.5 Z-1.5
G1 X175.5
G1 X174.0 Z-3.5
G1 X71.7372
G3 X70.2372 Y200.0595 I0.0 J-1.5
G1 Y161.3928
G1 Y159.8928 Z-1.5
G1 Y156.8928
G1 Y155.3928 Z-3.5
G1 Y100.0595
G3 X71.7372 Y98.5595 I1.5 J0.0
G1 X126.0
G1 X127.5 Z-1.5
G1 X130.5
G1 X132.0 Z-3.5
G1 X221.7372
G3 X222.1338 Y98.6129 I0.0 J1.5
G0 Z5.0
G0 Y66.5455
G0 Z-1.0
G1 F200.0 Z-3.0
G1 F400.0 X24.3856
G3 X22.8856 Y65.0455 I0.0 J-1.5
G1 Y57.0
G1 Y55.5 Z-1.5
G1 Y52.5
G1 Y51.0 Z-3.0
G1 Y40.0455
```

```
G3 X24.3856 Y38.5455 I1.5 J0.0
G1 X274.3856
G3 X275.8856 Y40.0455 I0.0 J1.5
G1 Y48.0
G1 Y49.5 Z-1.5
G1 Y52.5
G1 Y54.0 Z-3.0
G1 Y65.0455
G3 X274.3856 Y66.5455 I-1.5 J0.0
G1 X222.1338
G1 F200.0 Z-3.5
G1 F400.0 X24.3856
G3 X22.8856 Y65.0455 I0.0 J-1.5
G1 Y57.0
G1 Y55.5 Z-1.5
G1 Y52.5
G1 Y51.0 Z-3.5
G1 Y40.0455
G3 X24.3856 Y38.5455 I1.5 J0.0
G1 X274.3856
G3 X275.8856 Y40.0455 I0.0 J1.5
G1 Y48.0
G1 Y49.5 Z-1.5
G1 Y52.5
G1 Y54.0 Z-3.5
G1 Y65.0455
G3 X274.3856 Y66.5455 I-1.5 J0.0
G1 X222.1338
G1 F200.0 Y68.5669
G1 F400.0 X274.3856
G3 X275.8856 Y70.0669 I0.0 J1.5
G1 Y81.0
G1 Y82.5 Z-1.5
G1 Y85.5
G1 Y87.0 Z-3.5
G1 Y95.0669
G3 X274.3856 Y96.5669 I-1.5 J0.0
G1 X132.0
G1 X130.5 Z-1.5
G1 X127.5
G1 X126.0 Z-3.5
G1 X24.3856
G3 X22.8856 Y95.0669 I0.0 J-1.5
G1 Y86.0
G1 Y84.5 Z-1.5
G1 Y81.5
G1 Y80.0 Z-3.5
G1 Y70.0669
```

G3 X24.3856 Y68.5669 I1.5 J0.0
G1 X222.1338
G0 Z5.0
G0 Y36.5669
G0 Z-1.5
G1 F200.0 Z-3.5
G1 F400.0 X24.3856
G3 X22.8856 Y35.0669 I0.0 J-1.5
G1 Y26.0
G1 Y24.5 Z-1.5
G1 Y21.5
G1 Y20.0 Z-3.5
G1 Y10.0669
G3 X24.3856 Y8.5669 I1.5 J0.0
G1 X274.3856
G3 X275.8856 Y10.0669 I0.0 J1.5
G1 Y21.0
G1 Y22.5 Z-1.5
G1 Y25.5
G1 Y27.0 Z-3.5
G1 Y35.0669
G3 X274.3856 Y36.5669 I-1.5 J0.0
G1 X222.1338
G0 Z5.0
M5
M30

The G-code was first run by the cut-viewer software as seen below to simulate the cutting routes and behaviours to ensure the safety and reliability.

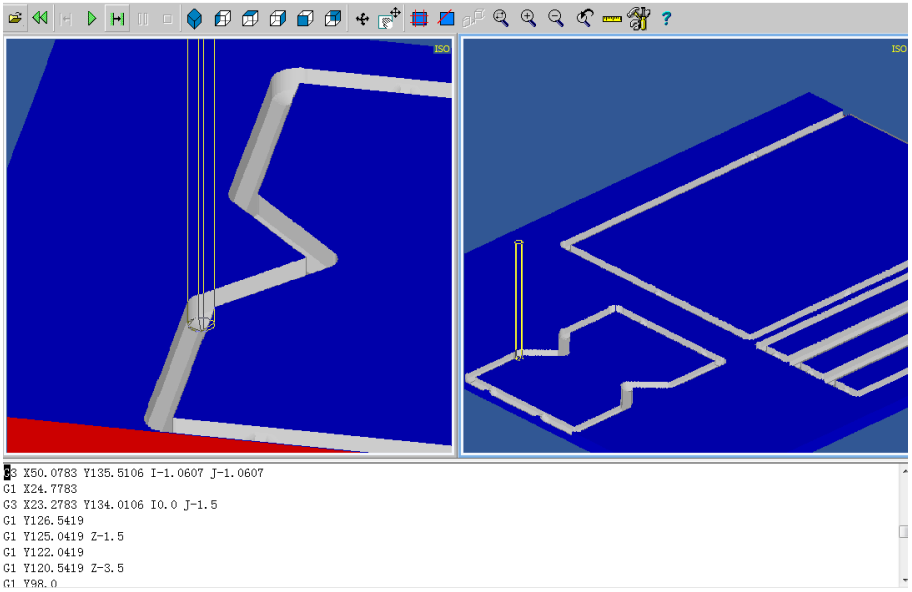

Figure 4-4. Simulation of g-code by cut viewer.

Apendix 5. Procedure of bonding tensile specimens with tabs

1. Sample preparation before bonding

- Clean the lab and working area.
- Prepare aluminium tabs in 25×50 mm size (four for one specimen tabing)
- Remove the impurities on the aluminium tab surfaces using abrasion paper to make a rougher surface for bonding. (Figure 5-1 (a))
- Similarly prepare the rougher surface of composite specimens on both side of the bonding area. (Figure 5-1(b))

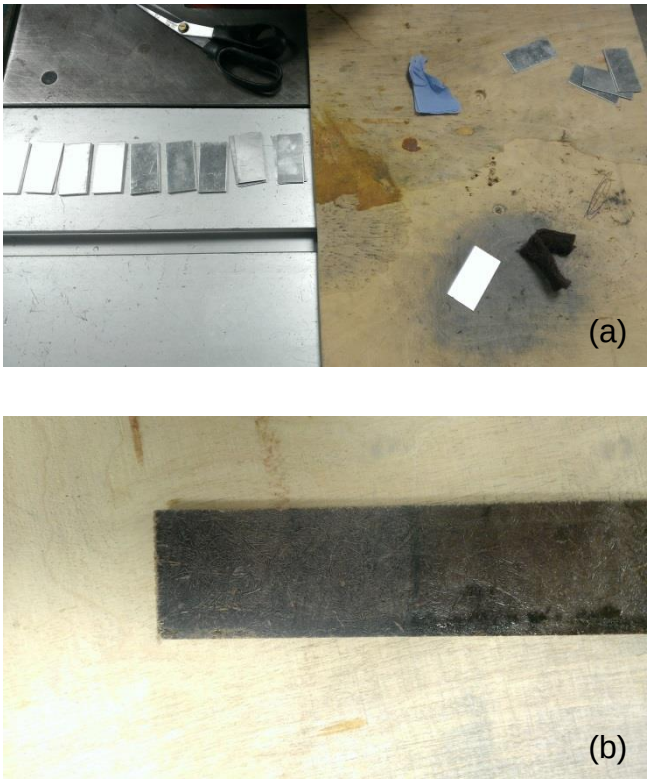

Figure 5-1. Preparation of (a) tab abrasion and (b) specimen abrasion.

2. Adhesive bonding

- Weight out Redux 420 A/B adhesive carefully: 10: 4 in weight ratio
- Mixe the part A and B adhesive together
- Clean the tab and specimen surface (both sides) using acetone to remove the contaminates

- Apply adhesive gently and slightly make it cove the tab surface
- Make the composite stand straight and place the adhesive surface of the tab on the composite part (Figure 5-2)
- For each end, clamp the tab and composites, and then remove the excess leaked adhesive as much as possible (Figure 5-2)
- Place the bonded parts in an oven at the temperature of 40 °C for 4 h.
- Clean area and dispose of any uncured epoxy resin material as hazardous waste.
- After curing, remove any resins on the tab surface which will be clamped in the tension testing.

Figure 5-2. Adhesive tab bonding procedure on tensile specimens.